Block-Interleaved Frequency Division Multiple Access and its Application in the Uplink of Future Mobile Radio Systems

von
Dipl.-Ing. Tobias Frank
geboren am 01.04.1979 in Laubach

Danksagung

Zum Gelingen der vorliegenden Arbeit haben sehr viele unterschiedliche Menschen beigetragen, denen ich an dieser Stelle ausdrücklich danken möchte.

Zunächst danke ich allen Kollegen am Fachgebiet Kommunikationstechnik. Meine Kollegen waren mir fachlich und organisatorisch, aber auch persönlich immer eine wertvolle Hilfe. Es hat meine Arbeit sehr bereichert, dass ich unter meinen Kollegen jederzeit kompetente Ansprechpartner für die unterschiedlichsten technischen Fragestellungen finden konnte. Außerdem haben Humor und Hilfsbereitschaft meiner Kollegen meiner Arbeit über manchen toten Punkt hinweggeholfen.

Ein besonderer Dank gilt Frau Professor Anja Klein, die mich bei meiner Arbeit intensiv angeleitet und betreut hat. Sie hat in vielen fruchtbaren Diskussionen wesentlich zum Inhalt und zur Form der vorliegenden Arbeit beigetragen. Ihre Unterstützung, insbesondere bei der Veröffentlichung der Ergebnisse, hat mir die Möglichkeit gegeben, die Inhalte meiner Arbeit mit vielen Fachleuten zu diskutieren und immer wieder kritisch zu überdenken. Weiterhin danke ich auch Herrn Professor Martin Bossert für die Übernahme des Korreferats und seine Einladung zum Vortrag an die Universität Ulm.

Die Einbindung meiner Arbeit in das europäische Forschungsprojekt WINNER hat mir ermöglicht, über den Tellerrand zu schauen und mein Thema als Teil eines Gesamtsystems zu sehen. Ich danke den Kollegen in den unterschiedlichsten Gremien des WINNER Projekts, insbesondere Frau Dr. Elena Costa, Herrn Professor Tommy Svensson und Herrn Professor Mikael Sternad, für die interessanten Gespräche und Rückmeldungen zu meiner Arbeit.

Den Studenten, die ich bei ihrer Bachelor-, Studien-, Diplom-, oder Masterarbeit betreut habe, danke ich dafür, dass sie mir geholfen haben, die Umgebungen zu implementieren, mit denen die Simulationsergebnisse in meiner Arbeit erzeugt wurden.

Mein Dank geht auch an meine Freunde und Verwandte in Oberhessen und in Darmstadt. Sie haben mich immer wieder auf andere Gedanken gebracht und haben mir geholfen, auch in anstrengenden Phasen zwischendurch abzuschalten.

Ich widme diese Arbeit meinen Eltern und möchte damit meiner Dankbarkeit Ausdruck geben, dass sie mir nicht nur das Studium ermöglicht und mir in vielerlei Beziehung den Rücken frei gehalten haben, sondern auch sonst immer für mich da waren und mir besonders in der Zeit, in der diese Arbeit entstanden ist, eine wertvolle Stütze waren.

Immenstaad, im Mai 2010   Tobias Frank

Kurzfassung

In der vorliegenden Arbeit wird ein neues Vielfachzugriffsverfahren mit dem Namen Block-Interleaved Frequency Division Multiple Access (B-IFDMA) vorgestellt und auf seine Eignung für die Anwendung in der Aufwärtsstrecke zukünftiger Mobilfunksysteme untersucht. Hierzu werden neue Algorithmen vorgestellt, die das Verfahren ergänzen, die Eigenschaften des Verfahrens werden analysiert, und sie werden mit denen anderer bekannter Vielfachzugriffsverfahren verglichen.

Zunächst wird ein neues, allgemeines, digitales Systemmodell eingeführt, das die gemeinsame Beschreibung von B-IFDMA und zahlreichen bereits bekannten und mit B-IFDMA verwandten Vielfachzugriffsverfahren ermöglicht. Hierdurch wird es möglich, die Zusammenhänge der verschiedenen Verfahren exakt und übersichtlich darzustellen. Unter anderem wird gezeigt, dass B-IFDMA als Orthogonal Frequency Division Multiple Access (OFDMA) Verfahren mit einer Vorcodierung der Daten und äquidistanter Anordnung gleichgroßer Blöcke mit benachbarten Unterträgern aufgefasst werden kann, wobei die Blöcke über die gesamte verfügbare Bandbreite gespreizt sind. Außerdem wird dargestellt, dass B-IFDMA als eine Verallgemeinerung von Single Carrier Frequency Division Multiple Access (SC-FDMA) verstanden werden kann.

Basierend auf dem neuen Systemmodell wird gezeigt, dass für B-IFDMA bei der Verwendung in der Aufwärtsstrecke eine einfache Empfängerstruktur verwendet werden kann. Diese Empfängerstruktur beruht auf einer Trennung der Signale verschiedener Nutzer im Frequenzbereich und einer anschließenden Entzerrung der Signale der einzelnen Nutzer mit Hilfe von Frequenzbereichs-Entzerrern und weist dadurch eine geringe Komplexität auf.

Anschließend werden verschiedene neue Algorithmen vorgestellt und diskutiert, die eine effiziente Anwendung von B-IFDMA in einem zukünftigen Mobilfunksystem ermöglichen. Im einzelnen werden

- ein Algorithmus mit geringer Komplexität zur Signalerzeugung für B-IFDMA im Zeitbereich,

- ein Algorithmus mit geringer Komplexität zur Anwendung von orthogonalen und nicht-orthogonalen Raum-Zeit Codes (engl. Space-Time Codes) für B-IFDMA,

- ein Algorithmus mit geringer Komplexität zur Anwendung von Raum-Vielfachzugriff (engl. Space-Division Multiple Access) für B-IFDMA und

- ein Algorithmus mit geringer Komplexität zur flexiblen Verwendung verschiedener Datenraten in einer Mobilfunkzelle für B-IFDMA bei gleichzeitiger Wahrung der Orthogonalität der Signale verschiedener Nutzer

beschrieben.

Abschließend werden in dieser Arbeit die Eigenschaften von B-IFDMA ausführlich hinsichtlich

- Ausnutzung von Diverstät in Frequenz, Zeit, Raum und über mehrere Nutzer,

- Verlusten durch Überhang durch Pilotsymbole für Kanalschätzung,

- Robustheit gegen Frequenzversatz,

- Effizienz der Leistungsverstärker und

- Komplexität bei der Implementierung

untersucht. Es stellt sich dabei heraus, dass die genannten Eigenschaften von B-IFDMA zum Teil stark von der gewählten Parametrisierung abhängen.

Ein wichtiges Ergebnis der Untersuchung der Eigenschaften von B-IFDMA ist, dass das Verfahren für eine hohe Zahl von Blöcken vornehmlich durch die gute Ausnutzung von Frequenzdiversität eine gute Bitfehler-Performanz erreicht, die durch den Einsatz von Raum-Zeit Codes noch verbessert wird. Dadurch kommt B-IFDMA, anders als Verfahren, die auf eine Adaption der Übertragung an den Übertragungskanal ausgerichtet sind, ohne Kenntnis des Übertragungskanals am Sender aus. Somit ist B-IFDMA besonders für nicht-adaptive Übertragung geeignet, die in Szenarien notwendig ist, in denen Kanalkenntnis am Sender nicht zur Verfügung gestellt werden kann, z.B. weil sich die Kanalbedingungen aufgrund hoher Geschwindigkeiten der Teilnehmer zu schnell ändern. Wie gezeigt wird, ist B-IFDMA robuster gegen Frequenzversatz, hat geringere Verluste durch Überhang durch Pilotsymbole für Kanalschätzung, hat eine höhere Leistungseffizienz als andere Verfahren und ist sehr flexibel. Es kann daher insgesamt als ein interessanter und geeigneter Kandidat für die Aufwärtstrecke bei nicht-adaptiver Übertragung in zukünftigen Mobilfunksystemen angesehen werden.

Abstract

In this thesis, a new multiple access scheme denoted as Block-Interleaved Frequency Division Multiple Access (B-IFDMA) is presented and investigated with respect to its suitability for an application in the uplink of future mobile radio systems. For that purpose, new algorithms are presented that complement the scheme. The properties of the scheme are analyzed and compared to the properties of other well-known multiple access schemes.

At first, a new, general, digital system model is introduced that makes a joint description of B-IFDMA and various other well-known multiple access schemes that are related to B-IFDMA possible and enables a clear and proper illustration of their relations. Amongst other things, it is shown that B-IFDMA can be considered as Orthogonal Frequency Division Multiple Access (OFDMA) with pre-coding of the data and with blocks of equal size of adjacent subcarriers that are equidistantly distributed over the total available bandwidth. Further on, it is identified that B-IFDMA can be regarded as a generalization of Single Carrier Frequency Division Multiple Access (SC-FDMA).

Based on the new system model, it is shown that, in the uplink, a simple receiver structure can be applied for B-IFDMA. The simple receiver structure is based on a separation of different users' signals in frequency domain and subsequent equalization applying frequency domain equalizers to the different users' signals, which leads to a low computational receiver complexity.

Subsequently, different new algorithms are presented and discussed that make an efficient application of B-IFDMA in a future mobile radio system possible. In particular,

- an algorithm for B-IFDMA signal generation in time domain providing a low computational complexity,

- an algorithm for application of orthogonal and non-orthogonal Space-Time Codes to B-IFDMA providing a low computational complexity,

- an algorithm for application of Space-Division Multiple Access to B-IFDMA providing a low computational complexity, and

- an algorithm for a flexible and efficient accommodation of different data rates to the users within a mobile radio cell providing a low computational complexity and maintaining the orthogonality of different users' signals

are described.

Finally, in this thesis, the properties of B-IFDMA regarding

- the exploitation of diversity in frequency, time, space and among different users,

- pilot symbol overhead for channel estimation,

- robustness to carrier frequency offsets,

- power efficiency of the power amplifiers, and

- computational complexity

are extensively investigated. It turns out that the properties of B-IFDMA in part strongly depend on the choice of the parameters.

As an important result of the investigation of the properties of B-IFDMA, the scheme is shown to provide a good bit error rate performance due to a good exploitation of frequency diversity for the assignment of a high number of subcarrier blocks. This performance is further improved by the application of Space Time Coding. Thus, in contrast to multiple access schemes that are focused on the adaptation of the transmission to the current channel conditions, B-IFDMA does not require any channel state information at the transmitter. Consequently, B-IFDMA is especially suited for non-adaptive transmission which is required in scenarios where channel state information at the transmitter cannot be provided, e.g., due to a high change rate of the channel conditions caused by a high user mobility. It is shown that, compared to other schemes, B-IFDMA is more robust to carrier frequency offsets, provides lower pilot symbol overhead for channel estimation, provides a higher power efficiency of the power amplifier and is very flexible. Thus, it can be concluded that B-IFDMA is an interesting and well-suited candidate for the non-adaptive uplink of future mobile radio systems.

Contents

Chapter 1

Introduction

1.1 The Radio Interface of Future Mobile Radio Systems

1.1.1 Evolution of Current Mobile Radio Systems

In recent years, terrestrial cellular mobile radio systems have been characterized by a rapid technological progress. After the introduction of the first generation (1G) mobile radio systems that were based on analog technology in the 1980s, in the 1990s the second generation (2G) mobile radio systems have been introduced that were based on digital technology. Examples and details of 1G and 2G mobile radio systems can be found, e.g., in [RP03]. Currently, in many countries all over the world, third generation (3G) mobile radio systems are operating. In many references, e.g., in [SH03], the Japanese mobile radio system denoted Freedom of Mobile Multimedia Access (FOMA), that has been launched in 2001, is referred to as the first commercial 3G mobile radio system worldwide. In Germany, 3G mobile radio systems are commercially available since 2004 [Ker04].

The International Telecommunication Union (ITU) has formulated a global standard for 3G mobile radio systems that is denoted as International Mobile Telecommunications (IMT)-2000 standard. Currently, the ITU has approved six radio interfaces for IMT-2000 [ITU01]. The six current IMT-2000 radio interfaces are

- Universal Terrestrial Radio Access for Frequency Division Duplex (UTRA-FDD) as part of the Universal Mobile Telecommunications Systems (UMTS) [3GP09, SW02],

- CDMA2000 [TIA99],

- Time Division - Code Division Multiple Access (TD-CDMA) and the Time Division - Synchronous Code Division Multiple Access (TD-SCDMA) as part of the Universal Terrestrial Radio Access for Time Division Duplex (UTRA-TDD) of UMTS [3GP08g, SW02],

- Enhanced Data Rates for GSM Evolution (EDGE) that is an evolution of the Global Systems for Mobile Communications (GSM) [3GP08d, 3GP08e],

- Digital Enhanced Cordless Telecommunications (DECT) [DEC97], and

- Internet Protocol - Orthogonal Frequency Division Multiple Access (IP-OFDMA) as part of the Institute of Electrical and Electronics Engineers (IEEE) standard 802.16 for Worldwide Interoperability for Microwave Access (WiMAX) [IEE00].

Compared to 2G systems that have been basically designed for voice oriented traffic, 3G systems provide mixed voice, data, and multimedia traffic, are packet oriented and are aiming at seamless global roaming [ITU01]. 3G systems provide peak data rates from 144 kbps in high mobility environments and up to 2 Mbps in low mobility environments [RP03].

In parallel to the current mobile radio systems, broadband wireless access systems have been introduced that provide wireless access to the internet with peak data rates of up to 54 Mbps [RP03] and even more if used in combination with multiple antenna techniques. Examples for broadband wireless access systems are

- IEEE 802.11 Wireless Local Area Network (WLAN) [IEE99],

- High Performance Local Area Network (HIPERLAN)-2 [ETS99], and

- Multimedia Mobile Access Communications Systems (MMAC) [RP03].

However, the broadband wireless access systems are designed for low mobility scenarios and, thus, are not suitable for mobile radio transmission.

The ITU has formulated a concept for the evolution of mobile radio systems beyond 3G that is denoted as IMT-Advanced [ITU08]. IMT-Advanced compliant systems are also often denoted as fourth generation (4G) mobile radio systems [DMO09]. Important requirements for IMT-Advanced compliant systems as formulated in [ITU08] are:

- a high degree of commonality of functionality worldwide while retaining the flexibility to support a wide range of services and applications in a cost efficient manner,

- compatibility of services within IMT-2000 and with fixed networks,

- capability of interworking with other radio access schemes,

- high quality mobile services,

- user equipment suitable for worldwide use,

- user-friendly applications, services and equipment,

- worldwide roaming capability, and

- enhanced peak data rates to support advanced services and applications (100 Mbps for high and 1 Gbps for low mobility were established for research).

Several consortia have started the evolution of 3G mobile radio systems towards IMT-Advanced. In the following, some activities in this field that are of particular interest for this thesis are briefly described.

The 3rd Generation Partnership Project (3GPP) has started the evolution by the standardisation of the 3GPP Long Time Evolution (LTE) [3GP08c, 3GP08b]. The 3GPP LTE standard can be regarded as an intermediate step from 3G mobile radio systems to the IMT-Advanced concept. The 3GPP system that is evolving 3GPP LTE targeting at the IMT-Advanced concept is known under the name 3GPP LTE-Advanced [3GP08f].

The IEEE is evolving the WiMAX system, cf. the IEEE 802.16 standard [IEE00], and is also targeting at fulfilling the requirements of the IMT-Advanced concept, especially with the standard 802.16m [IEE00].

In 2004, the European Union (EU) started a research project in a consortium of partners from the universities and from the industry, including manufacturers as well as operators. This research project was denoted as Wireless World Initiative New Radio (WINNER) [Moh06] and was finalized in 2005. The goal of this project and its succeeding project WINNER II that started in 2006 was to investigate and to propose an IMT-Advanced compliant mobile radio system concept. The project WINNER II was finalized in 2007. The author of this thesis was involved in the WINNER and WINNER II project in the research and development of a new IMT-Advanced compliant radio interface.

1.1.2   Requirements for the Radio Interface of Future Mobile Radio Systems

In order to meet the requirements for IMT-Advanced compliant mobile radio systems, significant changes compared to 3G systems are expected for the network structure as well as for the radio interface [ITU01]. In this thesis, the focus is on the radio interface.

For the radio interface of an IMT-Advanced compliant mobile radio system, the following key requirements can be identified, cf. [3GP08f, ITU01, WIN07d]:

- A high flexibility and granularity in terms of different data rates is required in order to make a flexible support of a wide range of services and applications possible.

- Low delays are required in order to enable also delay critical and interactive services such as online gaming. The requirement of low delays becomes even more important if relays are used in order to increase the system performance, because relaying introduces unavoidable additional delays to the system that have to be compensated by even lower delays for a single radio link.

- A power efficient use of the mobile terminal is required in order to provide user friendly standby and activity times of the mobile terminals.

- A good performance is required in order to provide high quality mobile services and in order to meet the targets of IMT-Advanced for the spectral efficiency, cf. [ITU01].

- Algorithms with low computational complexity that can handle high data rates at the transmitter as well as at the receiver are required in order to keep the costs for the mobile terminals as well as the costs for the base stations as low as possible.

- High user mobilities from 120 km/h up to 350 km/h have to be supported in order to provide high quality services even for mobile users [ITU01].

1.1.3   Multiple Access Schemes for Future Mobile Radio Systems

The properties of the radio interface strongly depend on the choice of the multiple access scheme [JWY05]. In this section, the state-of-the-art of multiple access schemes for the radio interfaces of future mobile radio systems is described.

In the following, multiple access schemes for uplink and downlink transmission are distinguished. The uplink is the link from the mobile terminal to a central terminal within a mobile radio cell that is connected to a fixed communication network. This central terminal is denoted as base station throughout this thesis. Vice versa, the downlink is the link from the base station to the mobile terminal. The reason that, in the following, uplink and downlink are distinguished is that the requirements for a multiple access scheme in the uplink and in the downlink are different. E.g., in the uplink, the power efficiency of the power amplifier is much more critical than in the downlink because the power supply for mobile terminals is based on batteries.

Further on, in the following, scenarios where reliable information of the current channel between mobile terminal and base station is available at the transmitter side and scenarios where this is not the case are distinguished. The information of the current channel between a certain mobile terminal and the base station is denoted as channel state information (CSI) throughout this thesis. In scenarios where reliable CSI is available at the transmitter, a good performance for the radio transmission can be provided by means of adaptation to the channel. Well-known techniques providing a good performance by an exploitation of reliable CSI at the transmitter side are, e.g., adaptive multi-user scheduling [ECV03], and adaptive power loading, modulation and coding [GC98]. In order to provide reliable CSI at the transmitter, in general, the CSI has to be determined at the receiver by means of channel estimation. Subsequently, the CSI has to be fed back to the transmitter. Thus, reliable CSI at the transmitter requires a high signal to noise and interference ratio in order to enable a reliable channel estimation. Further on, a low change rate of the channel conditions compared to the time required for feedback of the CSI from the receiver to the transmitter is necessary. In the following, scenarios exploiting the reliable CSI available at the transmitter in order to provide a good performance are denoted as scenarios for adaptive transmission.

However, for reasons like high user mobility or a bad signal to noise and interference ratio of the received signal, reliable CSI may not be available at the transmitter. In this case, adaptive transmission fails. Also in scenarios where the same information is transmitted to a group of users, as it is the case for broadcast and multicast services, adaptive transmission is not appropriate. In the following, these kinds of scenarios are denoted as scenarios for non-adaptive transmission. For non-adaptive transmission, the preferred strategy for provision of good performance is the exploitation of diversity [WIN05].

Further on, note that, in order to meet the targets of IMT-Advanced for the spectral efficiency, the application of multiple antenna techniques is required [JB04]. Thus, the compatibility of the multiple access scheme with appropriate multiple antenna

techniques is essential. Note that, for the choice of an appropriate multiple antenna technique, the question if reliable CSI is available at the transmitter or not is also important. If reliable CSI is available, the multiple antennas can be used for adaptation to the channel and to competitively exploit the different channel conditions of different users [JB04]. If reliable CSI is not available, the exploitation of spatial diversity by means of averaging of the channel conditions is an appropriate strategy.

The distinction between, on the one hand, uplink and downlink and, on the other hand, adaptive and non-adaptive transmission results in four possible combinations. In the following, for these four combinations, the state-of-the-art of the multiple access schemes for future mobile radio systems is described.

For adaptive downlink transmission, Orthogonal Frequency Division Multiple Access (OFDMA) [RMBG99] has been identified as an appropriate solution. OFDMA subdivides the available bandwidth in overlapping but mutually orthogonal narrowband subcarriers that are used for transmission. Due to the overlapping subcarriers the scheme is spectrally efficient. For OFDMA, the transmission of the data is organized in consecutive and mutually independent blocks that are separated by a guard interval that is typically designed as Cyclic Prefix (CP) [WG00]. Due to the block transmission with CP, for OFDMA, the orthogonality of the subcarriers can be maintained even for the transmission over frequency selective channels. Thus, simple receiver structures are possible even for high data rates. Moreover, OFDMA modulation and demodulation can be implemented in a computationally efficient way by the application of the Fast Fourier Transform (FFT) algorithm [Ach78]. Thus, OFDMA can be considered as a transmission scheme that enables high data rate transmission at acceptable costs. Additionally, OFDMA provides a high flexibility due to a flexible assignment of the subcarriers to users. In order to provide maximum gains for adaptive transmission, blocks of adjacent subcarriers are assigned to the users dependent on the user specific CSI. OFDMA is intended, e.g., as multiple access solution in the adaptive downlink of WiMAX [IEE00] as well as in the adaptive downlink of 3GPP LTE [3GP08a]. Moreover, OFDMA has been adopted as multiple access scheme for the adaptive downlink of the WINNER II system concept [WIN07a, WIN07b, WIN07c].

For the non-adaptive downlink, again OFDMA has been identified as an appropriate multiple access solution. However, in order to provide diversity, the subcarrier assignment is chosen in a different way compared to the adaptive downlink. In WiMAX, in 3GPP LTE and in the WINNER II system concept, for the non-adaptive downlink, OFDMA with subcarriers assigned to a user that are distributed over the total available bandwidth is adopted [IEE00, 3GP08a, WIN06, WIN07e]. Due to the distributed subcarriers, frequency diversity can be exploited.

In general, OFDMA is known to suffer from high fluctuations of the signal envelope [vNP00]. Thus, expensive highly linear power amplifiers are required that, especially in the uplink, result in undesirable cost for the mobile terminals. Moreover, due to the high envelope fluctuations, a power back-off is necessary that reduces the power efficiency of the power amplifier and, thus, reduces the activity time of the mobile terminals [RAC+02]. For downlink transmission, typically, the signal that is transmitted from the base station, is a superposition of the transmit signals of different users. Thus, for downlink transmission, high envelope fluctuations cannot be avoided and the choice of OFDMA is reasonable. For uplink transmission, only the signal of one user is transmitted from the mobile terminal. Thus, for uplink transmission, the fluctuations of the signal envelope can be kept low by an appropriate choice of the multiple access scheme.

For that reason, for adaptive uplink transmission, in 3GPP LTE, instead of OFDMA, a different block-transmission-based multiple access scheme with CP is used that is denoted as localized Single-Carrier Frequency Division Multiple Access (SC-FDMA) [3GP06, 3GP08a]. Localized SC-FDMA is based on an OFDMA scheme assigning adjacent subcarriers to the users dependent on the user specific CSI. In addition, a Discrete Fourier Transform (DFT) is applied to the data symbols before OFDMA modulation. The pre-coding of the data symbols by a DFT changes the properties of the OFDMA signal to those of a single carrier signal and results in a considerably decreased signal envelope of the transmit signal [XZG03]. However, in WiMAX as well as in the WINNER II system, OFDMA without DFT pre-coding assigning blocks of adjacent subcarriers to the users dependent on the user specific CSI is proposed also for adaptive uplink transmission and the high envelope fluctuations of the transmit signal are accepted [IEE00, WIN06, WIN07e]. One reason is that a DFT pre-coding of the data symbols before allocating them to blocks of adjacent subcarriers would make the application of adaptive modulation and coding schemes and adaptive power allocation much more complicated.

For non-adaptive uplink transmission, in 3GPP LTE, localized SC-FDMA is adopted, too [3GP08a]. In order to provide frequency diversity, frequency hopping (FH) is applied [SW02, 3GP08a]. However, the application of FH is expected to introduce additional undesired delays to the system and the pilot symbol overhead required for channel estimation is expected to be increased compared to localized SC-FDMA without FH. In WiMAX, in order to provide frequency diversity, for non-adaptive uplink transmission, OFDMA with a distributed subcarrier allocation is used accepting the low power efficiency and the high costs of the power amplifier due to the high envelope fluctuations of the transmit signal.

A promising multiple access scheme that has been intensively discussed in WINNER as well as in 3GPP LTE is Interleaved Frequency Division Multiple Access (IFDMA) [SDBS98]. IFDMA is based on an OFDMA scheme where the subcarriers assigned to a user are equidistantly distributed over the total available bandwidth in order to provide frequency diversity. In addition, a DFT is applied to the data symbols before OFDMA modulation [GRC+02, SDBS98]. The combination of the regular subcarrier allocation and the DFT pre-coding results in single carrier like low envelope fluctuations of the transmit signal [FKH08]. However, IFDMA is known to be sensitive to carrier frequency offsets, e.g., caused by the Doppler effect or oscillator imperfections [DLF04]. The sensitivity of IFDMA to frequency offsets has been investigated by the author of this thesis in [FKCS04] and [FKC07b]. Additionally, for IFDMA, a higher pilot symbol overhead for channel estimation is expected compared to localized SC-FDMA since for IFDMA an interpolation between the different interleaved subcarriers is, in general, not possible. The suitability of IFDMA for future mobile radio systems and its relation to other multiple access schemes has been investigated by the author of this thesis in [FKCS05a] and [FKC07b].

In WINNER and WINNER II, alternative multiple access solutions for non-adaptive uplink transmission have been under investigation. The author of this thesis was involved in the evaluation process of the different candidate multiple access schemes and, finally, in the development of a new multiple access solution [WIN06] aiming at a best possible compliance to the key requirements of the radio interface as formulated in Section 1.1.2. This new multiple access scheme is denoted as Block-Interleaved Frequency Division Multiple Access (B-IFDMA) and is in the focus of this thesis. B-IFDMA is based on an OFDMA scheme where blocks of adjacent subcarriers that are equidistantly distributed over the total available bandwidth are assigned to the users. In addition, a DFT is applied to the data symbols before OFDMA modulation. An initial work on B-IFDMA has been published in [SFF+07] by the author of this thesis together with other members of the respective task in the WINNER II project.

Note that, throughout this thesis, several new algorithms complementing B-IFDMA are introduced. The state-of-the-art of the respective algorithms is described in the corresponding sections.

1.2   Open Issues and Goals of the Thesis

In the following, the open issues related to B-IFDMA and its application to non-adaptive uplink transmission and the goals of this thesis are formulated. Since B-IFDMA is a new multiple access scheme, a new theoretical framework is required that

gives a precise definition of B-IFDMA and, at the same time, enables to place it in the context of other well known multiple access schemes. Further on, several algorithms are required in order to extend B-IFDMA towards the application of the scheme in a future mobile radio system. Finally, a detailed analysis of its properties is required in order to evaluate the scheme with respect to an application as multiple access solution in future mobile radio systems. Further on, a comparison of the properties of B-IFDMA to the properties of other candidate multiple access schemes that are currently under consideration for the non-adaptive uplink as described in Section 1.1.3 has to be performed.

In particular, the goals of this thesis are to answer the following questions:

1. How can a general system model be formulated that enables a joint description of B-IFDMA and other important multiple access solutions that are related to B-IFDMA and how is B-IFDMA related to them?

2. How does an appropriate receiver structure for B-IFDMA look like that provides a good performance and a reasonable computational complexity?

3. Is it possible to find a low complexity implementation for B-IFDMA signal generation in time domain and how does it look like?

4. How does an appropriate combination of B-IFDMA with multiple antenna techniques at the transmitter look like for non-adaptive uplink transmission and how can it it be implemented efficiently?

5. How does an appropriate combination of B-IFDMA with Space Division Multiple Access (SDMA) look like and how can it it be implemented efficiently?

6. How can a high flexibility and granularity in terms of different data rates be provided in a mobile radio cell using B-IFDMA?

7. How is the performance of B-IFDMA in the non-adaptive uplink of a future mobile radio system with respect to

   - frequency diversity, time diversity, spatial diversity and multi-user diversity,
   - pilot symbol overhead for channel estimation,
   - carrier frequency offsets, and
   - power efficiency of non-linear power amplifiers?

   and how does the performance depend on the parameters of the B-IFDMA signal?

8. How is the computational complexity of B-IFDMA for the application in the non-adaptive uplink of a future mobile radio system and how does the computational complexity depend on the parameters of the B-IFDMA signal?

9. How is the performance and the complexity of B-IFDMA compared to other important candidate multiple access schemes?

10. Which conclusions for the suitability and the parametrization of B-IFDMA in the non-adaptive uplink of a future mobile radio system can be drawn from the analysis of the performance and the computational complexity of B-IFDMA dependent on its parameters?

1.3 Contributions and Thesis Overview

In this section, an overview of the major contributions and the structure of the thesis is given. In the sequel, the contents of the following chapters is described, along with the contributions in each of them.

In Chapter 2, a new general system model is formulated that enables a joint description of B-IFDMA and other important multiple access solutions that are related to B-IFDMA. From the new general system model, a system model for B-IFDMA is derived and an appropriate receiver structure for B-IFDMA is proposed. Important basic properties of B-IFDMA are deduced and compared to those of other multiple access schemes that can be described by the new general system model. Finally, the relations between B-IFDMA and these multiple access schemes are analyzed and illustrated.

In Chapter 3, new algorithms are presented that extend the B-IFDMA scheme towards the application of the scheme in a future mobile radio system. For each algorithm, a detailed overview of the state-of-the-art is given. In particular, a new low complexity implementation for B-IFDMA in time domain is presented, a new approach for the application of space time coding to B-IFDMA with low complexity is presented, a new method for the application of SDMA to B-IFDMA providing low complexity is described, and a new approach for an efficient accommodation of different data rates in mobile radio systems using B-IFDMA is introduced.

In Chapter 4, the properties of B-IFDMA and their dependency on the parameters of the scheme are intensively analyzed and discussed and various new simulation results for coded transmission over a mobile radio channel considering correlated transmit

and receive antennas are presented. In particular, performance results for frequency diversity, time diversity, spatial diversity, and multi-user diversity are presented, the overhead for channel estimation is investigated, the computational effort required for B-IFDMA is given, and the robustness to frequency offsets is analyzed. Further on, the envelope fluctuations of the B-IFDMA transmit signal and the power efficiency of the power amplifiers is investigated for B-IFDMA. The analysis of the properties of B-IFDMA includes a comparison to the properties of other candidate multiple access schemes that are currently under consideration for the non-adaptive uplink as described in Section 1.1.3. At the end of the chapter, the results of the analysis of the properties of B-IFDMA and their consequences for the parametrization of B-IFDMA in a non-adaptive uplink scenario in a future mobile radio system are discussed.

Finally, a summary of the main conclusions of the thesis is presented in Chapter 5.

Chapter 2

System Model

2.1   Introduction

In this chapter, a communication system using block-transmission-based multiple access schemes with CP is described for uplink transmission. For this system, a new general discrete-time system model is introduced in the base-band. From the new general system model, a system model for B-IFDMA, which is in the focus of this thesis, is derived. It is shown that the new general system model enables a unified description of B-IFDMA and various other block-transmission-based multiple access schemes that are well-known from the literature. Important basic properties of B-IFDMA are deduced and compared to those of other multiple access schemes that can be described by the new general system model and that are currently discussed in the literature in the context of future mobile radio transmission. Finally, the relations between B-IFDMA and these multiple access schemes are analyzed and illustrated.

Throughout this thesis, all signals are represented by their discrete time equivalents in the complex base-band. Upper case bold letters denote matrices and lower case bold letters denote column vectors unless otherwise stated. Further on, $(\cdot)^\dagger$ denotes the pseudo-inverse, $(\cdot)^{-1}$ the inverse and $(\cdot)^{\mathrm{H}}$ the Hermitian of a matrix and $(\cdot)^{\mathrm{T}}$ the transpose, of a vector or a matrix, respectively. Finally, j denotes the square root of -1.

The remainder of the chapter is organized as follows: In Section 2.2, the communication system based on block transmission with CP is described. In Section 2.3, the general discrete-time base-band system model is introduced. Section 2.4 gives the system model for B-IFDMA and a discussion of the basic properties of B-IFDMA. In Section 2.5, B-IFDMA is compared to other multiple access schemes and the relations between the schemes are described. Section 2.6 concludes the chapter.

2.2   Description of the Communication System

In this section, a communication system using block-transmission-based multiple access schemes with CP is described for uplink transmission. An overview of the system is

given in Figure 2.1. In the remainder of this thesis, a communication system according to Figure 2.1 is considered.

After channel coding and interleaving, the data bits of each user are mapped to data symbols according to a bit mapping scheme such as Phase Shift Keying (PSK) or Quadrature Amplitude Modulation (QAM). Subsequently, the data symbols are organized in blocks that are, after serial to parallel conversion (S/P), modulated simultaneously according to the multiple access scheme that is used for transmission. The blocks of modulated data symbols are, then, parallel to serial (P/S) converted and a CP is inserted in between consecutive blocks of modulated data symbols in order to avoid interference between the blocks at the receiver. It is well-known that, for that purpose, the length of the CP has to be chosen larger than the maximum delay of the mobile radio channels of all users plus the maximum time offset between the received signals of the users [vNP00]. After insertion of the CP, a windowing of each block of modulated data symbols with CP is applied in order to form the spectrum of the transmit signal [vNP00]. The resulting signal is, then, digital to analog (D/A) converted and an appropriate radio frequency signal processing including modulation of the signal on a carrier and analogue filtering is applied. Subsequently, the resulting transmit signal is transmitted over a user specific mobile radio channel. Assuming uplink transmission, at the receiver, the signals that have been transmitted over different user specific channels are superimposed and noise is added.

The receiver performs the inverse operations of the transmitter in reversed order: After radio signal processing including analogue filtering and a shift of the signal in frequency domain from the carrier frequency down to the base-band, analogue to digital (A/D) conversion is applied and the window and the cyclic prefix are removed. Subsequently, after S/P conversion, the different users' signals are separated and estimates of the data symbols of each user are calculated block by block. The P/S converted estimates of the data symbols are then fed into a soft decision device, the soft bits at the output of the soft decision device are deinterleaved and estimates of the transmitted data bits are obtained by means of decoding.

The new ideas and algorithms presented throughout this thesis are exclusively related to the part of the communication system on the right of the vertical dashed line in Figure 2.1. Channel coding and interleaving at the transmitter side and the respective operations at the receiver side are not part of the models that are introduced in the following. Note that, for the performance analysis presented throughout this thesis, channel coding and interleaving are, however, considered.
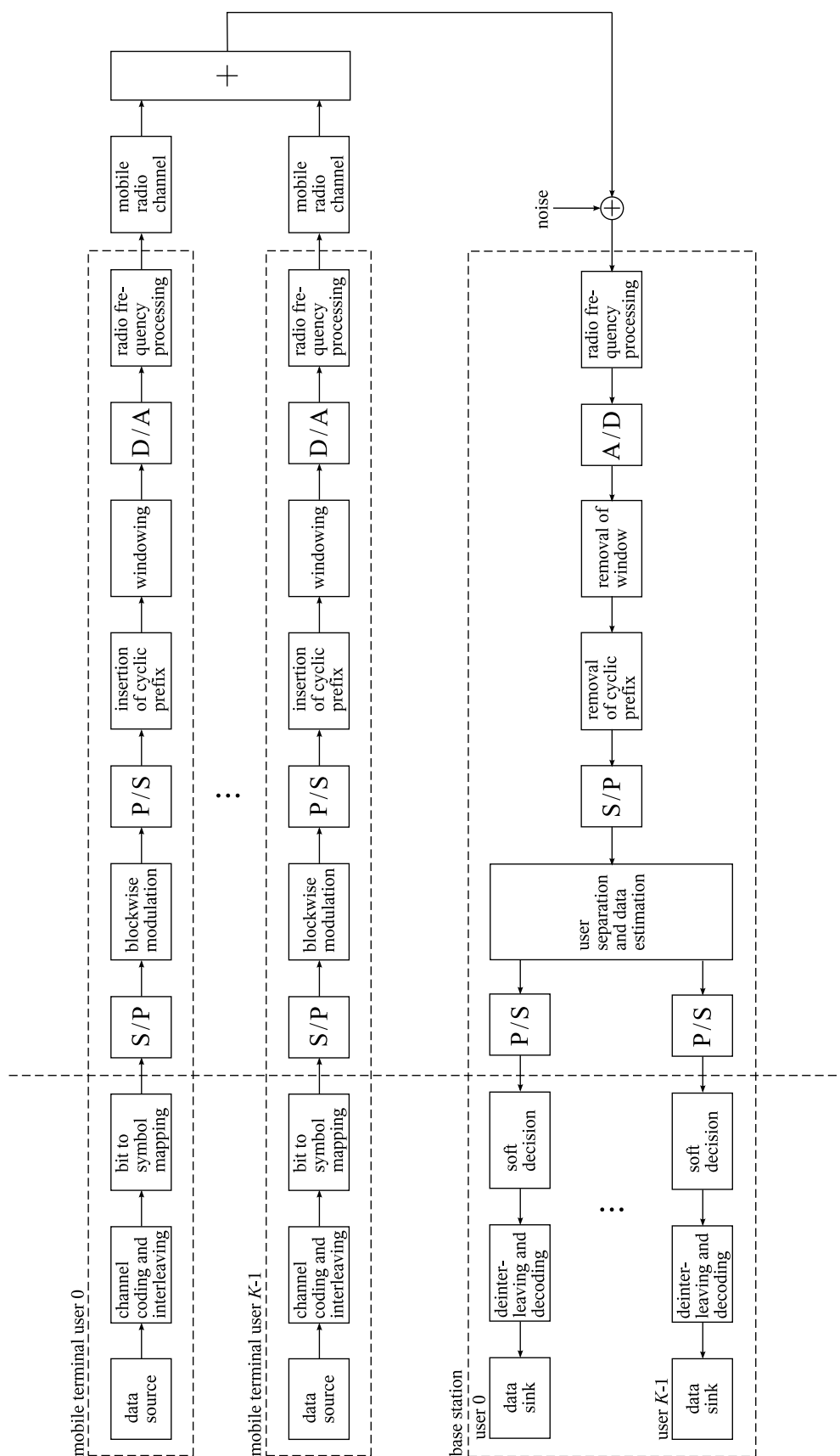
Figure 2.1: Model of a communication system with K users utilizing a block-transmission-based multiple access scheme with CP.

2.3 General Discrete-Time Base-Band System Model

2.3.1 Introduction

In this section, a general discrete-time base-band system model is defined for the uplink. The model describes the part of the system model given in Figure 2.1 between bit to symbol mapping and soft decision, i.e., the part of the model on the right of the vertical dashed line. In this part of the model, the transmission is performed blockwise. The blocks of modulated data symbols are assumed to be separated by a CP of appropriate length, cf. Section 2.2, and, thus, can be considered as mutually independent. In order to make a simple description of the blockwise transmission possible, in the following, a vector-matrix notation is introduced.

The remainder of Section 2.3 is organized as follows. In Section 2.3.2, an overview of the the general discrete-time base-band system model is given and the respective vectors for the signals are introduced. In Sections 2.3.3, 2.3.4 and 2.3.5, the transmitter, the channel and the receiver, respectively, of the discrete-time base-band system model are defined in detail.

2.3.2 Overview of the General Discrete-Time Base-Band System Model

In this section, an overview of the general discrete-time base-band system model is given. The model is illustrated in Figure 2.2.

As consecutive blocks of data symbols are modulated independently from each other, in the following, without loss of generality, only the transmission of one block of data symbols is described. In a system with K users indicated by $k = 0, \ldots, K-1$, let

$$\mathbf{d}^{(k)} = \left[d_0^{(k)}, \ldots, d_{Q-1}^{(k)} \right]^{\mathrm{T}} \tag{2.1}$$

denote a vector consisting of Q data symbols $d_q^{(k)}$, $q = 0, \ldots, Q-1$. The data symbols $d_q^{(k)}$ are taken from an arbitrary bit mapping scheme like PSK or QAM at symbol rate $1/T_{\mathrm{s}}$ and are assumed to be mutually independent and equiprobable. For the sake of simplicity, it is assumed that the number Q of data symbols per block is the same for all users.
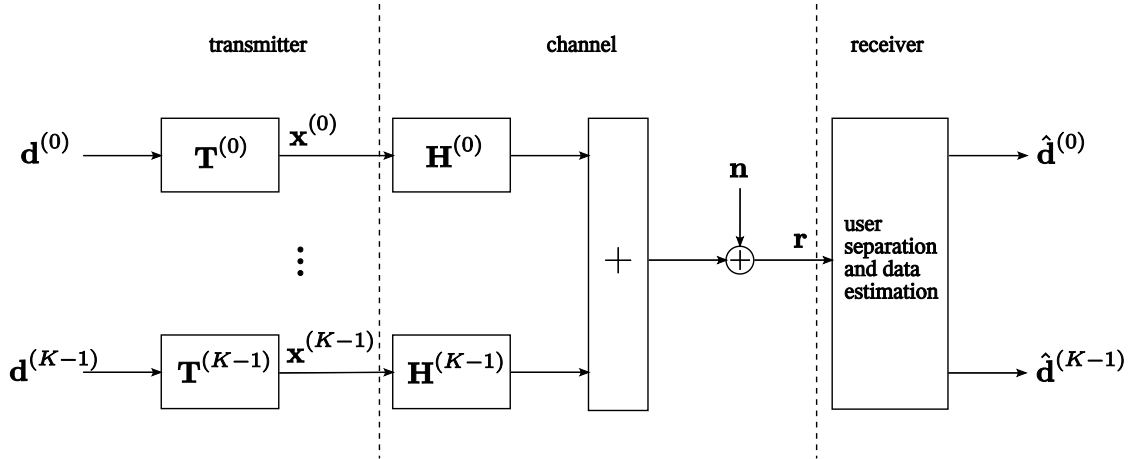
Figure 2.2:   General discrete-time base-band system model for K users utilizing a block-transmission-based multiple access scheme with CP.

The blockwise modulation according to the multiple access scheme that is used for transmission is defined by an $N \times Q$ matrix $\mathbf{T}^{(k)}$, where

$$N = K \cdot Q. \tag{2.2}$$

The vector consisting of modulated data symbols of user k can be described by

$$\mathbf{x}^{(k)} = \left[x_0^{(k)}, \dots, x_{N-1}^{(k)} \right]^{\mathrm{T}} \tag{2.3}$$

with elements $x_n^{(k)}$, $n = 0, \dots, N-1$, at sampling rate K/T_{s}. The modulated data vector is obtained from the data symbol vector $\mathbf{d}^{(k)}$ by

$$\mathbf{x}^{(k)} = \mathbf{T}^{(k)} \cdot \mathbf{d}^{(k)}. \tag{2.4}$$

After modulation, the modulated data vector $\mathbf{x}^{(k)}$ of user k is transmitted over a discrete-time overall channel that models the insertion and the removal of the CP, the radio frequency processing at transmitter and receiver and the transmission over the user specific mobile radio channel. The discrete-time overall channel for the transmission of $\mathbf{x}^{(k)}$ is described by the user specific $N \times N$ matrix $\mathbf{H}^{(k)}$.

After transmission over the channel $\mathbf{H}^{(k)}$, the signals of the different users are superimposed and noise is added. Let

$$\mathbf{n} = [n_0, \dots, n_{N-1}]^{\mathrm{T}} \tag{2.5}$$

denote a vector with N Additive White Gaussian Noise (AWGN) samples n_n, $n = 0, \ldots, N - 1$, at sampling rate K/T_s. The AWGN samples n_n are realizations of a zero mean circularly symmetric white Gaussian random process. It is further assumed that the AWGN samples n_n and data symbols $d_q^{(k)}$ are statistically independent.

The received block of modulated data symbols can be described by vector

$$\mathbf{r} = [r_0, \ldots, r_{N-1}]^\mathrm{T} \tag{2.6}$$

with

$$\mathbf{r} = \sum_{k=0}^{K-1} \mathbf{H}^{(k)} \cdot \mathbf{x}^{(k)} + \mathbf{n}. \tag{2.7}$$

From $\mathbf{r}$, estimates $\hat{\mathbf{d}}^{(k)}$ for the data symbol vectors $\mathbf{d}^{(k)}$ are calculated by means of user separation and data estimation.

In the following, the matrix $\mathbf{T}^{(k)}$ at the transmitter, the overall channel matrix $\mathbf{H}^{(k)}$ as well as the user separation and data estimation at the receiver are defined in detail.

2.3.3 Transmitter of the General Discrete-Time Base-Band System Model

In this section, the blockwise modulation described by matrix $\mathbf{T}^{(k)}$ is defined in detail. By this definition, a new transmitter model is introduced that enables a unified description of various well-known multiple access schemes based on block transmission with CP.

In general, the transmitter model considers user separation by Code Division Multiple Access (CDMA), Frequency Division Multiple Access (FDMA), and Time Division Multiple Access (TDMA). Due to the blockwise modulation, TDMA can be easily applied by the assignment of consecutive modulated data vectors to different users. Since for the general discrete-time base-band system model the different blocks are assumed to be mutually independent, in the model only the transmission of one block is described and, thus, the effect of TDMA is not visible. However, in the following, all schemes described by the general discrete-time base-band system model are considered to provide user separation by TDMA. Note that each of the multiple access schemes described by the transmitter model introduced in this section can be also combined with SDMA without modification of the transmit signal. Thus, in this context, user separation by SDMA is not regarded.

In the following, it is assumed that, within a modulated data vector, the signals of K users are separated by

- K_{c} orthogonal codes indexed by $k_{\mathrm{c}} = 0, \ldots, K_{\mathrm{c}} - 1$, and

- K_{f} orthogonal frequency resources indexed by $k_{\mathrm{f}} = 0, \ldots, K_{\mathrm{f}} - 1$.

The number K of users is, thus, given by

$$K = K_{\mathrm{c}} \cdot K_{\mathrm{f}} \tag{2.8}$$

and the user index k is related to the indices k_{c} and k_{f} by

$$k = k_{\mathrm{f}} + k_{\mathrm{c}} \cdot K_{\mathrm{f}}. \tag{2.9}$$

Let $\mathbf{S}^{(k_{\mathrm{c}})}$, $\mathbf{P}$, $\mathbf{M}^{(k_{\mathrm{f}})}$, and $\mathbf{F}_{\mathrm{N}}^{\mathrm{H}}$ denote a spreading matrix, a pre-coding matrix, a sub-carrier mapping matrix, and an Inverse Discrete Fourier Transform (IDFT) matrix, respectively.

The matrices $\mathbf{S}^{(k_{\mathrm{c}})}$, $\mathbf{P}$ and $\mathbf{M}^{(k_{\mathrm{f}})}$, and $\mathbf{F}_{\mathrm{N}}^{\mathrm{H}}$ can be interpreted as follows. In case of CDMA, the separation of different users' signals is performed by the $Q K_{\mathrm{c}} \times Q$ spreading matrix $\mathbf{S}^{(k_{\mathrm{c}})}$. Matrix $\mathbf{S}^{(k_{\mathrm{c}})}$ spreads each of the Q data symbols $d_q^{(k)}$ from the data symbol vector $\mathbf{d}^{(k)}$ of (2.1) with a spreading sequence with index k_{c} and with spreading factor K_{c}. Spreading sequences with different indices k_{c} are assumed to be mutually orthogonal.

The $Q K_{\mathrm{c}} \times Q K_{\mathrm{c}}$ pre-coding matrix $\mathbf{P}$ describes a non-redundant pre-coding of the data symbol vector $\mathbf{d}^{(k)}$ after spreading. If matrix $\mathbf{P}$ is chosen as identity matrix, the resulting scheme is a multi carrier scheme. Otherwise, matrix $\mathbf{P}$ distributes the information contained in each data symbol $d_q^{(k)}$ to the subcarriers assigned to a certain user. If $\mathbf{P}$ is chosen as Discrete Fourier Transform (DFT) matrix, the resulting scheme is a single carrier scheme. Note that also other non-redundant pre-coding operations can be used, e.g., by the choice of the pre-coding matrix as a Walsh-Hadamard matrix. In this case, the classification whether the scheme is a single carrier or a multi carrier scheme is not obvious.

In case of FDMA, user separation is performed by the $N \times Q K_{\mathrm{c}}$ matrix $\mathbf{M}^{(k_{\mathrm{f}})}$ with N of (2.2). The elements of matrix $\mathbf{M}^{(k_{\mathrm{f}})}$ are either 0 or 1. Each row and each column of matrix $\mathbf{M}^{(k_{\mathrm{f}})}$ can carry only one number 1. The sum of all elements of the matrix

has to be equal to QK_c. Thus, matrix $\mathbf{M}^{(k_f)}$ describes the mapping of the elements of the data symbol vector $\mathbf{d}^{(k)}$ after spreading and pre-coding to a set of QK_c subcarriers within the N subcarriers available in the system. Matrices $\mathbf{M}^{(k_f)}$ with different indices k_f are assumed to carry the numbers 1 in different rows. Thus, the subcarrier sets that are used for user separation performed by $\mathbf{M}^{(k_f)}$ are mutually orthogonal.

The $N \times N$ IDFT matrix $\mathbf{F}_N^H$ transforms its input signal from the DFT domain to the time domain and can be interpreted as an OFDM (Orthogonal Frequency Division Multiplex) modulation [vNP00]. The elements $\left[\mathbf{F}_N^H\right]_{m,n}$, $m, n = 0, \ldots, N-1$, of the IDFT matrix $\mathbf{F}_N^H$ are given by

$$\left[\mathbf{F}_N^H\right]_{m,n} = 1/\sqrt{N} \cdot e^{j\frac{2\pi}{N}mn}. \tag{2.10}$$

Combining the matrices $\mathbf{S}^{(k_c)}$, $\mathbf{P}$ and $\mathbf{M}^{(k_f)}$, and $\mathbf{F}_N^H$, the transmitter of the general discrete-time base-band system model performing blockwise modulation is defined as

$$\mathbf{T}^{(k)} = \mathbf{F}_N^H \cdot \mathbf{M}^{(k_f)} \cdot \mathbf{P} \cdot \mathbf{S}^{(k_c)}. \tag{2.11}$$

With this transmitter, that is illustrated in Figure 2.3, different multiple access schemes can be modelled by a different choice of the matrices $\mathbf{S}^{(k_c)}$, $\mathbf{P}$ and $\mathbf{M}^{(k_f)}$ in (2.11).
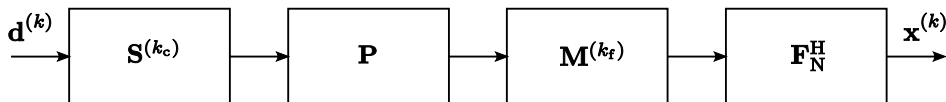
Figure 2.3: Transmitter of the general discrete-time base-band system model in Figure 2.1 of user k.

2.3.4 Channel of the General Discrete-Time Base-Band System Model

In this section, the overall channel described by matrix $\mathbf{H}^{(k)}$ is described in detail. It is assumed that the overall channel model in the base-band including the mobile radio channel between the mobile terminal of user k and the base station as well as filtering at transmitter and receiver can be approximated by a Finite Impulse Response (FIR) filter with L_c coefficients. This assumption is common for mobile radio applications, cf. [Pae99]. The filter coefficients of the FIR filter are assumed to be constant for the duration T of the transmission of a modulated data vector $\mathbf{x}^{(k)}$ plus the duration T_{CP} of the CP. Let

$$\mathbf{h}^{(k)} = \left[h_0^{(k)}, \ldots, h_{L_c-1}^{(k)}\right]^T \tag{2.12}$$

denote the vector of the L_c FIR filter coefficients at sampling rate K/T_s. In the following, vector $\mathbf{h}^{(k)}$ is denoted as channel vector. It can be assumed that the windowing has no impact of the part of the received signal that is used for data estimation [vNP00]. Thus, in the following, the impact of the insertion and removal of the window can be omitted. The impact of the CP can be described as follows: The insertion of the CP at the transmitter and the removal of the CP at the receiver transforms the linear convolution of the modulated data vector with CP with the channel vector $\mathbf{h}^{(k)}$ to a circular convolution of the modulated data vector $\mathbf{x}^{(k)}$ without CP with the channel vector $\mathbf{h}^{(k)}$ [WG00].

Thus, the transmission of the modulated data vector $\mathbf{x}^{(k)}$ over the channel described by the channel vector $\mathbf{h}^{(k)}$ can be described by

$$\mathbf{r} = \sum_{k=0}^{K-1} \mathbf{x}^{(k)} \circledast \mathbf{h}^{(k)} + \mathbf{n}, \qquad (2.13)$$

where $'\circledast'$ denotes circular convolution and $\mathbf{n}$ denotes the AWGN vector according to (2.5). For $L_\mathrm{c} \leq N$, let

$$\bar{\mathbf{h}}^{(k)} = \left[\bar{h}_0^{(k)}, \dots, \bar{h}_{N-1}^{(k)} \right]^{\mathrm{T}} \qquad (2.14)$$

denote the channel vector $\mathbf{h}^{(k)}$ complemented with zeros to the length N with N of (2.2), with

$$\bar{h}_n^{(k)} = \begin{cases} h_n^{(k)} & 0 \leq n \leq L_\mathrm{c} - 1 \\ 0 & \text{else} \end{cases} . \qquad (2.15)$$

Note that, usually, the CP is considerably shorter than the modulated data vector $\mathbf{x}^{(k)}$. Thus, the assumption $L_\mathrm{c} \leq N$ is justified. Let, further on, $\mathbf{H}^{(k)}$ denote a circulant matrix with $\bar{\mathbf{h}}^{(k)}$ in its first column. Thus, (2.13) can be expressed as

$$\mathbf{r} = \sum_{k=0}^{K-1} \mathbf{H}^{(k)} \cdot \mathbf{x}^{(k)} + \mathbf{n}, \qquad (2.16)$$

cf. Figure 2.2.

2.3.5 Receiver of the General Discrete-Time Base-Band System Model

In this section, the user separation and the data estimation in the receiver of the general discrete-time base-band system model is discussed and a simple receiver structure for schemes that do not suffer from Multiple Access Interference (MAI) contained in

the received signal is presented. For the sake of simplicity, optimum frequency synchronization and time synchronization between the transmitting mobile stations and the receiving base station is assumed.

In general, the receiver structure and the receiver complexity depend on the MAI and Inter Symbol Interference (ISI) properties of the received signal. If the received signal is MAI-free, the computational effort for user separation is low and user separation and compensation of the impact of the channel can be performed separately. If, in addition, the received signal is also ISI-free, the receiver structure becomes very simple. In this case, for optimum Maximum Likelihood (ML) data detection, after user separation, simply an amplitude and a phase correction has to be applied to each data symbol. A well-known example for multiple access schemes, where the received signal is MAI- and ISI-free, is OFDMA [vNP00].

If the received signal is MAI-free but contains ISI, in general, an equalizer has to be applied. According to [Pro95], Maximum Likelihood Sequence Estimation (MLSE) provides optimum ML equalization for this case. However, the complexity of this equalizer increases exponentially with the number of data symbols that are mutually interfering and, thus, especially for high symbol rates, can be considered as too complex. However, for the special case of block transmission with CP, a Frequency Domain Equalizer (FDE) can be applied [SKJ94]. Although this is a linear equalizer and, thus, not optimum in the sense of the ML criterion, it combines good performance and low computational effort when designed according to the Minimum Mean Square Error (MMSE) criterion [FABSE02]. However, the performance can be further improved by application of appropriate means to combat the residual ISI after application of the FDE, e.g. as proposed by the author of this thesis in [FKCS05c]. The application of an FDE provides a computational effort for the receiver that is similar to the computational effort for an OFDMA receiver, cf. [FABSE02]. A further improved performance such as proposed in [FKCS05c] is obtained at the expense of increased computational effort.

If the received signal contains MAI, in general, at the receiver, multi-user detection (MUD) has to be applied that requires a high computational effort. Thus, especially for high symbol rates and high numbers of users, block-transmission-based multiple access schemes with CP where MAI occurs can be considered as costly and, hence, not adequate for the uplink of future mobile radio systems [FK03].

In the following, at first, a new method for diagnosing whether the received signal contains MAI or ISI, respectively, is presented based on the generalized discrete-time base-band system. Subsequently, a general receiver model for FDMA schemes, where

the received signal is MAI-free, is presented that is based on user separation and equalization in frequency domain.

The occurrence of MAI at the received signal can be diagnosed as follows: Let

$$\mathbf{r}^{(k)} = \left[r_0^{(k)}, \ldots, r_{N-1}^{(k)} \right]^{\mathrm{T}} \tag{2.17}$$

denote the contribution of the signal of user k to the received signal vector $\mathbf{r}$ of (2.7) with

$$\mathbf{r} = \sum_{k=0}^{K-1} \mathbf{r}^{(k)}. \tag{2.18}$$

If the vectors $\mathbf{r}^{(k)}$ of different users are mutually orthogonal, i.e., if

$$\left(\mathbf{r}^{(k)} \right)^{\mathrm{H}} \cdot \mathbf{r}^{(\kappa)} = 0 \quad \forall \quad k, \kappa = 0, \ldots, K-1; \quad k \neq \kappa, \tag{2.19}$$

the received signal vector $\mathbf{r}$ is MAI-free. Equation (2.19) can be reformulated as follows: With $\mathbf{T}^{(k)}$ of (2.11) and $\mathbf{H}^{(k)}$ of (2.16), let

$$\mathbf{G}^{(k)} = \mathbf{H}^{(k)} \cdot \mathbf{T}^{(k)} \tag{2.20}$$

denote an $N \times Q$ matrix with column vectors

$$\mathbf{g}_q^{(k)} = \left[g_0^{(k)}, \ldots, g_{N-1}^{(k)} \right]^{\mathrm{T}}, \quad q = 0, \ldots, Q-1. \tag{2.21}$$

Regarding the MAI, the AWGN vector $\mathbf{n}$ does not have to be considered because MAI and AWGN are mutually independent. For the noise-free case, vector $\mathbf{r}^{(k)}$ is given by

$$\mathbf{r}^{(k)} = \mathbf{G}^{(k)} \cdot \mathbf{d}^{(k)} \tag{2.22}$$

with $\mathbf{d}^{(k)}$ of (2.1). Thus, (2.19) is equivalent to

$$\left(\mathbf{d}^{(k)} \right)^{\mathrm{H}} \left(\mathbf{G}^{(k)} \right)^{\mathrm{H}} \cdot \mathbf{G}^{(\kappa)} \mathbf{d}^{(\kappa)} = 0. \tag{2.23}$$

For arbitrary data symbol vectors $\mathbf{d}^{(k)}$ and $\mathbf{d}^{(\kappa)}$, (2.23) is fulfilled if

$$\left(\mathbf{G}^{(k)} \right)^{\mathrm{H}} \cdot \mathbf{G}^{(\kappa)} = \mathbf{0}_{Q \times Q}, \tag{2.24}$$

where $\mathbf{0}_{Q \times Q}$ denotes a $Q \times Q$ matrix with all elements equal to zero. Equation (2.24) is fulfilled if all column vectors $\mathbf{g}_q^{(k)}$ of the matrices $\mathbf{G}^{(k)}$ of different users are mutually orthogonal, i.e., if

$$\left(\mathbf{g}_p^{(k)} \right)^{\mathrm{H}} \cdot \mathbf{g}_q^{(\kappa)} = 0 \quad \forall \quad p, q = 0, \ldots, Q-1; \quad k, \kappa = 0, \ldots, K-1; \quad k \neq \kappa. \tag{2.25}$$

Thus, if (2.25) is fulfilled, the received signal vector $\mathbf{r}$ is MAI-free.

The occurrence of ISI can be diagnosed as follows: Equation (2.22) can be rewritten as a linear combination of the column vectors $\mathbf{g}_q^{(k)}$ of matrix $\mathbf{G}^{(k)}$ according to

$$\mathbf{r}^{(k)} = \sum_{q=0}^{Q-1} \mathbf{g}_q^{(k)} \cdot d_q^{(k)} \qquad (2.26)$$

with $d_q^{(k)}$ denoting the data symbols of vector $\mathbf{d}^{(k)}$, cf. (2.1). If the vectors $\mathbf{g}_q^{(k)}$ in the linear combination in (2.26) are mutually orthogonal, i.e. if

$$\left(\mathbf{g}_p^{(k)} \right)^{\mathrm{H}} \cdot \mathbf{g}_q^{(k)} = 0 \quad \forall \quad p, q = 0, \dots, Q-1; \quad p \neq q; \quad k = 0, \dots, K-1, \qquad (2.27)$$

there is no interference between the data symbols $d_q^{(k)}$ and, thus, vector $\mathbf{r}^{(k)}$ is ISI-free.

In the following, a general receiver structure for FDMA schemes where (2.25) holds is described. For the receiver structure, it is assumed that user separation and equalization are performed in frequency domain. The receiver structure is depicted in Figure 2.4. In a first step, the received signal vector $\mathbf{r}$ is transformed to the DFT domain by the application of an N-point DFT described by the $N \times N$ matrix $\mathbf{F}_{\mathrm{N}}$ defined analogous to (2.10). For FDMA schemes, user separation is given by the application of matrix $\left(\mathbf{M}^{(k)} \right)^{\dagger}$ to the received signal in the DFT domain.

After user separation, an FDE is applied to the received signal of each user. Let

$$\mathbf{\Gamma}^{(k)} = \left(\mathbf{M}^{(k)} \right)^{\dagger} \cdot \mathbf{F}_{\mathrm{N}} \cdot \mathbf{H}^{(k)} \cdot \mathbf{F}_{\mathrm{N}}^{\mathrm{H}} \cdot \mathbf{M}^{(k_{\mathrm{f}})}. \qquad (2.28)$$

Matrix $\mathbf{\Gamma}^{(k)}$ can be interpreted as follows: Since matrix $\mathbf{H}^{(k)}$ is circulant, $\mathbf{F}_{\mathrm{N}} \cdot \mathbf{H}^{(k)} \cdot \mathbf{F}_{\mathrm{N}}^{\mathrm{H}}$ is a diagonal matrix that describes the channel $\mathbf{H}^{(k)}$ in the DFT domain. Multiplication from the left by $\left(\mathbf{M}^{(k)} \right)^{\dagger}$ and multiplication from the right by $\mathbf{M}^{(k)}$ selects the Q diagonal elements of matrix $\mathbf{F}_{\mathrm{N}} \cdot \mathbf{H}^{(k)} \cdot \mathbf{F}_{\mathrm{N}}^{\mathrm{H}}$ that are relevant for the transmission of the
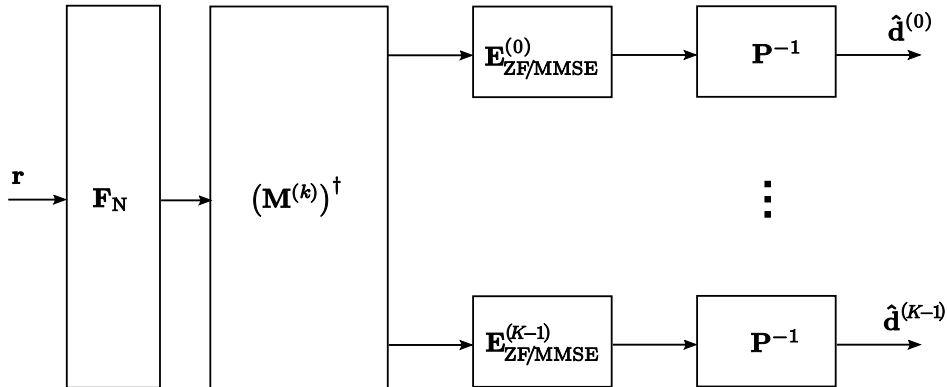
Figure 2.4: Receiver structure for FDMA schemes where (2.25) holds.

signal of user k. Thus, $\mathbf{\Gamma}^{(k)}$ is a $Q \times Q$ diagonal matrix that gives the channel of user k in the DFT domain. Let diag$(\cdot)$ denote a diagonal matrix with the elements of the argument vector on its main diagonal. Thus, the diagonal matrix $\mathbf{\Gamma}^{(k)}$ can be described by

$$\mathbf{\Gamma}^{(k)} = \mathrm{diag}\left(\left[\Gamma_0^{(k)}, \ldots, \Gamma_{Q-1}^{(k)}\right]^{\mathrm{T}}\right), \tag{2.29}$$

where

$$\begin{bmatrix} \Gamma_0^{(k)} \\ \vdots \\ \Gamma_{Q-1}^{(k)} \end{bmatrix} = \left(\mathbf{M}^{(k)}\right)^{\dagger} \cdot \mathbf{F}_N \cdot \bar{\mathbf{h}}^{(k)} \tag{2.30}$$

with $\bar{\mathbf{h}}^{(k)}$ of (2.14).

A linear FDE for user k based on the ZF criterion [SKJ94] is given by

$$\mathbf{E}_{\mathrm{ZF}}^{(k)} = \left(\mathbf{\Gamma}^{(k)}\right)^{-1}. \tag{2.31}$$

The FDE based on the Zero Forcing (ZF) criterion is formally equivalent to the amplitude and phase correction per data symbol required for schemes where the conditions from (2.25) and (2.27) hold, cf. [FABSE02].

A linear FDE for user k based on the MMSE criterion [SKJ94] is given by

$$\mathbf{E}_{\mathrm{MMSE}}^{(k)} = \left(\left(\mathbf{\Gamma}^{(k)}\right)^{\mathrm{H}}\mathbf{\Gamma}^{(k)} + \frac{\sigma_{\mathrm{n}}^2}{\sigma_{\mathrm{d}}^2}\mathbf{I}\right)^{-1}, \tag{2.32}$$

where σ_{n}^2 and σ_{d}^2 are the variance of the noise according to (2.5) and the variance of the data symbols according to (2.1), respectively.

For block transmission schemes where (2.25) holds and (2.27) is violated, the FDE based on the MMSE criterion outperforms the ZF FDE in terms of bit error rates since the MMSE FDE provides a trade-off between noise amplification and ISI reduction, cf. [FABSE02].

After application of the FDE, the pre-coding is reversed by the application of matrix $\mathbf{P}^{-1}$. An estimate $\hat{\mathbf{d}}^{(k)}$ for the data symbol vector $\mathbf{d}^{(k)}$ of user k is, thus, given by

$$\hat{\mathbf{d}}^{(k)} = \mathbf{P}^{-1} \cdot \mathbf{E}_{\mathrm{ZF/MMSE}}^{(k)} \cdot \left(\mathbf{M}^{(k)}\right)^{\dagger} \cdot \mathbf{F}_N \cdot \mathbf{r}. \tag{2.33}$$

Note that for TDMA schemes, the user separation is already given by the blockwise transmission. Thus, a simple form of the receiver model from Figure 2.4 can be also used for the description of TDMA schemes. In this case, $Q = N$ and instead of matrix $\left(\mathbf{M}^{(k)}\right)^{\dagger}$ the identity matrix $\mathbf{I}_N$ is applied.

2.4   System Model for B-IFDMA

In this section, a discrete-time base-band system model for B-IFDMA, that is the scheme in the focus of this thesis, is derived from the general discrete-time base-band system model of Section 2.3. For that purpose, the matrices $\mathbf{S}^{(k_c)}$, $\mathbf{P}$ and $\mathbf{M}^{(k_f)}$ used for modeling the blockwise modulation in (2.11) are chosen accordingly and a corresponding receiver structure is defined.

For B-IFDMA, no CDMA is used, i.e., the number K_c of orthogonal spreading codes is given by $K_c = 1$. Consequently, $K = K_f$, cf. (2.8), $k = k_f$, cf. (2.9), and the spreading matrix $\mathbf{S}^{(k_c)}$ is set to

$$\mathbf{S}^{(k_c)} = \mathbf{I}_Q. \tag{2.34}$$

Aiming at low envelope fluctuations of the transmit signal, a DFT is used for pre-coding [XZG03]. Thus, the pre-coding matrix is given by

$$\mathbf{P} = \mathbf{F}_Q, \tag{2.35}$$

where $\mathbf{F}_Q$ denotes a $Q \times Q$ DFT matrix analogous to (2.10). From (2.35) follows that the nature of a B-IFDMA signal is that of a single carrier signal, cf. Section 2.3.3.

For a B-IFDMA scheme, the user separation is realized by FDMA. In order to provide good frequency diversity, the subcarriers assigned to each user are distributed over the total available bandwidth. A symmetrical subcarrier allocation is used that organizes the set of Q subcarriers with Q of (2.1) that are assigned to user k in L subcarrier blocks, each containing M adjacent subcarriers. The L subcarrier blocks of user k are equidistantly distributed over the total available bandwidth. The number Q of subcarriers per block is given by

$$Q = L \cdot M. \tag{2.36}$$

For the sake of simplicity, in the following, it is assumed that the number M of sub-carriers per block and the number L of subcarrier blocks is the same for all users. An illustration of the subcarrier allocation of different users' subcarrier sets is given in Figure 2.5.

For a subcarrier allocation according to Figure 2.5, the subcarrier mapping matrix is given by

$$\mathbf{M}^{(k_f)} = \mathbf{M}_{\mathrm{BI}}^{(k)} \tag{2.37}$$
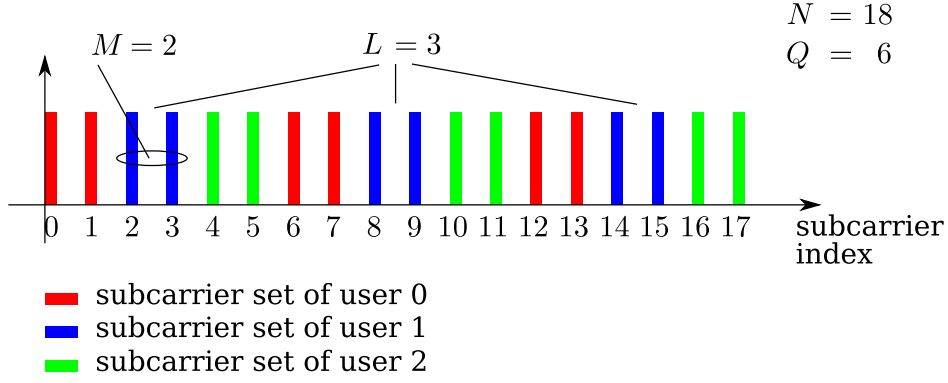
Figure 2.5: Subcarrier allocation of different users' subcarrier sets for B-IFDMA.

with elements

$$\left[\mathbf{M}_{\mathrm{BI}}^{(k)}\right]_{n,q} = \begin{cases} 1 & n = l \cdot \frac{N}{L} + m + kM \\ 0 & \text{else} \end{cases} , \quad l = 0, \ldots, L-1, \ m = 0, \ldots, M-1,$$

(2.38)

with $q = m + l \cdot M$. Thus, the modulated data vector for B-IFDMA is given by

$$\mathbf{x}_{\mathrm{BI}}^{(k)} = \mathbf{F}_{\mathrm{N}}^{\mathrm{H}} \cdot \mathbf{M}_{\mathrm{BI}}^{(k)} \cdot \mathbf{F}_{\mathrm{Q}} \cdot \mathbf{d}^{(k)}.$$

(2.39)

Note that for N and Q chosen as powers of 2, for the implementation of B-IFDMA according to (2.39), a high computational efficiency is provided by the use of the Fast Fourier Transform (FFT) algorithm for the DFT pre-coding and for the OFDM modulation [Ach78].

With the definition of the matrices in (2.34), (2.35) and (2.37), the degrees of freedom of a B-IFDMA signal of user k are given by the choice of

- the number L of subcarrier blocks and

- the number M of subcarriers per block.

Note that the number Q of subcarriers assigned to a user is given by the choice of L and M, cf. (2.36). Considering that B-IFDMA is combined with TDMA by the assignment of a number N_{t} consecutive modulated data vectors to a certain user, another degree of freedom is provided by the choice of the number N_{t}. The numbers L, M and N_{t} are denoted as signal parameters of B-IFDMA throughout this thesis.

For B-IFDMA, the insertion of the matrices from (2.34), (2.35) and (2.37) in (2.20) leads to

$$\left(\mathbf{g}_p^{(k)}\right)^{\mathrm{H}} \cdot \mathbf{g}_q^{(\kappa)} = 0 \ \ \forall \ \ p, q = 0, \ldots, Q-1; \ \ k, \kappa = 0, \ldots, K-1; \ \ k \neq \kappa, \quad (2.40)$$

i.e., the received signal is MAI-free. Moreover, the condition

$$\left(\mathbf{g}_p^{(k)}\right)^{\mathrm{H}} \cdot \mathbf{g}_q^{(k)} = 0 \quad \forall \quad p, q = 0, \ldots, Q-1; \quad p \neq q; \quad k = 0, \ldots, K-1 \qquad (2.41)$$

is violated, i.e., the received signal contains ISI and, thus, an equalizer is required.

A simple receiver structure for B-IFDMA in frequency domain is given by setting the matrices in the receiver model from Figure 2.4 to

$$\left(\mathbf{M}^{(k)}\right)^{\dagger} = \left(\mathbf{M}_{\mathrm{BI}}^{(k)}\right)^{\dagger} \qquad (2.42)$$

and

$$\mathbf{P}^{-1} = \mathbf{F}_{\mathrm{Q}}^{\mathrm{H}}. \qquad (2.43)$$

As discussed in Section 2.3.5, an FDE based on the MMSE criterion can be considered as an appropriate equalizer. Thus, for B-IFDMA, an estimate $\hat{\mathbf{d}}^{(k)}$ for the data symbol vector $\mathbf{d}^{(k)}$ is given by

$$\hat{\mathbf{d}}^{(k)} = \mathbf{F}_{\mathrm{Q}}^{\mathrm{H}} \cdot \mathbf{E}_{\mathrm{MMSE}}^{(k)} \cdot \left(\mathbf{M}_{\mathrm{BI}}^{(k)}\right)^{\dagger} \cdot \mathbf{F}_{\mathrm{N}} \cdot \mathbf{r}. \qquad (2.44)$$

Some special cases of B-IFDMA are well-known in the literature. For $Q = M = N$, B-IFDMA is equivalent to OFDM with DFT pre-coding. In [BR98], it is shown that for for this scheme the DFT for pre-coding and the OFDM modulation performed by an IDFT totally cancel out. Thus, in this case, the modulated data vector $\mathbf{x}^{(k)}$ is equivalent to the data symbol vector $\mathbf{d}^{(k)}$. The scheme is also referred to as Cyclic Prefix Only (CP-only) [WG00] and as single carrier modulation with FDE (SC-FDE) [FABSE02]. Throughout this thesis, the scheme is denoted as Single Carrier TDMA (SC-TDMA) in order to underline that the user separation is performed by TDMA.

For $M = 1$, B-IFDMA is equivalent to IFDMA. The author of this thesis has shown in [FKCS05a] that for this case the blockwise modulation of (2.39) can be simplified to the originally proposed time domain modulation for IFDMA in [SDBS98] that consists of a compression in time by factor K and a subsequent K-fold repetition of the modulated data vector followed by a user specific phase rotation, cf. [SDBS98]. IFDMA is also known under the name distributed Single Carrier FDMA (SC-FDMA) in 3GPP LTE [3GP06].

For $L = 1$, B-IFDMA is equivalent to localized FDMA (LFDMA), cf. [MLG06]. LFDMA is also known under the name localized SC-FDMA in 3GPP LTE [3GP06].

Since B-IFDMA includes localized SC-FDMA and distributed SC-FDMA as special cases, B-IFDMA can be, vice versa, regarded as a generalization of the SC-FDMA approach from 3GPP LTE [3GP06].

2.5 Overview of Block-transmission-based Multiple Access Schemes with CP and Their Relation to B-IFDMA

In this section, an overview of several well-known multiple access schemes based on block transmission with CP is given and their relation to B-IFDMA is shown.

An important multiple access scheme that is also considered throughout this thesis as a reference is OFDMA. For OFDMA, no CDMA is used and, thus, $K_c = 1$. Consequently, $K = K_f$ and $k = k_f$, cf. Section 2.3.3. Further on, no pre-coding is applied. Thus, the discrete-time base-band system model for OFDMA is given by setting

$$\mathbf{S}^{(k_c)} = \mathbf{I}_N \tag{2.45}$$

and

$$\mathbf{P} = \mathbf{I}_Q. \tag{2.46}$$

Matrix $\mathbf{M}^{(k)}$ is chosen as an $N \times Q$ matrix that defines the desired subcarrier mapping for user k according to the definition of $\mathbf{M}^{(k)}$ in Section 2.3.3.

For OFDMA in general, with (2.4) and (2.11), the modulated data vector is, thus, given by

$$\mathbf{x}^{(k)}_{\mathrm{OFDMA}} = \mathbf{F}^{\mathrm{H}}_N \cdot \mathbf{M}^{(k)} \cdot \mathbf{d}^{(k)}. \tag{2.47}$$

An OFDMA scheme with block-interleaved subcarrier mapping, also denoted as Block-Equidistant Frequency Division Multiple Access (B-EFDMA) [SFF$^+$07], is given by additionally setting

$$\mathbf{M}^{(k)} = \mathbf{M}^{(k)}_{\mathrm{BI}} \tag{2.48}$$

with $\mathbf{M}^{(k)}_{\mathrm{BI}}$ of (2.38).

From B-EFDMA, an OFDMA scheme with interleaved subcarrier allocation is obtained by setting $M = 1$. OFDMA with interleaved subcarrier allocation is denoted as interleaved OFDMA (I-OFDMA) throughout this thesis.

For all OFDMA schemes, the insertion of the matrices from (2.45), (2.46) and matrix $\mathbf{M}^{(k)}$ in (2.20) leads to

$$\left(\mathbf{g}^{(k)}_p\right)^{\mathrm{H}} \cdot \mathbf{g}^{(\kappa)}_q = 0 \ \ \forall \ \ p, q = 0, \dots, Q-1; \ \ k, \kappa = 0, \dots, K-1; \ \ k \neq \kappa. \tag{2.49}$$

i.e., the received signal is MAI-free. Moreover,

$$\left(\mathbf{g}_p^{(k)}\right)^{\mathrm{H}} \cdot \mathbf{g}_q^{(k)} = 0 \quad \forall \quad p, q = 0, \ldots, Q - 1; \quad p \neq q; \quad k = 0, \ldots, K - 1, \qquad (2.50)$$

i.e., the received signal is also ISI-free.

The receiver structure for OFDMA is given by the application of the respective matrices $\mathbf{P}$ and $\mathbf{M}^{(k)}$ that have been defined above for OFDMA to the receiver structure given in Figure 2.4. Note that as the received signal is ISI-free, a ZF FDE is applied that represents an optimum ML receiver for OFDMA [vNP00].

Other multiple access schemes that can be described by the general discrete-time base-band system model from Section 2.3 are

- Multi Carrier TDMA (MC-TDMA) [IEE99],

- Spread Spectrum Multi Carrier Multiple Access (SS-MC-MA) [KF97],

- Block-Transmission CDMA (BT-CDMA) [Mar04],

- Multi Carrier CDMA (MC-CDMA) [FK03],

- CDMA with Frequency Domain Orthogonal Signature Sequences (FDOSS-CDMA) [CC00],

- CDMA with Variable Spreading and Chip Repetition Factor (VSCRF-CDMA) [GKAS03].

The definition of these schemes based on the general discrete-time base-band system model from Section 2.3 is given in Appendix A.1.

An overview of the different multiple access schemes and their ISI and MAI properties is given in Table 2.1. The relation of B-IFDMA to the schemes shown in Table 2.1 is illustrated in Figure 2.6. At the arrows it is described what has to be changed in order to come from the scheme at the start of the arrow to the scheme at the end of the arrow. From Figure 2.6 it can be seen, e.g., that if the DFT pre-coding is omitted for B-IFDMA, B-EFDMA is obtained. As a second example, it can be seen from Figure 2.6 that SS-MC-MA can be obtained from B-IFDMA by setting $M = 1$, i.e., using only one subcarrier per block and replacing the DFT pre-coding by a Walsh Hadamard pre-coding.

Table 2.1: Overview over block-transmission based multiple access schemes with CP

Scheme	Reference	Spreading	Pre-Coding	Subcarrier Allocation	Multiple Access	ISI	MAI
SC-TDMA	[FABSE02]	-	DFT	full bandwidth	TDMA	yes	no
MC-TDMA	[IEE99]	-	-	full bandwidth	TDMA	no	no
B-EFDMA	[SFF$^+$07]	-	-	block-interleaved	FDMA	no	no
OFDMA	[vNP00]	-	-	arbitrary	FDMA	no	no
B-IFDMA	-	-	DFT	block-interleaved	FDMA	yes	no
SC-FDMA localized distributed	[3GP06]	- -	DFT DFT	blockwise interleaved	FDMA FDMA	yes yes	no no
SS-MC-MA	[KF97]	-	WH	interleaved	FDMA	yes	no
BT-CDMA	[Mar04]	orthogonal codes	DFT	full bandwidth	CDMA	yes	yes
MC-CDMA	[FK03]	orthogonal codes	-	full bandwidth	CDMA	no	yes
FDOSS-CDMA	[CC00]	FDOSS	DFT	full bandwidth	CDMA	yes	no
VSCRF-CDMA	[GKAS03]	WH	DFT	interleaved	CDMA +FDMA	yes	yes
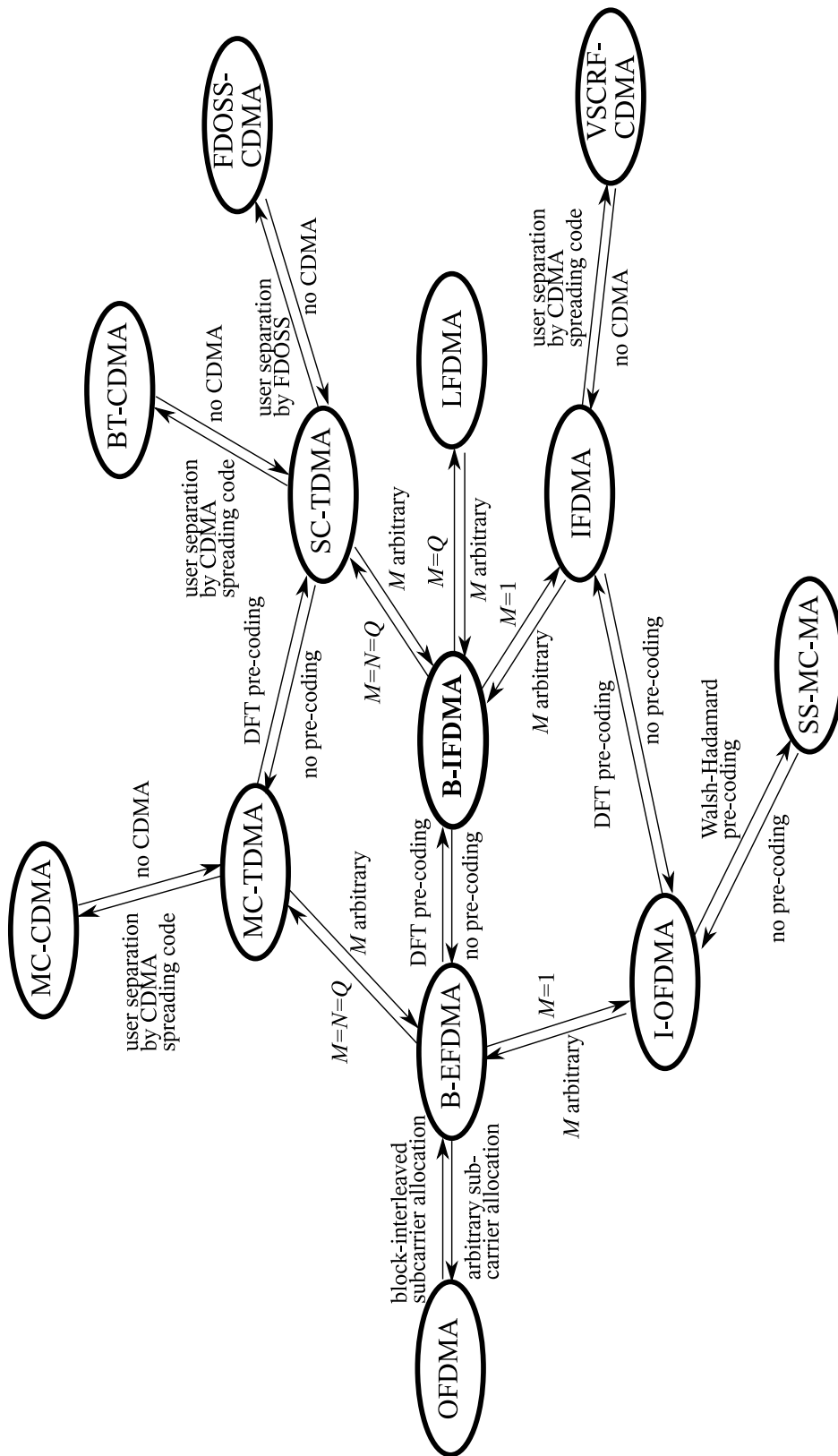
Figure 2.6:   Relation of B-IFDMA to other multiple access schemes based on block
transmission with CP.

2.6   Conclusions

In this chapter, a new general discrete-time base-band system model for block-transmission-based multiple access schemes with CP has been introduced. The new system model provides an appropriate framework for a unified description of various well-known block-transmission-based multiple access schemes with CP such as OFDMA, MC-CDMA and SC-FDMA. Moreover, the new system model has been used for the definition of B-IFDMA that is the scheme in the focus of this thesis. Based on the general discrete-time base-band system model, a new method for diagnosing whether the received signal contains MAI or ISI, respectively, has been presented. It has been shown that for B-IFDMA, the received signal is MAI free even for the transmission over a time dispersive channel in the uplink. Thus, for B-IFDMA, costly MUD techniques can be avoided. Nevertheless, the received signal for B-IFDMA has been shown to contain ISI and, thus, an equalizer is required. However, for B-IFDMA a simple receiver structure has been introduced that performs user separation and equalization in frequency domain. Finally, based on the new system model, B-IFDMA has been categorized amongst other block-transmission-based multiple access schemes with CP and the relation between B-IFDMA and the different schemes has been systematically described.

Chapter 3

New Algorithms for the Application of B-IFDMA in Future Mobile Radio Systems

3.1   Introduction

In this chapter, for B-IFDMA, new algorithms are introduced that are important in order to meet the challenging requirements a multiple access solution has to meet for future mobile radio systems, cf. Section 1.1. For the different algorithms, the state-of-the-art is given. Further on, the algorithms are extensively described and the properties of the algorithms when applied to B-IFDMA are discussed.

According to Section 1.1, for the radio interface of a future mobile radio system, a low computational complexity is important, especially for the mobile terminal, in order to keep the costs as low as possible. Although, due to the application of the FFT algorithm, the implementation of B-IFDMA presented in Section 2.4 already provides low computational effort, in this chapter, a new time domain implementation for B-IFDMA is introduced that provides a further reduced computational complexity compared to the implementation from Section 2.4.

The application of multiple antenna techniques has been identified to be a key technology for future mobile radio systems in order to provide a good performance [FG98, PNG03], which is an important issue for future mobile radio applications, cf. Section 1.1. Thus, it has to be shown that B-IFDMA can be well combined with appropriate multiple antenna techniques. Accordingly, throughout this chapter, new approaches for the application of Space-Time Block-Codes (STBCs) and for the application of Space Division Multiple Access (SDMA) to B-IFDMA are introduced and their properties when combined with B-IFDMA are discussed.

Further on, the air interface of a future mobile radio system has to provide a high flexibility and granularity in terms of different data rates, cf. Section 1.1. Due to the regular subcarrier allocation of B-IFDMA signals, the flexibility of the scheme is restricted. Consequently, a solution is required that provides a high flexibility and granularity in terms of different data rates for B-IFDMA. Thus, throughout this chapter, for B-IFDMA, a new approach for the accommodation of different data rates within one cell is presented.

The remainder of this chapter is organized as follows: In Section 3.2, new computationally efficient algorithms are presented for B-IFDMA modulation and demodulation in time domain. In Section 3.3, a new approach for the application of various STBCs to B-IFDMA is introduced that provides a good performance due to the exploitation of spatial diversity, low computational complexity and maintains the envelope characteristics of the B-IFDMA signal. In Section 3.4, the application of SDMA to B-IFDMA is described and a solution for a further reduction of the computational effort is proposed. In Section 3.5, for B-IFDMA, a new approach for the accommodation of different data rates within one cell is presented that provides sufficient flexibility and granularity in terms of different data rates for the application of B-IFDMA in a future mobile radio system.

3.2   Time Domain Implementation

3.2.1   Introduction

In this section, new implementations of B-IFDMA modulation and demodulation are presented. In Section 2.4, B-IFDMA has been introduced based on a general discrete-time base-band system model. This system model describes B-IFDMA as DFT pre-coded OFDMA with a block-interleaved subcarrier allocation and is an illustrative means for the description of the spectral characteristics of B-IFDMA such as frequency diversity provided by the block-interleaved subcarrier allocation and user separation by FDMA, cf. Section 2.4. Moreover, the description of B-IFDMA based on the discrete-time base-band system model separates important operations that are part of the B-IFDMA signal generation such as DFT pre-coding, subcarrier allocation and OFDM modulation and, thus, enables to describe the relation of B-IFDMA to other block-transmission-based multiple access schemes with CP in a systematic way.

In this section, an alternative implementation of B-IFDMA in time domain is presented. The time domain implementation of B-IFDMA has been introduced and discussed by the author of this thesis in [FKC07a]. It is based on a combination of the DFT pre-coding, the block-interleaved subcarrier mapping and the IDFT for OFDM modulation and exploits the symmetry of the subcarrier allocation for the provision of an even lower computational complexity than the implementation from Section 2.4. Moreover, the implementation in time domain gives a new perspective on the B-IFDMA signal, especially on the relation between the elements $x_n^{(k)}$ of the modulated data symbol vector $\mathbf{x}^{(k)}$ and the data symbols $d_q^{(k)}$.

The remainder of this section is organized as follows: An overview of relevant existing literature related to the B-IFDMA time domain implementation is given in Section 3.2.2. In Section 3.2.3.1, the new algorithm for time domain implementation of B-IFDMA modulation is introduced and discussed. In Section 3.2.3.2, for the special case $M = 1$, the time domain implementation of B-IFDMA modulation is further simplified and a new algorithm for an efficient time domain implementation is introduced for this case. In Section 3.2.4, the new algorithm for time domain implementation of B-IFDMA demodulation is introduced and discussed. Finally, Section 3.2.5 summarizes the main results of Section 3.2.

3.2.2 State-of-the-art

In the sequel, an overview of relevant existing literature related to the presented B-IFDMA time domain implementation is given. For some special cases of B-IFDMA, the time domain implementation is well known. As described in Section 2.4, for $Q = N$ with Q and N as defined in Section 2.3.2, B-IFDMA is equivalent to OFDM with DFT pre-coding. In [BR98] it is shown that for OFDM with DFT pre-coding the DFT and the OFDM modulation performed by an IDFT, cf. (2.39), totally cancel out each other and that, thus, the time domain implementation is trivial. For $Q = L$, B-IFDMA is equivalent to IFDMA, cf. Section 2.4. IFDMA modulation and demodulation in time domain are introduced in [SDBS98]. For $Q = M$, B-IFDMA is equivalent to localized SC-FDMA, cf. Section 2.4. For localized SC-FDMA, the modulation in time domain is described in [MLG06].

The B-IFDMA time domain implementation presented in this section generalizes the existing results for the time domain implementations of the aforementioned schemes to B-IFDMA and includes them as special cases. Additionally, for the special case $M = 1$, a novel algorithm for modulation in time domain is presented that reduces the computational effort compared to the algorithm presented in [SDBS98].

For OFDMA with interleaved subcarrier allocation, a time domain implementation has been proposed in [FC07]. This implementation is shown to reduce the computational complexity for OFDMA signal generation considerably. Since OFDMA with block-interleaved subcarrier mapping is equivalent to B-IFDMA with IDFT pre-coding of the data symbols before modulation, the B-IFDMA time domain implementation can be also regarded as a generalization of the approach described in [FC07] to OFDMA schemes with block-interleaved subcarrier allocation.

3.2.3   Modulation in Time Domain

3.2.3.1   Algorithm for Modulation in Time Domain

In this section, the time domain implementation of B-IFDMA modulation is derived. Throughout this section, the index 'BI' that has been introduced in order to distinguish the modulated data vector $\mathbf{x}_{\mathrm{BI}}^{(k)}$ from the modulated data vectors of other schemes is omitted, because throughout this section the modulated data vector for B-IFDMA is regarded exclusively.

For the derivation of the algorithm for B-IFDMA modulation, in the following, the matrix $\mathbf{F}_Q$ of (2.35) for DFT pre-coding, the matrix $\mathbf{M}_{\mathrm{BI}}^{(k)}$ of (2.37) for block-interleaved subcarrier allocation and the matrix $\mathbf{F}_N^{\mathrm{H}}$ of (2.10) for OFDM modulation of are combined.

In order to show the simplifications obtained by the exploitation of the symmetry of the block-interleaved subcarrier allocation, in the following, the elements of the vectors after DFT pre-coding, subcarrier allocation and OFDM modulation are regarded. For that purpose, (2.39) is reformulated as follows. Let

$$\mathbf{u}^{(k)} = \left[u_0^{(k)}, \ldots, u_{Q-1}^{(k)} \right]^{\mathrm{T}} \tag{3.1}$$

denote the DFT pre-coded data symbol vector according to

$$\mathbf{u}^{(k)} = \mathbf{F}_{\mathrm{Q}} \cdot \mathbf{d}^{(k)} \tag{3.2}$$

with $\mathbf{d}^{(k)}$ of (2.1) and with elements

$$u_p^{(k)} = \frac{1}{\sqrt{Q}} \sum_{q=0}^{Q-1} d_q^{(k)} \cdot e^{-j\frac{2\pi}{Q}pq}; \quad p = 0, \ldots, Q-1. \tag{3.3}$$

Let further

$$\bar{\mathbf{u}}^{(k)} = \left[\bar{u}_0^{(k)}, \ldots, \bar{u}_{N-1}^{(k)} \right]^{\mathrm{T}} \tag{3.4}$$

denote the pre-coded data symbol vector after subcarrier mapping with

$$\bar{\mathbf{u}}^{(k)} = \mathbf{M}_{\mathrm{BI}}^{(k)} \cdot \mathbf{u}^{(k)}. \tag{3.5}$$

Together with (2.38), the elements $\bar{u}_r^{(k)}$, $r = 0, \ldots, N-1$, of vector $\bar{\mathbf{u}}^{(k)}$ are given by

$$\bar{u}_r^{(k)} = \begin{cases} u_{lM+m}^{(k)} & \text{for} \quad r = l \cdot \frac{N}{L} + m + kM \\ 0 & \text{else} \end{cases}, \quad l = 0, \ldots, L-1, \quad m = 0, \ldots, M-1. \tag{3.6}$$

According to (2.39), the modulated data vector $\mathbf{x}^{(k)}$ is, thus, given by

$$\mathbf{x}^{(k)} = \mathbf{F}_N^H \cdot \bar{\mathbf{u}}^{(k)} \tag{3.7}$$

and the elements $x_n^{(k)}$, $n = 0, \ldots, N-1$, of vector $\mathbf{x}^{(k)}$ can be expressed as

$$x_n^{(k)} = \frac{1}{\sqrt{N}} \sum_{r=0}^{N-1} \bar{u}_r^{(k)} \cdot e^{j\frac{2\pi}{N}rn}. \tag{3.8}$$

The insertion of (3.6) and (3.3) into (3.8) results in

$$x_n^{(k)} = \frac{1}{\sqrt{QN}} \sum_{m=0}^{M-1} e^{j\frac{2\pi}{N}n(kM+m)} \sum_{q=0}^{Q-1} d_q^{(k)} \cdot e^{-j\frac{2\pi}{Q}qm} \sum_{l=0}^{L-1} e^{j\frac{2\pi}{L}l(n-q)}, \tag{3.9}$$

where

$$\sum_{l=0}^{L-1} e^{j\frac{2\pi}{L}l(n-q)} = \begin{cases} L & \text{for} \quad q = n + \mu L \\ 0 & \text{else} \end{cases} , \quad \mu = 0, \ldots, M-1. \tag{3.10}$$

With (3.10), (3.9) results in

$$x_n^{(k)} = \frac{L}{\sqrt{QN}} \sum_{\mu=0}^{M-1} d_{(n+\mu L)\bmod Q}^{(k)} \cdot e^{j\frac{2\pi}{N}nkM} \sum_{m=0}^{M-1} e^{-j2\pi m\left(\frac{n}{Q} - \frac{n}{N} + \frac{\mu}{M}\right)}, \tag{3.11}$$

where 'mod' denotes the modulo operation. Defining

$$\Theta_n^{(\mu,k)} = \frac{L}{\sqrt{QN}} e^{j\frac{2\pi}{N}nkM} \sum_{m=0}^{M-1} e^{-j2\pi m\left(\frac{n}{Q} - \frac{n}{N} + \frac{\mu}{M}\right)}, \tag{3.12}$$

(3.11) reduces to

$$x_n^{(k)} = \sum_{\mu=0}^{M-1} d_{(n+\mu L)\bmod Q}^{(k)} \cdot \Theta_n^{(\mu,k)}. \tag{3.13}$$

Equation (3.13) can be illustrated by the block diagram depicted in Figure 3.1. The sequence $d_{(n+\mu L)\bmod Q}^{(k)}$ in (3.13) can be interpreted as a compression of the sequence of data symbols $d_q^{(k)}$, $q = 0, \ldots, Q-1$, in time by factor N/Q, a subsequent N/Q-fold repetition and, finally, a cyclic shift of the N elements of the resulting sequence by μL. Thus, the sequence $d_{(n+\mu L)\bmod Q}^{(k)}$ represents a single carrier signal. Consequently, B-IFDMA can be considered as a superposition of M single carrier signals carrying the same data but weighted by different complex numbers $\Theta_n^{(\mu,k)}$. The expression $e^{j\frac{2\pi}{N}kM}$ in (3.12) represents a user specific frequency shift by kM times the subcarrier bandwidth.

Since the coefficients $\Theta_n^{(\mu,k)}$ in (3.13) are independent of the data symbols, they can be calculated offline and only the multiplication of $d_{(n+\mu L)\bmod Q}^{(k)}$ with $\Theta_n^{(\mu,k)}$ has to be performed online. Hence, the implementation of (3.13) requires only $M \cdot N$ complex
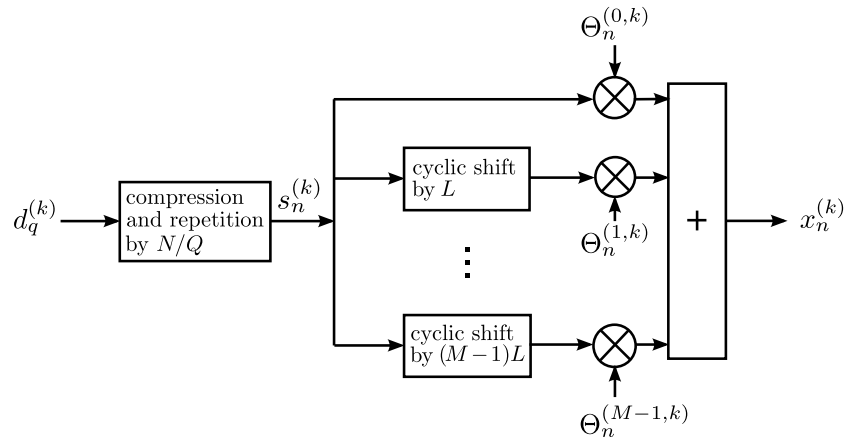
Figure 3.1: Time domain implementation for B-IFDMA modulation

multiplications. Thus, (3.13) represents a computationally efficient alternative to the implementation of B-IFDMA of (2.39). In Section 4.3, the computational effort required for (3.13) is extensively analyzed and compared to the computational effort required for (2.39). Further on, note that (3.13) represents an implementation for B-IFDMA modulation that does not necessarily need N and Q to be powers of 2 as it would be the case for an implementation of B-IFDMA modulation according to (2.39) using the Fast Fourier Transform (FFT) algorithm.

Note that the time domain implementation for B-IFDMA can be also applied to OFDMA with block-interleaved subcarrier allocation, because OFDMA with block-interleaved subcarrier allocation can be considered as B-IFDMA with IDFT pre-coding. For a time domain implementation of OFDMA modulation with block-interleaved subcarrier allocation, an additional Q-point IDFT has to be applied to the data symbol vector $\mathbf{d}^{(k)}$ in (3.13) before modulation.

3.2.3.2   Further Simplification for the Special Case $M = 1$

In the following, the special case $M = 1$ is described in detail and for this special case, a novel efficient time domain implementation is presented. For $M = 1$, $\Theta_n^{(\mu,k)}$ reduces to

$$\Theta_n^{(\mu,k)} = \sqrt{\frac{Q}{N}} e^{j\frac{2\pi}{N}kn} \tag{3.14}$$

and (3.13) simplifies to compression and repetition of the data symbols, subsequent user specific frequency shift and a normalization to $\sqrt{Q/N}$. This is equivalent to the time domain implementation of an IFDMA signal described in [SDBS98].

Inserting (3.14) into (3.13), the modulated data vector can be expressed as

$$x_n^{(k)} = \frac{1}{\sqrt{K}} \cdot d_{n \bmod Q}^{(k)} \cdot e^{j \frac{2\pi}{N} kn}. \tag{3.15}$$

Let the values of N be chosen such that $N \bmod 4 = 0$, i.e. N is an integer multiple of 4. Moreover, let also $K \bmod 4 = 0$ and $K \geq 4$. Note that these assumptions are in accordance with assumptions for practical applications, e.g., for an efficient accommodation of different data rates, N and Q are favorable to be chosen as powers of 2, cf. [FKCS05b] and Section 3.5.

Regarding the term $e^{j \frac{2\pi}{N} kn}$, $n = 0, \ldots, N-1$, it can be noticed that this term can be obtained from $e^{j \frac{2\pi}{N} km}$, $m = 0, \ldots, N/4 - 1$, according to

$$e^{j \frac{2\pi}{N} kn} = \begin{cases} e^{j \frac{2\pi}{N} km} & n = 0, ..., N/4 - 1, \ m = n \\ (j)^k \cdot e^{j \frac{2\pi}{N} km} & n = N/4, ..., N/2 - 1, \ m = n - N/4 \\ (-1)^k \cdot e^{j \frac{2\pi}{N} km} & n = N/2, ..., 3N/4 - 1, \ m = n - N/2 \\ (-j)^k \cdot e^{j \frac{2\pi}{N} km} & n = 3N/4, ..., N - 1, \ m = n - 3N/4 \end{cases}. \tag{3.16}$$

Together with (3.15), from (3.16) follows that also the elements $x_n^{(k)}$, $n = 0, \ldots, N-1$, can be obtained from the elements $x_m^{(k)}$, $m = 0, \ldots, N/4 - 1$, according to

$$x_n^{(k)} = \begin{cases} x_m^{(k)} & n = 0, ..., N/4 - 1, \ m = n \\ (j)^k \cdot x_m^{(k)} & n = N/4, ..., N/2 - 1, \ m = n - N/4 \\ (-1)^k \cdot x_m^{(k)} & n = N/2, ..., 3N/4 - 1, \ m = n - N/2 \\ (-j)^k \cdot x_m^{(k)} & n = 3N/4, ..., N - 1, \ m = n - 3N/4 \end{cases}. \tag{3.17}$$

The calculation of $(j)^k \cdot x_m^{(k)}$, $(-1)^k \cdot x_m^{(k)}$ and $(-j)^k \cdot x_m^{(k)}$ can be realized by switching the sign and/or exchanging the real and the imaginary part of $x_m^{(k)}$ and does not require any further mathematical operation. Thus, with the help of (3.17), the computational complexity for signal generation of B-IFDMA with $M = 1$ in terms of required complex multiplications can be reduced by a factor of 4 compared to the implementation according to (3.15). The simplified implementation of B-IFDMA modulation for $M = 1$ in time domain is depicted in Figure 3.2.

Note that the presented approach can be also used in order to further decrease the computational complexity of the approach described in [FC07] for an efficient implementation of OFDMA modulation with interleaved subcarrier allocation. For this purpose, the Q data symbols $d_q^{(k)}$ in (3.15) have to be replaced by the Q elements of their Q-point IDFT.

With the further reduction of the computational complexity of B-IFDMA with $M = 1$, the implementation according to (3.17) provides an interesting approach especially for generation of B-IFDMA transmit signals in low-cost mobile terminals for uplink transmission.

$$\left[d_0^{(k)}, \ldots, d_{Q-1}^{(k)}\right]^{\mathrm{T}} = \mathbf{d}^{(k)}$$

compression by N/Q and
repetition by $N/(4Q)$

$e^{j\frac{2\pi}{N}km}$; $m = 0, \ldots, N/4 - 1$

$$\left[x_0^{(k)}, \ldots, x_{N/4-1}^{(k)}\right]^{\mathrm{T}}$$

j^k $\quad$ $(-1)^k$ $\quad$ $(-j)^k$

$$\left[x_0^{(k)}, \ldots, x_{N/4-1}^{(k)} \mid x_{N/4}^{(k)}, \ldots, x_{2N/4-1}^{(k)} \mid x_{2N/4}^{(k)}, \ldots, x_{3N/4-1}^{(k)} \mid x_{3N/4}^{(k)}, \ldots, x_{N-1}^{(k)}\right]^{\mathrm{T}} = \mathbf{x}^{(k)}$$
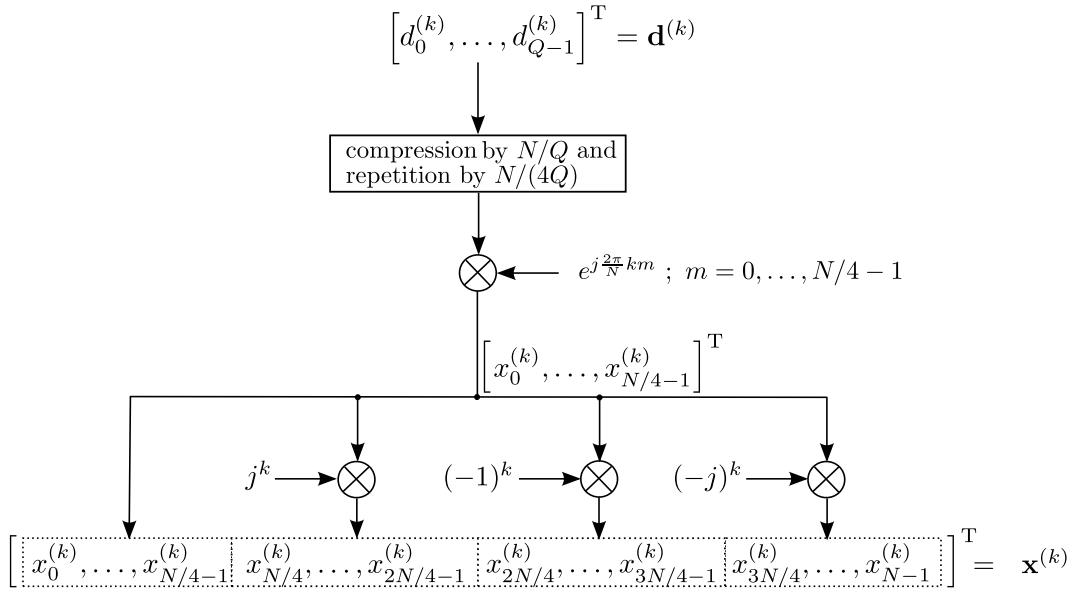
Figure 3.2: Low complexity implementation for B-IFDMA modulation with $M = 1$.

3.2.4 Demodulation in Time Domain

In this section, the time domain representation of B-IFDMA demodulation is derived. For the derivation of the algorithm for B-IFDMA demodulation, in the following, the matrix $\mathbf{F}_N$ of (2.44) for OFDM demodulation, the matrix $\left(\mathbf{M}_{\mathrm{BI}}^{(k)}\right)^{\dagger}$ of (2.44) for user separation, and the matrix $\mathbf{F}_Q^{\mathrm{H}}$ of (2.44) for compensation of the DFT pre-coding are combined.

In order to show the simplifications obtained by the exploitation of the symmetry of the block-interleaved subcarrier allocation, in the following, the elements of the vectors after OFDM demodulation, user separation and compensation of the DFT pre-coding are regarded. For that purpose, (2.44) is reformulated as follows.

The signal after compensation of the DFT pre-coding, i.e., the demodulated signal of user k, can be described by the $Q \times 1$ vector $\boldsymbol{\rho}^{(k)} = \left[\rho_0^{(k)}, \ldots, \rho_{Q-1}^{(k)}\right]^{\mathrm{T}}$ with

$$\boldsymbol{\rho}^{(k)} = \mathbf{F}_Q^H \cdot \left(\mathbf{M}_{\mathrm{BI}}^{(k)}\right)^{\dagger} \cdot \mathbf{F}_N \cdot \mathbf{r}. \tag{3.18}$$

Let $\bar{\mathbf{v}} = [\bar{v}_0, \ldots, \bar{v}_{N-1}]^{\mathrm{T}}$ denote the DFT of the received signal vector $\mathbf{r}$ of (2.16) after removal of the CP according to

$$\bar{\mathbf{v}} = \mathbf{F}_{\mathrm{N}} \cdot \mathbf{r} \tag{3.19}$$

with elements

$$\bar{v}_n = \frac{1}{\sqrt{N}} \sum_{s=0}^{N-1} r_s \cdot e^{-j\frac{2\pi}{N}sn}, \quad n = 0, \ldots, N-1. \tag{3.20}$$

Let, further on, $\bar{\mathbf{v}}^{(k)} = \left[\bar{v}_0^{(k)}, \ldots, \bar{v}_{Q-1}^{(k)}\right]^{\mathrm{T}}$ denote the DFT of the received signal vector after block-interleaved subcarrier demapping with

$$\bar{\mathbf{v}}^{(k)} = \left(\mathbf{M}_{\mathrm{BI}}^{(k)}\right)^{\dagger} \cdot \bar{\mathbf{v}}. \tag{3.21}$$

The elements $\bar{v}_p^{(k)}$, $p = 0, \ldots, Q-1$, are given by

$$\bar{v}_p^{(k)} = \begin{cases} \bar{v}_{lN/L+m+kM} & \text{for} \quad p = lM + m \\ 0 & \text{else} \end{cases}, \quad l = 0, \ldots, L-1, \ m = 0, \ldots, M-1. \tag{3.22}$$

Inserting (3.19) and (3.21) in (3.18), the demodulated B-IFDMA signal of user k results in

$$\boldsymbol{\rho}^{(k)} = \mathbf{F}_Q^{\mathrm{H}} \cdot \bar{\mathbf{v}}^{(k)}. \tag{3.23}$$

Thus, with (3.20) and (3.22), the elements $\rho_q^{(k)}$ of vector $\boldsymbol{\rho}^{(k)}$ can be expressed as

$$\rho_q^{(k)} = \frac{1}{\sqrt{QN}} \sum_{m=0}^{M-1} \sum_{s=0}^{N-1} r_s e^{j\frac{2\pi}{Q}mq} e^{-j\frac{2\pi}{N}skM} \cdot e^{-j\frac{2\pi}{N}sm} \sum_{l=0}^{L-1} e^{j\frac{2\pi}{L}l(q-s)}. \tag{3.24}$$

With

$$\sum_{l=0}^{L-1} e^{j\frac{2\pi}{L}l(q-s)} = \begin{cases} L & \text{for} \quad s = q + \nu L \\ 0 & \text{else} \end{cases}, \quad q = 0, \ldots, Q-1, \ \nu = 0, \ldots, N/L-1, \tag{3.25}$$

(3.24) can be reformulated as

$$\begin{aligned} \rho_q^{(k)} &= \frac{L}{\sqrt{QN}} \sum_{m=0}^{M-1} \sum_{\nu=0}^{N/L-1} r_{(q+\nu L)\mathrm{mod}N} e^{j\frac{2\pi}{Q}mq} e^{-j\frac{2\pi}{N}kM(q+\nu L)} \cdot e^{-j\frac{2\pi}{N}(q+\nu L)m} \\ &= \frac{L}{\sqrt{QN}} \sum_{\nu=0}^{N/L-1} r_{(q+\nu L)\mathrm{mod}N} e^{-j\frac{2\pi}{N}kM(q+\nu L)} \sum_{m=0}^{M-1} e^{j\frac{2\pi}{Q}m((q+\nu L)} e^{-j\frac{2\pi}{N}m(q+\nu L)} e^{+j\frac{2\pi}{M}(\nu\mathrm{mod}M)} \end{aligned} \tag{3.26}$$

Defining

$$\Psi_n^{(\nu,k)} = \left(\Theta_n^{(-\nu\mathrm{mod}M,k)}\right)^*, \tag{3.27}$$

with $n = (q + \nu L)\mathrm{mod}N$, $\nu = 0, \ldots, N/L-1$ and $q = 0, \ldots, Q-1$, (3.26) can be simplified to

$$\rho_q^{(k)} = \sum_{\nu=0}^{N/L-1} r_{(q+\nu L)\mathrm{mod}N} \cdot \Psi_{(q+\nu L)\mathrm{mod}N}^{(\nu,k)}. \tag{3.28}$$
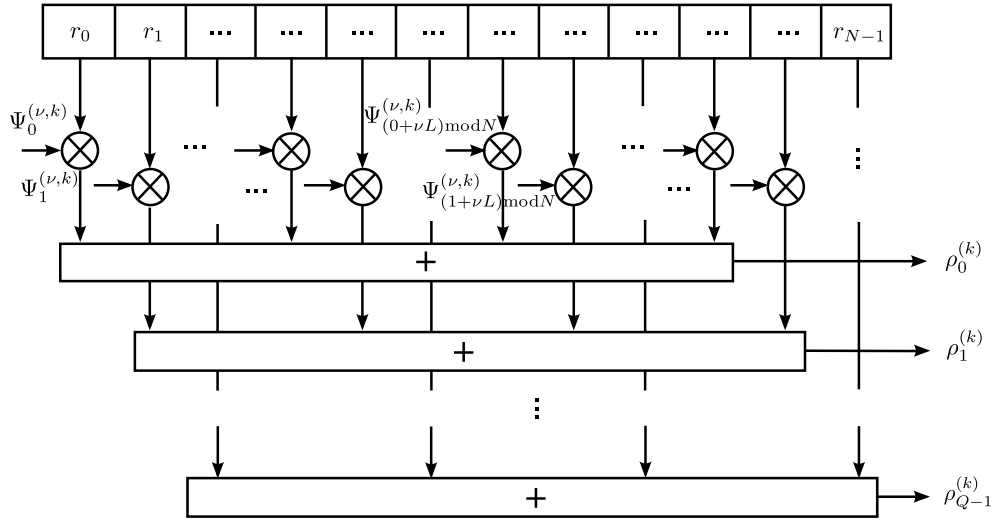
Figure 3.3: Time domain implementation for B-IFDMA demodulation

Equation (3.28) can be implemented as depicted in Figure 3.3. For each element $\rho_q^{(k)}$ of the demodulated signal, the N/L elements $r_{(q+\nu L)\mathrm{mod}N}$ from the received signal are multiplied with $\Psi_{(q+\nu L)\mathrm{mod}N}^{(\nu,k)}$ and summed up. Similar as for the modulation algorithm, the coefficients $\Psi_{(q+\nu L)\mathrm{mod}N}^{(\nu,k)}$ at the demodulator are independent from the data and, thus, can be calculated offline. Hence, the implementation of (3.28) requires $Q \cdot N/L = N \cdot M$ complex multiplications.

The time domain implementation of B-IFDMA demodulation according to (3.28) can be regarded as a generalization of the well known time domain implementation of IFDMA demodulation according to [SDBS98] and includes it as special case with $M = 1$.

Since OFDMA with block-interleaved subcarrier allocation can be regarded as IDFT pre-coded B-IFDMA, also the demodulator from (3.28) can be used for demodulation of OFDMA signals with block-interleaved subcarrier allocation by applying an additional Q-point DFT after demodulation.

3.2.5   Conclusions

In Section 3.2, new algorithms for B-IFDMA modulation and demodulation in time domain have been presented. The major results of the section can be summarized as follows:

- The presented algorithms exploit the symmetries contained in the B-IFDMA signal and provide a low computational complexity because they are based on a multiplication of the data symbols with complex numbers that can be calculated offline.

- The algorithm for B-IFDMA modulation in time domain shows that B-IFDMA can be considered as a superposition of M single carrier signals.

- As opposed to the implementation presented in Section 2.4, the efficient time domain implementation does not require the B-IFDMA signal parameters N and Q to be powers of 2.

- For the special case $M = 1$, a novel efficient implementation is presented that further reduces the computational complexity for modulation by factor 4.

- Due to the fact that B-IFDMA and OFDMA with block interleaved subcarrier allocation only differ in a DFT operation applied to the data symbols before modulation, the efficient algorithms for B-IFDMA can be also applied to OFDMA.

- The presented B-IFDMA time domain implementation represents a generalization of the respective algorithms for IFDMA modulation and demodulation.

3.3   Application of Space-Time Block-Codes to B-IFDMA

3.3.1   Introduction

In this section, the application of Space-Time Block-Codes (STBCs) to B-IFDMA is described. It is well known that the use of multiple antennas is an important technology to increase the spectral efficiency of a mobile radio system [FG98, PNG03]. For that reason, it is expected that in a future mobile radio system, a considerable number of mobile terminals will be equipped with more than one antenna [WIN05]. This is feasible because cross polarized antennas provide both, an effective decoupling of the antenna elements and compact physical dimensions. Hence, the application of multiple antenna techniques is possible even for small mobile phones [WIN05]. Further on, also mobile terminals in the form of laptops and personal digital assistants (PDAs) will be used that are appropriate for an integration of several spatially well separated antennas because the dimensions of these kinds of mobile terminals are in the order of several wavelengths [RP03].

Depending on whether or not channel state information is available, different multiple antenna techniques have to be used. As B-IFDMA is considered for the non-adaptive uplink, cf. Section 1.1.3, at the mobile terminal, multiple antenna techniques have to be applied that do not require channel state information at the transmitter side. Thus, the combination of B-IFDMA with multiple antenna techniques exploiting spatial diversity at the transmitter is a reasonable choice [PNG03].

Another important motivation for combining B-IFDMA with multiple antenna techniques providing spatial diversity is given by the fact that in future mobile radio applications the time diversity that can be exploited is limited. Time diversity is typically obtained at the expense of additional delays, e.g., by the application of channel coding and bit interleaving over several consecutive modulated data vectors. However, the delay constraints are tight because of delay critical services like online gaming etc. and due to the use of relay enhanced cells [WIN05]. Thus, besides frequency diversity, spatial diversity represents an important source of additional diversity.

In general, space-time coding can be regarded as an appropriate means for exploiting spatial diversity if channel knowledge at the transmitter is not available [PNG03]. Amongst the space-time codes (STCs), the STBCs have been attracting wide interest, especially for practical applications, because STBCs combine good performance with low effort for signal processing [Ala98, TJC99b]. Thus, in the following, the application of STBCs to B-IFDMA is considered.

Since B-IFDMA is aiming at the provision of low envelope fluctuations, cf. Section 2.4, the algorithm for an application of STBCs to B-IFDMA has to be designed such that the envelope of the B-IFDMA signal is not affected. Moreover, the algorithm for application of STBCs to B-IFDMA should

- provide low complexity, especially at the transmitter, in order to provide low cost for the mobile terminals,

- be applicable to the time domain implementation for B-IFDMA,

- be appropriate for a variety of STBCs,

- be appropriate for all special cases of B-IFDMA including B-IFDMA with $M = 1$, i.e. IFDMA,

- provide good performance for transmission over a mobile radio channel.

In this section, an approach is presented that fulfills the abovementioned requirements. The approach presented throughout this section has been published in [FKCK06] by the author of this thesis for the application of the Alamouti STBC to IFDMA.

Note that the implementation of multiple antenna techniques exploiting spatial diversity such as STBCs at the transmitter side can be complemented by the implementation of appropriate multiple antenna techniques such as SDMA at the receiver side. The application of SDMA at the base station will be regarded in Section 3.3 subsequent to the description of multiple antenna techniques at the transmitter side.

The remainder of this section is organized as follows: In Section 3.3.2, an overview of existing literature that is relevant for an application of STBCs to B-IFDMA is presented. In Section 3.3.3.1, a new space time encoder suitable for the application of various STBCs to B-IFDMA is presented. Due to the relevance of the Alamouti STBC for practical implementations, in Section 3.3.3.2, the space time encoder is formulated for the Alamouti STBC. The respective space time decoders are presented in Sections 3.3.4.1 and 3.3.4.2, respectively. In Section 3.3.5.1, an FDE for a joint compensation of the channels from the different transmit antennas to the receive antenna is presented that takes the coloration of the noise by the decoder of the STBC into account. Again, the particular formulation of the FDE for the Alamouti STBC is given in Section 3.3.5.2. Finally, Section 3.3.6 summarizes the major results of Section 3.3.

3.3.2   State-of-the-art

In the sequel, an overview of existing literature that is relevant for an application of STBCs to B-IFDMA is presented. Originally, STBCs such as introduced in [Ala98, TJC99b] have been proposed for single carrier transmission of the signal of one user over flat fading channels. The coding is applied to consecutive data symbols. For OFDM, the data symbols are transmitted simultaneously, but on adjacent subcarriers. However, the flat fading condition holds for each subcarrier. Thus, STBCs can be also applied to OFDM if the coding is applied to adjacent subcarriers. A respective approach that is denoted as Space Frequency Block Coding (SFBC) has been introduced in [BP00]. SFBC is originally formulated for a single user system, but in general, SFBC can be also applied to B-IFDMA. In contrast to OFDM, for B-IFDMA, the subcarriers carry the elements of the DFT of the data symbol vector $\mathbf{d}^{(k)}$ instead of the data symbols $d_q^{(k)}$, cf. Section 2.4. Thus, for application of SFBC to B-IFDMA, the codes have to be applied to the elements of the DFT of $\mathbf{d}^{(k)}$.

However, the application of SFBC requires a certain number $N_\mathrm{f} > 1$ of adjacent subcarriers providing identical channel conditions. E.g., for the Alamouti Code [Ala98], $N_\mathrm{f} = 2$ and for the code proposed in [GS01a], $N_\mathrm{f} = 4$ is required. Besides the fact that, due to the multi-path propagation, the channel changes in frequency direction, for B-IFDMA, different subcarriers are assigned to different users and, thus, for uplink transmission, the data at different subcarriers is transmitted over different channels. Hence, the application of SFBC to B-IFDMA results in constraints to the minimum possible number M of subcarriers per block, i.e., the condition $M \geq N_\mathrm{f}$ has to be fulfilled. Consequently, especially to B-IFDMA with M=1 SFBC cannot be applied at all.

Moreover, the encoding of the elements of the DFT of the B-IFDMA signal would affect the envelope of the transmit signal. E.g., for the Alamouti code, a pairwise exchange of the elements of the DFT of $\mathbf{d}^{(k)}$ is required, followed by taking the complex conjugate and an inversion of the sign of one element in every pair. Applying SFBC, due to the exchange of the elements of the DFT of $\mathbf{d}^{(k)}$, the resulting signal is no longer an authentic DFT pre-coded OFDMA signal. Thus, the envelope fluctuations of the signal are increased. Results for this effect are given in Appendix B.1. For the abovementioned reasons, an alternative solution for an application of STBCs to B-IFDMA is desired that avoids the disadvantages of the application of SFBC to B-IFDMA.

In [MP00], an approach for the application of Alamouti STBC to OFDM encoding groups of consecutive modulated data vectors has been described. However, an application of this technique to B-IFDMA would affect the envelope characteristics of the B-IFDMA transmit signal, because this approach requires a further DFT operation in addition to the DFT pre-coding. Thus, the approach from [MP00] is not appropriate for an application to B-IFDMA.

In [TIA04, AD01, ZG03], the application of STBCs to single-carrier schemes assigning all subcarriers to one user has been described. The approaches from [TIA04, AD01, ZG03] meet most of the requirements formulated in Section 3.3.1. However, since for B-IFDMA the subcarriers are assigned to different users, a modification of the approaches from [TIA04, AD01, ZG03] to the multi-user case is required. Moreover, in [TIA04, AD01], only the application of the Alamouti STBC is considered. The scheme presented in [ZG03] is formulated only for the application of rate 1/2 orthogonal STBCs. For application in a future mobile radio system, however, a more generic approach considering various STBCs that are not necessarily orthogonal and that are not restricted to rate 1/2 is desirable. Finally, for the MMSE equalizers presented in [TIA04, AD01, ZG03], white noise is assumed. However, this assumption is typically

Table 3.1: Comparison of STCs from relevant existing literature to the proposed approach.

reference	does not affect signal envelope	considers colored noise	considers subcarriers assigned to different users	formulated for
[BP00]	✘	✘	✘	STCs in general
[MP00]	✘	✘	✘	Alamouti STBC
[TIA04]	✔	✘	✘	Alamouti STBC
[AD01]	✔	✘	✘	Alamouti STBC
[ZG03]	✔	✘	✘	Alamouti STBC, orthogonal STBCs rate 1/2
new approach	✔	✔	✔	orth. and non-orth. STBCs, even with rate $\neq 1/2$

violated by the application of space-time decoding before equalization. Thus, in order to improve the performance, the coloration of the noise has to be considered.

The approach that is introduced in the following extends the approaches from [TIA04, AD01, ZG03] to the application of STBCs to B-IFDMA and is not limited to orthogonal STBCs with code rate 1/2. Thus, also STBCs with other rates such as given in [TJC99a, GS01b] and quasi-orthogonal STBCs such as described, e.g., in [PF01] can be applied. Moreover, an FDE based on the MMSE criterion is presented that takes the coloration of the noise into account. An overview and a comparison of the existing approaches with the new approach is given in Table 3.1.

3.3.3   Encoder

3.3.3.1   Generalized Encoder

In this section, a new approach for the application of various STBCs to B-IFDMA is described. The approach is based on applying the respective STBC to the elements of the DFTs of several data symbol vectors $\mathbf{d}^{(k)}$. In particular, the elements of the DFTs of a block of A consecutive data symbol vectors $\mathbf{d}^{(k)}$ are encoded. The encoded

elements of the DFTs are transmitted from n_T different transmit antennas and in N_t consecutive modulated data vectors. The code rate is, thus, given by

$$R = \frac{A}{N_t}. \tag{3.29}$$

It is assumed that the channel does not change for the duration of the transmission of N_t consecutive modulated data vectors. For the sake of simplicity and without loss of generality, in the following, $n_R = 1$ receive antenna is assumed. In order to distinguish the A consecutive data symbol vectors that are used for the STBC, throughout this section, an index a, $a = 0, \ldots, A - 1$, is introduced for the data symbol vector $\mathbf{d}^{(k)}$ and its DFT. Thus, (3.2) can be rewritten as

$$\mathbf{u}_a^{(k)} = \mathbf{F}_Q \cdot \mathbf{d}_a^{(k)}. \tag{3.30}$$

The encoding in space and time and a comparison to the single antenna case is illustrated in Figure 3.4. From Figure 3.4 it can be seen that, for the single antenna case, on the subcarriers of a certain user k, the elements $u_{a,q}^{(k)}$, $q = 0, \ldots, Q - 1$, of the DFT of $\mathbf{d}_a^{(k)}$ are transmitted. The code is applied to the A elements $u_{a,q}^{(k)}$ transmitted on the same subcarrier q but in different modulated data vectors, which is illustrated by the black double line. Thus, the elements $u_{a,q}^{(k)}$, at subcarrier q are encoded independently of the elements $u_{a,p}^{(k)}$, $p = 0, \ldots, Q - 1$ at subcarrier p for $p \neq q$. The A elements $u_{a,q}^{(k)}$ at subcarrier q are encoded in space and time. The encoded elements $c_{m,n,q}^{(k)}$ are, thus, transmitted on the same subcarrier, but in different modulated data vectors and from different antennas.

In the following, the encoding in space and time is described by a general STBC encoding matrix in the DFT domain. For that purpose, the encoded elements $c_{m,n,q}^{(k)}$ transmitted from the m-th transmit antenna, $m = 0, \ldots, n_T - 1$, and in the n-th modulated data vector, $n = 0, \ldots, N_t - 1$, are collected in a $Q \times 1$ vector

$$\mathbf{c}_{m,n}^{(k)} = \left[c_{m,n,0}^{(k)}, \ldots, c_{m,n,Q-1}^{(k)} \right]^T. \tag{3.31}$$

The vectors $\mathbf{c}_{m,n}^{(k)}$ can be organized in a matrix

$$\mathbf{C}^{(k)} = \begin{bmatrix} \mathbf{c}_{0,0}^{(k)} & \cdots & \mathbf{c}_{0,N_t-1}^{(k)} \\ \vdots & \ddots & \vdots \\ \mathbf{c}_{n_t-1,0}^{(k)} & \cdots & \mathbf{c}_{n_T-1,N_t-1}^{(k)} \end{bmatrix}. \tag{3.32}$$

Matric $\mathbf{C}^{(k)}$ is a general STBC encoding matrix that describes the encoded elements of the DFTs of the A vectors $\mathbf{d}_a^{(k)}$. The columns of matrix $\mathbf{C}^{(k)}$ describe the encoding in space, i.e., the vectors $\mathbf{c}_{m,n}^{(k)}$ that are transmitted from the n_T transmit antennas.
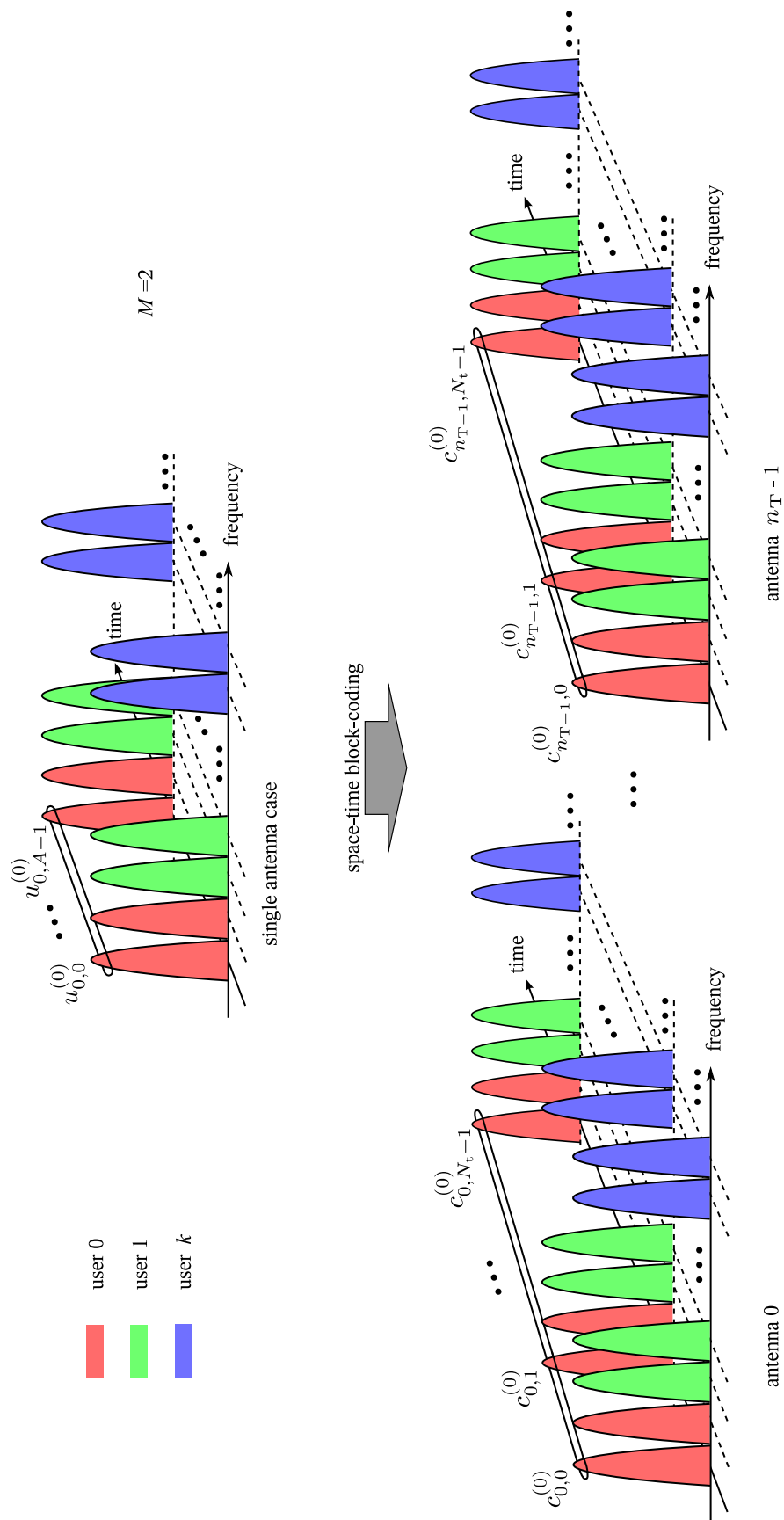
Figure 3.4: Illustration of the application of STBCs to B-IFDMA.

The rows of matrix $\mathbf{C}^{(k)}$ describe the encoding in time, i.e., the vectors $\mathbf{c}_{m,n}^{(k)}$ that are transmitted in N_{t} consecutive modulated data vectors. For B-IFDMA, the n-th modulated data vector $\mathbf{x}_{m,n}^{(k)}$ that is transmitted from the m-th transmit antenna applying a STBC described by the general encoding matrix $\mathbf{C}^{(k)}$ is, thus, given by

$$\mathbf{x}_{m,n}^{(k)} = \mathbf{F}_N^{\mathrm{H}} \cdot \mathbf{M}_{\mathrm{BI}}^{(k)} \cdot \mathbf{c}_{m,n}^{(k)}. \tag{3.33}$$

The relation between the vectors $\mathbf{c}_{m,n}^{(k)}$ and the data symbol vectors $\mathbf{d}_a^{(k)}$ depends on the STBC that is used. However, for a variety of STBCs, the relation between the vectors $\mathbf{c}_{m,n}^{(k)}$ and the data symbol vectors $\mathbf{d}_a^{(k)}$ provides similarities. In the following, a generic description for the relation between the vectors $\mathbf{c}_{m,n}^{(k)}$ and the data symbol vectors $\mathbf{d}_a^{(k)}$ is given that can be applied to various STBCs. In order to give a generic description of the relation between $\mathbf{c}_{m,n}^{(k)}$ and $\mathbf{d}_a^{(k)}$, in the sequel, some set definitions are introduced. Let

$$\mathcal{V} = \{(m,n)|m = 0,\ldots,n_{\mathrm{T}}-1; n = 0,\ldots,N_{\mathrm{T}}-1\} \tag{3.34}$$

denote the set of all possible couples (m,n) and let

$$\mathcal{V}_1 \subseteq \mathcal{V} \tag{3.35}$$

denote a subset of $\mathcal{V}$ that is dependent on the considered STBC. Let, finally,

$$\mathcal{V}_2 = \mathcal{V} \setminus \mathcal{V}_1 \tag{3.36}$$

denote the relative complement of $\mathcal{V}_1$ in $\mathcal{V}$. Thus, for a variety of STBCs the relation between vectors $\mathbf{c}_{m,n}^{(k)}$ and $\mathbf{d}_a^{(k)}$ can be expressed in the form of

$$\mathbf{c}_{m,n}^{(k)} = \begin{cases} f_{m,n} \cdot \mathbf{u}_a^{(k)} & = & f_{m,n} \cdot \mathbf{F}_{\mathrm{Q}} \cdot \mathbf{d}_a^{(k)} & \text{for } (m,n) \in \mathcal{V}_1 \\ f_{m,n} \cdot \left(\mathbf{u}_a^{(k)}\right)^* & = & f_{m,n} \cdot \left(\mathbf{F}_{\mathrm{Q}} \cdot \mathbf{d}_a^{(k)}\right)^* & \text{for } (m,n) \in \mathcal{V}_2 \end{cases}, \tag{3.37}$$

where $f_{m,n}$ represents a real-valued weighting factor and the relation between m, n and a is given by the respective STBC.

Matrix $\mathbf{C}^{(k)}$ describes the encoding of the elements of the DFTs of the A vectors $\mathbf{d}_a^{(k)}$. Thus, an implementation of the encoding in space and time according to (3.32) and (3.37) requires access to the respective elements of the DFTs. However, using the time domain implementation from Section 3.2, for B-IFDMA, access to the elements of the DFTs of $\mathbf{d}_a^{(k)}$ is not provided. Thus, in the following, an equivalent matrix is derived that describes the encoding in space and time for the data symbol vectors $\mathbf{d}_a^{(k)}$. For that purpose, a Q-point IDFT is applied to the vectors $\mathbf{c}_{m,n}^{(k)}$ in matrix $\mathbf{C}^{(k)}$.

The resulting $Q \times 1$ vectors $\boldsymbol{\xi}_{m,n}^{(k)}$ are given by

$$\boldsymbol{\xi}_{m,n}^{(k)} = \begin{cases} f_{m,n} \cdot \mathbf{F}_Q^{\mathrm{H}} \cdot \mathbf{F}_Q \cdot \mathbf{d}_a^{(k)} &= f_{m,n} \cdot \mathbf{d}_a^{(k)} & \text{for} \quad (m,n) \in \mathcal{V}_1 \\ f_{m,n} \cdot \mathbf{F}_Q^{\mathrm{H}} \cdot \left(\mathbf{F}_Q \cdot \bar{\mathbf{d}}_a^{(k)} \right)^* &= \mathbf{F}_Q^{\mathrm{H}} \cdot \mathbf{F}_Q^{\mathrm{H}} \cdot \left(\mathbf{d}_a^{(k)} \right)^* & \text{for} \quad (m,n) \in \mathcal{V}_2 \end{cases} . \quad (3.38)$$

As

$$\mathbf{F}_Q^{\mathrm{H}} \cdot \mathbf{F}_Q^{\mathrm{H}} \cdot \mathbf{d}_a^{(k)} = \bar{\mathbf{d}}_a^{(k)}, \quad (3.39)$$

with

$$\bar{\mathbf{d}}^{(k)} = \left[d_{a,0}^{(k)}, d_{a,Q}^{(k)}, d_{a,Q-1}^{(k)}, \ldots, d_{a,1}^{(k)} \right]^{\mathrm{T}} \quad (3.40)$$

denoting a permuted version of the the data symbol vector $\mathbf{d}_a^{(k)}$, the vectors $\boldsymbol{\xi}_{m,n}^{(k)}$ can be simplified to

$$\boldsymbol{\xi}_{m,n}^{(k)} = \begin{cases} f_{m,n} \cdot \mathbf{d}_a^{(k)} & \text{for} \quad (m,n) \in \mathcal{V}_1 \\ f_{m,n} \cdot \left(\bar{\mathbf{d}}_a^{(k)} \right)^* & \text{for} \quad (m,n) \in \mathcal{V}_2 \end{cases} . \quad (3.41)$$

Similar as in (3.32), the vectors $\boldsymbol{\xi}_{m,n}^{(k)}$ can be organized in a matrix $\boldsymbol{\Xi}^{(k)}$ that is given by

$$\boldsymbol{\Xi}^{(k)} = \begin{bmatrix} \boldsymbol{\xi}_{0,0}^{(k)} & \cdots & \boldsymbol{\xi}_{0,N_{\mathrm{t}}-1}^{(k)} \\ \vdots & \ddots & \vdots \\ \boldsymbol{\xi}_{n_{\mathrm{t}}-1,0}^{(k)} & \cdots & \boldsymbol{\xi}_{n_{\mathrm{T}}-1,N_{\mathrm{t}}-1}^{(k)} \end{bmatrix}. \quad (3.42)$$

With (3.38), the expression for the modulated data vector $\mathbf{x}_{m,n}^{(k)}$ given in (3.33) can be modified to

$$\mathbf{x}_{m,n}^{(k)} = \underbrace{\mathbf{F}_N^{\mathrm{H}} \cdot \mathbf{M}_{\mathrm{BI}}^{(k)} \cdot \mathbf{F}_Q}_{\text{B-IFDMA modulation}} \cdot \boldsymbol{\xi}_{m,n}^{(k)}. \quad (3.43)$$

From (3.43) it can be seen that, compared to single antenna transmission as described in (2.39), the application of a STBC to B-IFDMA requires just to replace the data symbol vector $\mathbf{d}^{(k)}$ by the encoded data symbol vectors $\boldsymbol{\xi}_{m,n}^{(k)}$ and is independent from the implementation that is used for B-IFDMA modulation. Moreover, the application of STBC to B-IFDMA according to (3.43) does not require access to the elements of the DFTs of $\mathbf{d}_a^{(k)}$ as it is the case for an implementation according to (3.33).

From (3.38) it can be seen that the encoding in space and time according to (3.43) can be implemented in a computationally efficient way: According to (3.38), only a multiplication by factor $f_{m,n}$, a permutation of the elements of the data vector $\mathbf{d}_a^{(k)}$ and taking the complex conjugate of the data symbols $d_{a,q}^{(k)}$ is required. Note that, for many codes, $f_{m,n} \in \{-1; 1\}$ holds, cf. [PNG03], and, thus, the multiplication with $f_{m,n}$ reduces to switching the sign of the data symbols $d_{a,q}^{(k)}$. As $\bar{\mathbf{d}}_a^{(k)}$ consists of the same elements as $\mathbf{d}_a^{(k)}$, hence, even for application of a STBC, the transmit signal at each transmit antenna provides the same signal envelope as the transmit signal for single

antenna transmission as long as $|f_{m,n}| = 1$. As the presented approach for application of STBCs is based on encoding the elements of the DFTs of $\mathbf{d}_a^{(k)}$ that are transmitted on the same subcarrier, the approach can be also applied to B-IFDMA with $M = 1$ subcarrier per block.

3.3.3.2 Alamouti Encoder

In the following, from the general STBC encoding matrix of (3.32), the STBC encoding matrix for the special case $n_{\mathrm{T}} = 2$ using the well-known Alamouti STBC [Ala98] is derived. This case is of particular interest because many future user terminals are expected to be equipped with 2 cross-polarized antennas [WIN05].

For the Alamouti STBC, $A = N_{\mathrm{t}} = n_{\mathrm{T}} = 2$. Thus, the code rate is $R = 1$. Further on, $\mathcal{V}_1$ of (3.35) and $\mathcal{V}_2$ of (3.36) are given by

$$\mathcal{V}_1 = \{(0,0), (1,0)\} \tag{3.44}$$

and

$$\mathcal{V}_2 = \{(0,1), (1,1)\}, \tag{3.45}$$

respectively. Finally,

$$f_{0,0} = f_{1,0} = f_{1,1} = 1 \tag{3.46}$$

and

$$f_{0,1} = -1. \tag{3.47}$$

Thus, with (3.37), for the Alamouti code, matrix $\mathbf{C}^{(k)}$ of (3.32) is given by

$$\mathbf{C}^{(k)} = \left[\begin{array}{cc} \mathbf{u}_0^{(k)} & -\left(\mathbf{u}_1^{(k)}\right)^* \\ \mathbf{u}_1^{(k)} & \left(\mathbf{u}_0^{(k)}\right)^* \end{array} \right] \tag{3.48}$$

with $\mathbf{u}_a^{(k)}$ of (3.30). Consequently, with (3.38) to (3.41), matrix $\mathbf{\Xi}^{(k)}$ of (3.42) is given by

$$\mathbf{\Xi}^{(k)} = \left[\begin{array}{cc} \mathbf{d}_0^{(k)} & -\left(\bar{\mathbf{d}}_1^{(k)}\right)^* \\ \mathbf{d}_1^{(k)} & \left(\bar{\mathbf{d}}_0^{(k)}\right)^* \end{array} \right]. \tag{3.49}$$

The encoding in space and time according to matrix $\mathbf{\Xi}^{(k)}$ in (3.49) can be interpreted as follows. Let $\mathbf{x}_{m,n}^{(k)}$ denote the n-th modulated data vector that is transmitted from the m-th transmit antenna according to (3.43). Thus, for the application of the Alamouti STBC to B-IFDMA, in order to obtain the first modulated data vector $\mathbf{x}_{0,0}^{(k)}$ to be transmitted from the first transmit antenna, B-IFDMA modulation has to be applied

to $\mathbf{d}_0^{(k)}$. At the same time, in order to obtain $\mathbf{x}_{1,0}^{(k)}$ at the second transmit antenna, B-IFDMA modulation has to be applied to $\mathbf{d}_1^{(k)}$. Further on, in order to obtain the second modulated data vector $\mathbf{x}_{0,1}^{(k)}$ to be transmitted from the first transmit antenna, B-IFDMA modulation has to be applied to $-\left(\bar{\mathbf{d}}_1^{(k)}\right)^*$. At the same time, in order to obtain $\mathbf{x}_{1,1}^{(k)}$ at the second transmit antenna, B-IFDMA modulation has to be applied to $\left(\bar{\mathbf{d}}_0^{(k)}\right)^*$. The resulting approach for the application of the Alamouti STBC to B-IFDMA is depicted in Figure 3.5. It requires only low additional computational effort compared to the single antenna transmission because only a switching of the signs, taking the complex conjugate and a permutation of the data symbols $d_{a,q}^{(k)}$ is required.

Further examples for the STBC encoding matrices of orthogonal and non-orthogonal STBCs with different code rates are given in Appendix B.2.
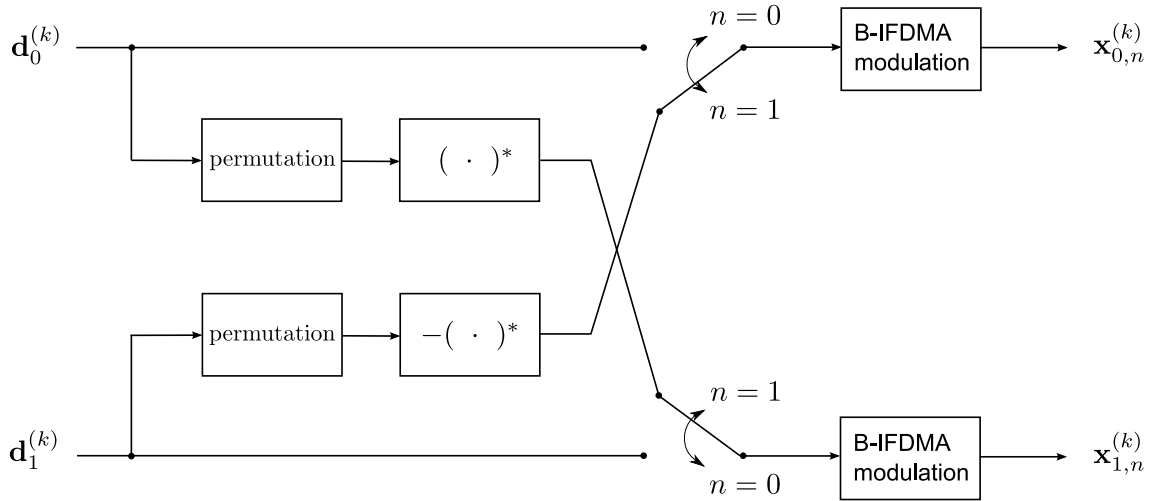
Figure 3.5: Application of Alamouti STBC to B-IFDMA. $\mathbf{x}_{0,n}^{(k)}$ and $\mathbf{x}_{1,n}^{(k)}$ denote the n-th modulated data vector at the first and the second transmit antenna, respectively.

3.3.4   Decoder

3.3.4.1   Generalized Decoder

In general, the decoders for different STBCs have to be designed individually. However, for orthogonal STBCs, a generalized decoder that corresponds to the encoder from Section 3.3.3.1 can be described. In the following, this generalized encoder is introduced.

Let $\mathbf{H}_m^{(k)}$ denote the channel matrix of the channel between the m-th transmit antenna and the receive antenna defined according to the channel matrix $\mathbf{H}^{(k)}$ introduced in Section 2.3.4. Analogous to (2.7), the n-th received data vector $\mathbf{r}_n$ is given by

$$\mathbf{r}_n = \sum_{k=0}^{K-1} \sum_{m=0}^{n_T-1} \mathbf{H}_m^{(k)} \cdot \mathbf{F}_N^{\mathrm{H}} \cdot \mathbf{M}_{\mathrm{BI}}^{(k)} \cdot \mathbf{c}_{m,n}^{(k)} + \mathbf{n}_n, \tag{3.50}$$

with $\mathbf{c}_{m,n}^{(k)}$ of (3.31) and with $\mathbf{n}_n$ denoting the the n-th AWGN vector defined according to (2.5).

In the following, the n-th received vector $\bar{\mathbf{v}}_n^{(k)}$ of user k in frequency domain after user separation is regarded. Analogous to (3.21),

$$\bar{\mathbf{v}}_n^{(k)} = \left[\bar{v}_{n,0}^{(k)}, \ldots, \bar{v}_{n,Q-1}^{(k)} \right]^{\mathrm{T}} \tag{3.51}$$

is given by

$$\bar{\mathbf{v}}_n^{(k)} = \left(\mathbf{M}_{\mathrm{BI}}^{(k)} \right)^{\dagger} \cdot \mathbf{F}_N \cdot \mathbf{r}_n. \tag{3.52}$$

Assuming that the subcarriers are perfectly orthogonal, the decoding at a subcarrier with index q is independent from the decoding at other subcarriers. Thus, in the following, the description of the decoding algorithm can be reduced to a single subcarrier. In order to obtain a simple expression for the relation between a certain element $\bar{v}_{n,q}^{(k)}$ of $\bar{\mathbf{v}}_n^{(k)}$ and the respective elements $c_{m,n,q}^{(k)}$ of $\mathbf{c}_{m,n}^{(k)}$, an expression for the overall channel $\Gamma_{m,q}^{(k)}$ of user k from the m-th transmit antenna to the receive antenna at subcarrier q is defined analogous to (2.30). This expression is given by replacing the channel vector $\bar{\mathbf{h}}^{(k)}$ in (2.30) by the channel vector $\bar{\mathbf{h}}_m^{(k)}$ denoting the channel between the m-th transmit antenna and the receive antenna and results in

$$\begin{bmatrix} \Gamma_{0,m}^{(k)} \\ \vdots \\ \Gamma_{Q-1,m}^{(k)} \end{bmatrix} = \left(\mathbf{M}_{\mathrm{BI}}^{(k)} \right)^{\dagger} \cdot \mathbf{F}_N \cdot \bar{\mathbf{h}}_m^{(k)} \tag{3.53}$$

with $\mathbf{M}_{\mathrm{BI}}^{(k)}$ of (2.37).

Let

$$\bar{\mathbf{n}}_n^{(k)} = \left[\bar{n}_{n,0}^{(k)}, \ldots, \bar{n}_{n,Q-1}^{(k)} \right]^{\mathrm{T}} \tag{3.54}$$

denote the noise part of $\bar{\mathbf{v}}_n^{(k)}$ with

$$\bar{\mathbf{n}}_n^{(k)} = \left(\mathbf{M}_{\mathrm{BI}}^{(k)} \right)^{\dagger} \cdot \mathbf{F}_N \cdot \mathbf{n}_n. \tag{3.55}$$

Thus, from insertion of (3.50) in (3.52) follows that the elements $\bar{v}_{n,q}^{(k)}$ of $\bar{\mathbf{v}}_n^{(k)}$ are given by

$$\bar{v}_{n,q}^{(k)} = \sum_{m=0}^{n_T-1} \Gamma_{m,q}^{(k)} \cdot c_{m,n,q}^{(k)} + \bar{n}_{n,q}^{(k)} \tag{3.56}$$

with $c_{m,n,q}^{(k)}$ of (3.31). Defining

$$\bar{\mathbf{v}}_q^{(k)} = \left[\bar{v}_{0,q}^{(k)}, \ldots, \bar{v}_{N_t-1,q}^{(k)}\right]^{\mathrm{T}}, \tag{3.57}$$

$$\mathbf{\Gamma}_q^{(k)} = \left[\Gamma_{0,q}^{(k)}, \ldots, \Gamma_{n_{\mathrm{T}}-1,q}^{(k)}\right]^{\mathrm{T}}, \tag{3.58}$$

$$\mathbf{C}_q^{(k)} = \begin{bmatrix} c_{0,0,q}^{(k)} & \cdots & c_{0,N_t-1,q}^{(k)} \\ \vdots & \ddots & \vdots \\ c_{n_t-1,0,q}^{(k)} & \cdots & c_{n_{\mathrm{T}}-1,N_t-1,q}^{(k)} \end{bmatrix}, \tag{3.59}$$

and

$$\bar{\mathbf{n}}_q^{(k)} = \left[\bar{n}_{0,q}^{(k)}, \ldots, \bar{n}_{N_t-1,q}^{(k)}\right]^{\mathrm{T}}, \tag{3.60}$$

(3.56) can rewritten as

$$\left(\bar{\mathbf{v}}_q^{(k)}\right)^{\mathrm{T}} = \left(\mathbf{\Gamma}_q^{(k)}\right)^{\mathrm{T}} \cdot \mathbf{C}_q^{(k)} + \left(\bar{\mathbf{n}}_q^{(k)}\right)^{\mathrm{T}}. \tag{3.61}$$

In order to obtain generalized expressions that are valid for the different orthogonal STBCs, it is common to regard the real part and the imaginary part of the encoded signals separately, cf. [LS03]. Thus, in the following, the matrix $\mathbf{C}_q^{(k)}$ is decomposed into expressions that describe its real and imaginary part, respectively. Let

$$\breve{u}_{a,q}^{(k)} = \mathrm{Re}\left\{u_{a,q}^{(k)}\right\} \tag{3.62}$$

and

$$\tilde{u}_{a,q}^{(k)} = \mathrm{Im}\left\{u_{a,q}^{(k)}\right\} \tag{3.63}$$

denote the real and the imaginary part of the elements $u_{a,q}^{(k)}$ of the DFT pre-coded data vector $\mathbf{d}_a^{(k)}$, respectively. Let, further on, $\mathbf{K}_a$ and $\mathbf{L}_a$ denote $n_{\mathrm{T}} \times N_t$ matrices that, dependent on the STBC that is regarded, describe the encoding in space and time of the real part $\breve{u}_{a,q}^{(k)}$ and the imaginary part $\tilde{u}_{a,q}^{(k)}$, respectively. In particular, dependent on the STBC that is regarded, the matrix $\mathbf{K}_a$ describes from which antennas and in which modulated data vectors the real part of $u_{a,q}^{(k)}$ has to be transmitted. The matrix $\mathbf{L}_a$ describes the same for the imaginary part of $u_{a,q}^{(k)}$. Thus, the STBC encoding matrix $\mathbf{C}_q^{(k)}$ can be can be written as follows:

$$\mathbf{C}_q^{(k)} = \sum_{a=0}^{A-1} \left(\mathbf{K}_a \cdot \breve{u}_{a,q}^{(k)} + j \cdot \mathbf{L}_a \cdot \tilde{u}_{a,q}^{(k)}\right). \tag{3.64}$$

In the following, the description of matrix $\mathbf{C}_q^{(k)}$ according to (3.64) is used in order to give the relation between $\bar{v}_{n,q}^{(k)}$, $\breve{u}_{a,q}^{(k)}$ and $\tilde{u}_{a,q}^{(k)}$. For that purpose, let

$$\mathbf{B}_{\mathrm{Re},q}^{(k)} = \left[\left(\left(\mathbf{\Gamma}_q^{(k)}\right)^{\mathrm{T}} \cdot \mathbf{K}_0\right)^{\mathrm{T}}, \ldots, \left(\mathbf{\Gamma}_q^{(k)} \cdot \mathbf{K}_{A-1}\right)^{\mathrm{T}}\right] \tag{3.65}$$

and

$$\mathbf{B}_{\mathrm{Im},q}^{(k)} = \left[\left(\left(\mathbf{\Gamma}_q^{(k)} \right)^{\mathrm{T}} \cdot \mathbf{L}_0 \right)^{\mathrm{T}}, \ldots, \left(\mathbf{\Gamma}_q^{(k)} \cdot \mathbf{L}_{A-1} \right)^{\mathrm{T}} \right]. \tag{3.66}$$

The $1 \times N_{\mathrm{t}}$ vector $\left(\mathbf{\Gamma}_q^{(k)} \right)^{\mathrm{T}} \cdot \mathbf{K}_a$ respresents the vector of overall channel coefficients the real part of $u_{a,q}^{(k)}$ is multiplied with during transmission in the n-th modulated data vector. The $1 \times N_{\mathrm{t}}$ vector $\left(\mathbf{\Gamma}_q^{(k)} \right)^{\mathrm{T}} \cdot \mathbf{L}_a$ represents the same for the imaginary part of $u_{a,q}^{(k)}$.

Finally, let

$$\breve{\mathbf{u}}_q^{(k)} = \left[\breve{u}_{0,q}^{(k)}, \ldots, \breve{u}_{A-1,q}^{(k)} \right]^{\mathrm{T}} \tag{3.67}$$

and

$$\tilde{\mathbf{u}}_q^{(k)} = \left[\tilde{u}_{0,q}^{(k)}, \ldots, \tilde{u}_{A-1,q}^{(k)} \right]^{\mathrm{T}} \tag{3.68}$$

denote vectors stacking the A elements $\breve{u}_{a,q}^{(k)}$ and $\tilde{u}_{a,q}^{(k)}$, respectively, at subcarrier q.

With the above introduced definitions, (3.61) can be rewritten as

$$\bar{\mathbf{v}}_q^{(k)} = \mathbf{B}_{\mathrm{Re},q}^{(k)} \cdot \breve{\mathbf{u}}_q^{(k)} + j \cdot \mathbf{B}_{\mathrm{Im},q}^{(k)} \cdot \tilde{\mathbf{u}}_q^{(k)} + \bar{\mathbf{n}}_q^{(k)}. \tag{3.69}$$

Equation (3.69) can be interpreted as follows. Vector $\bar{\mathbf{v}}_q^{(k)}$ describes the N_{t} elements of the DFT of the received signal of user k at subcarrier q. The right side of (3.69) gives the dependency of $\bar{\mathbf{v}}_q^{(k)}$ from the real part $\breve{\mathbf{u}}_q^{(k)}$ and from the imaginary part $\tilde{\mathbf{u}}_q^{(k)}$ of the elements of the DFT of the data symbols $d_{a,q}^{(k)}$ of user k at subcarrier q. Dependent on the STBC, real part and imaginary part of the elements of the DFT of the data symbols $d_{a,q}^{(k)}$ are transmitted from different antennas and in different modulated data vectors and, consequently, weighted by different channel coefficients $\Gamma_{m,q}^{(k)}$. These channel coefficients $\Gamma_{m,q}^{(k)}$ are contained in the matrices $\mathbf{B}_{\mathrm{Re},q}^{(k)}$ and $\mathbf{B}_{\mathrm{Im},q}^{(k)}$, respectively. Finally, $\bar{\mathbf{n}}_q^{(k)}$ describes the noise at subcarrier q of user k.

With

$$\mathbf{B}_q^{(k)} = \left[\mathbf{B}_{\mathrm{Re},q}^{(k)}, j \cdot \mathbf{B}_{\mathrm{Im},q}^{(k)} \right], \tag{3.70}$$

(3.69) can be simplified to

$$\bar{\mathbf{v}}_q^{(k)} = \mathbf{B}_q^{(k)} \cdot \begin{bmatrix} \breve{\mathbf{u}}_q^{(k)} \\ \tilde{\mathbf{u}}_q^{(k)} \end{bmatrix} + \bar{\mathbf{n}}_q^{(k)}. \tag{3.71}$$

Introducing the abbreviation

$$\breve{\mathbf{u}}_q^{(k)} = \begin{bmatrix} \breve{\mathbf{u}}_q^{(k)} \\ \tilde{\mathbf{u}}_q^{(k)} \end{bmatrix}, \tag{3.72}$$

(3.71) can be simplified to

$$\bar{\mathbf{v}}_q^{(k)} = \mathbf{B}_q^{(k)} \cdot \check{\mathbf{u}}_q^{(k)} + \bar{\mathbf{n}}_q^{(k)}. \tag{3.73}$$

In (3.73), each element $\bar{v}_{m,q}^{(k)}$ of $\bar{\mathbf{v}}_q^{(k)}$ depends on several elements of the vector $\check{\mathbf{u}}_q^{(k)}$ because, in general, several elements in a row of matrix $\mathbf{B}_q^{(k)}$ are non-zero. However, for any orthogonal STBC, at the receiver side, the elements of the vector $\check{\mathbf{u}}_q^{(k)}$ can be decoupled by a transformation of matrix $\mathbf{B}_q^{(k)}$ to a diagonal matrix [LS03]. This transformation makes the application of an algorithm possible that provides low computational complexity for data estimation. The decoupling of the elements of vector $\check{\mathbf{u}}_q^{(k)}$ is denoted as space-time decoding [LS03].

In the following, the transformation of matrix $\mathbf{B}_q^{(k)}$ in (3.71) to a diagonal matrix is described. For any orthogonal STBC, the transformation of matrix $\mathbf{B}_q^{(k)}$ to a diagonal matrix can be achieved by multiplication from the left with $\left(\mathbf{B}_q^{(k)}\right)^{\mathrm{H}}$ and taking the real part, i.e., by $\mathrm{Re}\left\{\left(\mathbf{B}_q^{(k)}\right)^{\mathrm{H}} \cdot \mathbf{B}_q^{(k)}\right\}$, cf. [LS03]. In its upper half, the resulting $2A \times 2A$ diagonal matrix

$$\boldsymbol{\Delta}_q^{(k)} = \mathrm{Re}\left\{\left(\mathbf{B}_q^{(k)}\right)^{\mathrm{H}} \cdot \mathbf{B}_q^{(k)}\right\} \tag{3.74}$$

carries the sum of the absolute values squared of the elements of vector $\left(\boldsymbol{\Gamma}_q^{(k)}\right)^{\mathrm{T}} \cdot \mathbf{K}_a$ on its main diagonal. In its lower half, it carries the sum of the absolute values squared of the elements of vector $\left(\boldsymbol{\Gamma}_q^{(k)}\right)^{\mathrm{T}} \cdot \mathbf{L}_a$ on its main diagonal.

With (3.74) and exploiting the fact that the elements of the vector $\check{\mathbf{u}}_q^{(k)}$ are real-valued, a decoupling of the elements of $\check{\mathbf{u}}_q^{(k)}$ can be obtained by multiplication of (3.71) from the left with $\left(\mathbf{B}_q^{(k)}\right)^{\mathrm{H}}$ and taking the real part of the resulting expression. Thus, STBC decoding for B-IFDMA is given by

$$\begin{aligned}
\mathrm{Re}\left\{\left(\mathbf{B}_q^{(k)}\right)^{\mathrm{H}} \cdot \bar{\mathbf{v}}_q^{(k)}\right\} &= \mathrm{Re}\left\{\left(\mathbf{B}_q^{(k)}\right)^{\mathrm{H}} \cdot \mathbf{B}_q^{(k)}\right\} \cdot \check{\mathbf{u}}_q^{(k)} + \mathrm{Re}\left\{\left(\mathbf{B}_q^{(k)}\right)^{\mathrm{H}} \cdot \bar{\mathbf{n}}_q^{(k)}\right\} \\
&= \boldsymbol{\Delta}_q^{(k)} \cdot \check{\mathbf{u}}_q^{(k)} + \bar{\mathbf{w}}_q^{(k)},
\end{aligned} \tag{3.75}$$

where

$$\bar{\mathbf{w}}_q^{(k)} = \mathrm{Re}\left\{\left(\mathbf{B}_q^{(k)}\right)^{\mathrm{H}} \cdot \bar{\mathbf{n}}_q^{(k)}\right\}. \tag{3.76}$$

Equation (3.75) gives a description of STBC decoding at subcarrier q. In order to describe the decoding from (3.75) jointly for all subcarriers, let

$$\mathbf{B}^{(k)} = \left[\left(\mathbf{B}_0^{(k)}\right)^{\mathrm{T}}, \ldots, \left(\mathbf{B}_{Q-1}^{(k)}\right)^{\mathrm{T}}\right]^{\mathrm{T}}, \tag{3.77}$$

$$\bar{\boldsymbol{\nu}}^{(k)} = \left[\left(\bar{\mathbf{v}}_0^{(k)}\right)^{\mathrm{T}}, \ldots, \left(\bar{\mathbf{v}}_{Q-1}^{(k)}\right)^{\mathrm{T}}\right]^{\mathrm{T}}, \tag{3.78}$$

$$\boldsymbol{\Delta}^{(k)} = \begin{bmatrix} \boldsymbol{\Delta}_0^{(k)} & \mathbf{0}_{2A \times 2A} & \ldots & \mathbf{0}_{2A \times 2A} \\ \mathbf{0}_{2A \times 2A} & \ddots & \ldots & \mathbf{0}_{2A \times 2A} \\ \vdots & \ldots & \ddots & \vdots \\ \mathbf{0}_{2A \times 2A} & \ldots & \mathbf{0}_{2A \times 2A} & \boldsymbol{\Delta}_{Q-1}^{(k)} \end{bmatrix}, \tag{3.79}$$

$$\breve{\mathbf{u}}^{(k)} = \left[\left(\breve{\mathbf{u}}_0^{(k)} \right)^{\mathrm{T}}, \ldots, \left(\breve{\mathbf{u}}_{Q-1}^{(k)} \right)^{\mathrm{T}} \right]^{\mathrm{T}}, \tag{3.80}$$

and

$$\bar{\mathbf{w}}^{(k)} = \left[\left(\bar{\mathbf{w}}_0^{(k)} \right)^{\mathrm{T}}, \ldots, \left(\bar{\mathbf{w}}_{Q-1}^{(k)} \right)^{\mathrm{T}} \right]^{\mathrm{T}}, \tag{3.81}$$

where $\mathbf{0}_{2A \times 2A}$ denotes a $2A \times 2A$ matrix with all elements equal to zero.

With (3.77)-(3.81), (3.75) can be rewritten as

$$\mathrm{Re}\left\{ \left(\mathbf{B}^{(k)} \right)^{\mathrm{H}} \cdot \bar{\boldsymbol{\nu}}^{(k)} \right\} = \boldsymbol{\Delta}^{(k)} \cdot \breve{\mathbf{u}}^{(k)} + \bar{\mathbf{w}}^{(k)}. \tag{3.82}$$

Note that due to the multiplication with $\left(\mathbf{B}^{(k)} \right)^{\mathrm{H}}$, the noise $\bar{\mathbf{w}}^{(k)}$ in (3.82) is no longer white, because the matrices $\mathbf{B}_q^{(k)}$ in $\mathbf{B}^{(k)}$ depend on $\boldsymbol{\Gamma}_q^{(k)}$ and, thus, are different for different subcarriers q.

3.3.4.2 Alamouti Decoder

In the following, the application of the Alamouti decoder is described for the special case $n_{\mathrm{T}} = 2$. From matrix $\mathbf{C}^{(k)}$ of (3.48) follows that, for the Alamouti STBC, the matrix $\mathbf{C}_q^{(k)}$ of (3.59) is given by

$$\mathbf{C}_q^{(k)} = \begin{bmatrix} u_{0,q}^{(k)} & -\left(u_{1,q}^{(k)} \right)^* \\ u_{0,q}^{(k)} & \left(u_{0,q}^{(k)} \right)^* \end{bmatrix}. \tag{3.83}$$

Thus, for Alamouti STBC, (3.61) is given by

$$\left[\bar{v}_{0,q}^{(k)}, \bar{v}_{1,q}^{(k)} \right] = \left[\Gamma_{0,q}^{(k)}, \Gamma_{0,q}^{(k)} \right] \cdot \begin{bmatrix} u_{0,q}^{(k)} & -\left(u_{1,q}^{(k)} \right)^* \\ u_{0,q}^{(k)} & \left(u_{0,q}^{(k)} \right)^* \end{bmatrix} + \left[\bar{n}_{0,q}^{(k)}, \bar{n}_{1,q}^{(k)} \right]. \tag{3.84}$$

From (3.83) follows that, with (3.64), the matrices $\mathbf{K}_a$ and $\mathbf{L}_a$, $a = 0, \ldots, 1$, are given by

$$\mathbf{K}_0 = \begin{bmatrix} 1 & 0 \\ 0 & 1 \end{bmatrix}, \tag{3.85}$$

$$\mathbf{K}_1 = \begin{bmatrix} 0 & -1 \\ 1 & 0 \end{bmatrix}, \tag{3.86}$$

$$\mathbf{L}_0 = \begin{bmatrix} 1 & 0 \\ 0 & -1 \end{bmatrix}, \tag{3.87}$$

and

$$\mathbf{L}_1 = \begin{bmatrix} 0 & 1 \\ -1 & 0 \end{bmatrix}. \tag{3.88}$$

Thus, $\mathbf{B}_{\mathrm{Re},q}^{(k)}$ of (3.65) and $\mathbf{B}_{\mathrm{Im},q}^{(k)}$ of (3.66) result in

$$\mathbf{B}_{\mathrm{Re},q}^{(k)} = \begin{bmatrix} \Gamma_{0,q}^{(k)} & \Gamma_{1,q}^{(k)} \\ \Gamma_{1,q}^{(k)} & -\Gamma_{0,q}^{(k)} \end{bmatrix} \tag{3.89}$$

and

$$\mathbf{B}_{\mathrm{Im},q}^{(k)} = \begin{bmatrix} \Gamma_{0,q}^{(k)} & -\Gamma_{1,q}^{(k)} \\ -\Gamma_{1,q}^{(k)} & \Gamma_{0,q}^{(k)} \end{bmatrix}, \tag{3.90}$$

respectively. With (3.89) and (3.90), (3.84) can be rewritten as

$$\begin{bmatrix} \bar{v}_{0,q}^{(k)} \\ \bar{v}_{1,q}^{(k)} \end{bmatrix} = \begin{bmatrix} \Gamma_{0,q}^{(k)} & \Gamma_{1,q}^{(k)} & j \cdot \Gamma_{0,q}^{(k)} & -j \cdot \Gamma_{1,q}^{(k)} \\ -\Gamma_{1,q}^{(k)} & \Gamma_{0,q}^{(k)} & -j \cdot \Gamma_{1,q}^{(k)} & j \cdot \Gamma_{0,q}^{(k)} \end{bmatrix} \cdot \begin{bmatrix} \breve{u}_{0,q}^{(k)} \\ \breve{u}_{1,q}^{(k)} \\ \tilde{u}_{0,q}^{(k)} \\ \tilde{u}_{1,q}^{(k)} \end{bmatrix} + \begin{bmatrix} \bar{n}_{0,q}^{(k)} \\ \bar{n}_{1,q}^{(k)} \end{bmatrix}. \tag{3.91}$$

Alamouti decoding at subcarrier q can be obtained by multiplication of (3.91) from the left with

$$\left(\mathbf{B}_q^{(k)}\right)^{\mathrm{H}} = \begin{bmatrix} \Gamma_{0,q}^{(k)} & \Gamma_{1,q}^{(k)} & j \cdot \Gamma_{0,q}^{(k)} & -j \cdot \Gamma_{1,q}^{(k)} \\ -\Gamma_{1,q}^{(k)} & \Gamma_{0,q}^{(k)} & -j \cdot \Gamma_{1,q}^{(k)} & j \cdot \Gamma_{0,q}^{(k)} \end{bmatrix}^{\mathrm{H}} \tag{3.92}$$

and taking the real part. The decoded signal is, thus, given by

$$\mathrm{Re}\left\{ \left(\mathbf{B}_q^{(k)}\right)^{\mathrm{H}} \cdot \begin{bmatrix} \bar{v}_{0,q}^{(k)} \\ \bar{v}_{1,q}^{(k)} \end{bmatrix} \right\} = \mathbf{\Delta}_q^{(k)} \cdot \begin{bmatrix} \breve{u}_{0,q}^{(k)} \\ \breve{u}_{1,q}^{(k)} \\ \tilde{u}_{0,q}^{(k)} \\ \tilde{u}_{1,q}^{(k)} \end{bmatrix} + \mathrm{Re}\left\{ \begin{bmatrix} \Gamma_{0,q}^{(k)} & -\Gamma_{1,q}^{(k)} \\ \Gamma_{1,q}^{(k)} & \Gamma_{0,q}^{(k)} \\ j \cdot \Gamma_{0,q}^{(k)} & -j \cdot \Gamma_{1,q}^{(k)} \\ -j \cdot \Gamma_{1,q}^{(k)} & j \cdot \Gamma_{0,q}^{(k)} \end{bmatrix}^{*} \cdot \begin{bmatrix} \bar{n}_{0,q}^{(k)} \\ \bar{n}_{1,q}^{(k)} \end{bmatrix} \right\} \tag{3.93}$$

with

$$\mathbf{\Delta}_q^{(k)} = \begin{bmatrix} |\Gamma_{0,q}^{(k)}|^2 + |\Gamma_{1,q}^{(k)}|^2 & 0 & 0 & 0 \\ 0 & |\Gamma_{0,q}^{(k)}|^2 + |\Gamma_{1,q}^{(k)}|^2 & 0 & 0 \\ 0 & 0 & |\Gamma_{0,q}^{(k)}|^2 + |\Gamma_{1,q}^{(k)}|^2 & 0 \\ 0 & 0 & 0 & |\Gamma_{0,q}^{(k)}|^2 + |\Gamma_{1,q}^{(k)}|^2 \end{bmatrix}. \tag{3.94}$$

3.3.5   Equalizer

3.3.5.1   Generalized Equalizer

In the following, data estimation performed by a generalized equalizer that takes the colored noise into account is described. The equalizer can be applied for all STBCs considered in Section 3.3.4.1. Equation (3.82) describes the decoded signal at the receiver. Note that $\breve{\mathbf{u}}^{(k)}$ contains the real and the imaginary part of the elements of the DFTs of $\mathbf{d}_a^{(k)}$. Thus, estimates $\hat{d}_{a,q}^{(k)}$ of the data symbols $d_{a,q}^{(k)}$ contained in $\mathbf{d}_a^{(k)}$ can be obtained from estimates of the elements of $\breve{\mathbf{u}}^{(k)}$. As $\boldsymbol{\Delta}^{(k)}$ is a diagonal matrix, the elements of vector $\breve{\mathbf{u}}^{(k)}$ are mutually independent but still scaled by the diagonal elements of matrix $\boldsymbol{\Delta}^{(k)}$. Given the decoded signal of (3.82), estimates of the elements of $\breve{\mathbf{u}}^{(k)}$ can be obtained by the application of a linear FDE. The FDE is based on the minimization of the expected squared error $\mathbf{e}^{(k)}$ between $\boldsymbol{\mathcal{E}}_{\mathrm{MMSE}}^{(k)} \cdot \mathrm{Re}\left\{\left(\mathbf{B}^{(k)}\right)^{\mathrm{H}} \cdot \bar{\boldsymbol{\nu}}^{(k)}\right\}$ and $\breve{\mathbf{u}}^{(k)}$, cf. (3.82), given by

$$\mathbf{e}^{(k)} = E\left\{\left\|\boldsymbol{\mathcal{E}}_{\mathrm{MMSE}}^{(k)} \cdot \mathrm{Re}\left\{\left(\mathbf{B}^{(k)}\right)^{\mathrm{H}} \cdot \bar{\boldsymbol{\nu}}^{(k)}\right\} - \breve{\mathbf{u}}^{(k)}\right\|^2\right\}, \tag{3.95}$$

with $\boldsymbol{\mathcal{E}}_{\mathrm{MMSE}}^{(k)}$ denoting a $2AQ \times 2AQ$ equalizer matrix. The derivation of the equalizer matrix $\boldsymbol{\mathcal{E}}_{\mathrm{MMSE}}^{(k)}$ is given in Appendix B.3. The result is given by

$$\boldsymbol{\mathcal{E}}_{\mathrm{MMSE}}^{(k)} = \begin{bmatrix} \boldsymbol{\mathcal{E}}_{\mathrm{MMSE},0}^{(k)} & \mathbf{0}_{2A\times 2A} & \cdots & \mathbf{0}_{2A\times 2A} \\ \mathbf{0}_{2A\times 2A} & \ddots & \cdots & \mathbf{0}_{2A\times 2A} \\ \vdots & \cdots & \ddots & \vdots \\ \mathbf{0}_{2A\times 2A} & \cdots & \mathbf{0}_{2A\times 2A} & \boldsymbol{\mathcal{E}}_{\mathrm{MMSE},Q-1}^{(k)} \end{bmatrix} \tag{3.96}$$

with

$$\boldsymbol{\mathcal{E}}_{\mathrm{MMSE},q}^{(k)} = \left(\left(\boldsymbol{\Delta}_q^{(k)}\right)^{\mathrm{T}} \boldsymbol{\Delta}_q^{(k)} + \frac{\sigma_{\mathrm{n}}^2}{\sigma_{\mathrm{d}}^2} \cdot \mathrm{tr}\left\{\left(\mathbf{B}_q^{(k)}\right)^{\mathrm{H}} \mathbf{B}_q^{(k)}\right\} \cdot \mathbf{I}_{2A}\right)^{-1} \cdot \left(\boldsymbol{\Delta}_q^{(k)}\right)^{\mathrm{T}}, \tag{3.97}$$

where $\mathrm{tr}\left\{\cdot\right\}$ denotes the trace of a matrix. The linear FDE of (3.96) compensates the impact of matrix $\boldsymbol{\Delta}^{(k)}$ in (3.82) taking into account the colored noise $\bar{\mathbf{w}}^{(k)}$. The FDE jointly performs spatial equalization and a compensation of the impact of the multipath channel. Thus, in the case that STBC is used, this FDE replaces the FDE of (2.32).

From equation (3.82), an estimate $\left(\breve{\mathbf{u}}^{(k)}\right)'$ of vector $\breve{\mathbf{u}}^{(k)}$ of (3.80) can be obtained by the application of the equalizer from (3.96) as follows:

$$\begin{aligned} \left(\breve{\mathbf{u}}^{(k)}\right)' &= \boldsymbol{\mathcal{E}}_{\mathrm{MMSE}}^{(k)} \cdot \mathrm{Re}\left\{\left(\mathbf{B}^{(k)}\right)^{\mathrm{H}} \cdot \bar{\boldsymbol{\nu}}^{(k)}\right\} \\ &= \boldsymbol{\mathcal{E}}_{\mathrm{MMSE}}^{(k)} \cdot \boldsymbol{\Delta}^{(k)} \cdot \breve{\mathbf{u}}^{(k)} + \boldsymbol{\mathcal{E}}_{\mathrm{MMSE}}^{(k)} \cdot \bar{\mathbf{w}}^{(k)}. \end{aligned} \tag{3.98}$$

In the following, the application of the equalizer at subcarrier q of user k is described. Analogous to (3.80), let $\left(\breve{\mathbf{u}}_q^{(k)}\right)'$ denote estimates of the vectors $\breve{\mathbf{u}}_q^{(k)}$. Further on, let $\left(\breve{\mathbf{u}}_q^{(k)}\right)'$ and $\left(\tilde{\mathbf{u}}_q^{(k)}\right)'$ denote estimates of the vectors $\breve{\mathbf{u}}_q^{(k)}$ and $\tilde{\mathbf{u}}_q^{(k)}$ of (3.72), respectively. With (3.98), the estimates $\left(\breve{\mathbf{u}}_q^{(k)}\right)'$ and $\left(\tilde{\mathbf{u}}_q^{(k)}\right)'$ are given by

$$
\left[\begin{array}{c} \left(\breve{\mathbf{u}}_q^{(k)}\right)' \\ \left(\tilde{\mathbf{u}}_q^{(k)}\right)' \end{array}\right] = (\breve{\mathbf{u}}_q^{(k)})' = \boldsymbol{\mathcal{E}}_{\mathrm{MMSE},q}^{(k)} \cdot \mathrm{Re}\left\{\left(\mathbf{B}_q^{(k)}\right)^{\mathrm{H}} \cdot \bar{\mathbf{v}}_q^{(k)}\right\},
\tag{3.99}
$$

where

$$
(\breve{\mathbf{u}}_q^{(k)})' = \left[\left(\breve{u}_{0,q}^{(k)}\right)', \ldots, \left(\breve{u}_{A-1,q}^{(k)}\right)'\right]^{\mathrm{T}}
\tag{3.100}
$$

and

$$
(\tilde{\mathbf{u}}_q^{(k)})' = \left[\left(\tilde{u}_{0,q}^{(k)}\right)', \ldots, \left(\tilde{u}_{A-1,q}^{(k)}\right)'\right]^{\mathrm{T}}.
\tag{3.101}
$$

From $\left(\breve{\mathbf{u}}_q^{(k)}\right)'$ and $\left(\tilde{\mathbf{u}}_q^{(k)}\right)'$, estimates $\hat{\mathbf{d}}_a^{(k)}$ of the A data symbol vectors $\mathbf{d}_a^{(k)}$ can be calculated. For that purpose, the elements $\left(\breve{u}_{a,q}^{(k)}\right)'$ and $\left(\tilde{u}_{a,q}^{(k)}\right)'$ are reorganized in vectors

$$
(\breve{\mathbf{u}}_a^{(k)})' = \left[\left(\breve{u}_{a,0}^{(k)}\right)', \ldots, \left(\breve{u}_{a,Q-1}^{(k)}\right)'\right]^{\mathrm{T}}
\tag{3.102}
$$

and

$$
(\tilde{\mathbf{u}}_a^{(k)})' = \left[\left(\tilde{u}_{a,0}^{(k)}\right)', \ldots, \left(\tilde{u}_{a,Q-1}^{(k)}\right)'\right]^{\mathrm{T}}.
\tag{3.103}
$$

Estimates $\hat{\mathbf{d}}_a^{(k)}$ can, thus, be calculated from

$$
\hat{\mathbf{d}}_a^{(k)} = \mathbf{F}_Q^{\mathrm{H}} \cdot \left(\left(\breve{\mathbf{u}}_a^{(k)}\right)' + j \cdot \left(\tilde{\mathbf{u}}_a^{(k)}\right)'\right).
\tag{3.104}
$$

3.3.5.2 Space-Time Equalizer for the Alamouti Scheme

In the following, the equalization in space and time is described for the special case of Alamouti STBC. For Alamouti STBC, the equalizer is given by

$$
\boldsymbol{\mathcal{E}}_{\mathrm{MMSE},q}^{(k)} = \left(\left(\boldsymbol{\Delta}_q^{(k)}\right)^{\mathrm{H}} \boldsymbol{\Delta}_q^{(k)} + \frac{\sigma_{\mathrm{n}}^2}{\sigma_{\mathrm{d}}^2} \cdot \left(|\Gamma_{0,q}^{(k)}|^2 + |\Gamma_{1,q}^{(k)}|\right) \cdot \mathbf{I}_4\right)^{-1} \cdot \left(\boldsymbol{\Delta}_q^{(k)}\right)^{\mathrm{H}}
\tag{3.105}
$$

with $\mathbf{\Delta}_q^{(k)}$ of (3.94). With the equalizer given in (3.105) and $\left(\mathbf{B}_q^{(k)}\right)^{\mathrm{H}}$ of (3.92),

$$
\begin{bmatrix}
\left(\breve{u}_{0,q}^{(k)}\right)' \\[4pt]
\left(\breve{u}_{1,q}^{(k)}\right)' \\[4pt]
\left(\tilde{u}_{0,q}^{(k)}\right)' \\[4pt]
\left(\tilde{u}_{1,q}^{(k)}\right)'
\end{bmatrix}
= \boldsymbol{\mathcal{E}}_{\mathrm{MMSE},q}^{(k)} \cdot \mathrm{Re}\left\{ \left(\mathbf{B}_q^{(k)}\right)^{\mathrm{H}} \cdot
\begin{bmatrix}
\left(\bar{v}_{0,q}^{(k)}\right)' \\[4pt]
\left(\bar{v}_{1,q}^{(k)}\right)'
\end{bmatrix}
\right\}
\tag{3.106}
$$

is calculated from equation (3.99). The elements of $\left[\left(\breve{u}_{0,q}^{(k)}\right)', \left(\breve{u}_{1,q}^{(k)}\right)', \left(\tilde{u}_{0,q}^{(k)}\right)', \left(\tilde{u}_{1,q}^{(k)}\right)'\right]^{\mathrm{T}}$
for $q = 0, \ldots, Q-1$ are reorganized in the vectors $\left(\breve{\mathbf{u}}_0^{(k)}\right)'$, $\left(\breve{\mathbf{u}}_0^{(k)}\right)'$, $\left(\tilde{\mathbf{u}}_0^{(k)}\right)'$ and $\left(\tilde{\mathbf{u}}_1^{(k)}\right)'$
according to (3.102) and (3.103), respectively. Finally, the estimates estimates $\hat{\mathbf{d}}_0^{(k)}$ and
$\hat{\mathbf{d}}_1^{(k)}$ for the data symbol vectors $\mathbf{d}_0^{(k)}$ and $\mathbf{d}_1^{(k)}$, respectively, are obtained from

$$
\hat{\mathbf{d}}_0^{(k)} = \mathbf{F}_Q^{\mathrm{H}} \cdot \left(\left(\breve{\mathbf{u}}_0^{(k)}\right)' + j \cdot \left(\tilde{\mathbf{u}}_0^{(k)}\right)' \right)
\tag{3.107}
$$

and

$$
\hat{\mathbf{d}}_1^{(k)} = \mathbf{F}_Q^{\mathrm{H}} \cdot \left(\left(\breve{\mathbf{u}}_1^{(k)}\right)' + j \cdot \left(\tilde{\mathbf{u}}_1^{(k)}\right)' \right),
\tag{3.108}
$$

respectively, according to (3.104).

3.3.6   Conclusions

In Section 3.3 a new approach for the application of STBCs to B-IFDMA is presented
that enables the exploitation of spatial transmit diversity for B-IFDMA. The exploita-
tion of spatial transmit diversity by means of the presented approach represents a
well suited supplementation of B-IFDMA when multiple antennas are available at the
transmitter. The major properties of the approach can be summarized as follows: The
presented approach

- leaves the low envelope fluctuations of the B-IFDMA transmit signal unchanged.

- requires only low computational effort at the transmitter because it can be im-
  plemented by means of permutation of the data symbols, taking the complex
  conjugate and switching of the sign of the data symbols before modulation.

- can be combined with the low complexity time domain implementation for B-
  IFDMA modulation introduced in Section 3.2.

- makes the application of various STBCs to B-IFDMA possible.

- provides improved performance compared to existing approaches because it considers the coloration of the noise.

3.4 Application of Space Division Multiple Access to B-IFDMA

3.4.1 Introduction

After having introduced the combination of B-IFDMA with appropriate techniques for the use of multiple transmit antennas in Section 3.3, in this section, the combination of B-IFDMA with appropriate techniques for the use of multiple receive antennas is regarded. It is well known that, if the receiver is equipped with multiple antennas, Space Division Multiple Access (SDMA) is an appropriate means to increase the spectral efficiency of a mobile radio system. The reason is that with the aid of the multiple receive antennas a spatial reuse of the time and frequency resources is possible for the different users within a cell of a mobile radio system [TV05]. For future mobile radio systems, SDMA is considered as an important multiple antenna technique [Mac08, Deg05, WIN07a, WIN07b, WIN07c]. For that reason, the suitability of B-IFDMA for a combination with SDMA can be considered as an important criterion for the application of B-IFDMA to future mobile radio systems. Throughout Section 3.4, it is shown how SDMA can be applied to B-IFDMA. The approach presented in this section has been described in [AFK10] by the author of this thesis.

The remainder of this section is organized as follows: In Section 3.4.2, an overview of existing literature that is relevant for the application of SDMA to B-IFDMA is given. In Section 3.4.3, the system model for B-IFDMA defined in Section 2 is extended to a scenario where the base station is equipped with multiple receive antennas. In particular, in Section 3.4.3.1, assumptions for the extension of the system model are formulated. In Section 3.4.3.2, the joint transmit signal of a group of users that transmit on the same time frequency resources is described, followed by a description of the joint channel from the terminals of these users to the multiple receive antennas of the base station in Section 3.4.3.3. Section 3.4.3.4 gives a description of the receiver structure based on a system matrix that is defined throughout this section. In Section 3.4.4, linear multi-user detectors for the application of SDMA to B-IFDMA are presented. Finally, Section 3.4.5 summarizes the main results of Section 3.4.

3.4.2   State-of-the-art

In the sequel, an overview of existing literature that is relevant for the application of
SDMA to B-IFDMA in the uplink is presented. In [Deg05], the application of SDMA
to OFDM is described. Further on, in [VdPG$^+$00], the application of SDMA to DFT
precoded OFDM is regarded, which corresponds to the special case of SDMA applied
to B-IFDMA with $M = N = Q$ and $L = 1$, cf. Section 2.5, with Q and N of (2.2)
and L and M of (2.36). The approach presented in this section can be regarded as
an extension of the approaches presented in [Deg05] and [VdPG$^+$00] to B-IFDMA.
In [PL07], an approach for a spatial reuse of the time and frequency resources for the
transmission of several data streams is described for IFDMA, i.e., for the special case
of B-IFDMA with $M = 1$, cf. Section 2.5. However, in [PL07], for each time frequency
ressource, only the data stream of one user is considered. Thus, the approach presented
in this section can be regarded as an extension of the approach in [PL07] from IFDMA
to B-IFDMA in general, and considering data streams that belong to different users.

3.4.3   System Model for Application of Space-Division Multiple Access to B-IFDMA

3.4.3.1   System Assumptions

In the following, the system model for B-IFDMA from Section 2 is extended to a
scenario where the base station is equipped with $n_R > 1$ receive antennas. For the
sake of simplicity and without loss of generality, the mobile terminals are assumed to
be equipped with $n_T = 1$ transmit antenna.

For the application of SDMA, the users within a cell have to be grouped. The grouping
depends on the properties of the channels between the respective user terminals and the
n_R receive antennas at the base station. In the following, it is assumed that the grouping
is performed such that the signals of all users within a certain group can be spatially
well separated at the base station. Thus, the users within one group can share the same
subcarriers and the same modulated data vectors for transmission. Algorithms for user
grouping according to their spatial separability are extensively discussed in [Mac08].
For grouping in the case that instantaneous channel state information is not available,
an algorithm based on second order statistics of the channel is presented in [FGH07].
In the remainder of this section, it is assumed that the grouping problem is solved and,
thus, the grouping is not addressed.

In the following, let K_s denote the number of users within a given group sharing the same block-interleaved subcarrier set and the same modulated data vectors for transmission. Consequently, compared to the system model for B-IFDMA from Section 2, instead of K_f users, a number of up to $K = K_\mathrm{f} \cdot K_\mathrm{s}$ users can be served by a cell in the mobile radio system. Assuming perfect synchronization, signals transmitted on different subcarrier sets and in different modulated data vectors are mutually orthogonal. Thus, for sake of simplicity and without loss of generality, in the following, only one block-interleaved subcarrier set is regarded. For that reason, throughout Section 3.4 the notation of the signal vectors and of the matrices changes compared to the notation introduced in Section 2. Instead of index k that has been introduced in Section 2 for B-IFDMA in order to distinguish users transmitting on different subcarrier sets, in the following, the index $\kappa = 0, \ldots, K_\mathrm{s} - 1$ is introduced in order to distinguish the K_s users within one group sharing the same subcarrier set. At the same time, index k is omitted.

In Figure 3.6, an overview of the considered system model for the regarded subcarrier set assuming a base station equipped with multiple antennas is given. In the following, the vectors and matrices from Figure 3.6 are explained. Note that a detailed description of the relations between the vectors and matrices shown in Figure 3.6 is given in the adjacent subsections. In line with the replacement of index k by index κ mentioned above, $\mathbf{d}^{(\kappa)}$ denotes the data symbol vectors of the K_s users within one group. Except for the user index, $\mathbf{d}^{(\kappa)}$ is defined according to (2.1). The vectors $\mathbf{u}^{(\kappa)}$ denote the data symbol vectors of the K_s users after DFT pre-coding analogous to (3.2). The data symbol vectors $\mathbf{d}^{(\kappa)}$ of the users in the group are B-IFDMA modulated by the matrices $\mathbf{F}_Q$, $\mathbf{M}_\mathrm{BI}$ and $\mathbf{F}_N^\mathrm{H}$, cf. (2.39). Note that, for the block interleaved subcarrier mapping matrix $\mathbf{M}_\mathrm{BI}$, compared to the definition in (2.37), the user index is omitted as the subcarrier mapping is the same for all K_s users in the group.

The modulated data vectors $\mathbf{x}^{(\kappa)}$ are transmitted over the channel that is modelled by matrix $\mathbf{H}$. In particular, matrix $\mathbf{H}$ describes the channels between the transmit antennas of the mobile terminals of the K_s users in the group and the n_R receive antennas at the base station and contains the respective $K_\mathrm{s} \cdot n_\mathrm{R}$ channel matrices $\mathbf{H}^{(\eta,\kappa)}$, $\eta = 0, \ldots, n_\mathrm{R} - 1$, that are defined analogous to (2.16).

At the receiver, at each receive antenna, AWGN is added. The AWGN is modelled by n_R vectors $\mathbf{n}_\eta$. Each vector $\mathbf{n}_\eta$ is defined analogous to (2.5). The received signals at the n_R receive antennas at the base station are described by the n_R received signal vectors $\mathbf{r}_\eta$. At the base station receiver, the vectors $\mathbf{r}_\eta$ are transformed to the DFT domain by matrix $\mathbf{F}_N$ and a subcarrier demapping performed by matrix $\mathbf{M}_\mathrm{BI}^\dagger$ is applied. The resulting n_R signals at the output of the subcarrier demapper are described by the

vectors $\mathbf{s}_\eta$. Afterwards, multi-user detection is applied to the vectors $\mathbf{s}_\eta$ that delivers estimates $\hat{\mathbf{u}}^{(\kappa)}$ of the vectors $\mathbf{u}^{(\kappa)}$. From $\hat{\mathbf{u}}^{(\kappa)}$, estimates $\hat{\mathbf{d}}^{(\kappa)}$ of the data symbol vectors $\mathbf{d}^{(\kappa)}$ are obtained by an IDFT operation performed by matrix $\mathbf{F}_Q^{\mathrm{H}}$.

3.4.3.2   Transmitter

In the following, a transmitter model is introduced that describes the combined modulated data vectors of all users of a group. The data vectors of the K_s users can be stacked into a $KQ \times 1$ vector

$$\mathbf{d} = \left[\left(\mathbf{d}^{(0)} \right)^{\mathrm{T}}, \dots, \left(\mathbf{d}^{(K_\mathrm{s}-1)} \right)^{\mathrm{T}} \right]^{\mathrm{T}}. \tag{3.109}$$

The modulated data vector of user κ is given by

$$\mathbf{x}^{(\kappa)} = \mathbf{F}_N^{\mathrm{H}} \cdot \mathbf{M}_{\mathrm{BI}} \cdot \mathbf{F}_Q \cdot \mathbf{d}^{(\kappa)}. \tag{3.110}$$

Note that, in general, the Kroenecker product of the identity matrix $\mathbf{I}_W$ with an arbitrary $X \times Y$ matrix $\mathbf{Z}$, with $W, X, Y \in \mathbb{N}$, results in a $WX \times WY$ block diagonal matrix with W replica of matrix $\mathbf{Z}$ on its main diagonal. Thus, the Kroenecker product provides an appropriate means to describe the modulated data vectors $\mathbf{x}^{(\kappa)}$ of the K_s users jointly in a clearly arranged manner. With '$\otimes$' denoting the Kroenecker product of two matrices, the stacked modulated data vector

$$\mathbf{x} = \left[\left(\mathbf{x}^{(0)} \right)^{\mathrm{T}}, \dots, \left(\mathbf{x}^{(K_\mathrm{s}-1)} \right)^{\mathrm{T}} \right]^{\mathrm{T}} \tag{3.111}$$

for all K_s users is given by

$$\mathbf{x} = \left(\mathbf{I}_{K_\mathrm{s}} \otimes \mathbf{F}_N^{\mathrm{H}} \right) \cdot \left(\mathbf{I}_{K_\mathrm{s}} \otimes \mathbf{M}_{\mathrm{BI}} \right) \cdot \left(\mathbf{I}_{K_\mathrm{s}} \otimes \mathbf{F}_Q \right) \cdot \mathbf{d}. \tag{3.112}$$

Let $\mathbf{u}$ denote a vector stacking the vectors $\mathbf{u}^{(\kappa)}$ after DFT pre-coding according to

$$\mathbf{u} = \left[\left(\mathbf{u}^{(0)} \right)^{\mathrm{T}}, \dots, \left(\mathbf{u}^{(K_\mathrm{s}-1)} \right)^{\mathrm{T}} \right]^{\mathrm{T}}. \tag{3.113}$$

As

$$\mathbf{u}^{(\kappa)} = \mathbf{F}_Q \cdot \mathbf{d}^{(\kappa)}, \tag{3.114}$$

vector $\mathbf{u}$ is given by

$$\mathbf{u} = \left(\mathbf{I}_{K_\mathrm{s}} \otimes \mathbf{F}_Q \right) \cdot \mathbf{d}. \tag{3.115}$$

With (3.115), (3.112) can be rewritten as

$$\mathbf{x} = \left(\mathbf{I}_{K_\mathrm{s}} \otimes \mathbf{F}_N^{\mathrm{H}} \right) \cdot \left(\mathbf{I}_{K_\mathrm{s}} \otimes \mathbf{M}_{\mathrm{BI}} \right) \cdot \mathbf{u}. \tag{3.116}$$
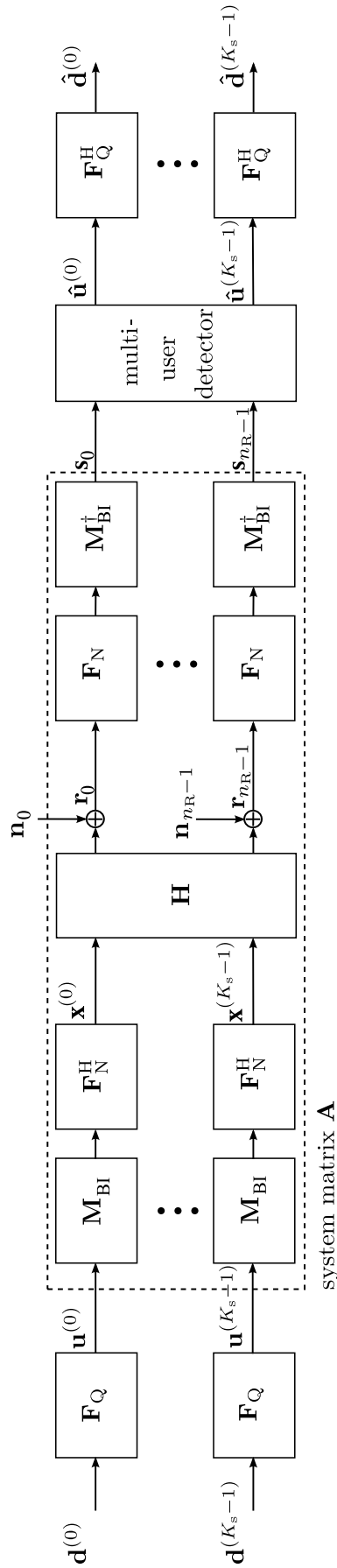
Figure 3.6: System model for the application of SDMA to B-IFDMA for one group of K_{s} users sharing the same set of block-interleaved subcarriers.

3.4.3.3   Channel

In the following, the channel between the user terminals and the base station is modelled for the transmission of the modulated data vectors of all users of one group. Let $\mathbf{H}^{(\eta,\kappa)}$ denote the $N \times N$ circulant channel matrix according to (2.16) for user κ from the transmit antenna to the η-th receive antenna. Collecting the channel matrices $\mathbf{H}^{(\eta,\kappa)}$ in one $n_{\mathrm{R}}N \times K_{\mathrm{s}}N$ matrix, $\mathbf{H}$ results in

$$
\mathbf{H} = \begin{bmatrix} \mathbf{H}^{(0,0)} & \cdots & \mathbf{H}^{(0,K_{\mathrm{s}}-1)} \\ \vdots & \ddots & \vdots \\ \mathbf{H}^{(n_{\mathrm{R}}-1,0)} & \cdots & \mathbf{H}^{(n_{\mathrm{R}}-1,K_{\mathrm{s}}-1)} \end{bmatrix}.
\tag{3.117}
$$

Let $\bar{\mathbf{n}}$ denote an $n_{\mathrm{R}}N \times 1$ stacked AWGN vector consisting of the $N \times 1$ noise vectors $\mathbf{n}_{\eta}$ analogous to (2.13) at the n_{R} receive antennas with

$$
\bar{\mathbf{n}} = \left[(\mathbf{n}_0)^{\mathrm{T}}, \ldots, (\mathbf{n}_{n_{\mathrm{R}}-1})^{\mathrm{T}} \right]^{\mathrm{T}}.
\tag{3.118}
$$

Thus, the $n_{\mathrm{R}}N \times 1$ stacked received signal vector $\bar{\mathbf{r}}$ consisting of the $N \times 1$ received signal vectors $\mathbf{r}_{\eta}$ at the n_{R} receive antennas according to

$$
\bar{\mathbf{r}} = \left[(\mathbf{r}_0)^{\mathrm{T}}, \ldots, \left(\mathbf{r}_{n_{\mathrm{R}}-1)}\right)^{\mathrm{T}} \right]^{\mathrm{T}}
\tag{3.119}
$$

is given by

$$
\bar{\mathbf{r}} = \mathbf{H} \cdot \mathbf{x} + \bar{\mathbf{n}}.
\tag{3.120}
$$

3.4.3.4   System Matrix and Receiver

In the following, the receiver structure for the application of SDMA to B-IFDMA is presented. At the receiver, OFDM demodulation and subcarrier demapping are applied to the received signal vectors $\mathbf{r}_{\eta}$, cf. Figure 3.6. The output of the subcarrier demapper is described by vector $\mathbf{s}$ stacking the n_{R} vectors $\mathbf{s}_{\eta}$ with

$$
\mathbf{s}_{\eta} = \mathbf{M}_{\mathrm{BI}}^{\dagger} \cdot \mathbf{F}_N \cdot \mathbf{r}_{\eta}
\tag{3.121}
$$

according to

$$
\mathbf{s} = \left[(\mathbf{s}_0)^{\mathrm{T}}, \ldots, \left(\mathbf{s}_{n_{\mathrm{R}}-1)}\right)^{\mathrm{T}} \right]^{\mathrm{T}}.
\tag{3.122}
$$

Similar as in Section 3.4.3.2, the Kroenecker product can be used in order to describe the relation between $\bar{\mathbf{r}}$ of (3.119) and $\mathbf{s}$:

$$
\mathbf{s} = \left(\mathbf{I}_{n_{\mathrm{R}}} \otimes \mathbf{M}_{\mathrm{BI}}^{\dagger} \right) \cdot \left(\mathbf{I}_{n_{\mathrm{R}}} \otimes \mathbf{F}_{\mathrm{N}} \right) \cdot \bar{\mathbf{r}}.
\tag{3.123}
$$

In the following, an $n_\mathrm{R}Q \times K_\mathrm{s}Q$ system matrix $\mathbf{A}$ is introduced. This system matrix $\mathbf{A}$ gives a joint description of block interleaved subcarrier mapping and OFDM modulation at the transmitter side, transmission over the channel, and OFDM demodulation and subcarrier demapping at the receiver side, cf. Figure 3.6. With the aid of the system matrix $\mathbf{A}$, the relation between vector $\mathbf{u}$ and vector $\mathbf{s}$ can be easily described. From $\mathbf{s}$, the multi-user detector calculates estimates for $\mathbf{u}$ by a compensation of the system matrix $\mathbf{A}$. From the insertion of (3.116) and (3.119) in (3.123) follows that

$$\mathbf{A} = \left(\mathbf{I}_{n_\mathrm{R}} \otimes \mathbf{M}_\mathrm{BI}^\dagger\right) \cdot (\mathbf{I}_{n_\mathrm{R}} \otimes \mathbf{F}_\mathrm{N}) \cdot \mathbf{H} \cdot \left(\mathbf{I}_{K_\mathrm{s}} \otimes \mathbf{F}_\mathrm{N}^\mathrm{H}\right) \cdot (\mathbf{I}_{K_\mathrm{s}} \otimes \mathbf{M}_\mathrm{BI}) \tag{3.124}$$

and

$$\mathbf{s} = \mathbf{A} \cdot \mathbf{u}. \tag{3.125}$$

However, a compensation of matrix $\mathbf{A}$ in order to perform multi-user detection would require high computational effort. Thus, in the following, the structure of the system matrix $\mathbf{A}$ is further analyzed in order to find a computationally efficient solution for the compensation of matrix $\mathbf{A}$.

In order to deduce the properties of the system matrix $\mathbf{A}$, in the following, the submatrices of $\mathbf{A}$ are regarded. Let $\bar{\mathbf{A}}^{(\eta,\kappa)}$ denote a $Q \times Q$ submatrix of $\mathbf{A}$ with

$$\mathbf{A} = \begin{bmatrix} \bar{\mathbf{A}}^{(0,0)} & \cdots & \bar{\mathbf{A}}^{(0,K_\mathrm{s}-1)} \\ \vdots & \ddots & \vdots \\ \bar{\mathbf{A}}^{(n_\mathrm{R}-1,0)} & \cdots & \bar{\mathbf{A}}^{(n_\mathrm{R}-1,K_\mathrm{s}-1)} \end{bmatrix}. \tag{3.126}$$

The submatrix $\bar{\mathbf{A}}^{(\eta,\kappa)}$ describes the channel in frequency domain between the mobile terminal of a certain user κ and one of the receive antennas η at the base station and is given by

$$\bar{\mathbf{A}}^{(\eta,\kappa)} = \mathbf{M}_\mathrm{BI}^\dagger \cdot \mathbf{F}_N \cdot \mathbf{H}^{(\eta,\kappa)} \cdot \mathbf{F}_N^\mathrm{H} \cdot \mathbf{M}_\mathrm{BI}. \tag{3.127}$$

Hence, the matrix $\bar{\mathbf{A}}^{(\eta,\kappa)}$ is equivalent to the matrix described in (2.28) applying the channel matrix $\mathbf{H}^{(\eta,\kappa)}$ in place of $\mathbf{H}^{(k)}$ and the block interleaved subcarrier mapping matrix $\mathbf{M}_\mathrm{BI}^{(k)}$ defined in (2.37) in place of $\mathbf{M}^{(k)}$. Consequently, $\bar{\mathbf{A}}^{(\eta,\kappa)}$ is a $Q \times Q$ diagonal matrix, cf. comments on (2.28)-(2.30).

With the submatrices $\bar{\mathbf{A}}^{(\eta,\kappa)}$ being diagonal matrices, $\mathbf{A}$ provides a structure as depicted in Figure 3.7 on the left. In the following, the structure of matrix $\mathbf{A}$ is exploited in order to provide an efficient implementation for the multi-user detector. Due to the structure of matrix $\mathbf{A}$, the elements of matrix $\mathbf{A}$ can be rearranged such that the resulting matrix $\check{\mathbf{A}}$ has a block-diagonal structure, as indicated in Figure 3.7 on the right. This block-diagonal structure is beneficial for the formulation of a multi-user detector with low computational effort, cf. [Deg05].
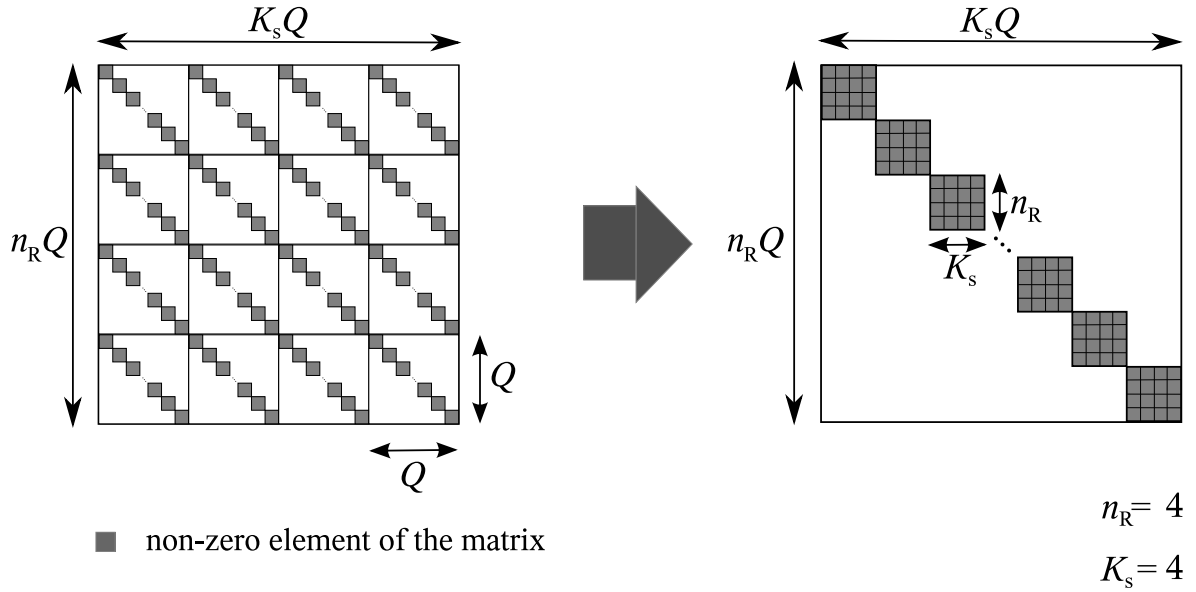
$n_R= 4$

$K_s= 4$

Figure 3.7: Structure of the system matrix $\mathbf{A}$ and the modified matrix $\breve{\mathbf{A}}$ with rearranged elements depicted for $K_s = n_R = 4$.

In the following, the rearrangement of the elements of $\mathbf{A}$ is described. For that purpose, let $\bar{A}_{q,q}^{(\eta,\kappa)}$ denote the element on the main diagonal of $\bar{\mathbf{A}}^{(\eta,\kappa)}$ in the q-th row and q-th column. Let, further on,

$$\underline{\mathbf{A}}_q = \begin{bmatrix} \bar{A}_{q,q}^{(0,0)} & \cdots & \bar{A}_{q,q}^{(0,K_s-1)} \\ \vdots & \ddots & \vdots \\ \bar{A}_{q,q}^{(n_R-1,0)} & \cdots & \bar{A}_{q,q}^{(n_R-1,K_s-1)} \end{bmatrix} \tag{3.128}$$

denote an $n_R \times K_s$ matrix that contains all elements of the system matrix $\mathbf{A}$ that are related to the subcarrier with index q.

With the above introduced definitions, the $n_R Q \times K_s Q$ block-diagonal matrix $\breve{\mathbf{A}}$ is given by

$$\breve{\mathbf{A}} = \begin{bmatrix} \underline{\mathbf{A}}_0 & \mathbf{0}_{n_R \times K_s} & \cdots & \mathbf{0}_{n_R \times K_s} \\ \mathbf{0}_{n_R \times K_s} & \underline{\mathbf{A}}_1 & \cdots & \mathbf{0}_{n_R \times K_s} \\ \vdots & \vdots & \ddots & \vdots \\ \mathbf{0}_{n_R \times K_s} & \mathbf{0}_{n_R \times K_s} & \cdots & \underline{\mathbf{A}}_{Q-1} \end{bmatrix}. \tag{3.129}$$

The block-diagonal structure of matrix $\breve{\mathbf{A}}$ enables a decoupled description of the data transmission on the different subcarriers q. Thus, from this new block-diagonal matrix $\breve{\mathbf{A}}$, a per-subcarrier multi-user detector can be derived that performs user separation by the compensation of the Q small matrices $\underline{\mathbf{A}}_q$ instead of the large matrix $\mathbf{A}$. The compensation of Q small matrices $\underline{\mathbf{A}}_q$ provides a lower computational effort compared to a compensation of one large matrix $\mathbf{A}$, cf. [Deg05].

In the following, the respective vectors containing the part of the data that is transmitted at subcarrier q are defined. Let

$$\underline{\mathbf{v}}_q = [v_{0,q}, \ldots, v_{n_{\mathrm{R}}-1,q}]^{\mathrm{T}} \tag{3.130}$$

denote a vector consisting of the elements $v_{\eta,q}$ of the vectors $\mathbf{s}_\eta$ on the q-th subcarrier. Let, further on,

$$\underline{\mathbf{u}}_q = \left[u_q^{(0)}, \ldots, u_q^{(K_{\mathrm{s}}-1)}\right]^{\mathrm{T}} \tag{3.131}$$

denote a vector consisting of the elements $u_q^{(\kappa)}$ of the DFT of the data symbols of the users κ that are transmitted on the q-th subcarrier. Let, finally,

$$\underline{\mathbf{n}}_q = [n_{0,q}, \ldots, n_{K_{\mathrm{s}}-1,q}]^{\mathrm{T}} \tag{3.132}$$

denote a vector consisting of the elements $n_{\eta,q}$ of the AWGN vectors

$$\breve{\mathbf{n}}_\eta = \mathbf{M}_{\mathrm{BI}}^{\dagger} \cdot \mathbf{F}_N \cdot \mathbf{n}_\eta \tag{3.133}$$

after DFT and subcarrier demapping on the q-th subcarrier. Thus, the data transmission per subcarrier can be described by

$$\underline{\mathbf{v}}_q = \underline{\mathbf{A}}_q \cdot \underline{\mathbf{u}}_q + \underline{\mathbf{n}}_q. \tag{3.134}$$

Let $\hat{\underline{\mathbf{u}}}_q$ denote an estimate of vector $\underline{\mathbf{u}}_q$ and let $\underline{\mathbf{W}}_q$ denote a $K_{\mathrm{s}} \times n_{\mathrm{R}}$ receive filter for the subcarrier with index q. Applying a linear receive filter, vector $\hat{\underline{\mathbf{u}}}_q$ is calculated from vector $\underline{\mathbf{v}}_q$ by

$$\hat{\underline{\mathbf{u}}}_q = \underline{\mathbf{W}}_q \cdot \underline{\mathbf{v}}_q. \tag{3.135}$$

3.4.4 Linear Multi-User Detection

In the following, from the per-subcarrier description of the data transmission in (3.134), linear multi-user detectors that perform user separation and compensation of the channel per subcarrier are given. A multi-user detector according to the ZF criterion is given by

$$\underline{\mathbf{W}}_q = \left(\left(\underline{\mathbf{A}}_q \right)^{\mathrm{H}} \cdot \underline{\mathbf{A}}_q \right)^{-1} \cdot \left(\underline{\mathbf{A}}_q \right)^{\mathrm{H}}. \tag{3.136}$$

A multi-user detector according to the MMSE criterion is given by

$$\underline{\mathbf{W}}_q = \left(\left(\underline{\mathbf{A}}_q \right)^{\mathrm{H}} \cdot \underline{\mathbf{A}}_q + \frac{\sigma_{\underline{\mathrm{n}}}^2}{\sigma_{\underline{\mathrm{u}}}^2} \cdot \mathbf{I}_{K_{\mathrm{s}}} \right)^{-1} \cdot \left(\underline{\mathbf{A}}_q \right)^{\mathrm{H}}, \tag{3.137}$$

where $\sigma_{\underline{\mathrm{u}}}^2$ and $\sigma_{\underline{\mathrm{n}}}^2$ denote the variances of the elements of $\hat{\underline{\mathbf{u}}}_s$ and $\underline{\mathbf{n}}_s$, respectively, assuming uncorrelated data symbols and additive white Gaussian noise as described in Section 2.3.2.

From $\hat{\underline{\mathbf{u}}}_q$, an estimate $\hat{\mathbf{d}}^{(\kappa)}$ of the data vector $\mathbf{d}^{(\kappa)}$ of user κ is obtained by resorting the elements $u_q^{(\kappa)}$ of $\hat{\underline{\mathbf{u}}}_q$ in vectors $\hat{\mathbf{u}}^{(\kappa)} = \left[d_0^{(\kappa)}, \ldots, d_{Q-1}^{(\kappa)} \right]^{\mathrm{T}}$ and subsequent IDFT according to

$$\hat{\mathbf{d}}^{(\kappa)} = \mathbf{F}_{\mathrm{Q}}^{\mathrm{H}} \cdot \hat{\mathbf{u}}^{(\kappa)}. \tag{3.138}$$

Note that for B-IFDMA, if the channel properties do not change significantly within one block of M adjacent subcarriers with M of (2.36), the per-subcarrier notation enables a further simplification by calculating only one multi-user detector $\underline{\mathbf{W}}_q$ according to (3.136) or (3.137), respectively, for each subcarrier block and using this multi-user detector for user separation and compensation of the channel at all subcarriers within the block.

3.4.5   Conclusions

In Section 3.4, the application of SDMA to B-IFDMA is presented. The major results of this section can be summarized as follows.

- A system model that enables the derivation of a per-subcarrier approach for linear multi-user detectors for B-IFDMA with SDMA has been presented.

- The presented approach extends the existing algorithms for application of SDMA to DFT pre-coded OFDM to B-IFDMA and shows that B-IFDMA is suited for a combination with SDMA.

- It is shown that, if the channel properties do not change significantly within one block of M adjacent subcarriers, the per-subcarrier approach for linear multi-user detection can be further simplified by calculating the multi-user detector per subcarrier block instead of calculating the multi-user detector per subcarrier. This property, that is made possible by the block-interleaved subcarrier allocation of B-IFDMA, enables a reduction of the computational complexity for multi-user detection.

- The presented approach makes an increased spectral efficiency for B-IFDMA applied in a mobile radio cell possible, because in a system applying B-IFDMA combined with SDMA several users can share the same time frequency resources.

3.5 Efficient Accommodation of Different Data Rates

3.5.1 Introduction

In this section, a new approach for an efficient accommodation of different data rates in mobile radio systems using B-IFDMA is introduced. Future mobile radio systems have to support a variety of different services ranging from low data rate services like Voice Over IP (VoIP) to high data rate services like video transmission [WIN07d]. Thus, a high flexibility and granularity in terms of different data rates is required.

In general, different data rates can be provided by different means such as adaptation of the modulation scheme and the code rate, assignment of different numbers of modulated data vectors to a user within a given time frame, or assignment of different numbers of subcarriers to a user, respectively. The provision of different data rates by an adaptation of the modulation and coding scheme (MCS) is, however, only possible to a limited extent. On the one hand, for a given number of resources that are assigned to a user, the data rate obtained by an adaptation of the MCS cannot exceed the channel capacity. On the other hand, if, for a given number of resources assigned to a user, the data rate obtained by an adaptation of the MCS is much lower than the channel capacity, the bandwidth efficiency of the system is decreased, which cannot be accepted.

Compared to the adaptation of the MCS, the provision of different data rates can be made much more effective by a combination of the adaptation of the MCS with the assignment of different numbers of resources to a user. For that reason, it is convenient to establish a TDMA component in the air interface of the mobile radio system, cf. Section 2.3.3. TDMA enables a flexible assignment of variable numbers of modulated data vectors within a given time frame to a user. However, the adaptation of the data rate solely by a combination of adaptive MCS and TDMA component would introduce unacceptably large delays, especially for low data rates. The reason is that using TDMA, in order to provide low average data rates, the transmission is organized in short bursts with high instantaneous data rates. Hence, the time to wait to fill the buffers between consecutive bursts is long and causes delays. Thus, in order to meet the tough requirements on flexibility in terms of different data rates and, at the same time, low delays, cf. Section 1.1.2, in addition to the TDMA component, the assignment of different numbers of subcarriers to the users is required.

Typically, for a mobile radio cell, the resource allocation is performed by a resource allocation algorithm running in a central resource scheduler at the base station. Thus, the information about assigned resources for uplink transmission has to be transmitted over the air to the user terminals, which causes signalling overhead. Due to block interleaved subcarrier allocation for B-IFDMA signals, the subcarrier assignment is restricted and the development of an approach for the assignment of different numbers of subcarriers to the users within one cell that maintains the orthogonality of the different users' signals and avoids a waste of resources due to an awkward subcarrier assignment is a challenging task. In particular, an according approach has to meet the following demands:

Regarding the B-IFDMA signal of a certain user,

- all subcarrier blocks assigned to that particular user have to have the same size,

- the subcarrier blocks assigned to that particular user have to be equidistant, and

- in order to maximize the frequency diversity, the blocks of subcarriers have to be spread over the total available bandwidth.

In addition, regarding the signals of the different users within one cell,

- the subcarrier sets assigned to the users must not overlap in order to maintain the orthogonality of the different users' signals and, thus, to avoid MAI,

- the probability that a user is blocked, although the number of subcarriers that is required to provide the data rate requested by the user is available in the system, has to be kept low,

- the approach for an accommodation of different numbers of subcarriers should provide low signalling overhead, because signalling overhead affects the spectral efficiency of the mobile radio system, and

- the approach for an accommodation of different numbers of subcarriers should make efficient resource allocation algorithms possible in order to keep the hardware costs of the resource scheduler as well as the delays caused by the runtime of the resource allocation algorithm as low as possible.

In the sequel, a new approach is presented that meets the above mentioned criteria and, thus, is well suited for the accommodation of different data rates for B-IFDMA in future mobile radio systems. This approach has been published by the author of this thesis in [FKCS05b] and [FKC07b]. Note that the approach presented in this section, although formulated and described for B-IFDMA, can be also applied to B-EFDMA, because for both schemes the subcarrier allocation is similar.

The remainder of this section is organized as follows: In Section 3.5.2, an overview of existing literature that is relevant for the presented new approach is given. In Section 3.5.3, constraints on important system parameters are formulated that provide the basis for the new approach for accommodation of different numbers of subcarriers for B-IFDMA. The new approach is introduced in Section 3.5.4. In Section 3.5.5, important special cases are addressed. Finally, Section 3.5.6 summarizes the main results of Section 3.5.

3.5.2 State-of-the-art

In this section, an overview of existing literature that is relevant for the presented new approach is given. To the best of the author's knowledge there are no proposals for the accommodation of different numbers of block-interleaved subcarriers in a system, neither for B-IFDMA nor for block-interleaved OFDMA. However, a similar problem has been already addressed in the context of CDMA by the assignment of spreading codes with different spreading factors. The resulting approach is well known as Orthogonal Variable Spreading Factor (OVSF-) Codes, cf., e.g., [Sza05, SW02] and references therein. For a specific parametrization, the new approach that is presented in this section for the assignment of different subcarriers to the users, is similar to the code tree of the OVSF-Codes [SW02] that is used for the assignment of different CDMA spreading codes.

3.5.3 Formulation of Constraints on the System Parameters

In this section, constraints on the system parameters are formulated. The introduction of constraints is motivated by the fact that a B-IFDMA signal has many degrees of freedom. On the one hand, this leads to a high flexibility. On the other hand, for the accommodation of B-IFDMA signals with different parameters in a system, the many degrees of freedom result in a high signalling overhead and a high computational

complexity for the subcarrier allocation algorithms due to a high number of admitted parameter combinations.

The constraints introduced in this section are formulated in order to reach two goals: On the one hand, the development of an algorithm that meets the demands formulated in Section 3.5.1 shall be made possible for B-IFDMA. On the other hand, important system properties like performance and flexibility shall be affected as little as possible.

In the following, let $Q^{(k)}$, $L^{(k)}$ and $M^{(k)}$ denote the number of subcarriers, the number of subcarrier blocks and the number of subcarriers per block, respectively, that are assigned to user k. Analogous to (2.36), let

$$Q^{(k)} = L^{(k)} \cdot M^{(k)}. \tag{3.139}$$

Without loss of generality, it is assumed that the N subcarriers available in the system are indexed by $n = 0, \ldots, N-1$ starting from the subcarrier at the lowest frequency. According to the definition in Section 2.4, the subcarrier blocks are equidistant. The distance between two adjacent subcarrier blocks assigned to user k can be described by the difference $D^{(k)}$ of the indices of the subcarriers at the lowest frequency within each of the two blocks.

Subcarriers with signal parameters $Q^{(k)}$, $L^{(k)}$, $M^{(k)}$ and $D^{(k)}$ assigned to user k are, in the following, denoted as a block-interleaved subcarrier set. A block-interleaved subcarrier set is well-defined by the signal parameters $L^{(k)}$, $M^{(k)}$, $D^{(k)}$ and the position of a dedicated subcarrier within the set. In the following, without loss of generality, this position is defined by the index $I^{(k)}$ of the subcarrier with the lowest frequency in the set. The signal parameters for a B-IFDMA signal are illustrated in Figure 3.8.

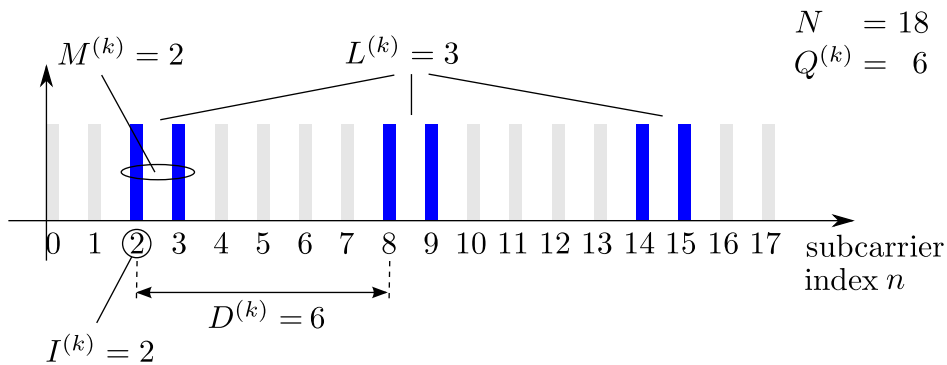Figure 3.8: Signal parameters for the B-IFDMA signal of user k for $N = 18$, $Q^{(k)} = 6$, $L^{(k)} = 3$, $M^{(k)} = 2$, $D^{(k)} = 6$ and $I^{(k)} = 2$.

In order to illustrate the benefits of the constraints introduced in this section, for comparison, in the following, a straightforward approach without constraints for accommodation of different numbers of block-interleaved subcarriers is regarded. For

this straightforward approach, the subcarrier sets assigned to a user are found, user by user, by a search for an available subcarrier set amongst all admitted combinations of the signal parameters $L^{(k)}$, $M^{(k)}$, $D^{(k)}$ and $I^{(k)}$ for a given number $Q^{(k)}$ according to the data rate request of user k. For the first combination of $L^{(k)}$, $M^{(k)}$, $D^{(k)}$ and $I^{(k)}$ that fits to the subcarriers that are available in the system, the according block-interleaved subcarrier set is assigned to user k. A high frequency diversity is achieved by starting the search with the largest admitted values for $L^{(k)}$ and $D^{(k)}$ and decreasing them step by step if the current parameter combinations do not fit to the subcarriers available in the system. When all admitted parameter combinations have been tested and no parameter combination fits to the subcarriers available in the system, the user is blocked.

The subcarrier allocation based on the straightforward approach has the following properties:

- The signalling overhead is high because the approach requires the signalling of the complete set of parameters $L^{(k)}$, $M^{(k)}$, $D^{(k)}$ and $I^{(k)}$. Moreover, there are many admitted values for each of the parameters leading to a high number of bits required for the signalling of each parameter.

- Due to the high degree of freedom for the parametrization of a B-IFDMA signal, the number of admitted parameter combinations is very high. Thus, especially for systems with high numbers of subcarriers, the computational complexity of the search is high.

- Due to the high number of admitted parameter combinations, the impact of a certain allocation of block-interleaved subcarriers to a user on the system as a whole is hard to describe. Especially the consequences for further assignments of subcarrier sets to users that will join the system at a later point in time cannot be described in a systematic and simple way.

- The probability that a user is blocked because none of the parameter combinations fits to the subcarriers available in the system is high. The reason for that is that a few awkwardly assigned sets of block-interleaved subcarriers may prevent a high number of other subcarrier sets from being assigned. Especially for signals with relatively prime parameters $L^{(k)}$ and $M^{(k)}$, an allocation without destroying the orthogonality different users' signals is difficult. A corresponding example is depicted in Figure 3.9. The parameters of the subcarrier set of user $k = 0$ that are depicted in red are $Q^{(0)} = 5$, $L^{(0)} = 5$, $M^{(0)} = 1$ and $I^{(0)} = 0$. In addition, two examples for allocations of B-IFDMA subcarrier sets of another user with
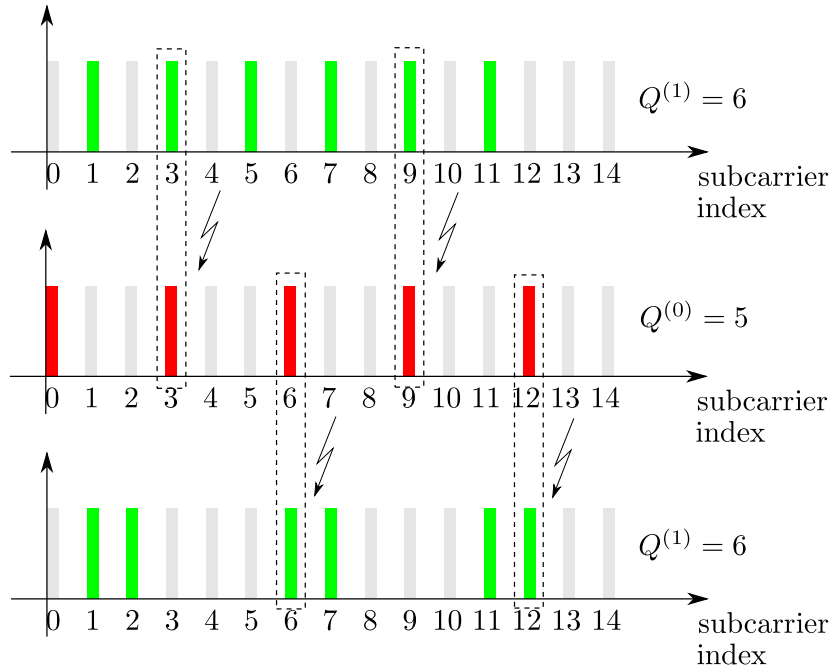
Figure 3.9: Example for the assignment of a subcarrier set with $Q^{(0)} = 5$ to user $k = 0$ and two alternative assignments of subcarrier sets with $Q^{(1)} = 6$ to user $k = 1$.

index $k = 1$ are given that are depicted in green. It can be seen that, for both examples, collisions with the subcarrier set of user $k = 0$ cannot be avoided although, for user $k = 1$, there are 10 subcarriers available in the system and the number of subcarriers assigned to user $k = 1$ is only $Q^{(1)} = 6$. The reason for the collisions is that, for both examples, $Q^{(0)}$ and $Q^{(1)}$ and, thus, also $L^{(0)}$ and $L^{(1)}$ are relatively prime.

In order to improve the subcarrier allocation, the system parameters are constrained as follows. Let

$$N = \prod_{r=0}^{R-1} p_r \qquad (3.140)$$

denote a factor decomposition of N, where p_r, $r = 1, \ldots, R - 1$, denote $R - 1$ prime numbers and where $p_0 = 1$. Note that, in general, the decomposition of a number N into $R - 1$ prime factors is unique except for the order of the prime factors. With the indexing of the prime factors in (3.140), an order is implicitly defined, because a distinct index is assigned to every prime factor.

In the following, in a cell, R different values are admitted for $L^{(k)}$ and $M^{(k)}$, respectively. Let L_l denote the R admitted values of $L^{(k)}$ with index $l = 0, \ldots, R - 1$. The admitted

values L_l are defined as products of the factors p_r according to

$$L_l = \prod_{r=0}^{R-1-l} p_r.$$

(3.141)

Consequently, the values L_l obtained according to (3.141) are integer multiples of each other.

Let, similarly, M_m denote the R admitted values of $M^{(k)}$ with index $m = 0, \ldots, R-1$. With L_l of (3.141), the R admitted values M_m are defined as

$$M_m = \frac{N}{L_{R-1-m}} = \frac{N}{\prod\limits_{r=0}^{m} p_r}.$$

(3.142)

Consequently, also the values M_m obtained according to (3.142) are integer multiples of each other. Further on, from (3.141) and (3.142) follows that, for $Q^{(k)} \leq N$, $Q^{(k)}$ is an integer divisor of N, because

$$\frac{N}{Q^{(k)}} = \frac{N}{L_l \cdot M_m} = \frac{N}{L_l \frac{N}{L_{R-1-m}}} = \frac{L_{R-1-m}}{L_l}$$

(3.143)

is an integer for all $l, m \in \{0, ..., R-1\}$ that fulfill $L_l \leq L_{R-1-m}$. A comparison of the left side of (3.143) and the right side of (3.143) shows that the condition $L_l \leq L_{R-1-m}$ is equivalent to the condition $Q^{(k)} \leq N$.

An important consequence of the constraints introduced in (3.141) and (3.142) is that an assignment of subcarrier sets with parameters $M^{(k)}$ and $L^{(k)}$ that are relatively prime for different users is prevented and, thus, the probability for blocking as depicted in Figure 3.9 is reduced. Moreover, the constraints formulated in (3.141) and (3.142) cause a considerable reduction of the number of admitted parameter combinations for B-IFDMA. Thus, they provide both, a reduction of the computational effort of the search for available subcarrier sets and a reduced signalling effort.

These advantages are obtained at the expense of a decreased flexibility and granularity in terms of numbers of subcarriers that can be assigned to a user. However, by the choice of N providing many small prime factors, a flexibility and granularity in terms of different numbers of subcarriers can be provided that can be considered as sufficient for practical applications. For N chosen as a power of 2, the flexibility and granularity is similar to the flexibility and granularity for resource allocation provided by the OVSF-Codes that are used in CDMA-based mobile radio systems. E.g., assuming a subcarrier bandwidth of $\Delta f \approx 40$ kHz, cf. [WIN05], and assuming N to be a power

of 2, for the presented approach, the provided instantaneous symbol rates are roughly given by $2^n \cdot 40$ kBaud, $n = 0, ..., \text{ld}(N)$. The exact values for the symbol rates are a little lower due to the overhead of the guard interval. Note that, as mentioned in Section 3.5.1, the granularity in terms of different data rates can be further increased by a combination of the assignment of different numbers of subcarriers to a user with TDMA and with an adaptive MCS.

In addition to the constraints formulated in (3.141) and (3.142), the signal parameter $D^{(k)}$ can be expressed dependent on N and $L^{(k)}$ according to

$$D^{(k)} = \frac{N}{L^{(k)}}. \tag{3.144}$$

Note that the admitted values of $L^{(k)}$ according to (3.141) imply that $D^{(k)}$ chosen according to (3.144) is also an integer divisor of N.

With (3.144), the signalling can be further reduced because only the parameters $L^{(k)}$, $M^{(k)}$ and $I^{(k)}$ have to be signaled and signalling of parameter $D^{(k)}$ can be omitted. Moreover, (3.144) provides maximum diversity for all users, because the subcarrier blocks are distributed over the total available bandwidth.

In order to make a simple and well-structured description of the allocation possible, finally, the admitted values of $I^{(k)}$ are constrained. Let $I_{l,m}$ denote the index of the subcarrier with the lowest frequency of the subcarrier set with parameters M_m and L_l. The admitted values of $I_{l,m}$ dependent on M_m and L_l are constrained to

$$I_{l,m} \in \{n | n = \eta \cdot M_m \wedge 0 \leq \eta < L_l \wedge 0 \leq n < N, \eta \in \mathbb{N}\}. \tag{3.145}$$

The constraint described in (3.145) means that, e.g., the subcarrier set depicted in Figure 3.8 can be only placed at positions that correspond to indices $I^{(k)} = 0, 2$ or 4, respectively, i.e., the admitted indices have to be multiple integers of the number $M^{(k)}$ of subcarriers per block and, further on, have to be chosen such that the subcarrier with the highest frequency is still within the system bandwidth.

The impact of the constraints introduced above on the signalling overhead can be summarized as follows:

- The number of admitted values for the parameters $L^{(k)}$ and $M^{(k)}$, respectively, is reduced to R. The number R is maximum for the special case that N is a power of 2. In this case, $R = \text{ld}(N) + 1$, cf. (3.140). Without any constraints, instead, N admitted values would have to be considered. For $N = 1024$, this corresponds

to a reduction of the number of bits required for signalling due to introduction of the constraints described above from 10 bits to 4 bits for each of the two signal parameters $L^{(k)}$ and $M^{(k)}$.

- The parameter $D^{(k)}$ does not have to be signalled any more. Without any constraints, also for $D^{(k)}$, up to N different admitted values have to be considered that corresponds to a number of 10 bits required for signalling if $N = 1024$ is assumed.

- The number of admitted values for the parameter $I^{(k)}$ is restricted. This can be exploited as follows: Assuming a minimum admitted number M_0 of subcarriers per block, which is a reasonable assumption for B-IFDMA, cf. [WIN06], instead of N admitted values for $I^{(k)}$, only N/M_0 admitted values have to be considered. Thus, the signalling effort is reduced by $\mathrm{ld}(M_0)$ bits compared to the case without any constraints. Similarly, the assumption of a minimum admitted number L_0 of subcarrier blocks provides a further reduction of $\mathrm{ld}(L_0)$ bits.

Moreover, the constraints from (3.140) - (3.145) enable efficient algorithms for subcarrier allocation based on a tree structure that is introduced in the next section.

3.5.4   Tree-based Subcarrier Allocation

In this section, based on the constraints introduced in Section 3.5.3, a tree structure is introduced. This tree structure provides a basis for efficient algorithms for the allocation of different numbers of subcarriers for B-IFDMA and provides a simple, well-structured and illustrative description of the consequences of a certain subcarrier allocation for the system.

The R admitted values L_l for $L^{(k)}$ according to (3.141) can be illustrated by a tree with R levels that are indexed by $l = 0, \ldots, R-1$. Each level corresponds to one of the R admitted values L_l. The nodes at level $l = 0$ and level $l = R-1$ are referred to as root and as leaves of the tree, respectively. The N leaves of the tree represent the N subcarriers available in the system.

At level l, the tree has
$$S_l = \frac{N}{L_l} \tag{3.146}$$
nodes. Every node at level l represents a set of L_l interleaved subcarriers with distance N/L_l corresponding to the L_l leaves originating from the respective node. An illustration of the tree for L_l with $N = 24$, $p_0 = 1$, $p_1 = 2$, $p_2 = 2$, $p_3 = 3$ and $p_4 = 2$ with p_r of

(3.140) is given in Figure 3.10. Note that (3.140) defines an order of the prime factors of N. With this order, the order of the admitted values L_l for $L^{(k)}$ is also defined, cf. (3.141). Thus, also the structure of the tree and of the numbers S_l of nodes at level l is defined by the order of the factors p_r in (3.140). However, as, in general, several different orders of the prime factors of a number N can be defined, for a given number N, in general, different trees are possible.

Let, without loss of generality, for a tree as depicted in Figure 3.10, the nodes of the tree be indexed in ascending order from the left to the right and let $s_l = 0, \ldots, S_l - 1$ denote the indices of the nodes at level l. The difference of the indices of two nodes at level l is, in the following, denoted as the distance of these nodes at level l. The subcarrier indices n are related to the N indices $s_l = 0, \ldots, N - 1$ of the nodes at level $R - 1$, i.e., the indices of the leaves, by

$$n = \sum_{r=0}^{R-2} \left\lfloor \frac{s_{R-1} \bmod L_r}{L_{r+1}} \right\rfloor \cdot \frac{N}{L_r}, \tag{3.147}$$

where $\lfloor \cdot \rfloor$ returns the closest integer smaller or equal to the argument. In the following, it is explained how the tree is used for subcarrier assignment. The assignment of a block-interleaved subcarrier set with $L^{(k)} = L_l$ subcarrier blocks and $M^{(k)} = M_m$ subcarriers per block to user k is equivalent to the assignment of M_m nodes at level l to this user as long as the distance of the assigned nodes at level l is equal to S_l/M_m. An illustration of the assignment of nodes to a user is given in Figure 3.11. E.g., the assignment of $L^{(k)} = 4$ blocks with $M^{(k)} = 2$ subcarriers per block to user k is equivalent to the assignment of 2 nodes at level $l = 2$, because for the tree that is depicted in Figure 3.11, $L_2 = 4$. The nodes at level 2 assigned to user k have to have a distance of $6/2 = 3$. Assuming that the 6 nodes at level $l = 2$ are numbered from the left to the right, there are 3 possibilities for the assignment: The nodes with indices $s_2 = 0$ and $s_2 = 3$, the nodes with indices $s_2 = 1$ and $s_2 = 4$ or the nodes with indices $s_2 = 3$ and $s_2 = 5$, respectively. In the given example, the nodes with indices $s_2 = 3$ and $s_2 = 5$ are assigned. The assigned nodes are indicated by green circles.

When a node in the tree is assigned to a certain user, this node and the children of the node, i.e., all nodes originating from this node, have to be marked as occupied and cannot be assigned to any other user. Moreover, also all nodes on the direct path to the root of the tree have to be marked as occupied. In Figure 3.11, the occupied nodes are indicated by green crosses. Note that all assignments of nodes in the tree according to the rules described above meet the constraints for $I_{l,m}$ given in (3.145).

In the following, the benefit of the tree structure for the subcarrier allocation is illustrated by an example. In Figure 3.12 a), $N = 24$ subcarriers are depicted. Some of
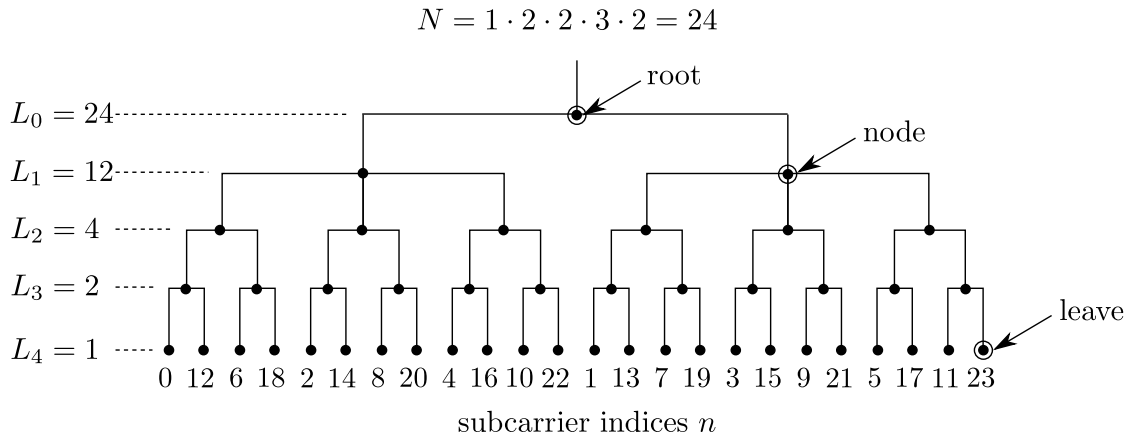
Figure 3.10: Example for a tree for L_l with $N = 24$, $p_0 = 1$, $p_1 = 2$, $p_2 = 2$, $p_3 = 3$ and $p_4 = 2$ with p_r of (3.140).
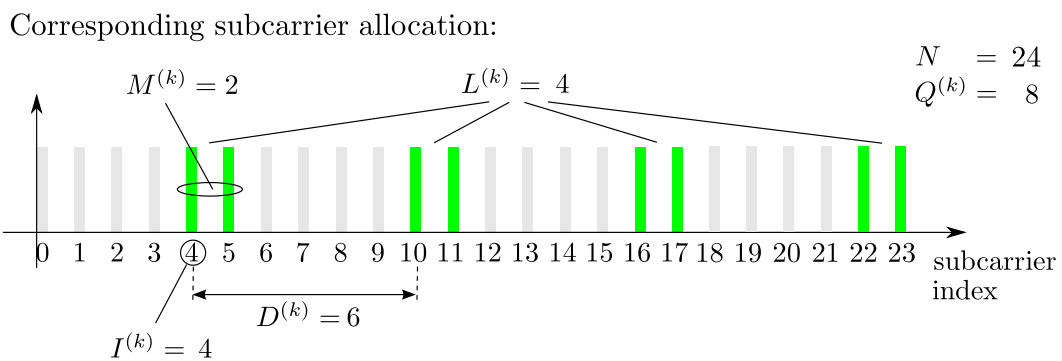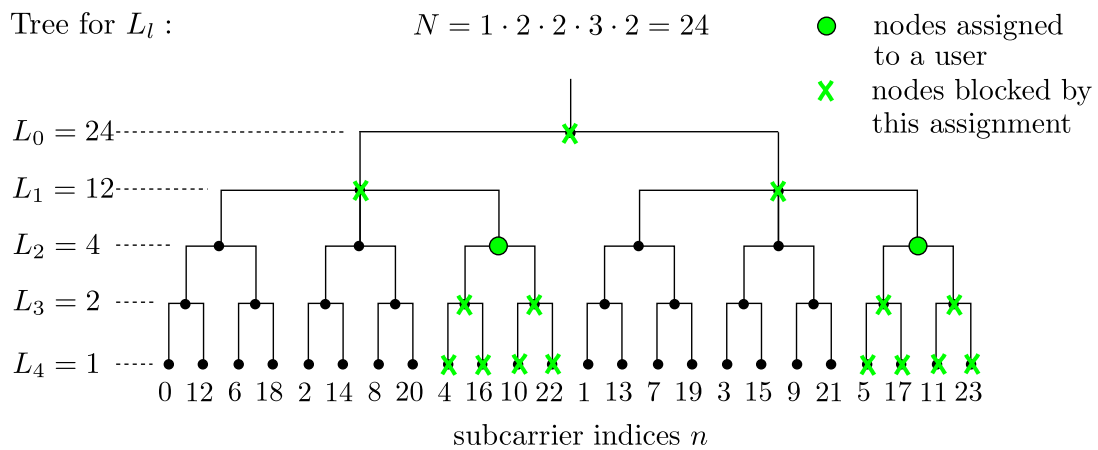

Figure 3.11: Illustration of the accommodation of a subcarrier set with parameters $L^{(k)} = 4$, $M^{(k)} = 2$ and $I^{(k)} = 4$.

them are not available for subcarrier allocation because they are already assigned to other users. It is assumed that two users $k = 0$ and $k = 1$ are joining the system. To user $k = 0$, a number of $Q^{(0)} = 8$ subcarriers and to user $k = 1$, a number of $Q^{(1)} = 4$ block-interleaved subcarriers shall be assigned. It is not obvious where the subcarriers can be allocated and it is even not obvious if the two subcarrier sets can be allocated or not. In the given example there is only one solution for this assignment which can be found, e.g., by an exhaustive search among all possible parameter combinations for block-interleaved subcarrier sets with $Q^{(0)} = 8$ and $Q^{(1)} = 4$, respectively. Applying the constraints introduced in Section 3.5.3, the possible parameter combinations can be reduced. Assuming a decomposition of $N = 24$ with $p_0 = 1$, $p_1 = 2$, $p_2 = 2$ $p_3 = 3$ and $p_4 = 2$, cf. (3.140), the admitted values for $L^{(k)}$ result in $L_0 = 24$, $L_1 = 12$, $L_2 = 4$, $L_3 = 2$ and $L_4 = 1$, cf. (3.141). The admitted values for $M^{(k)}$ result in $M_0 = 24$, $M_2 = 12$, $M_2 = 6$, $M_3 = 2$ and $M_4 = 1$, cf. (3.142). Thus, the only admitted parametrization for user $k = 0$ is $L^{(0)} = 4$ and $M^{(0)} = 2$. For user $k = 1$, only the parameters $L^{(1)} = M^{(1)} = 2$ or the parameters $L^{(1)} = 4$ and $M^{(1)} = 1$ are admitted, respectively. For user $k = 0$, the admitted start indices $I^{(0)}$ are $0, 2$ and 4, cf. (3.145). For user $k = 1$, the admitted start indices $I^{(1)}$ are $0, 2, 4, 6, 8, 10$ for $L^{(1)} = M^{(1)} = 2$ or $0, 2, 4, 1, 3, 5$ for $L^{(1)} = 4$ and $M^{(1)} = 1$, respectively, cf. (3.145). It can be seen that, even having introduced the constraints from Section 3.5.3, still a large number of admitted subcarrier allocations has to be checked whether it is feasible or not. Note, that for each subcarrier set that is considered, the positions of all $Q^{(k)}$ subcarriers in the set have to be checked whether they are occupied or not.

In Figure 3.12 b), the tree structure according to the situation shown in Figure 3.12 a) is depicted. Following the above introduced rules for subcarrier allocation using the tree, for the subcarriers that are already occupied, the nodes on the direct path from the respective leaves to the root of the tree have to be marked as occupied as it is done in Figure 3.12 b) by the black crosses. Thus, the rules for subcarrier allocation using the tree cause a further reduction of the number of possible subcarrier allocations in addition to the constraints formulated in Section 3.5.3. The reason is, that using the tree, the interdependencies between different subcarrier allocations is now taken into consideration. If only one subcarrier, that is part of an admitted subcarrier set, is already occupied, the whole set has to be marked as unavailable. From Figure 3.12 b) is can be seen that, thus, the introduction of the tree brings an additional simplification of the subcarrier allocation procedure. For the given example, for user $k = 0$, two available nodes at level $l = 2$ with distance $S_2/M^{(0)} = 6/2 = 3$ have to be found. Obviously, this is only given for the nodes with index $s_2 = 2$ and with index $s_2 = 5$. For user $k = 1$, either two available nodes at level $l = 3$ with distance $S_3/M^{(1)} = 12/2 = 3$ or one available node at level $l = 2$ have to be found. Using the

tree, it can be seen that assigning the available nodes at level $l = 1$ to user $k = 1$ would lead to an occupation of the nodes with index $s_2 = 2$ and with index $s_2 = 5$ at level $l = 2$. In this case, the subcarrier set for user $k = 0$ could not be assigned at all. The feasibility to describe the impact of a certain subcarrier allocation on other subcarrier allocations in the system is a further advantage of the tree structure. The only possibility to assign subcarriers for user $k = 1$ is the assignment of the subcarriers corresponding to the node with index $s_2 = 0$ at level $l = 2$. In Figures 3.12 c) and d), the above described results of the search are illustrated. The subcarrier set that can be assigned to user $k = 0$ and the corresponding nodes in the tree are marked in green, the respective subcarrier set and nodes in the tree for user $k = 1$ are marked in blue.

In the example presented above it has been shown that the introduction of the tree structure brings the following additional benefits:

- The computational complexity for the search of available subcarrier sets is further reduced compared to the introduction of constraints described in Section 3.5.3. One reason is, that the application of the tree makes possible to take also the interdependencies of different subcarrier allocations into consideration and, thus, further reduces the search space for possible subcarrier allocations. A second reason is that, for a given number $L^{(k)}$, the available numbers L_l of subcarriers per block can be directly determined from the S_l nodes at level l of the tree. Thus, instead of a check of all $Q^{(k)}$ subcarriers in the set, only a check of $S_l < Q^{(k)}$ nodes at level L_l in the tree is required in order to decide whether a subcarrier set can be assigned or not.

- The tree provides a simple and well-structured description of the consequences of a subcarrier allocation for the system, especially for the subcarriers that will be available for users joining the system at a later point in time.

However, the subcarrier allocation algorithm using a tree for the admitted values of $L^{(k)}$ becomes the more complex the larger $M^{(k)}$ and the lower $L^{(k)}$. The reason is that, one the one hand, according to (3.146), S_l increases with decreasing L_l. On the other hand, the number of equidistant nodes that has to be assigned to a user at a certain level l of the tree is equal to $M^{(k)}$. Thus, for large values of $M^{(k)}$ and low values of $L^{(k)}$, an alternative solution with lower complexity is desirable. Similar to the tree introduced based on the R different admitted values of $L^{(k)}$, that has been introduced above, a tree structure can be also defined for the R admitted values of $M^{(k)}$. The tree for the admitted values of $M^{(k)}$ is dual to the tree for the admitted values of $L^{(k)}$ and

a)

available subcarriers

unavailable subcarriers

b) Corresponding tree for L_l, l=0,...,4: $N = 1 \cdot 2 \cdot 2 \cdot 3 \cdot 2 = 24$

$L_0 = 24$

$L_1 = 12$

$L_2 = 4$ $s_2 = 0$ $s_2 = 1$ $s_2 = 2$ $s_2 = 3$ $s_2 = 4$ $s_2 = 5$

$L_3 = 2$

$L_4 = 1$

0 12 6 18 2 14 8 20 4 16 10 22 1 13 7 19 3 15 9 21 5 17 11 23

subcarrier indices n

✗ unavailable nodes

c)

available subcarriers   subcarrier set with $Q^{(0)} = 8$

unavailable subcarriers   subcarrier set with $Q^{(1)} = 4$

d) Corresponding tree for L_l, l=0,...,4: $N = 1 \cdot 2 \cdot 2 \cdot 3 \cdot 2 = 24$

$L_0 = 24$

$L_1 = 12$

$L_2 = 4$ $s_2 = 0$ $s_2 = 1$ $s_2 = 2$ $s_2 = 3$ $s_2 = 4$ $s_2 = 5$

$L_3 = 2$

$L_4 = 1$

0 12 6 18 2 14 8 20 4 16 10 22 1 13 7 19 3 15 9 21 5 17 11 23

subcarrier indices n

✗ unavailable nodes

●/● nodes assigned for a subcarrier set with $Q^{(0)} = 8$ / $Q^{(1)} = 4$ subcarriers

✗/✗ nodes occupied by the assignment of the subcarrier set with $Q^{(0)} = 8$ / $Q^{(1)} = 4$
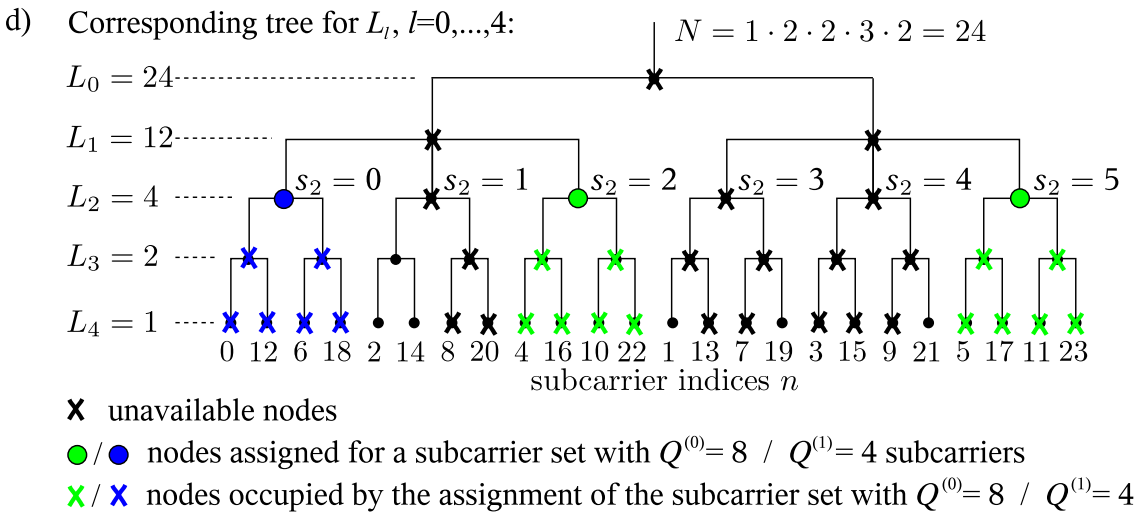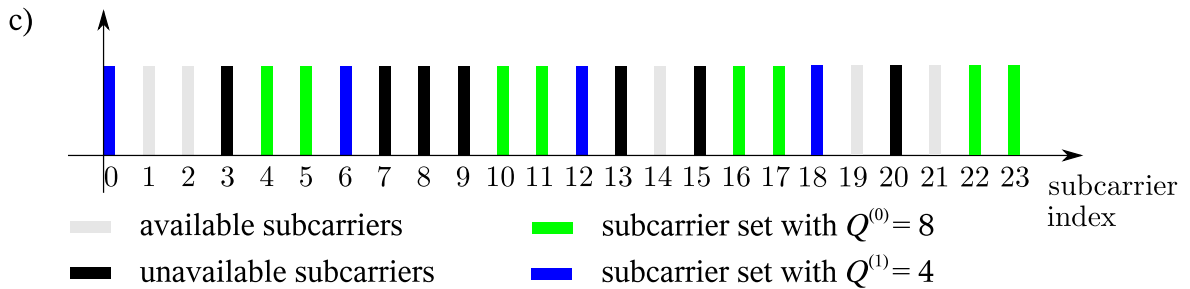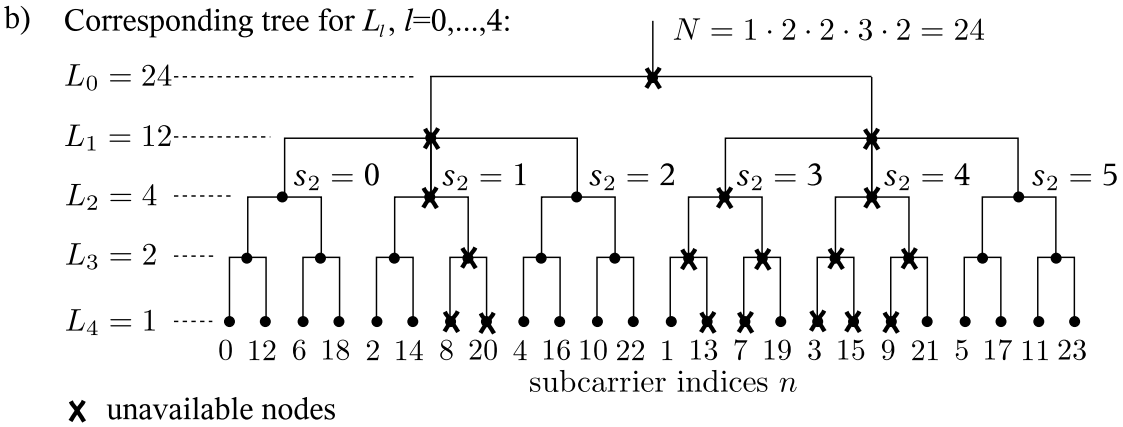
Figure 3.12: Example for tree based subcarrier allocation.

does not provide any additional information but provides lower complexity for large values of $M^{(k)}$ and low values of $L^{(k)}$.

In the following, the tree for the admitted values M_m of $M^{(k)}$ is described. It provides R levels indexed by $m = 0, \ldots, R - 1$. Each level corresponds to one of the R admitted values M_m. Again, the nodes at level $m = 0$ and $m = R - 1$ are referred to as root and as leaves of the tree, respectively, and the N leaves of the tree represent the N subcarriers available in the system. At level m, the tree has

$$S_m = \frac{N}{M_m} \tag{3.148}$$

nodes. Every node at level m represents a set of M_m adjacent subcarriers corresponding to the M_m leaves originating from the respective node. Without loss of generality, let the nodes of the tree be indexed in ascending order from the left to the right and let $s_m = 0, \ldots, S_m - 1$ denote the indices of the nodes at level m. The subcarrier indices n are related to the indices s_{R-1} of the nodes at level $R - 1$, i.e., the indices of the leaves, by

$$n = s_{R-1}. \tag{3.149}$$

Thus, the assignment of a block-interleaved subcarrier set with $M^{(k)} = M_m$ subcarriers per block and $L^{(k)} = L_l$ blocks of subcarriers to user k is equivalent to the assignment of L_l nodes at level m to this user as long as the distance of the assigned nodes at level l is equal to S_m/L_l. When a node in the tree is assigned to a certain user, this node and the children of the node have to be marked as occupied. Moreover, also all nodes on the direct path to the root of the tree have to be marked as occupied.

Again, all assignments of nodes in the tree according to the rules described above meet the constraints for $I_{l,m}$ given in (3.145).

The tree for the admitted values of $M^{(k)}$ has similar properties as the tree for the admitted values of $L^{(k)}$. However, the following properties of the tree are different:

- From the S_m nodes at level m of the tree, the available numbers M_m of subcarriers per block can be directly read out. Thus, the $S_m < Q^{(k)}$ nodes at level M_m in the tree can be checked in order to decide whether a subcarrier set can be assigned or not.

- For B-IFDMA signals with a high number $M^{(k)}$ of subcarriers per block and a low number $L^{(k)}$ of subcarrier blocks, the search for available resources using the tree for the admitted values of $M^{(k)}$ provides a lower complexity than a search using

the tree for the admitted values of $L^{(k)}$. The reason is that, on the one hand, according to (3.148), S_m decreases with increasing $M^{(k)}$. On the other hand, the number of equidistant nodes that has to be assigned to a user at a certain level l of the tree is equal to $L^{(k)}$.

E.g., for IFDMA, i.e., B-IFDMA with $M^{(k)} = 1$, the tree for the admitted values L_l of $L^{(k)}$ is more appropriate, whereas, for localized SC-FDMA, i.e., B-IFDMA with $L^{(k)} = 1$, the tree for the admitted values M_m of $M^{(k)}$ is preferred.

3.5.5   Important Special Cases

In this section, important special cases of the tree-based subcarrier allocation are addressed that are considered as relevant for practical applications.

The choice of N according to

$$N = z^k, \quad k \in \mathbb{N}, \tag{3.150}$$

where z denotes an arbitrary prime number, leads to a symmetric structure of the tree. For the special case $z = 2$, the tree is similar to the well known tree for OVSF codes [Sza05, SW02] and references therein. For this case, the maximum granularity and flexibility in terms of different numbers of subcarriers that can be assigned to a user is provided. For IFDMA and LFDMA with $z = 2$, the tree-based allocation presented in this section is similar to the use of the OVSF codes. Consequently, also well known algorithms, e.g., for Dynamic Code Assignment (DCA) [MS00] can be directly applied.

For the special case of a B-IFDMA system assuming a minimum admitted number M_0 of subcarriers per block, the tree structure for L_l can be further simplified. The simplified tree is obtained by replacing N by N/M_0 and M_m by M_m/M_0 for the tree for L_l defined in Section 3.5.4. The simplified tree for L_l is illustrated in Figure 3.13. It is equivalent to the left half of the original tree for L_l depicted in Figure 3.11 and its leaves represent the indices of the subcarriers with the lowest frequency within each subcarrier block. As each leave of this tree now represents a block of $M_0 = 2$ subcarriers, the same block-interleaved subcarrier set as allocated in the tree from Figure 3.11 is obtained by assignment of $M^{(k)}/M_0 = 1$ node at level $l = 2$.

Assuming a minimum admitted number M_0 of subcarriers per block, also the tree structure for M_m can be simplified. All nodes at the levels m with $M_m < M_0$ can be

$$N = 1 \cdot 2 \cdot 2 \cdot 3 \cdot 2 = 24$$

$$M_0 = 2$$

● nodes assigned to a user for $M^{(k)} = 2$ and $L^{(k)} = 4$

✗ nodes blocked by this assignment

$L_1 = 12$

$L_2 = 4$

$L_3 = 2$

$L_4 = 1$

0 12 6 18 2 14 8 20 4 16 10 22
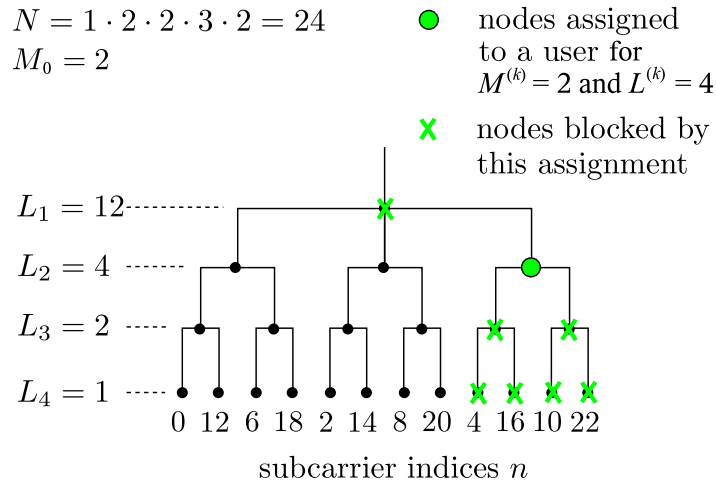
subcarrier indices n

Figure 3.13: Simplification of the tree for L_l in Figure 3.11 assuming $M_0 = 2$.

cut. The indices n of the lowest subcarriers within each block that is related to a leave of the simplified tree for M_m can be obtained from the indices s_m of the leaves by

$$n = M_0 \cdot s_m. \tag{3.151}$$

Similarly, for a system with a given minimum number L_0 of subcarrier blocks, a simplified tree for M_m is obtained by replacing N by N/L_0 and L_l by L_l/L_0 for the tree for M_m defined in Section 3.5.4. The resulting tree is equivalent to the branch of the original tree for M_m whose leaves give the indices of the subcarriers of the block with the lowest frequencies within each subcarrier set.

Assuming a system with a given minimum number L_0 of subcarrier blocks, also the tree for L_l can be simplified by cutting all nodes at the levels l, where $L_l < L_0$. The indices n of the subcarriers in the block with the lowest frequencies in the subcarrier set can be obtained from the indices s_l of the leaves of the simplified tree by

$$n = \sum_{r=0}^{l-1} \left\lfloor \frac{s_l \bmod L_r}{L_{r+1}} \right\rfloor \cdot \frac{N}{L_r}. \tag{3.152}$$

3.5.6 Conclusions

In Section 3.5, a new approach for accommodation of different data rates is introduced for B-IFDMA. The major results of the section can be summarized as follows: The presented approach

- makes an efficient assignment of block-interleaved subcarrier sets with different numbers of subcarriers per user within one cell possible.

- offers the accommodation of a wide range of different data rates to the users in one cell without introducing undesired large delays for buffering of the data, because the assignment of different numbers of subcarriers allows to adapt the instantaneous symbol rate that is used for transmission.

- provides maximum frequency diversity for all users, because, for all users, the subcarrier blocks are distributed over the total available bandwidth.

- avoids MAI, because it guarantees that every subcarrier is exclusively assigned to a single user and, thus, the approach maintains the orthogonality of different users' signals.

- provides low signalling effort by introducing constraints for the B-IFDMA signal parameters.

- reduces the probability that a user is blocked if a sufficient number of subcarriers to serve the user is available in the system, which is obtained by avoiding an assignment of block-interleaved subcarrier sets with relatively prime parameters.

- provides a simple and well-structured description of the consequences of a subcarrier allocation for the system, especially for the subcarriers that will be available for users joining the system at a later point in time, which is obtained by organizing the admitted signal parameters in a tree-structure.

- provides low computational effort, because instead of an exhaustive search a computationally efficient tree-based algorithm is used for subcarrier allocation.

- obtains its advantages at the expense of constraints on the B-IFDMA signal parameters, but for an appropriate choice of the number N of subcarriers in the system, e.g., as a power of 2, the remaining flexibility and granularity in terms of different numbers of subcarriers that can be assigned to a user can be considered as sufficient for practical applications.

- can be easily combined with TDMA and an adaptation of the MCS in order to further increase the granularity and flexibility of the scheme in terms of different data rates.

- can be applied for B-IFDMA including IFDMA and LFDMA as special cases as well as for B-EFDMA.

Chapter 4

Analysis of the Properties of B-IFDMA

4.1 Introduction

In this chapter, important properties of B-IFDMA and their dependency on the B-IFDMA signal parameters are analyzed. As introduced in Section 2.4, the B-IFDMA signal parameters are

- the number L of subcarrier blocks,

- the number M of subcarriers per block, and

- the number N_t of consecutive modulated data vectors that are assigned to a certain user.

The number Q of subcarriers assigned to a certain user is given by $Q = L \cdot M$, cf. (2.36).

Since B-IFDMA is a new scheme, a detailed quantitative analysis of its properties is required in order to evaluate the scheme with respect to an application in the uplink of future mobile radio systems. The properties can be categorized in performance analysis, complexity analysis and investigation of real world effects.

Throughout this chapter, for the performance analysis

- the bit error rate (BER) dependent on the signal to noise ratio (SNR) is investigated for different signal parameters. As the amount of diversity that is exploited by B-IFDMA is reflected in the BER performance, the BER dependent on the SNR is also used as a metric for the diversity properties of B-IFDMA.

- the overhead due to pilot symbols required for channel estimation is investigated. The use of pilot symbols for channel estimation results in an additional amount of energy that is required for the transmission of each data symbol. Consequently, the insertion of pilot symbols leads to a degradation of the required SNR in order to provide a certain BER performance compared to a transmission without pilot symbols. This SNR degradation is used as a metric for the overhead due to pilot symbols required for channel estimation.

For the complexity analysis,

- the computational effort required for B-IFDMA in a mobile terminal and in a base station, respectively, is analyzed in terms of required numbers of complex multiplications and divisions.

For the investigation of real world effects,

- the robustness to carrier frequency offsets is analyzed. It can be measured by the performance degradation in presence of carrier frequency offsets compared to the case where carrier frequency offsets do not occur. For that reason, also for the analysis of the robustness of B-IFDMA to carrier frequency offsets, the BER versus the SNR is used as a metric.

- the envelope fluctuations of the B-IFDMA transmit signal are analyzed in terms of the Peak-to-Average Power Ratio (PAPR), cf. [vNP00], the Cubic Metric (CM), cf. [SSJ06], and the required power back-off (BO) for the power amplifier in order to avoid undesired out-of-band radiations due to the non-linear distortions caused by the power amplifier.

A summary of the quantitatively investigated properties and the metrics used is shown in Table 4.1. Note that, in addition to the quantitative analysis of the envelope fluctuations for B-IFDMA, also a qualitative discussion of the power efficiency of the power amplifier for B-IFDMA dependent on its signal parameters is presented.

Besides the analysis of the properties of B-IFDMA, a comparison of the properties of B-IFDMA to the properties of the candidate multiple access schemes that are currently under consideration for the non-adaptive uplink as described in Section 1.1.3 is performed. In particular, throughout this chapter, the properties of B-IFDMA including IFDMA and localized SC-FDMA as special cases are compared to the properties of OFDMA and to the properties of localized SC-FDMA with FH. The major results of this chapter have been published in [SFE+09] by the author of this thesis .

The remainder of this chapter is organized as follows. The performance analysis is given in Section 4.2. Section 4.3 gives results for the computational effort required for B-IFDMA. In Section 4.4, the real world effects are addressed. The robustness of B-IFDMA to carrier frequency offsets is analyzed, the envelope of the B-IFDMA transmit signal is investigated and the power efficiency of the scheme is discussed. Finally, in Section 4.5, the results from Chapter 4 are summarized and concluded.

Table 4.1: Properties of B-IFDMA quantitatively investigated throughout this chapter
and respective metrics.

property	metric
performance, diversity exploited	BER versus SNR
pilot symbol overhead for channel estimation	SNR degradation
computational complexity	number of multiplications and divisions
robustness to carrier frequency offsets	BER versus SNR
envelope fluctuations	PAPR, CM, BO

4.2   Performance

4.2.1   Overview

In this section, the performance of B-IFDMA for coded transmission over a mobile
radio channel and the diversity exploited by B-IFDMA are analyzed. Section 4.2 is
organized as follows: In Section 4.2.2, the frequency diversity exploited by B-IFDMA is
analyzed dependent on its signal parameters and compared to the frequency diversity
exploited by OFDMA and localized SC-FDMA with FH. Note that throughout the
performance analysis, IFDMA and localized SC-FDMA are regarded as special cases
of B-IFDMA, cf. Section 2.5, whereas localized SC-FDMA with FH is regarded as an
individual scheme. Section 4.2.3 discusses the time diversity exploited by a combination
of B-IFDMA with FEC coding and bit interleaving over consecutive modulated data
vectors. In Section 4.2.4, the performance gains due to a combination of B-IFDMA
with spatial diversity exploiting schemes like the approach for STBC from Section
3.3 and Maximum Ratio Combining (MRC) are quantified. Section 4.2.5 discusses
the multi-user diversity provided by B-IFDMA and its limits in presence of unreliable
channel quality information at the transmitter. The performance degradation due to
the pilot symbol overhead required for channel estimation is quantified in Section 4.2.6
and compared to the respective results for localized SC-FDMA with FH.

4.2.2   Frequency Diversity

In this section, the frequency diversity properties of B-IFDMA are analyzed and compared to the frequency diversity provided by OFDMA and localized SC-FDMA with FH. For that purpose, performance results for coded B-IFDMA transmission over a mobile radio channel are presented and discussed. For the performance analysis, the BER is investigated dependent on the SNR. For the definition of the SNR, an AWGN with a two-sided power spectral density $S_{NN}(f) = N_0/2$ is assumed. Further on, let E_{b} denote the energy that is spent per transmission of an information bit. In the following, the SNR is defined in terms of E_{b}/N_0.

For the performance analysis, the system parameters are chosen according to the WINNER system design presented in [WIN07c] and are summarized in Table 4.2. A system bandwidth of $B = 40$ MHz and a total number of $N = 1024$ subcarriers is considered. It is assumed that the system is operating at a carrier frequency of $f_0 = 3.7$ GHz. The length of the guard interval is chosen as $T_{\mathrm{CP}} = 3.2$ μs. With the length of a modulated data vector of $T = N/B = 1024/(40 \text{ MHz}) = 25.6$ μs, the guard interval results in an overhead of $T_{\mathrm{CP}}/T = 12.5$ %. A Quarternary Phase Shift Keying (QPSK) mapping and a convolutional code with rate 1/2 with constraint length 6 are considered. The according code polynomials are given in Table 4.2. At the receiver, the Max-Log-MAP decoding algorithm [RHV97] is used. A random bit interleaving over $N_{\mathrm{t}} = 4$ consecutive modulated data vectors is assumed. This corresponds to the case where 4 consecutive modulated data vectors are assigned to a user by means of TDMA and where all 4 modulated data vectors are used for bit interleaving.

As channel model, the WINNER channel described in [WIN07f] is used. The considered scenario is an urban wide area scenario that complies to the respective scenario details formulated in [WIN07f]. It is assumed that the channel is perfectly known at the receiver, i.e., the effect of channel estimation errors is omitted.

For the discussion of the performance results, the coherence time T_{c} and the coherence bandwidth B_{c} of the mobile radio channel play an important role. Since in the literature various different definitions for coherence time and coherence bandwidth are used, in the following, both quantities are defined.

Let c_0 and v denote the speed of light and the velocity of a mobile station, respectively. Let, further on,

$$f_{\mathrm{D,max}} = f_0 \cdot \frac{v}{c_0} \tag{4.1}$$

Table 4.2: List of Parameters

System Parameters	
system bandwidth	$B = 40$ MHz
total number of subcarriers	$N = 1024$
carrier frequency	$f_0 = 3.7$ GHz
guard interval	$T_{\mathrm{CP}} = 3.2\ \mu$s
Link Parameters	
modulation	QPSK
code	convolutional code, rate 1/2
code polynomials	133,171
constraint length	6
decoder	Max-Log-MAP [RHV97]
interleaving	random over $N_{\mathrm{t}} = 4$ modulated data vectors
Channel	
channel model	WINNER mobile radio channel [WIN07f]
scenario	wide area, urban [WIN07f]
channel estimation	perfect
user velocity	$v = 70$ km/h
Coherence time	$T_{\mathrm{c}} \approx 2.1$ ms
Coherence bandwidth	$B_{\mathrm{c}} \approx 550$ kHz
Simulation Parameters	
sampling rate	$K/T_{\mathrm{s}} = 1/(25$ ns$)$

denote the maximum Doppler frequency for this mobile station. Assuming that the Doppler frequency is solely caused by the movement of the mobile station, the coherence time T_c can be defined as

$$T_c = \frac{1}{2 \cdot f_{D,\max}} = \frac{1}{B_D}, \tag{4.2}$$

where $B_D = 2 \cdot f_{D,\max}$ is the well-known Doppler bandwidth [Kam08]. The coherence time defined according to (4.2) gives the time required for the mobile station to cover a distance of half a wavelength and is equivalent to the maximum possible sampling interval for the mobile radio channel in time according to the sampling theorem [FK03]. For the considered channel, assuming a user velocity of $v = 70$ km/h, the coherence time is given by $T_c \approx 2.1$ ms. It can be assumed that the mobile radio channel is almost time invariant within a time interval of length $T_c/5 \approx 0.42$ ms. From a comparison of this value to the duration $T + T_{CP} = 28.8$ μs of a modulated data vector with CP follows that the channel is almost constant for the transmission of more than 14 consecutive modulated data vectors. Thus, even if bit interleaving over N_t consecutive modulated data vectors is applied, almost no time diversity can be exploited as long as $N_t \leq 14$.

The coherence bandwith B_c can be defined as

$$B_c = \frac{1}{\Delta\tau}, \tag{4.3}$$

where $\Delta\tau$ denotes the time difference between the first and the last received propagation path of the mobile radio channel which is well-known as the maximum channel excess delay [Pae99]. Similar to the definition of T_c, that gives the maximum possible sampling interval for the mobile radio channel in time direction, the definition of the coherence bandwidth B_c gives the maximum possible sampling interval for the mobile radio channel in frequency direction according to the sampling theorem [FK03]. For the considered channel, the coherence bandwidth is given by $B_c \approx 550$ kHz. Again, it can be assumed that the channel is almost constant within a bandwidth of $B_c/5 \approx 110$ kHz.

The amount of frequency diversity that is exploited by B-IFDMA depends on the B-IFDMA signal parameters. In the following, the performance is investigated for a fixed given number Q of subcarriers assigned to a user. This corresponds to the assumption of a fixed given data rate. For example, assuming $Q = 32$, a number of $Q = 32$ data symbols are transmitted within the time $T + T_{CP} = 28,8$ μs. Each data symbol contains 2 coded bits due to the QPSK modulation and 1 information bit due to the code rate 1/2. Thus, the resulting data rate that is, in the following, denoted as instantaneous net bit rate, results in 32 bit/28,8 μs=1.11 Mbps. Accordingly, $Q = 64$ and $Q = 128$ corresponds to instantaneous net bit rates of 2.22 Mbps and 4.44 Mbps, respectively.

In the following, the performance is investigated by means of Monte Carlo simulations of the BER dependent on the E_b/N_0 for given values of Q. Since N_t is fixed to $N_t = 4$ as described in Table 4.2 and since $Q = L \cdot M$, the remaining degree of freedom for the B-IFDMA signal parameters is given by the choice of either L or M. For the performance analysis, in the sequel, L is used as parameter. A single mobile radio cell is considered. The considered sampling rate for data transmission is $K/T_s = 1/(25 \text{ ns}) = 40$ mega samples per second with K and T_s as defined in Section 2.3.2. The signals of the different users within the cell are assumed to be perfectly orthogonal. Thus, only one users' signal is regarded. Moreover, perfect slow power control is assumed and, thus, the slow fading of the mobile radio channel as well as the dependency of the quality of the link on the distance of the mobile terminal to the base station is omitted.

In Figures 4.1-4.3 the performance results are presented for $Q = 128$, $Q = 64$ and $Q = 32$, respectively. It can be seen that for all data rates, the BER performance of B-IFDMA improves with an increasing number L of subcarrier blocks. Moreover, a comparison of Figures 4.1-4.3 shows that for a data rate of 4.44 Mbps, the performance for $L = 1$ is significantly better than for the respective curves for $L = 1$ for 2.22 Mbps and 1.11 Mbps. At the same time, the performance for $L = Q$ is only slightly different for 4.44 Mbps, 2.22 Mbps and 1.11 Mbps.
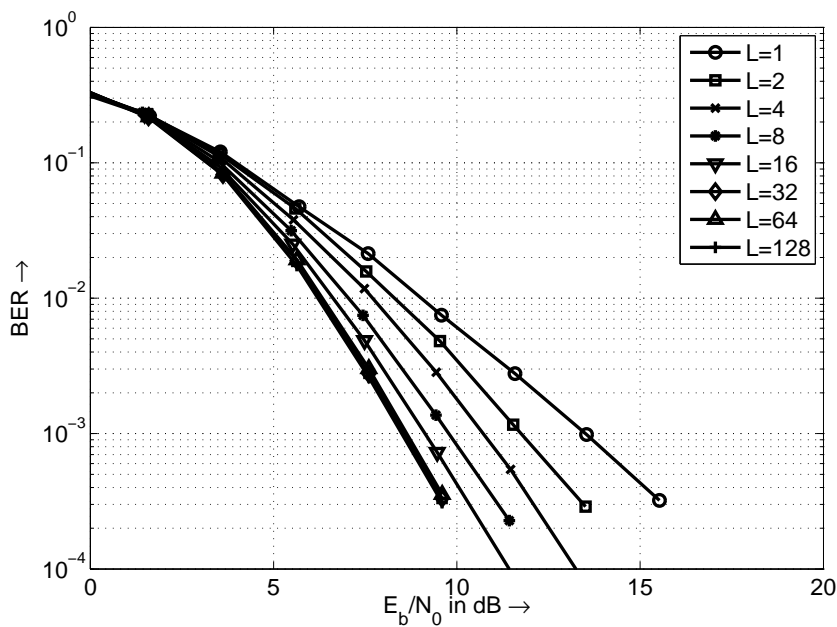

Figure 4.1: BER versus E_b/N_0 for coded transmission with $Q = 128$ subcarriers per user, i.e., for an instantaneous net bit rate of 4.44 Mbps, dependent on the number L of subcarrier blocks.

The required E_b/N_0 for a BER of 10^{-3}, that is a typical value required for speech
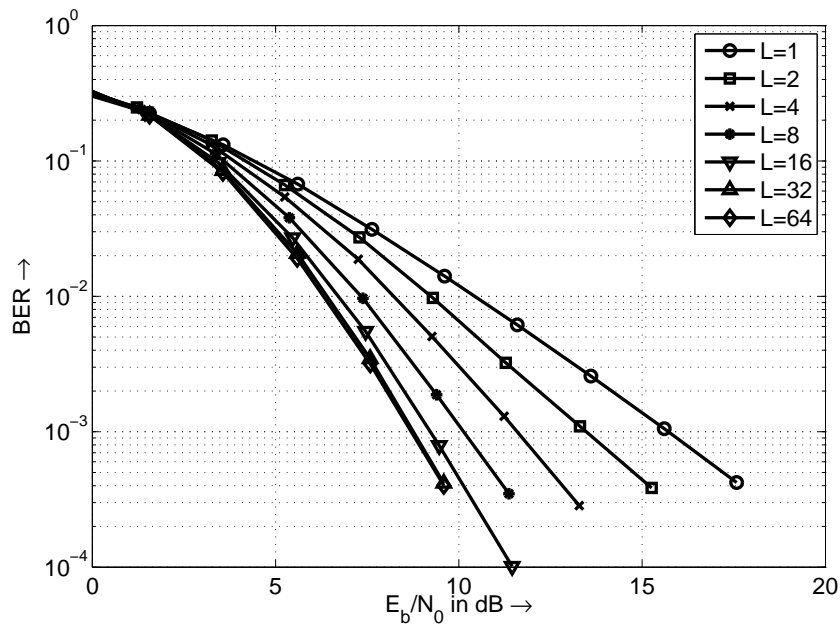
Figure 4.2: BER versus E_{b}/N_0 for coded transmission with $Q = 64$ subcarriers per user, i.e., for an instantaneous net bit rate of 2.22 Mbps, dependent on the number L of subcarrier blocks.

Figure 4.3: BER versus E_{b}/N_0 for coded transmission with $Q = 32$ subcarriers per user, i.e., for an instantaneous net bit rate of 1.11 Mbps, dependent on the number L of subcarrier blocks.
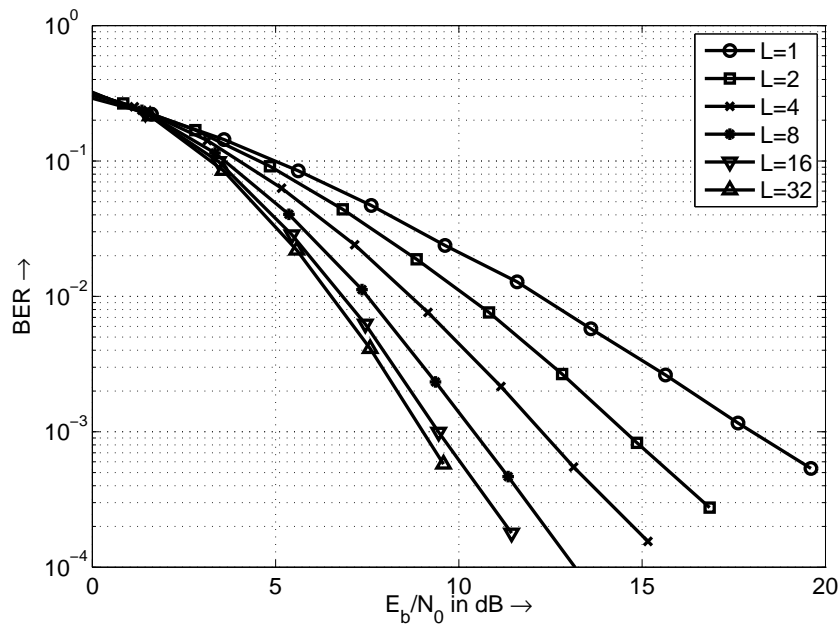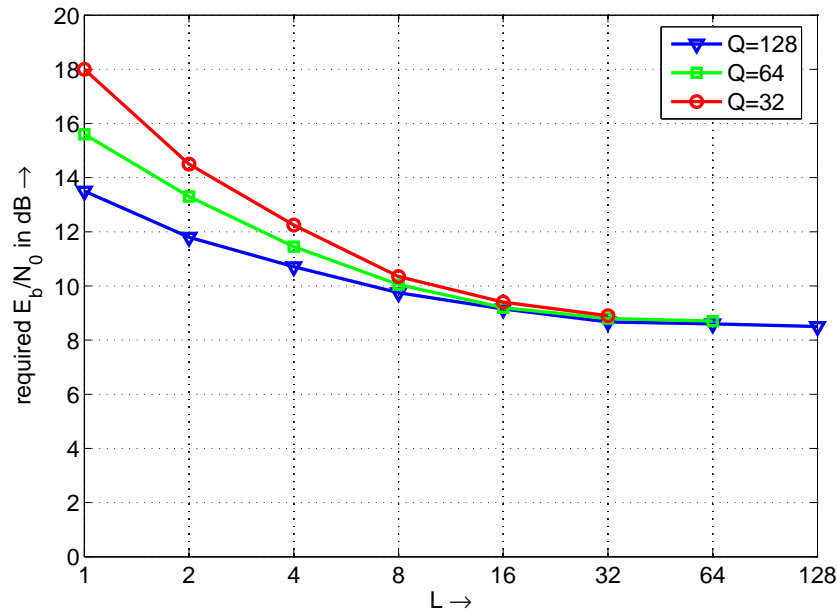
Figure 4.4: Required E_b/N_0 at a BER of 10^{-3} for different data rates dependent on the number L of subcarrier blocks.

transmission, is depicted in Figure 4.4. For packet transmission, it is also appropriate to regard a BER of 10^{-3}. The reason is that, in a future mobile radio system, in addition to the forward error correction code, for packet transmission, Automatic Repeat Request (ARQ) or Hybrid Automatic Repeat Request (HARQ) techniques will be used [Ea06, WIN05] that provide a BER that is considerably lower than 10^{-3}.

In Figure 4.4, it can be seen that the required E_b/N_0 at a BER of 10^{-3} decreases with an increasing L. The decrease is the more pronounced the lower the data rate. For low values of L, the required E_b/N_0 at a BER of 10^{-3} is the higher the lower the data rate. For high values of L, the required E_b/N_0 at a BER of 10^{-3} is similar for all data rates.

The results from Figures 4.1-4.3 and from Figure 4.4 can be interpreted as follows. The amount of frequency diversity exploited by B-IFDMA increases with an increasing number L of subcarrier blocks. The reason for that is that each of the subcarrier blocks experiences a fading of the channel that is almost independent of the fading in other blocks as long as the spacing between the blocks is larger than B_c. For $L \geq B/B_c$, the performance saturates because the spacing between the subcarrier blocks becomes smaller than B_c and, thus, no additional frequency diversity is exploited. For the given channel, $B/B_c \approx 73$. Consequently, for $L \geq 64$, no further performance gains are

obtained. Figure 4.4 shows that already for $L = 32$ the performance is similar to the performance for $L = 64$.

The different required E_b/N_0 at a BER of 10^{-3} at low values of L for different data rates can be explained as follows. A high data rate corresponds to a high number Q of subcarriers per user. The number M of subcarriers per block is given by $M = Q/L$, cf. (2.36). Consequently, for small values of L, M is in the order of magnitude of Q. The larger the values of M, the more the channel conditions are changing within one block. Thus, even within a block of subcarriers, a certain amount of frequency diversity is exploited that is dependent on M. For the given channel, the ratio of coherence bandwidth B_c and subcarrier bandwidth Δf with

$$\Delta f = B/N \approx 39 \text{ kHz} \tag{4.4}$$

is given by $B_\mathrm{c}/\Delta f \approx 15$. E.g., for $L = 1$ and $Q = M = 32$, the bandwidth of a subcarrier block is a little larger than $2 \cdot B_\mathrm{c}$, whereas for $L = 1$ and $Q = M = 128$, the bandwidth of a subcarrier block is a little larger than $8 \cdot B_\mathrm{c}$.

The similar required E_b/N_0 at a BER of 10^{-3} at high values of L for different data rates can be explained as follows. For high values of L, the numbers M of subcarriers per block are small and, thus, the bandwidth of a block is smaller than B_c. Consequently, the channel conditions do not change significantly within a block and the frequency diversity that is exploited is dominated by the number L of subcarrier blocks and almost independent of M. E.g., for $L = 16$ and $Q = M = 32$, the bandwidth of a subcarrier block is approximately $B_\mathrm{c}/7$.

It can be concluded that, in order to provide maximum frequency diversity, the number L of subcarrier blocks should be in the order of magnitude of B/B_c. For instantaneous data rates corresponding to an assignment of $Q \leq B/B_\mathrm{c}$ to a user, maximum frequency diversity is obtained by the choice of the maximum possible number L, i.e. for $M = 1$, which is equivalent to IFDMA.

In the following, the performance of B-IFDMA is compared to the performance of OFDMA. The performance results for uncoded transmission are shown in Figure 4.5 for B-IFDMA and OFDMA. Except for the coding, the parameters are the same as the parameters from Table 4.2. It is assumed that for B-IFDMA a linear MMSE FDE according to Section 2.4 is used. For OFDMA, a linear ZF FDE is considered, because it is well-known that for OFDMA an MMSE FDE does not provide any performance gain as the subcarriers are mutually independent [Kam08].

From Figure 4.5 it can be seen that for B-IFDMA the BER performance improves with increasing number L of subcarriers per block, whereas the performance of OFDMA is
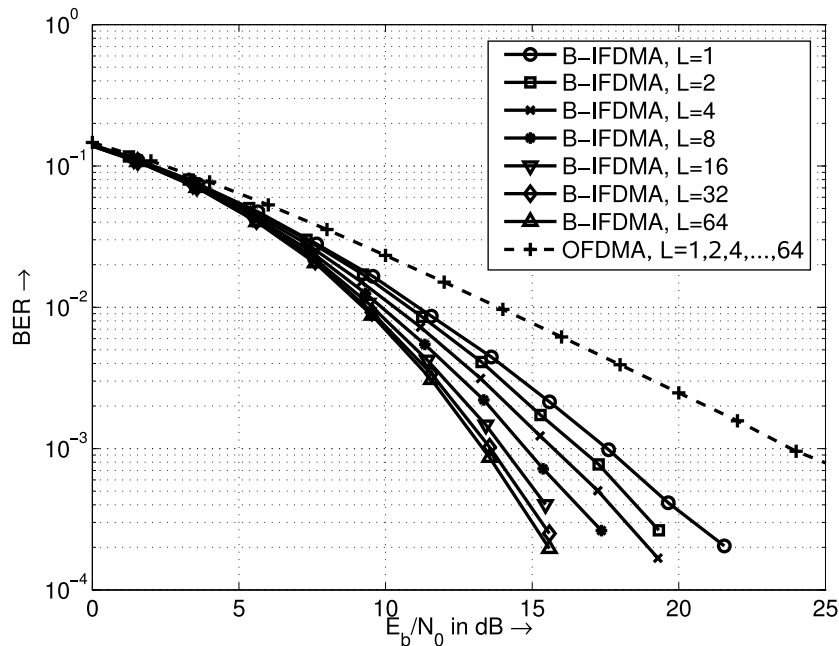
Figure 4.5: BER versus E_{b}/N_0 for uncoded transmission with $Q = 64$ subcarriers per user for B-IFDMA with different numbers L of subcarrier blocks and comparison to the uncoded performance of OFDMA.

independent of L. Moreover, for every L, the BER performance of B-IFDMA is better than the performance of OFDMA.

The performance results from Figure 4.5 can be explained as follows. Due to the DFT pre-coding of the data symbols, B-IFDMA distributes the information contained in every data symbol to all Q subcarriers that are used for transmission of a certain user's signal. Consequently, even without error control coding, frequency diversity is exploited and, similar as in Figures 4.1-4.3, B-IFDMA benefits from an increasing number L of subcarrier blocks. In contrast to B-IFDMA, for OFDMA, only one data symbol is transmitted on each subcarrier. Thus, the performance of OFDMA for uncoded transmission is equivalent to the performance for transmission over a one-tap Rayleigh channel, i.e., frequency diversity cannot be exploited regardless of the subcarrier allocation that is used.

From Figure 4.5 it can be concluded that for uncoded transmission even for the special case $L = 1$ where all subcarriers are concentrated in a localized portion of the bandwidth, B-IFDMA outperforms OFDMA by ≈ 2.8 dB at a BER of 10^{-2}. Similar to the coded transmission, the performance of B-IFDMA increases with increasing number L of subcarrier blocks. For $L = Q = 64$, the maximum diversity is provided and OFDMA
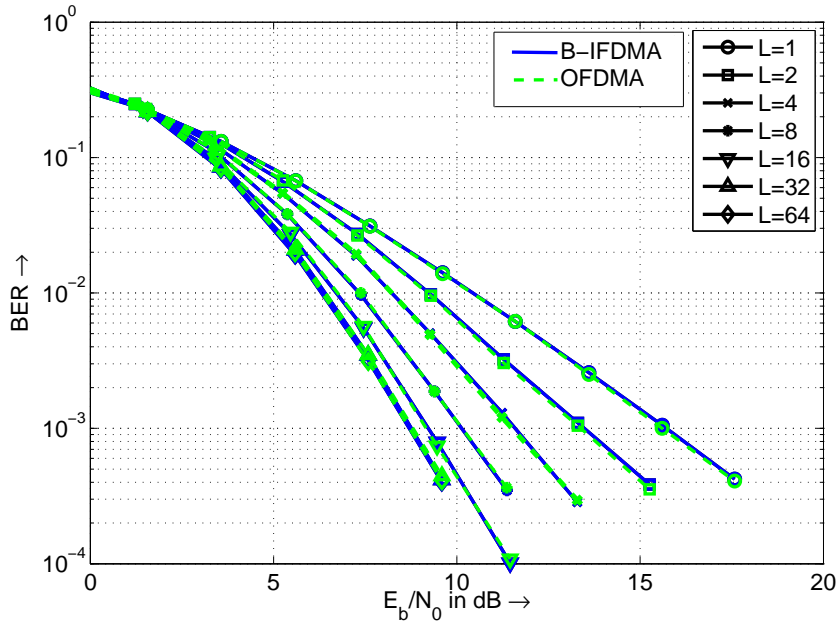
Figure 4.6: BER versus E_b/N_0 for coded transmission with $Q = 64$ subcarriers per user for B-IFDMA and OFDMA with different numbers L of subcarrier blocks.

is outperformed by ≈ 4.7 dB at a BER of 10^{-2}.

However, for real mobile radio systems, typically error control coding is used. Thus, a comparison of the performance of B-IFDMA to the performance of OFDMA considering error control coding is required, which is presented in the following. Both schemes use the same codes, the same decoders, the same interleaving as given in Table 4.2, and the same subcarrier allocation. The respective performance results are depicted in Figure 4.6. The performance results for B-IFDMA correspond to those from Figure 4.2. From Figure 4.6 it can be seen that for the given assumptions, the performance of B-IFDMA and OFDMA is very similar for coded transmission. The reason is that through coding and interleaving over the subcarriers for OFDMA, a similar amount of frequency diversity can be exploited as for B-IFDMA.

In the following, the performance of B-IFDMA with $L = 1$ combined with FH is analyzed and compared to the performance of B-IFDMA with $L = Q$ without FH. As shown in Section 2.4, B-IFDMA with $L = 1$ is equivalent to localized SC-FDMA. B-IFDMA with $L = 1$ provides low frequency diversity due to the subcarrier allocation localized in a small portion of the available bandwidth. As discussed in Section 1.1.3, in 3GPP LTE it is proposed to use B-IFDMA with $L = 1$ combined with FH in order to increase the diversity that is exploited by the scheme.

The application of FH to B-IFDMA with $L = 1$ can be explained as follows. For each modulated data vector, a subcarrier set with index $I^{(k)}$ according to the definition in Section 3.5.3 is assigned to user k. If the index $I^{(k)}$ changes from one modulated data vector to the next, for each modulated data vector, the signal of user k experiences different channel conditions. The different channel conditions can be exploited by the application of error control coding together with a bit interleaving over the number N_t of consecutive modulated data vectors that are assigned to user k. Note that, if $I^{(k)}$ changes from one modulated data vector to the next, N_t also describes the number of hops within the consecutive modulated data vectors that are assigned to user k.

In Figure 4.7, performance results for B-IFDMA with $L = 1$ combined with FH are depicted for different numbers N_t of hops and for different data rates, i.e., different numbers Q of subcarriers per user. Performance results for B-IFDMA with $L = Q = 128$ are given as a reference. Note that the performance of B-IFDMA with $L = Q = 128$ is similar to the performance of B-IFDMA with $L = Q = 64$ and $L = Q = 32$, cf. Figures 4.1-4.4. Thus, in Figure 4.7 the performance of B-IFDMA with $L = Q = 64$ and $L = Q = 32$ is omitted. For the analysis of B-IFDMA with $L = 1$ combined with FH, again, perfect orthogonality of the different users' signals is assumed and only the signal of one user is considered. The parameters are chosen according to Table 4.2, except for the interleaving depth that is set to $N_\mathrm{t} = 4, 8$ and 12 and the index $I^{(k)}$ that is chosen randomly for each modulated data vector.

From the results in Figure 4.7 it can be seen that the performance in terms of BER of B-IFDMA with $L = 1$ combined with FH improves with increasing number N_t of hops and with increasing data rate, i.e., with increasing number Q of subcarriers per user. Compared to the performance results of B-IFDMA with $L = 1$ without FH that are shown in Figures 4.1-4.3, the performance of B-IFDMA with $L = 1$ combined with FH is considerably improved. However, even for $N_\mathrm{t} = 12$ and $Q = 128$, the performance of B-IFDMA with $L = 1$ combined with FH is worse compared to the performance of B-IFDMA with $L = Q = 128$ without FH, cf. Figure 4.7.

The results can be explained as follows. The larger the values of N_t, the more modulated data vectors experience different channel conditions that are exploited by error control coding and bit interleaving. Thus, the performance of B-IFDMA with $L = 1$ combined with FH increases with increasing values of N_t. The larger the number Q, the more frequency diversity is already provided within one block of adjacent subcarriers. Thus, the performance of B-IFDMA with $L = 1$ combined with FH increases with increasing values of Q.

From the results it can be concluded that, in order to obtain a frequency diversity that is comparable to the one provided by B-IFDMA with $L = 128$, N_t would have to be
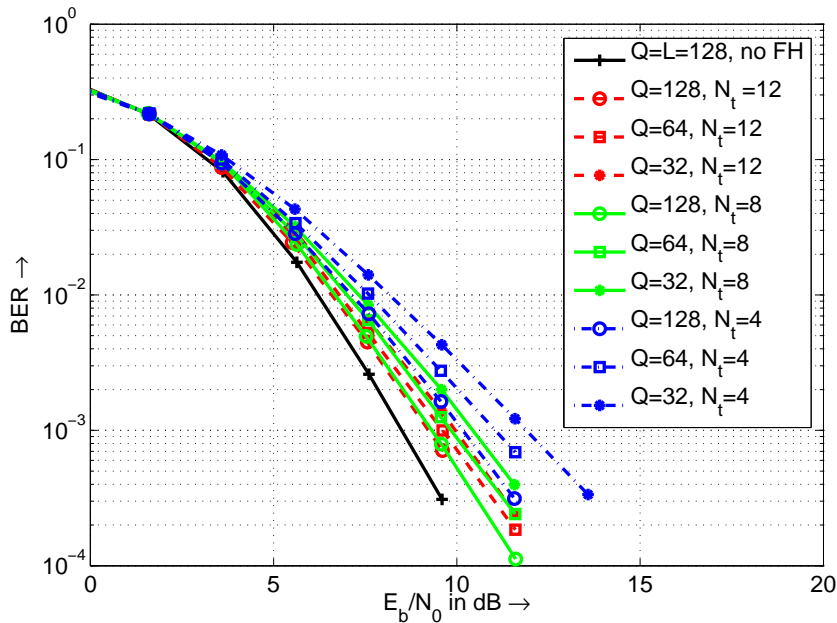
Figure 4.7: BER versus E_b/N_0 for coded transmission of B-IFDMA with $L = 1$ combined with FH for different numbers N_t of hops and different data rates and for B-IFDMA with $Q = L = 128$ without FH.

significantly larger than $N_t = 12$. But note that the application of bit interleaving over N_t consecutive modulated data vectors introduces delays into the system, because the data bits have to be buffered for the time required for the transmission of N_t modulated data vectors. Thus, a large number N_t causes additional delays compared to a transmission using B-IFDMA without FH, where N_t can be low. Consequently, in order to meet the goal of low delays for the radio interface, B-IFDMA with large values of L and without FH can be regarded as the preferred solution because it provides a good performance at lower delays than B-IFDMA with $L = 1$ and FH.

4.2.3 Time Diversity

In this section, the properties of B-IFDMA with respect to the exploitation of time diversity are analyzed and discussed. In general, for B-IFDMA, it is assumed that the channel is time invariant during the transmission of a modulated data vector with CP, cf. Section 2.3.4. Consequently, in general, B-IFDMA does not exploit time diversity. However, time diversity can be easily provided, e.g., by the application of channel coding and interleaving of the coded bits over several consecutive modulated data vectors. Note that the application of bit interleaving over N_t consecutive modulated
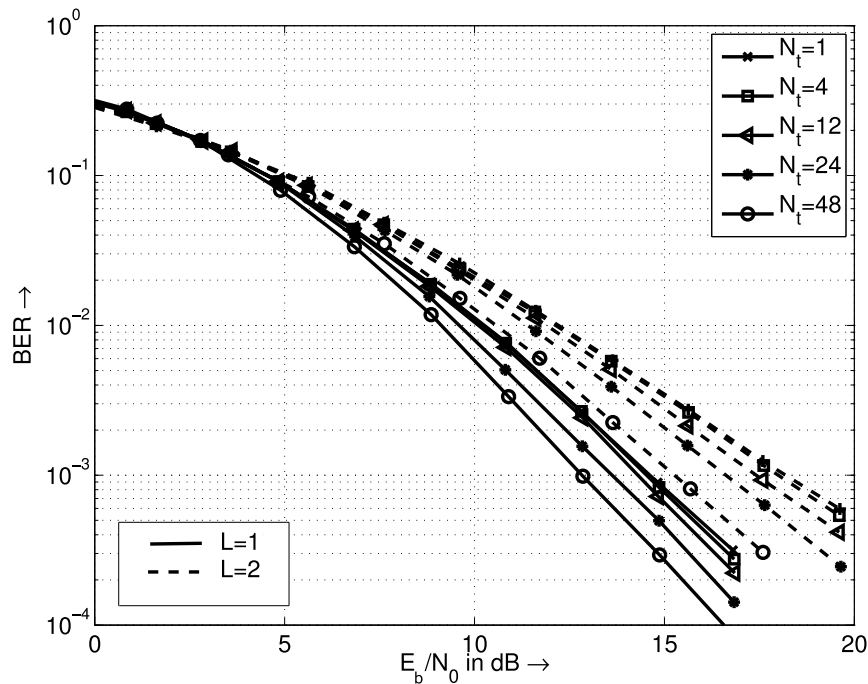
Figure 4.8: BER versus E_b/N_0 for coded transmission with $Q = 32$ subcarriers per user for B-IFDMA with different numbers N_t of consecutive modulated data vectors used for bit interleaving.

data vectors introduces delays to the system, because the data bits have to be buffered for the time required for the transmission of N_t modulated data vectors.

Figure 4.8 shows performance results for B-IFDMA exploiting time diversity by means of channel coding and bit interleaving dependent on the number N_t of consecutive modulated data vectors that are used for the bit interleaving. For the results in Figure 4.8, an instantaneous net bit rate of 1.11 Mbps, i.e., $Q = 32$ is assumed and the number L of subcarrier blocks is $L = 1$ and $L = 2$, respectively. Except for the interleaving depth, the simulation parameters correspond to those given in Table 4.2. In Figure 4.9, the required E_b/N_0 at a BER of 10^{-3} is depicted dependent on the number N_t.

In Figures 4.8 and 4.9, it can be seen that the performance increases with increasing numbers N_t. For $L = 1$, the performance improvement with increasing number N_t is more pronounced than for $L = 2$. Further on, even for $N_t = 48$ the performance gains due to time diversity are smaller than the performance gains due to exploitation of frequency diversity that can be achieved by the doubling of the number L of subcarrier blocks from $L = 1$ to $L = 2$.

The results can be explained as follows. For a given number N_t, the time that is used
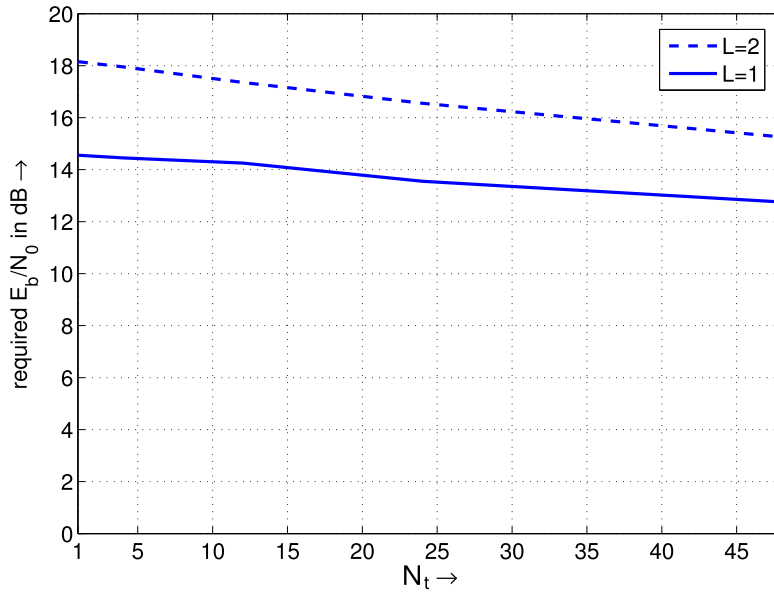
Figure 4.9: Required E_b/N_0 for $Q = 32$ subcarriers per user at a BER of 10^{-3} for B-IFDMA and for $L = 1$ and 2 with different numbers N_t of consecutive modulated data vectors used for bit interleaving.

for a spreading of the coded bits can be expressed as $\Delta T = (T + T_{CP}) \cdot N_t$, where $T + T_{CP}$ denotes the time required for transmission of a modulated data vector with CP. For the numbers N_t that are considered in Figures 4.8 and 4.9, ΔT is lower than the coherence time T_c of the channel. According to the definition of the coherence time T_c in (4.2), within N_t consecutive modulated data vectors the respective realizations of the channel $\mathbf{H}^{(k)}$ are still correlated and, thus, the amount of time diversity that can be exploited is low. The numbers N_t and their relation to the coherence time T_c, are given in Table 4.3. For $L = 1$ the frequency diversity that is exploited is also low and, thus, the exploitation of time diversity results in a performance improvement that is more pronounced as for $L = 2$, where already a considerable amount of frequency diversity is exploited.

From the results in Figures 4.8 and 4.9 it can be concluded that for the given parametrization that is typical for a future mobile radio scenario with high user mobility, a considerable performance improvement due to an exploitation of time diversity requires a large number N_t of consecutive modulated data vectors. Since a large number N_t of consecutive modulated data vectors results in undesired additional delays, aiming at a radio interface with low delays, the exploitation of time diversity can be regarded as an inappropriate means for performance improvement. In order to provide a coherence time T_c that is in the order of a few durations $T + T_{CP}$ of a modulated data

vector with CP, the user velocity would have to be in the order of $v = 1000$ km/h.

Table 4.3: Numbers N_t in Figures 4.8 and 4.9 and their relation to the coherence time.

N_t	1	4	12	24	48
$\Delta T/T_\text{c}$	0.01	0.05	0.16	0.33	0.66

4.2.4 Spatial Diversity

In this section, the exploitation of spatial diversity is analyzed and discussed for B-IFDMA. Special attention is paid to the question if, in case of existing means for provision of spatial diversity, the exploitation of frequency diversity for B-IFDMA still provides significant additional performance gains.

In the following, the user terminals are assumed to be equipped with 2 antennas. The antenna distance is assumed to be $\lambda/2$, where λ denotes the wavelength. Note that an antenna distance of $\lambda/2$ is a typical value for a mobile terminal [PNG03, WJ94]. At a carrier frequency of 3.7 GHz, the antenna distance of $\lambda/2$ corresponds to ≈ 4 cm. Again, the parameters from Table 4.2 are used. Note that the WINNER channel model takes spatial correlations of the antennas into account [WIN07f]. For the exploitation of spatial diversity, the approach for application of STBCs to B-IFDMA from Section 3.3 is used and an Alamouti STBC is applied.

In Figures 4.10-4.12 the coded performance at instantaneous net bit rates of 4.44 Mbps, 2.22 Mbps and 1.11 Mbps, respectively, is depicted corresponding to Q=128, Q=64 and Q=32 subcarriers per user, respectively. As a reference, the performance for single antenna transmission from Figures 4.1-4.3 is also given.

In Figures 4.10-4.12 it can be seen that the performance of B-IFDMA with Alamouti STBC is considerably improved compared to the performance for single antenna transmission. In particular, for B-IFDMA with Alamouti STBC, the slope of the curves is increased compared to the slope of the curves for single antenna transmission. The performance gains compared to single antenna transmission are the higher the lower the number L of subcarrier blocks for B-IFDMA. However, even for a data rate of 4.44 Mbps and for the case of $L = Q$ where maximum frequency diversity is provided, the performance gains due to an exploitation of spatial diversity are still in the order of 2 dB.

The results can be explained as follows. The increased slope of the curves indicates the increased diversity order through exploitation of spatial diversity. For a low number of subcarrier blocks, i.e., for low frequency diversity, the exploitation of spatial diversity results in a considerable reduction of the effect of the channel fading and, thus, results in a considerable performance improvement. For a high number of subcarrier blocks, the effect of the channel fading is already reduced by the exploitation of frequency diversity. Thus, the effect of spatial diversity is less pronounced but still considerable. From the performance improvement due to the exploitation of spatial diversity it can be concluded that the combination of B-IFDMA with an Alamouti STBC can be considered as a promising solution for improving the performance of B-IFDMA.

In the following, the amount of spatial diversity that is exploited is further increased by the introduction of multiple receive antennas at the base station. It is assumed that $n_R = 2$ receive antennas are used. The antenna distance at the receiver is assumed to be 5λ. At a carrier frequency of 3.7 GHz, an antenna distance of 5λ corresponds to ≈ 40 cm that can be considered as a typical antenna distance for a base station. In addition to the application of an Alamouti STBC at the transmitter, Maximum Ratio Combining (MRC) is applied at the receiver. Figures 4.13-4.15 show the resulting performance normalized to the array gain, i.e. in terms of the BER versus $E_b/(n_R \cdot N_0)$, i.e., E_b/N_0 normalized to the number of receive antennas. Again, as a reference, the single antenna performance is depicted.

In Figures 4.13-4.15 it can be seen that due to the additional use of multiple receive antennas the performance is further increased, even if the array gain is not considered. Again, the performance gain compared to the single antenna transmission is the higher the lower the frequency diversity provided by B-IFDMA. The reason is that the introduction of $n_R = 2$ receive antennas provides a significantly improved diversity order, especially due to the fact that the antenna distance at the receiver is considerably larger than the wavelength and, thus, the receive antennas can be assumed to be almost uncorrelated.

In Figure 4.16, the required E_b/N_0 is depicted for a BER of 10^{-3}. Again, the array gain for MRC is not considered because it would cause only a shift of the curves for B-IFDMA with Alamouti and MRC of 3 dB. Figure 4.16 shows the performance gains due to frequency diversity for different antenna configurations. The amount of frequency diversity is reflected in the difference of the required E_b/N_0 normalized to n_R between low values of L and high values of L for a given value of Q and for a given antenna configuration. It can be seen that, for a transmission applying STBC at the transmitter, compared to single antenna transmission, the performance gains due to frequency diversity are lower. This effect is further increased if, in addition to STBC at

Figure 4.10: BER versus E_b/N_0 for coded transmission of B-IFDMA with Alamouti STBC at $Q = 128$ subcarriers per user, i.e., at 4.44 Mbps.

Figure 4.11: BER versus E_b/N_0 for coded transmission of B-IFDMA with Alamouti STBC at $Q = 64$ subcarriers per user, i.e., at 2.22 Mbps.
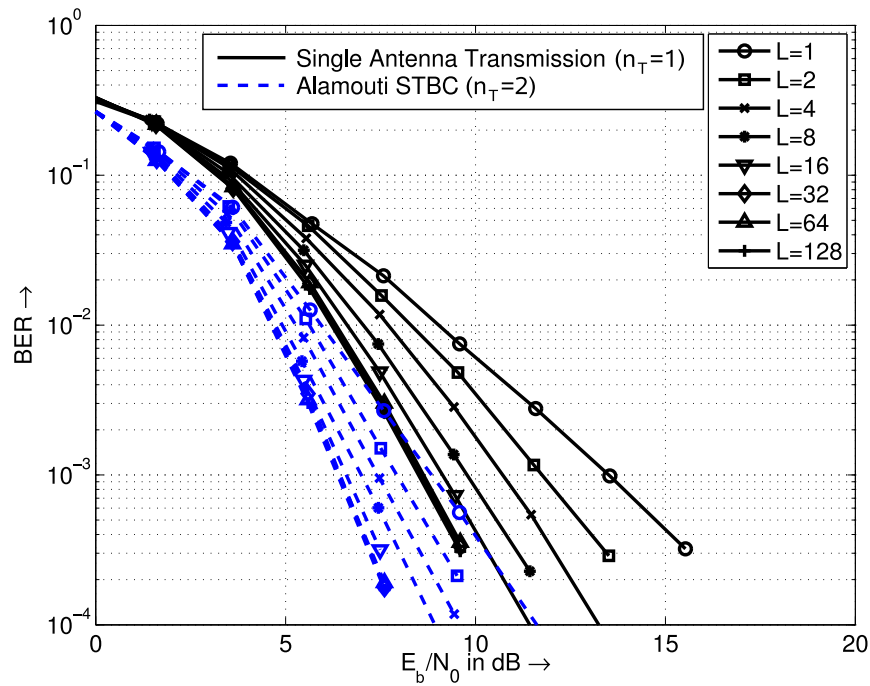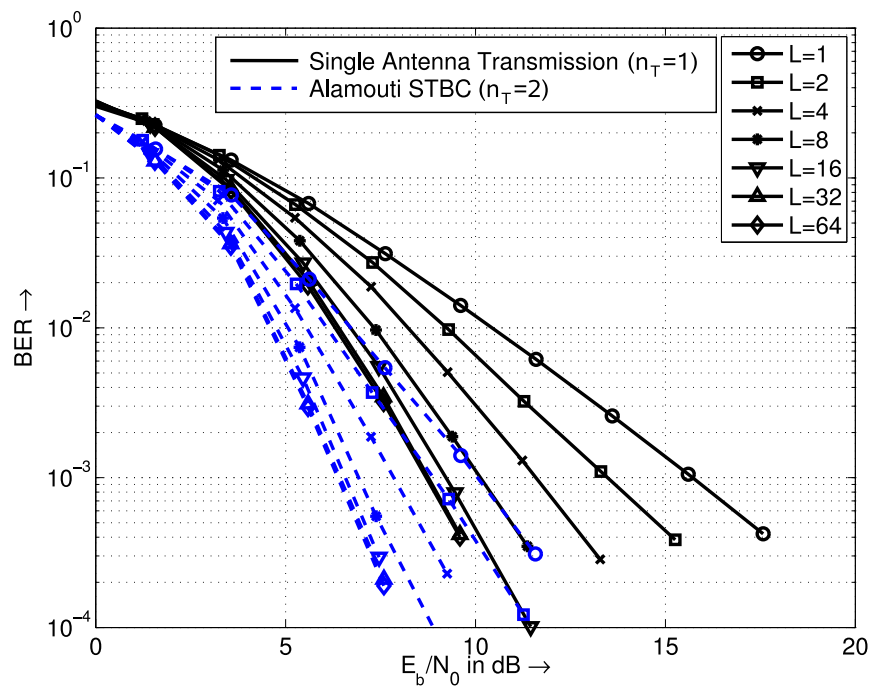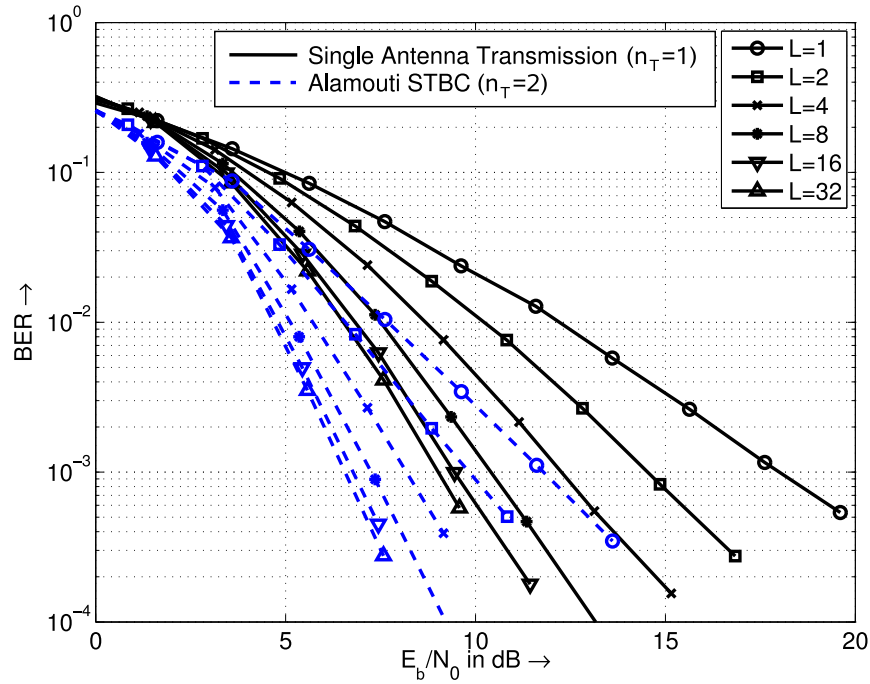
Figure 4.12: BER versus E_b/N_0 for coded transmission of B-IFDMA with Alamouti STBC at $Q = 32$ subcarriers per user, i.e., at 1.11 Mbps.
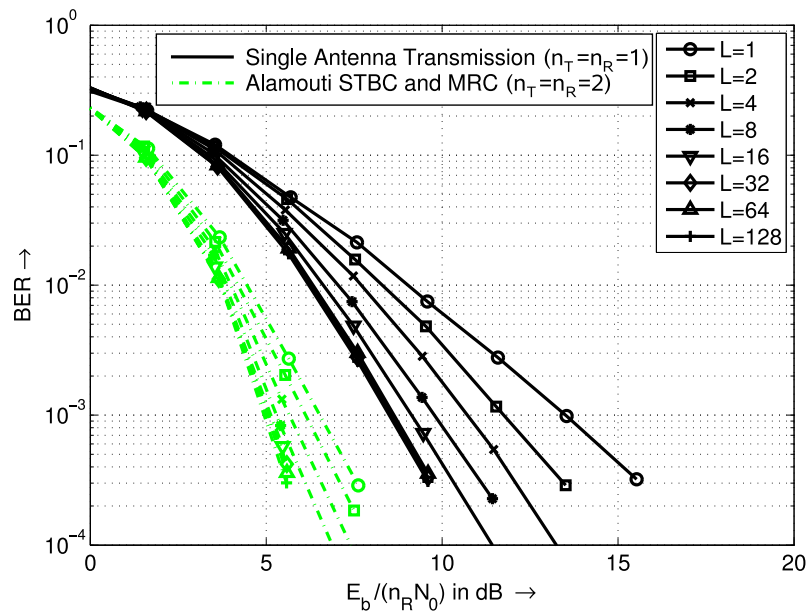

Figure 4.13: BER versus $E_b/(n_R \cdot N_0)$ for coded transmission of B-IFDMA with Alamouti STBC and MRC at $Q = 128$ subcarriers per user, i.e., at 4.44 Mbps.
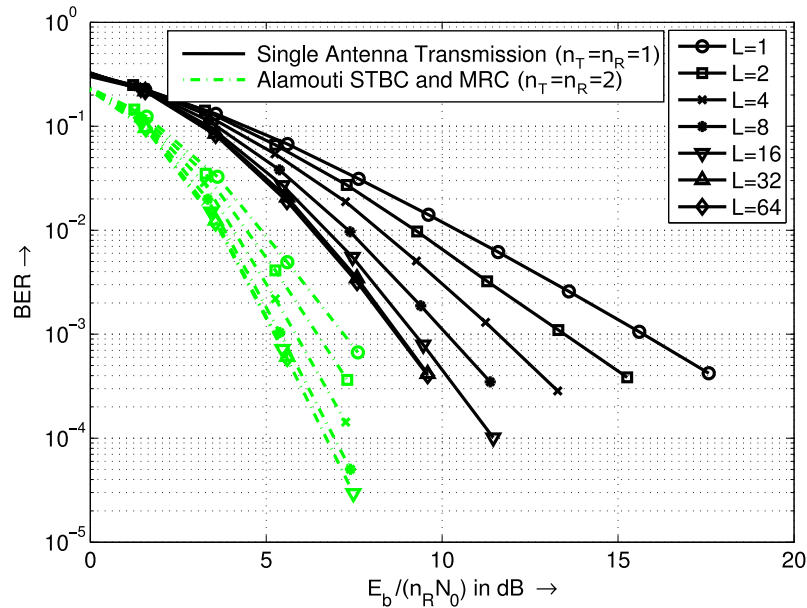
Figure 4.14: BER versus $E_b/(n_R \cdot N_0)$ for coded transmission of B-IFDMA with Alamouti STBC and MRC at $Q = 64$ subcarriers per user, i.e., at 2.22 Mbps.

the transmitter, also MRC at the receiver is applied. E.g., regarding the transmission at an instantaneous net bit rate of 1.11 Mbps, for B-IFDMA with Alamouti STBC, the difference between the required E_b/N_0 at a BER of 10^{-3} for $L = 1$ and for $L = 32$ is $\approx$ 5 dB. For B-IFDMA with Alamouti and MRC it reduces to $\approx$ 3 dB, whereas for single antenna transmission it is $\approx$ 9 dB. The reason is that, compared to the single antenna case, if spatial diversity is exploited, the effect of the channel fading is already reduced. Thus, if spatial diversity is exploited the performance gains through frequency diversity are lower compared to the single antenna case. However, it can be concluded that even if spatial diversity is exploited at transmitter and receiver, the performance gains due to an exploitation of frequency diversity are still significant.

In the following, the new approach for application of STBCs to B-IFDMA from Section 3.3 is compared to an approach where the coloration of the noise due to the STBC decoder, cf. Section 3.3.5.2, is not considered at the receiver. Again, an Alamouti STBC and an antenna distance of $\lambda/2$ are assumed at the transmitter. At the receiver, $n_R = 1$ receive antenna is assumed. The corresponding results are depicted in Figure 4.17.

It can be seen that the new approach considerably outperforms the approach that does not consider the coloration of the noise. Thus, the new approach is shown to provide a better performance compared to approaches that are state-of-the-art, cf. Section 3.3.2.
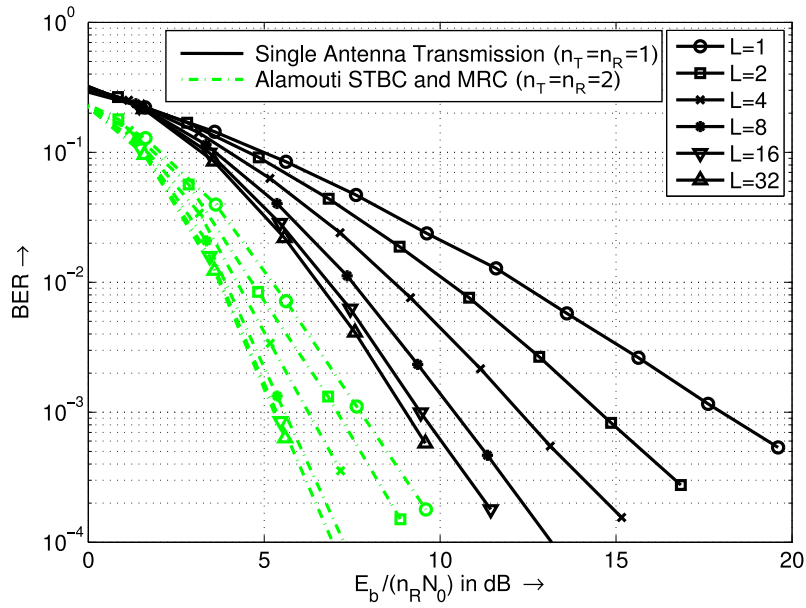
Figure 4.15: BER versus $E_b/(n_{\mathrm{R}} \cdot N_0)$ for coded transmission of B-IFDMA with Alamouti STBC and MRC at $Q = 32$ subcarriers per user, i.e., at 1.11 Mbps.
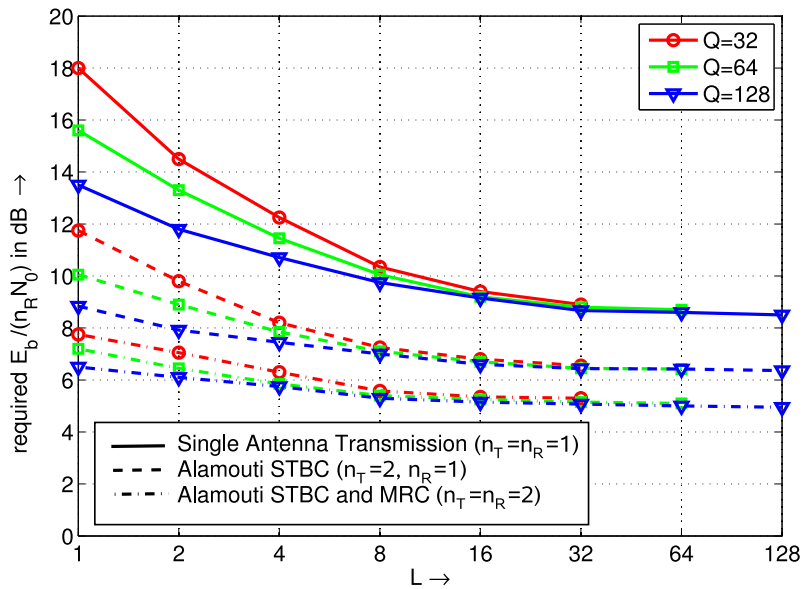
Figure 4.16: Required $E_b/(n_{\mathrm{R}} \cdot N_0)$ at a BER of 10^{-3} for different data rates dependent on the number L of subcarrier blocks for different antenna configurations.

The performance gain of the new approach is almost independent of the number Q of subcarriers per user.
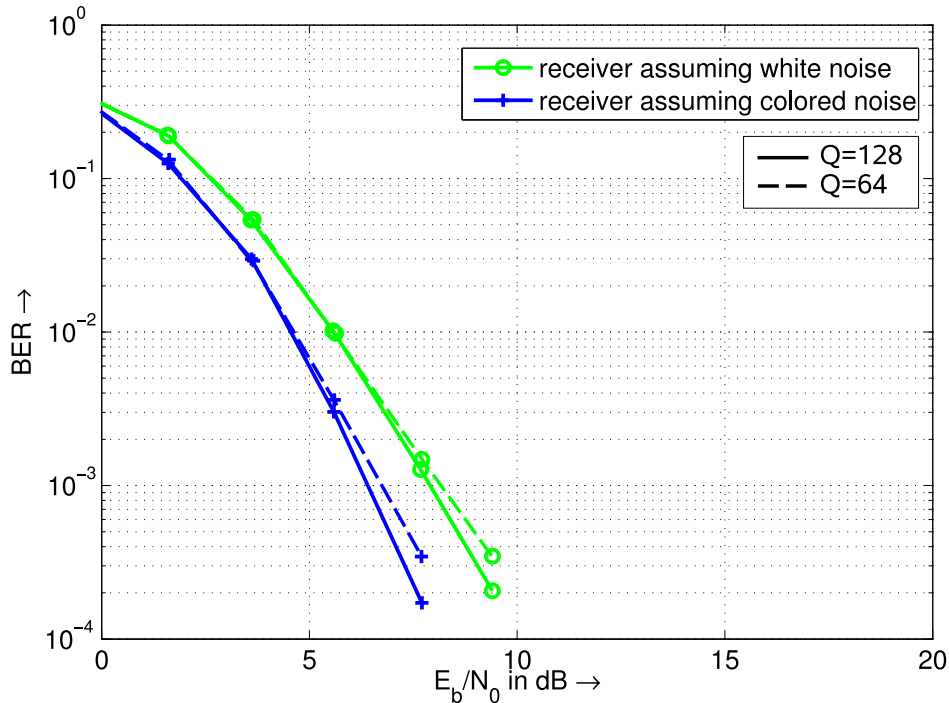
Figure 4.17: BER versus E_b/N_0 for coded transmission of B-IFDMA with Alamouti STBC at $Q = L = 128$ and $Q = L = 64$ subcarriers per user, i.e., at 4.44 Mbps and 2.22 Mbps, respectively.

4.2.5 Multi-User Diversity

In this section, the properties of B-IFDMA are discussed in the context of multi-user diversity. In order to exploit multi-user diversity, reliable channel state information (CSI) at the transmitter is required. Under perfect assumptions, a transmission exploiting multi-user diversity provides a better performance than a transmission where the channel knowledge at the transmitter is not exploited. However, if the reliability of the CSI that is available at the transmitter is affected, e.g., by outdating or channel estimation errors, the performance decreases. At a certain reliability level of the CSI, the performance of a transmission exploiting multi-user diversity may become worse than the performance of a transmission where other sources of diversity like frequency diversity, that do not require reliable channel state information at the transmitter, are exploited.

In this section, quantitative performance results for localized SC-FDMA, i.e., B-IFDMA with $L = 1$, exploiting multi-user diversity are presented dependent on the

reliability of the CSI. Note that localized SC-FDMA has been adopted as multiple access scheme for adaptive transmission in 3GPP LTE, cf. Section 1.1.3. The reliability level of the CSI, for that the use of B-IFDMA exploiting frequency diversity becomes superior to the use of localized SC-FDMA using exploiting multi-user diversity, is determined by a comparison of the performance results from this section with the performance of B-IFDMA with a large number L of subcarrier blocks from Section 4.2.2.

In the following, a system with K users and $K = N/Q$ available subcarrier sets is regarded. Each subcarrier set contains Q subcarriers. In order to exploit multi-user diversity, multi-user scheduling has to be performed. It is assumed that, at the base station, a multi-user scheduler determines the channel quality of all subcarrier sets for the channels of all users. Having determined the channel qualities, the multi-user scheduler tries to find that assignment of K subcarrier sets to the K users that provides the best channel quality for all users. In the following, the performance provided by the selection of the best subcarrier set and of the user with the best channel quality is analyzed.

The channel quality for each subcarrier set can be described in terms of the average SNR over all subcarriers in the set. An according channel quality metric is given as follows: Let $\kappa = 0, \ldots, K - 1$ denote the index of the K available subcarrier sets that can be described by the subcarrier mapping matrix $\mathbf{M}^{(\kappa)}$ that is, analogous to (2.38), defined by

$$\left[\mathbf{M}^{(\kappa)}\right]_{n,q} = \begin{cases} 1 & n = l \cdot \frac{N}{L} + m + \kappa M \\ 0 & \text{else} \end{cases}. \tag{4.5}$$

Note that, compared to the definition in (2.38), the index κ is used instead of the index k because the subcarrier set described by $\mathbf{M}^{(\kappa)}$ is not yet assigned to a certain user k.

Let, further on, $\hat{\mathbf{\Gamma}}^{(k,\kappa)}$ denote an overall channel matrix of user k with subcarrier set κ. The overall channel matrix $\hat{\mathbf{\Gamma}}^{(k,\kappa)}$ is defined as

$$\mathbf{\Gamma}^{(k,\kappa)} = \left(\mathbf{M}^{(\kappa)}\right)^{\dagger} \cdot \mathbf{F}_{\mathrm{N}} \cdot \mathbf{H}^{(k)} \cdot \mathbf{F}_{\mathrm{N}}^{\mathrm{H}} \cdot \mathbf{M}^{(\kappa)}, \tag{4.6}$$

analogous to (2.28). Note that $\mathbf{\Gamma}^{(k,\kappa)}$ is a $Q \times Q$ diagonal matrix and carries the channel coefficients of the Q subcarriers of the respective subcarrier set on its main diagonal.

Let $\hat{\mathbf{\Gamma}}^{(k,\kappa)}$ denote an estimate of the overall channel matrix $\mathbf{\Gamma}^{(k,\kappa)}$. Assuming a constant noise power for the AWGN, the above mentioned metric for the channel quality of the κ-th subcarrier set of user k is given by

$$Q^{(k,\kappa)} = \frac{1}{Q} \sum_{q=0}^{Q-1} \left| \left[\hat{\mathbf{\Gamma}}^{(k,\kappa)}\right]_{q,q} \right|^2, \tag{4.7}$$

where $[\cdot]_{m,n}$ denotes the element in the m-th row and in the n-th column of a matrix. The quality metric defined in (4.7) describes the mean attenuation of the channel for the subcarriers within subcarrier set κ. The larger the value for $Q^{(k,\kappa)}$, the lower the attenuation.

In real mobile radio systems, the channel quality information is not perfect. Basically, the following effects have to be taken into account:

- The channel quality information is obtained by means of channel estimation. Thus, a channel estimation error occurs.

- The channel quality information is outdated because the channel is estimated from the received signal at the base station. The information, which subcarrier set has been selected for every user, has to be fed back to the respective mobile stations before it can be used for uplink transmission. In the time interval that is required for channel estimation and feedback, the channel changes.

In the following, a model for the above mentioned errors is described. For that purpose, let

$$\check{\mathbf{t}}^{(k,\kappa)} = \left[\check{t}_0^{(k,\kappa)}, \ldots, \check{t}_{Q-1}^{(k,\kappa)} \right]^{\mathrm{T}} \tag{4.8}$$

denote the vector of the diagonal elements of the estimate $\hat{\boldsymbol{\Gamma}}^{(k,\kappa)}$ of the overall channel matrix with

$$\check{t}_q^{(k,\kappa)} = \left[\hat{\boldsymbol{\Gamma}}^{(k,\kappa)} \right]_{q,q}. \tag{4.9}$$

Vector $\check{\mathbf{t}}^{(k,\kappa)}$ is normalized according to

$$\mathbf{t}^{(k,\kappa)} = \frac{\check{\mathbf{t}}^{(k,\kappa)}}{\sqrt{\left(\check{\mathbf{t}}^{(k,\kappa)} \right)^{\mathrm{H}} \cdot \check{\mathbf{t}}^{(k,\kappa)}}}. \tag{4.10}$$

Assuming a pilot assisted channel estimation based on the least squares algorithm [Kam08], the channel estimation error can be described by an additive Gaussian noise term with power $\frac{\sigma_n^2}{P_{\mathrm{pilot}}}$, where σ_n^2 denotes the variance of the AWGN and P_{pilot} denotes the power of the pilot signal that is used for channel estimation [SFK06]. Let $\mathbf{t}_{\mathrm{OD}}^{(k,\kappa)}$ denote the outdated version of $\mathbf{t}^{(k,\kappa)}$ and let

$$\mathbf{n}_{\mathrm{e}} = [n_{\mathrm{e},0}, \ldots, n_{\mathrm{e},Q-1}]^{\mathrm{T}} \tag{4.11}$$

denote a Gaussian noise vector whose elements $n_{\mathrm{e},q}$, $q = 0, \ldots, Q-1$, are independent zero-mean Gaussian random variables with $E\left\{ \mathbf{n}_{\mathrm{e}}^{\mathrm{H}} \cdot \mathbf{n}_{\mathrm{e}} \right\} = 1/Q$. An estimate $\hat{\mathbf{t}}^{(k,\kappa)}$ for vector $\mathbf{t}^{(k,\kappa)}$ is, thus, given by

$$\hat{\mathbf{t}}^{(k,\kappa)} = \mathbf{t}_{\mathrm{OD}}^{(k,\kappa)} + \sqrt{\frac{\sigma_n^2}{P_{\mathrm{pilot}}}} \cdot \mathbf{n}_{\mathrm{e}}. \tag{4.12}$$

The vector $\mathbf{t}_{\text{OD}}^{(k,\kappa)}$ of the outdated channel coefficients can be modelled as follows. Let ρ describe the correlation between $\mathbf{t}^{(k,\kappa)}$ and $\mathbf{t}_{\text{OD}}^{(k,\kappa)}$. The correlation coefficient ρ is dependent on the time interval ΔT_{f} between the reception of the pilot symbols for channel estimation and the adapted transmission after feedback of the selected subcarrier set to the transmitter. Assuming a Jakes distribution of the channel coefficients, ρ can be can be described by

$$\rho = J_0 \left(2\pi v^{(k)} \frac{f_0}{c_0} \Delta T_{\text{f}} \right), \tag{4.13}$$

where $J_0(\cdot)$, $v^{(k)}$, f_0 and c_0 denote the zero-order Bessel function, the velocity of the mobile terminal of user k, the carrier frequency and the speed of light, respectively, cf. [WJ94].

According to [HEK05], the vector $\mathbf{t}_{\text{OD}}^{(k,\kappa)}$ of the channel coefficients considering an outdating according to (4.13) can be described by

$$\mathbf{t}_{\text{OD}}^{(k,\kappa)} = \rho \cdot \mathbf{t}^{(k,\kappa)} + \sqrt{1 - \rho^2} \cdot \mathbf{n}_{\text{e}}. \tag{4.14}$$

Since both effects, the channel estimation error and the outdating error, can be assumed to be statistically independent, (4.12) and (4.14) can be combined to

$$\hat{\mathbf{t}}^{(k,\kappa)} = \rho \cdot \mathbf{t}^{(k,\kappa)} + \left(\sqrt{1 - \rho^2} + \sqrt{\frac{\sigma_n^2}{P_{\text{pilot}}}} \right) \cdot \mathbf{n}_{\text{e}}. \tag{4.15}$$

In the following, the performance of localized SC-FDMA, i.e., B-IFDMA with $L = 1$, in terms of BER versus E_{b}/N_0 assuming an adaptive selection of the best subcarrier set κ and of the user with the best channel quality in terms of the quality metric from (4.7) taking into account the outdating and the channel estimation error according to (4.15) is analyzed. For the sake of simplicity, throughout this section, assuming an adaptive selection of the best subcarrier set is denoted adaptive transmission. The parameters that are used for this investigation are given in Table 4.2.

Figure 4.18 depicts performance results for adaptive transmission of B-IFDMA with and $L = 1$ for $Q = 64$, i.e., for an instantaneous net bit rate of 2.22 Mbps. The performance is given dependent on the time interval ΔT_{f} between reception of the pilot symbols for channel estimation and the adapted transmission of the data symbols. ΔT_{f} is normalized to the coherence time T_{c} of the channel. For $Q = 64$ subcarriers, the bandwidth of the subcarrier block is approximately 4.5 times the coherence bandwidth B_{c}. $K = N/Q = 16$ users are considered for the selection of the optimum subcarrier set.

From Figure 4.18 it can be seen that with decreasing values of $\Delta T_\mathrm{f}/T_\mathrm{c}$, the slope of the BER curves increases. Further on, with decreasing values of $\Delta T_\mathrm{f}/T_\mathrm{c}$, the BER curves show a parallel shift to the right. As a reference, in Figure 4.18, also the performance of B-IFDMA with $L = Q = 64$ and $L = 1$, respectively, without adaptive selection of the best resources is given. For the sake of simplicity, throughout this section, assuming a transmission without an adaptive selection of the best subcarrier set is denoted non-adaptive transmission.

The results from Figure 4.18 can be explained as follows. Due to the selection of the best resources for transmission, multi-user diversity is exploited. The selection of the best resources changes the statistics of the channel compared to the case without selection and causes an increased slope of the BER curve due to the exploitation of multi-user diversity. Moreover, due to the selection of subcarrier sets that provide a low mean attenuation, for a given transmit power, an improvement of the mean SNR at the receiver is provided compared to non-adaptive transmission. This improvement of the mean SNR causes the parallel shift of the curves to the left. Both effects are well-known and are described, e.g., in [CVY05]. The effects are the more pronounced the lower the error due to outdating and channel estimation. For the investigated E_b/N_0 values, the error is dominated by the outdating effect and is, thus, increasing with increasing $\Delta T_\mathrm{f}/T_\mathrm{c}$. For large values of $\Delta T_\mathrm{f}/T_\mathrm{c}$, the BER performance converges to the BER performance of non-adaptive transmission using B-IFDMA with $L = 1$, i.e., the adaptive selection of resources does not provide any advantage, because the channel quality information it is based on is too erroneous. Further on, it can be seen that, at a given target BER, for a certain value of $\Delta T_\mathrm{f}/T_\mathrm{c}$, the performance of adaptive transmission using B-IFDMA with $L = 1$ becomes worse than the performance of non-adaptive transmission using B-IFDMA with $L = Q$.

Figure 4.19 depicts the required E_b/N_0 for a target BER of 10^{-3} dependent on $\Delta T_\mathrm{f}/T_\mathrm{c}$. The results show that the performance gain due to adaptive transmission decreases with increasing values of ΔT_f. For $\Delta T_\mathrm{f} \approx 0.7 \cdot T_\mathrm{c}$, the required E_b/N_0 is similar to the required E_b/N_0 for non-adaptive transmission using B-IFDMA with $L = 1$ because the channel quality information is too erroneous. Further on, for $\Delta T_\mathrm{f} \gtrsim 0.5 \cdot T_\mathrm{c}$, the required E_b/N_0 for adaptive transmission using B-IFDMA with $L = 1$ is higher than the required E_b/N_0 for non-adaptive transmission using B-IFDMA with $L = Q$.

For a mobile radio system with parameters according to Table 4.2 this result can be interpreted as follows. Assuming that the minimum possible value for ΔT_f is 2 ms, the condition $\Delta T_\mathrm{f} \gtrsim 0.5 \cdot T_\mathrm{c}$ corresponds to a maximum user velocity of ≈ 35 km/h up to that adaptive transmission using B-IFDMA with $L = 1$ is beneficial. For higher velocities, non-adaptive transmission using B-IFDMA with $L = Q$ is preferable. Note
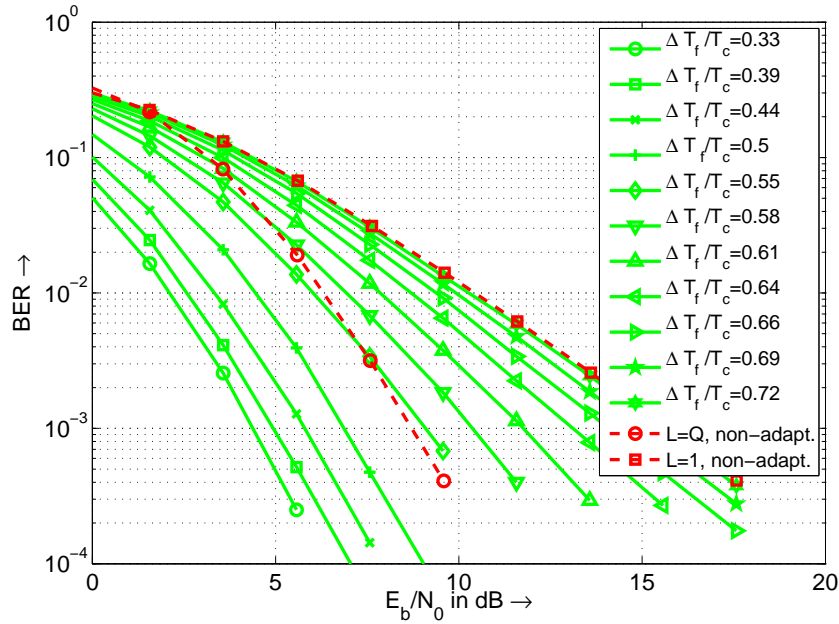
Figure 4.18: BER versus E_b/N_0 for coded transmission with $Q = 64$ subcarriers per user, i.e., for an instantaneous net bit rate of 2.22 Mbps, for adaptive transmission using B-IFDMA with $L = 1$ dependent on $\Delta T_f/T_c$ and for non-adaptive transmission using B-IFDMA with $L = 1$ and $L = Q$, respectively, as references.

that the provision of $\Delta T_f = 2$ ms will be a challenging task because in this time the channel quality information of all resources of all users has to be determined at the base station and and the assigned subcarrier sets have to be fed back to the mobile terminals. Further on, note that for the presented results the overhead required for determination of this channel quality information as well as the overhead required for a feedback of this information to the mobile terminal is not considered. Regarding the fact that the bandwidth of a subcarrier block with $Q = 64$ subcarriers is $\approx 4.5\ B_c$, it can be expected that for a lower number Q the performance for adaptive transmission is further improved. But note that, if at the same time a higher number $K = N/Q$ users has to be served, the time ΔT_f between reception of the pilots and adaptive transmission will be increased because the channel quality of all K channels has to be estimated at the base station based on pilots received from the K users.

From these results it can be concluded that adaptive transmission is only beneficial in a scenario with low user velocity. In the case of a higher user mobility, adaptive transmission fails and non-adaptive transmission exploiting frequency diversity as provided by B-IFDMA with a high number L of subcarrier blocks is an appropriate means in order to provide a good performance.
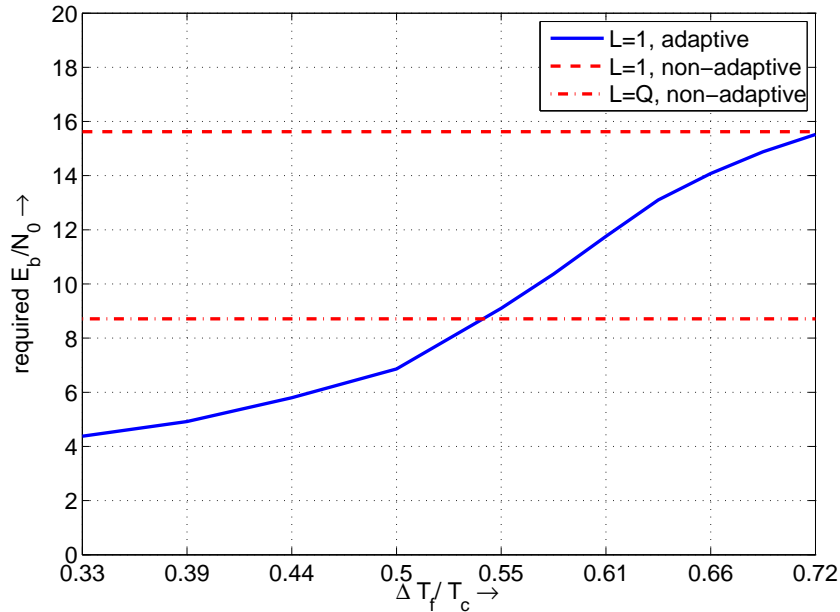
Figure 4.19: Required E_{b}/N_0 at a BER of 10^{-3} for different data rates for adaptive transmission using B-IFDMA with $L = 1$ dependent on $\Delta T_{\mathrm{f}}/T_{\mathrm{c}}$ and for non-adaptive transmission of B-IFDMA with $L = 1$ and $L = Q$, respectively, as references.

4.2.6 Overhead for Channel Estimation

In this section, for B-IFDMA transmission, the performance degradation due to pilot symbol overhead required for channel estimation is analyzed and discussed. For B-IFDMA, pilot assisted channel estimation can be assumed to be appropriate, cf. [SK07, LFDLD06]. However, the insertion of pilot symbols in the B-IFDMA signal reduces the number of data symbols that can be transmitted within a given number of consecutive modulated data vectors and for a given number of subcarriers. The effect of the insertion of pilot symbols can, thus, be considered as an additional amount of energy that is required for the transmission of each data symbol. Consequently, the insertion of pilot symbols leads to a degradation of the required SNR compared to a transmission without pilot symbols.

In the following, the SNR degradation due to pilot symbol overhead for channel estimation is described for B-IFDMA. A block of M adjacent subcarriers and a number of N_{t} consecutive modulated data vectors is regarded. In this resource, $M \cdot N_{\mathrm{t}}$ symbols including both, pilot symbols and data symbols, can be transmitted.

From the definitions of B_{c} and T_{c} in (4.3) and (4.2), respectively, follows that, according to the sampling theorem, at least one pilot symbol is required per coherence bandwidth

B_c and per coherence time T_c. However, in order to obtain a good performance for channel estimation, for practical applications, the introduction of an oversampling factor F is common, cf. [FK03].

In the following, it is assumed that the distance of the subcarrier blocks is large compared to the coherence bandwidth. With $\lceil \cdot \rceil$ returning the closest integer greater than or equal to the argument, for one subcarrier set and N_t consecutive modulated data vectors, the required numbers P_f and P_t of pilot symbols in frequency direction and time direction, respectively, can be written as

$$P_f = \left\lceil \frac{M \cdot \Delta f \cdot F}{B_c} \right\rceil,\tag{4.16}$$

where Δf denotes the subcarrier bandwidth, and

$$P_t = \left\lceil \frac{N_t \cdot (T + T_{CP}) \cdot F}{T_c} \right\rceil,\tag{4.17}$$

respectively, where $T + T_{CP}$ denotes the time required for transmission of one modulated data vector with cyclic prefix. The total number P of pilot symbols required for one subcarrier set and N_t consecutive modulated data vectors is given by

$$P = P_f \cdot P_t.\tag{4.18}$$

Assuming that the mean energy of a pilot symbol is equal to the mean energy of a data symbol, the SNR degradation in dB results in

$$\Upsilon = 10 \cdot \log_{10} \left(\frac{M \cdot N_t}{M \cdot N_t - P_f \cdot P_t} \right),\tag{4.19}$$

where $M \cdot N_t$ is the number of both pilot symbols and data symbols and $M \cdot N_t - P_f \cdot P_t$ is the number of data symbols that are transmitted in a subcarrier set and in N_t consecutive modulated data vectors. Note that with the definition according to (4.19), Υ can be directly combined with the E_b/N_0 that is used throughout this thesis.

Figure 4.20 illustrates the SNR degradation due to pilot overhead for channel estimation for B-IFDMA dependent on the number M of subcarriers per block and the number N_t of consecutive modulated data vectors. For the results in Figure 4.20, an oversampling factor of $F = 5$ is assumed that can be considered as a reasonable choice for channel estimation [SK09]. The system parameters correspond to those given in Table 4.2.

From the results in Figure 4.20 it can be concluded that the SNR degradation due to pilot symbol overhead becomes critical especially for small numbers M of subcarriers
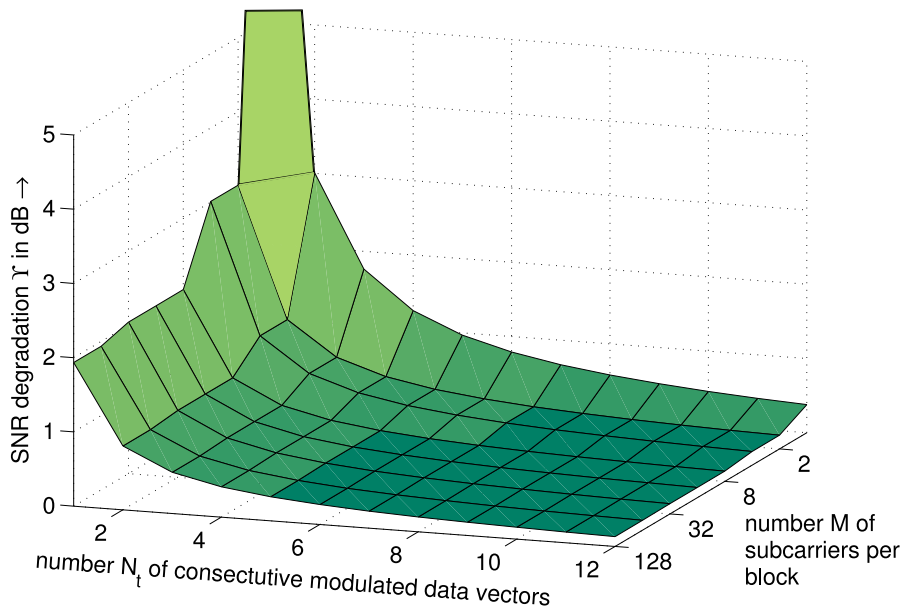
Figure 4.20: SNR degradation due to pilot symbol overhead for channel estimation dependent on the number M of subcarriers per block and the number N_t of consecutive modulated data vectors.

per block and small numbers N_t of consecutive modulated data vectors. For the extreme case of $M = 1$, i.e., for IFDMA, and $N_t = 1$, the overhead goes to infinity and a transmission of data symbols is not possible. The reason is that, for IFDMA, all subcarriers fade independently and, thus, one pilot symbol is required for each subcarrier. The gradient of the SNR degradation is maximum for small values of M and N_t.

From a comparison of the results in Figure 4.20 to the performance results from Section 4.2 it can be seen that for a given instantaneous data rate and for $L \leq B/B_c$ there is a general trade-off between optimum diversity and minimum channel estimation overhead, because for a given instantaneous net bit rate increasing the number M of subcarriers per block in order to reduce the pilot symbol overhead results in a decreased number L of subcarrier blocks.

As described in Section 4.2, an alternative solution to the spreading of the subcarriers over the total available bandwidth is the application of FH to B-IFDMA with $L = 1$. In the sequel, the pilot symbol overhead for B-IFDMA with $L = 1$ and FH is discussed. Assuming that for every hop a different set of subcarriers is used and that the different subcarrier sets provide maximum diversity, i.e., the channel conditions at different hops are mutually independent, every hop requires the transmission of pilot symbols. Let

N_t denote the number of hops. Thus, for B-IFDMA with $L = 1$ combined with FH, the SNR degradation due to pilot symbol overhead is given by

$$\bar{\Upsilon} = 10 \cdot \log_{10} \left(\frac{Q \cdot N_t}{Q \cdot N_t - P_f \cdot \bar{P}_t} \right), \tag{4.20}$$

with

$$\bar{P}_t = N_t. \tag{4.21}$$

From (4.20) it can be calculated that for B-IFDMA with $L = 1$ and FH, the pilot symbol overhead is ≈ 2 dB. In contrast to B-IFDMA without FH, the SNR degradation does not decrease with an increasing number N_t, because for each hop a new channel estimation is required. Compared to the results from Figure 4.20, the overhead for B-IFDMA with $L = 1$ and FH is higher except for B-IFDMA with $M = 1$ and $N_t \leq 3$ as well as for $M = 2$ and $N_t = 1$. The higher pilot symbol overhead required for channel estimation is a considerable disadvantage of B-IFDMA with $L = 1$ and FH compared to B-IFDMA without FH. Note that the presented results for pilot symbol overhead are independent of the DFT pre-coding of B-IFDMA and, thus, are the same for B-EFDMA, cf. Section 2.5.

4.3   Complexity

4.3.1   Mobile Terminal

In this section, the computational complexity of the digital signal processing required for B-IFDMA signal generation in the mobile terminal is analyzed and compared to the respective effort for OFDMA. The frequency domain implementation presented in Section 2 and the time domain implementation presented in Section 3.2 are regarded. Since complex multiplications and divisions require much more computational effort compared to additions and subtractions [Ach78], in the sequel, only the required numbers of multiplications and divisions are considered.

The computational effort for B-IFDMA signal generation in frequency domain is given by the effort for Q-point DFT pre-coding and N-point OFDM modulation, cf. (2.39). It is assumed that the subcarrier allocation operation can be implemented with negligible effort, because it can be implemented without performing any complex multiplications or additions. Assuming that both Q and N are powers of 2, the Fast Fourier Transform (FFT) algorithm [Ach78] can be applied. The number of complex multiplications

required for an N-point FFT or Inverse FFT (IFFT), respectively, is $1/2N \cdot \mathrm{ld}(N)$ [Ach78]. Thus, the computational effort for B-IFDMA signal generation in frequency domain is given by

$$MUL^{(f)}_{\mathrm{B-IFDMA,Tx}} = \frac{1}{2}Q \cdot \mathrm{ld}(Q) + \frac{1}{2}N \cdot \mathrm{ld}(N) \tag{4.22}$$

complex multiplications per mobile terminal and per modulated data vector. For the time domain implementation, the case $M = 1$ and the case $M > 1$ have to be distinguished because for $M = 1$, the simplification from Section 3.2.3.2 can be applied whereas for $M > 1$ the algorithm from Section 3.2.3.1 has to be used. From (3.13) and (3.17), respectively, it can be seen that the computational effort for B-IFDMA signal generation in time domain is given by

$$MUL^{(t)}_{\mathrm{B-IFDMA,Tx}} = \begin{cases} M \cdot N & M > 1 \\ \frac{N}{4} & M = 1 \end{cases} \tag{4.23}$$

complex multiplications per mobile terminal and per modulated data vector.

For OFDMA, compared to (4.22), the DFT pre-coding is omitted. Thus, for OFDMA, the computational effort for signal generation in frequency domain is given by

$$MUL^{(f)}_{\mathrm{OFDMA,Tx}} = \frac{1}{2}N \cdot \mathrm{ld}(N) \tag{4.24}$$

complex multiplications per mobile terminal and per modulated data vector. In general, for OFDMA, there is no efficient implementation in time domain.

In Sections 2.4 and 2.5, it has been shown that B-IFDMA can be regarded as block-interleaved OFDMA with DFT pre-coding of the data. If the DFT is omitted, the resulting scheme is block-interleaved OFDMA, that is also known as B-EFDMA [WIN06, SFE$^+$09]. Thus, B-EFDMA can be obtained by B-IFDMA modulation with an additional Q-point IDFT before modulation which cancels out the DFT pre-coding. Thus, also for B-EFDMA, the efficient implementation of the B-IFDMA modulation in time domain can be used complemented by an IDFT. Thus, the computational effort for time domain implementation of B-EFDMA is given by

$$MUL^{(t)}_{\mathrm{B-EFDMA,Tx}} = \begin{cases} M \cdot N + \frac{1}{2}Q \cdot \mathrm{ld}(Q) & M > 1 \\ \frac{N}{4} + \frac{1}{2}Q \cdot \mathrm{ld}(Q) & M = 1 \end{cases} \tag{4.25}$$

For the implementation in frequency domain, the computational effort for B-EFDMA is the same as for OFDMA.

For B-IFDMA, OFDMA and B-EFDMA signal generation, no complex divisions are required.

In Figure 4.21, the respective numbers of complex multiplications are depicted dependent on the number M of subcarriers per block for $N = 1024$ subcarriers in the system and $Q = 64$ subcarriers per user, i.e., an instantaneous net bit rate of 2.22 Mbps assuming QPSK modulation and error control coding with rate 1/2. Taking the duration $T + T_{\mathrm{CP}} = 28.8 \ \mu s$ of a modulated data vector with cyclic prefix, that is obtained assuming the system parameters from Table 4.2, into account, from the required numbers of multiplications per modulated data vector, the required numbers of complex multiplications per second can be calculated. It is given by the multiplication of the number of complex multiplications per modulated data vector with $1/(T + T_{\mathrm{CP}}) \approx 34722$. In Figure 4.21, the required number of complex multiplications per second is given on the vertical axis on the right.
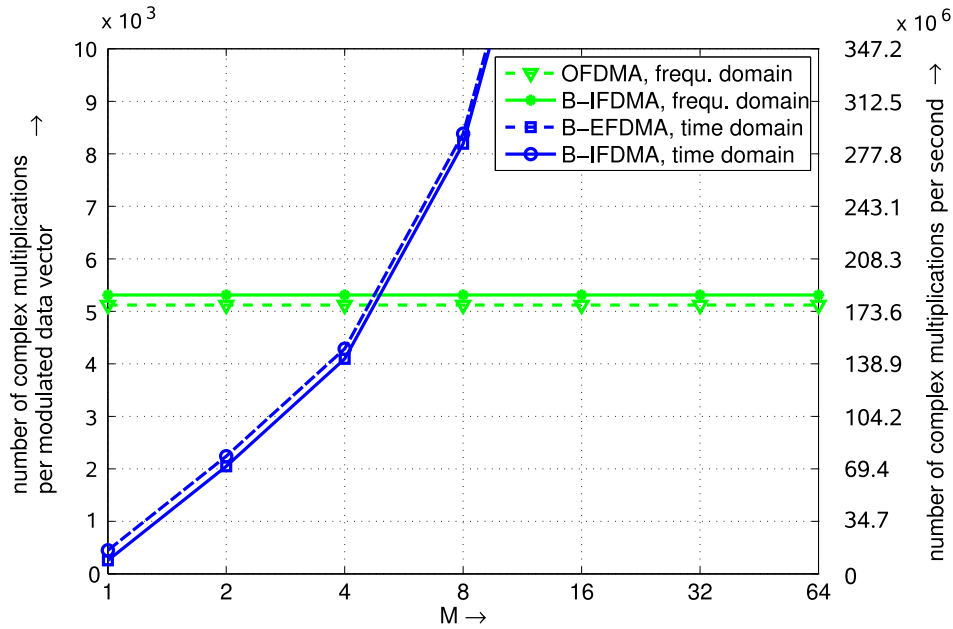
Figure 4.21: Computational complexity for signal generation in terms of required complex multiplications per mobile terminal dependent on the number M of subcarriers per block for $Q = 64$ and $N = 1024$.

Figure 4.21 shows that, for implementation in frequency domain, the computational effort of B-IFDMA is similar to that of OFDMA. The reason is, that the additional Q-point FFT for pre-coding requires only a small number of complex multiplications compared to the N-point IFFT for OFDM modulation, which is true as long as Q is significantly smaller than N. The implementation in time domain has a computational complexity that increases with increasing number M of subcarriers per block whereas the computational complexity for the implementation in frequency domain is independent of M. For $M \leq 4$, for the time domain implementation, a lower computational effort is required than for the frequency domain implementation. Again, the computational complexity of B-IFDMA is similar to that of OFDMA, because the additional

effort of the Q-point IFFT required for OFDMA is small.

For $M > 4$, the time domain implementation can be considered as inappropriate because it requires a significantly higher number of complex multiplications than the implementation in frequency domain. Regarding today's markets for available Digital Signal Processors (DSPs), it can be seen that DSPs providing several hundred millions of complex multiplications per second are already available. Thus, the computational power required for OFDMA and B-IFDMA modulation in future mobile terminals is already on the market. However, as computational power is always a source of costs, a low complexity solution as provided for B-IFDMA with $M < 4$ can be still regarded as an interesting option in order to make low cost mobile terminals possible.

4.3.2 Base Station

In this section, the computational complexity of digital signal processing required for a B-IFDMA receiver at the base station is analyzed and compared to the respective effort for OFDMA. As in Section 4.3.1, the frequency domain implementation presented in Section 2 and the time domain implementation presented in Section 3.2 are regarded and only the required numbers of multiplications and divisions are considered.

A fully loaded system with K users is assumed, where Q subcarriers are assigned to each user. For channel estimation, a simple pilot-based channel estimation algorithm as presented in [SFK06] is assumed which is appropriate for both, B-IFDMA and OFDMA. The computational effort of the B-IFDMA base station receiver implemented in frequency domain is given by the effort of OFDM demodulation, the effort for K channel estimations, the effort for the applications of K frequency domain equalizers and K times the effort for a Q-point IDFT to reverse the DFT pre-coding, cf. (2.33). As in Section 4.3.1, it is assumed that the subcarrier demapping operation can be implemented with negligible effort. Further on, as in Section 4.3.1, it is assumed that both Q and N are powers of 2 and that, thus, OFDM demodulation is performed by an N-point FFT and the IDFT is implemented using the IFFT algorithm.

The computational effort for K channel estimations is given as follows: In order to obtain an estimate of the channel coefficient, for every subcarrier carrying a pilot symbol within each of the K subcarrier sets, the respective received pilot symbol has to be multiplied with the inverse of the transmitted pilot symbol. Thus, for the channel estimation algorithm presented in [SFK06], one multiplication for each pilot within each of the K subcarrier sets is required. Consequently, in general, the computational

complexity of the channel estimation algorithm depends on the number of pilots within a subcarrier set and, thus, on the B-IFDMA signal parameters, cf. Section 4.2.6. In the following, for the complexity of the channel estimation, as a worst case it is assumed that channel estimation has to be performed for every subcarrier in each subcarrier set. As discussed in Section 4.2.6, this would be the case for B-IFDMA with $L = 1$. Thus, the computational effort for channel estimation results in $K \cdot Q$ complex multiplications per base station.

For frequency domain equalization, the received signal has to be multiplied with the inverse of a matrix, cf. (2.31) and (2.32). As the matrix to be inverted is a diagonal matrix, cf. Section 2.3.5, the matrix inversion can be performed by an inversion of the diagonal elements of the matrix. Thus, the multiplication of the received signal with the equalizer matrix, cf. (2.33), can be implemented by a division of the received signal at every subcarrier by the respective diagonal element. Thus, the required computational effort for frequency domain equalization is given by $K \cdot Q$ complex divisions per base station.

Thus, in total, the computational effort for the B-IFDMA base station receiver implemented in frequency domain is given by

$$MUL^{(f)}_{\text{B−IFDMA,Rx}} = \frac{1}{2}N \cdot \mathrm{ld}(N) + K \cdot Q + K \cdot \frac{1}{2}Q \cdot \mathrm{ld}(Q) \qquad (4.26)$$

complex multiplications and

$$DIV^{(f)}_{\text{B−IFDMA,Rx}} = K \cdot Q \qquad (4.27)$$

complex divisions per base station per modulated data symbol vector.

In order to obtain the computational effort for the B-IFDMA base station receiver with demodulation implemented in time domain, the computational effort of the N-point FFT in (4.26) has to be replaced by the effort required for K demodulators implemented in time domain according to (3.28). As the output of the demodulator is a signal in time domain and equalization is performed in frequency domain, an additional Q-point DFT is required for each of the K users. Thus, the computational effort of the respective base station receiver is given by

$$MUL^{(t)}_{\text{B−IFDMA,Rx}} = \frac{K \cdot N}{L} + 2K \cdot \frac{1}{2}Q \cdot \mathrm{ld}(Q) + K \cdot Q \qquad (4.28)$$

complex multiplications and

$$DIV^{(t)}_{\text{B−IFDMA,Rx}} = K \cdot Q \qquad (4.29)$$

complex divisions per base station and per modulated data symbol vector.

For OFDMA, compared to (4.26), the DFT pre-coding does not have to be reversed at the receiver. Thus, for OFDMA, the computational effort for the OFDMA base station receiver implemented in frequency domain is given by

$$MUL^{(f)}_{\text{OFDMA,Rx}} = \frac{1}{2} N \cdot \text{ld}(N) + K \cdot Q \tag{4.30}$$

complex multiplications and

$$DIV^{(f)}_{\text{OFDMA,Rx}} = K \cdot Q \tag{4.31}$$

complex divisions per base station and per modulated data symbol vector. Similar as for the OFDMA modulation, in general, there is also no efficient time domain implementation for OFDMA demodulation.

Since, as explained in Section 4.3.1, B-EFDMA can be regarded as IDFT pre-coded B-IFDMA, the computational effort of a base station receiver for B-EFDMA using the time domain demodulation from Section 3.2.4 is given by the computational complexity of the B-IFDMA receiver, where the IDFT after frequency domain equalization, cf. Figure 2.4 in Section 2.3.5, is omitted and, thus, is given by

$$MUL^{(t)}_{\text{B-EFDMA,Rx}} = \frac{K \cdot N}{L} + K \cdot \frac{1}{2} Q \cdot \text{ld}(Q) + K \cdot Q \tag{4.32}$$

complex multiplications and

$$DIV^{(t)}_{\text{B-EFDMA,Rx}} = K \cdot Q \tag{4.33}$$

complex divisions per base station per modulated data vector.

In Figure 4.22, the respective numbers of complex multiplications are depicted for $Q = 64$. The system parameters are chosen according to Table 4.2. The required number of complex divisions is the same for all schemes that are regarded throughout this section and independent from the B-IFDMA signal parameters. It is given by $K \cdot Q = N = 1024$ complex divisions per base station per modulated data vector. As in Section 4.3.1, from the required numbers of multiplications per modulated data vector, the required numbers of complex multiplications per second can be calculated. It is given by the multiplication of the number of complex multiplications per modulated data vector with $1/(T + T_{\text{CP}}) \approx 34722$. In Figure 4.22, the required number of complex multiplications per second is given on the vertical axis on the right. Figure 4.22 shows that, in general, for B-IFDMA, the computational effort at the base station is slightly higher than for OFDMA, because for B-IFDMA the DFT pre-coding has to

be reversed at the receiver side. Again, the implementation in time domain shows a computational complexity that increases with an increasing number M of subcarriers per block whereas the computational complexity for the implementation in frequency domain is independent of M. However, at the base station receiver, the demodulation in time domain requires a significantly higher computational effort compared to frequency domain demodulation for all numbers M. The reason is that in case of time domain demodulation one demodulator is required for each user whereas for frequency domain modulation an N-point DFT together with the subcarrier demapping performs user separation jointly for all users. Thus, at the base station receiver, for uplink transmission, the implementation in frequency domain is clearly preferable.
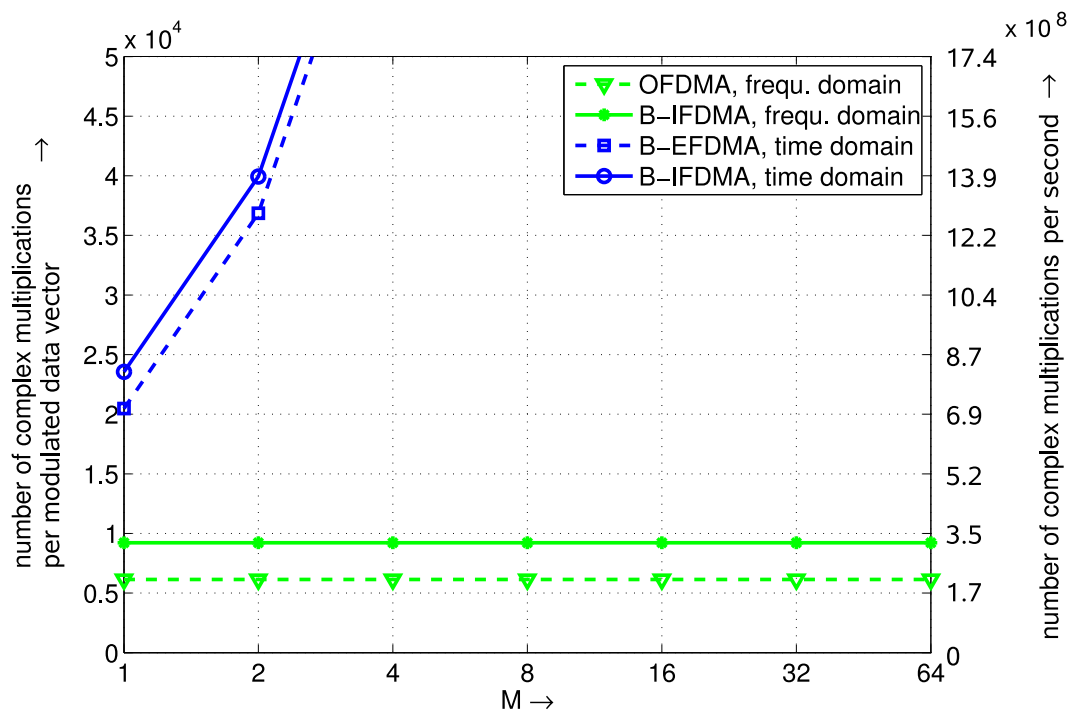
Figure 4.22: Computational complexity in terms of required complex multiplications per base station and per modulated data symbol dependent on the number M of subcarriers per block.

4.4 Real World Effects

4.4.1 Overview

In this section, B-IFDMA is analyzed with respect to real world effects. Section 4.4 is organized as follows: In Section 4.4.2, the robustness of B-IFDMA to carrier frequency offsets is investigated dependent on the B-IFDMA signal parameters. Section

4.4.2 discusses the power efficiency of the mobile terminal using B-IFDMA considering realistic pulse shaping and non-linear power amplifiers.

4.4.2 Carrier Frequency Offsets

In this section, the robustness of B-IFDMA to carrier frequency offsets is investigated dependent on the B-IFDMA signal parameters.

For mobile radio applications, carrier frequency offsets are typically caused by oscillator imperfections due to low cost oscillators or Doppler shifts due to the mobility of the users [WIN05]. If, due to the aforementioned reasons, the frequency of the received signals of the different users is not exactly the same and, moreover, exactly the same as the frequency of the oscillator at the receiver and if no frequency synchronization is applied, the orthogonality between the subcarriers of the different signals is destroyed and inter-carrier interference (ICI) occurs. This is a fundamental property of OFDM based signals, cf. [vNP00], and is, thus, also true for B-IFDMA that, in Section 2.5, has been shown to be a DFT pre-coded OFDMA scheme.

Since, for B-IFDMA, the signal contains subcarriers of different users, in general, the following two types of ICI can be distinguished: Interference between the subcarriers of the same user that is, in the following, denoted as self-interference (SI) and interference between subcarriers of different users that is, in the following, denoted as multiple access interference (MAI). Note that both kinds of interference occur if no synchronization is applied.

However, especially for uplink transmission, frequency synchronization is a challenging task. The reason is that, in general, in the uplink, the carrier frequency offsets of different users' signals are different because the velocities causing Doppler shifts are different and because the oscillators in the different mobile terminals may show different frequency imperfections.

The carrier frequency offset of the different users' signals can be estimated at the receiver side, e.g., using pilot symbols contained in the subcarrier sets of the different users' signals. If estimates of the carrier frequency offsets of the different users' signals are available at the receiver, a compensation of the SI is possible. For that purpose, after user separation, the subcarrier sets of the different users have to be shifted by the negative of their respective carrier frequency offset. However, the compensation of MAI is much more difficult and requires computationally complex joint detection techniques.

In the following, let $\Delta f_{\mathrm{CFO}}^{(k)}$ denote the carrier frequency offset of user k. A normalization of the carrier frequency offset $\Delta f_{\mathrm{CFO}}^{(k)}$ to the subcarrier bandwidth Δf of (4.4) results in the relative carrier frequency offset

$$\Delta \bar{f}_{\mathrm{CFO}}^{(k)} = \frac{\Delta f_{\mathrm{CFO}}^{(k)}}{\Delta f}. \tag{4.34}$$

As the carrier frequency offsets may be caused, e.g., by oscillator imperfections, in the following, the relative carrier frequency offset $\Delta \bar{f}_{\mathrm{CFO}}^{(k)}$ is modelled as a random variable that is uniformly distributed in $\left[-\Delta \bar{f}_{\mathrm{CFO,max}}^{(k)}, \Delta \bar{f}_{\mathrm{CFO,max}}^{(k)} \right]$ with $\Delta \bar{f}_{\mathrm{CFO,max}}^{(k)}$ denoting the maximum relative carrier frequency offset of user k that occurs.

In the following, the carrier frequency offsets $\Delta f_{\mathrm{CFO}}^{(k)}$ are assumed to be known at the receiver, i.e., it is assumed that $\Delta f_{\mathrm{CFO}}^{(k)}$ has been perfectly estimated at the receiver. Thus, the SI of user k can be compensated by shifting the subcarrier set of every user by the negative carrier frequency offset $-\Delta f_{\mathrm{CFO}}^{(k)}$. Further on, it is assumed that, due to the high complexity, the compensation of MAI at the receiver is not feasible.

In order to analyze the robustness of B-IFDMA to carrier frequency offsets independently of the diversity that is exploited, a B-IFDMA transmission over an AWGN channel with carrier frequency offsets is regarded.

Figure 4.23 depicts the performance results in terms of BER versus E_{b}/N_0 without coding for the robustness investigations of B-IFDMA to carrier frequency offsets assuming $N = 1024$ subcarriers in the system, $Q = 64$ subcarriers per user, $K = 16$ users and $\Delta \bar{f}_{\mathrm{CFO,max}}^{(k)} = 10\%$ for all users. The performance is shown dependent on the number M of subcarriers per block. It can be seen that the higher the number M of subcarriers per block the better the performance. The reason for that is that the strongest ICI is caused by neighboring subcarriers. The impact of neighboring subcarriers belonging to the same user causes SI and, thus, can be compensated. The impact of neighboring subcarriers belonging to different users causes MAI and, thus, cannot be compensated. Thus, increasing the number of neighboring subcarriers belonging to the same user increases the robustness of B-IFDMA to MAI at the expense of additional SI that, however, can be compensated.

In Figure 4.24, the required E_{b}/N_0 at a BER of 10^{-3} is depicted. From Figure 4.24 it can be seen that already for low numbers $M > 1$ of subcarriers per block the robustness of B-IFDMA to carrier frequency offsets is significantly improved.

Together with the results from Section 4.2 it can be concluded that, for application in a mobile radio system, B-IFDMA enables the combination of both, increased robustness
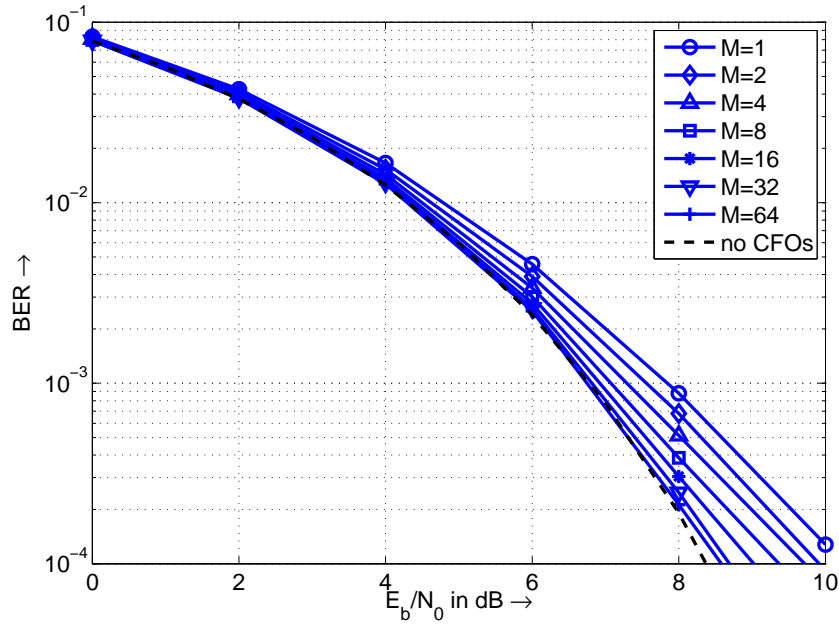
Figure 4.23: Performance of B-IFDMA with different numbers M of subcarriers per block in presence of carrier frequency offsets with $\Delta \bar{f}_{\mathrm{CFO,max}}^{(k)} = 10\%$ for all users and for $Q = 64$ subcarriers per user.
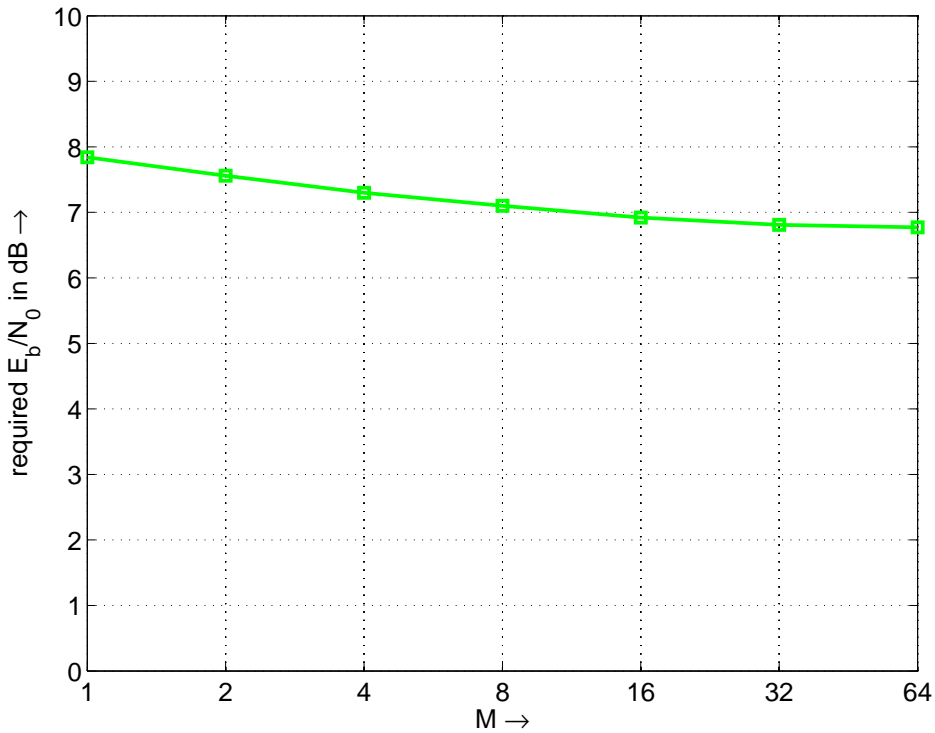

Figure 4.24: Required E_{b}/N_0 at a BER of 10^{-3} for B-IFDMA dependent on the number M of subcarriers per block in presence of carrier frequency offsets with $\Delta \bar{f}_{\mathrm{CFO,max}}^{(k)} = 10\%$ for all users.

to carrier frequency offsets and the exploitation of frequency diversity. This property is an essential advantage compared to, on the one hand, IFDMA that provides good frequency diversity but suffers from high sensitivity to carrier frequency offsets and, on the other hand, localized SC-FDMA that provides good robustness to carrier frequency offsets but only poor frequency diversity.

4.4.3   Power Efficiency

4.4.3.1   Introduction

In Section 4.4.3, the power efficiency of the mobile terminal is discussed from different perspectives. The power efficiency of the mobile terminal is increased by

- low envelope fluctuations of the transmit signal [vNP00, RAC+02],

- a high average power of the transmit signal within a modulated data vector [RAC+02, Cey05] compared to the maximum output power of the amplifier that is possible for this signal given a certain amount of envelope fluctuations, and

- joining a so-called sleep mode, i.e., switching off several parts of power consuming hardware components in the mobile terminal when they are not used, cf. [FN01].

In the following, at first, the envelope properties of the B-IFDMA transmit signal are investigated dependent on the B-IFDMA signal parameters. Note that for the evaluation of the envelope characteristics of the B-IFDMA transmit signal the analysis of the modulated data vector is not sufficient because, compared to the analog transmit signal, the modulated data vector does not consider the impact of the pulse shaping and the windowing of the signal. Thus, an extension of the signal model for the B-IFDMA signal is introduced that gives a good approximation of the analog transmit signal. Further on, note that for the evaluation of the signal envelope, different metrics are common. Thus, the results of the analysis of the B-IFDMA signal envelope shown throughout this section are presented in terms of several metrics. Some of the results have been published by the author of this thesis in [FKH08].

After the analysis of the envelope properties, the impact of the average power of the transmit signal within a modulated data vector on the power efficiency and its dependency on the B-IFDMA signal parameters are discussed. Finally, the efficiency of

sleep modes and its dependency on the B-IFDMA signal parameters is regarded. The analysis of the power efficiency of B-IFDMA has been published by the author of this thesis in [SFE$^+$09].

The remainder of this section is organized as follows. In Section 4.4.3.2, an approximation of the analog B-IFDMA transmit signal is introduced that is based on oversampling of the modulated data vector. In Section 4.4.3.3, a selection of different well-known metrics for the envelope fluctuations of a signal is recalled and briefly discussed. Section 4.4.3.4 gives the results of the analysis of the B-IFDMA signal envelope based on the different metrics from Section 4.4.3.3. Section 4.4.3.5 discusses the power efficiency dependent on the average power of a B-IFDMA signal within a modulated data vector and Section 4.4.3.6 regards the efficiency of sleep modes for B-IFDMA.

4.4.3.2 Signal Model for the Oversampled Transmit Signal

In this section, in order to approximate the analog transmit signal, the model of the B-IFDMA transmit signal from Section 2.3.2 is extended by the introduction of oversampling, pulse shaping and windowing.

Let
$$\mathbf{x}_{\mathrm{OS}}^{(k)} = \left[x_{\mathrm{OS},0}^{(k)}, \ldots, x_{\mathrm{OS},N\cdot S-1}^{(k)} \right]^{\mathrm{T}} \tag{4.35}$$
denote the oversampled modulated data vector with oversampling factor S. The elements $x_{\mathrm{OS},n}^{(k)}$, $n = 0, \ldots, S \cdot N - 1$, are given by

$$x_{\mathrm{OS},n}^{(k)} = \begin{cases} x_m^{(k)} & n = m \cdot S, \quad m = 0, \ldots, N-1 \\ 0 & \text{else} \end{cases}, \tag{4.36}$$

where $x_m^{(k)}$ denotes the elements of the modulated data vector in (2.39).

For the pulse shaping, a circular convolution of $\mathbf{x}_{\mathrm{OS}}^{(k)}$ with the vector representation of a pulse shaping filter given by

$$\mathbf{g} = [g_0, \ldots, g_{R_{\mathrm{f}}-1}]^{\mathrm{T}} \tag{4.37}$$

with samples g_r, $r = 0, \ldots, R_{\mathrm{f}} - 1$ at sampling rate $S \cdot K/T_{\mathrm{s}}$ is considered, where $R_{\mathrm{f}} \leq S \cdot N$ denotes the length of the filter and where K/T_{s} denotes the sampling rate of the modulated data vector $\mathbf{x}^{(k)}$ of (2.3). The circular convolution with the pulse shaping filter $\mathbf{g}$ in time domain is equivalent to a shaping of the spectrum implemented in the DFT domain. The reason for the description of this kind of spectrum shaping is

that, for OFDM and OFDMA, a shaping by an ideal lowpass filter implemented in the DFT domain is common, cf. [vNP00]. Thus, in order to provide a fair comparison of B-IFDMA to OFDMA, the same kind of spectrum shaping is applied.

The pulse shaped signal is given by

$$\mathbf{x}_{\text{PS}}^{(k)} = \mathbf{x}_{\text{OS}}^{(k)} \circledast \mathbf{g}, \tag{4.38}$$

where $\circledast$ denotes circular convolution.

The effect in DFT domain of oversampling and pulse shaping is schematically depicted in Figure 4.25. As shown in Figure 4.25 b), the insertion of zeros in the time domain signal due to oversampling leads to a periodic repetition of the DFT of $\mathbf{x}^{(k)}$ from Figure 4.25 a). As pulse shaping filter, an ideal lowpass filter in DFT domain is assumed, cf. Figure 4.25 c). The application of the pulse shaping filter $\mathbf{g}$ according to (4.38) is equivalent to a multiplication of the samples of the DFT of vector $\mathbf{x}_{\text{OS}}^{(k)}$ depicted in Figure 4.25 b) with the samples of the DFT of the ideal lowpass filter vector $\mathbf{g}$ from Figure 4.25 c). The DFT of the resulting vector $\mathbf{x}_{\text{PS}}^{(k)}$ is depicted in Figure 4.25 d). From a comparison of Figure 4.25 d) with Figure 4.25 a) it can be seen that oversampling and filtering with an ideal lowpass filter in DFT domain is equivalent to a zero-padding of the DFT of the modulated data vector $\mathbf{x}^{(k)}$ in the DFT domain.

Let $S \cdot N_{\text{CP}}$ denote the number of samples for the oversampled CP, where N_{CP} denotes the number of samples of the CP at sample rate K/T_{s}. The oversampled signal

$$\mathbf{x}_{\text{CP}}^{(k)} = \left[x_{\text{CP},0}^{(k)} \ldots, x_{\text{CP},S\cdot(N+N_{\text{CP}})-1}^{(k)} \right]^{\text{T}} \tag{4.39}$$

after the insertion of a CP at sample rate $K \cdot S/T_{\text{s}}$ can be described by

$$\mathbf{x}_{\text{CP}}^{(k)} = \left[\left(\mathbf{x}_{\text{Prefix}}^{(k)} \right)^{\text{T}} \ \left(\mathbf{x}_{\text{PS}}^{(k)} \right)^{\text{T}} \right]^{\text{T}}, \tag{4.40}$$

where

$$\mathbf{x}_{\text{Prefix}}^{(k)} = \left[x_{\text{PS},S\cdot(N-N_{\text{CP}})}^{(k)}, \ldots, x_{\text{PS},S\cdot N-1}^{(k)} \right]^{\text{T}}. \tag{4.41}$$

In order to reduce the out-of-band radiation of the signal, for practical implementations, after pulse shaping, a windowing is applied, cf. [vNP00]. Let

$$\mathbf{w} = \left[w_0, \ldots, w_{S\cdot(N+N_{\text{CP}})-1} \right]^{\text{T}} \tag{4.42}$$

denote the vector representation of a time domain window with elements w_s, $s = 0, \ldots, S \cdot (N_{\text{CP}} + N) - 1$, at sampling rate $S \cdot K/T_{\text{s}}$. The oversampled DFT precoded OFDMA signal with CP after windowing

$$\mathbf{x}_{\text{w}}^{(k)} = \left[x_{\text{w},0}^{(k)}, \ldots, x_{\text{w},S\cdot(N+N_{\text{CP}})-1}^{(k)} \right]^{\text{T}} \tag{4.43}$$
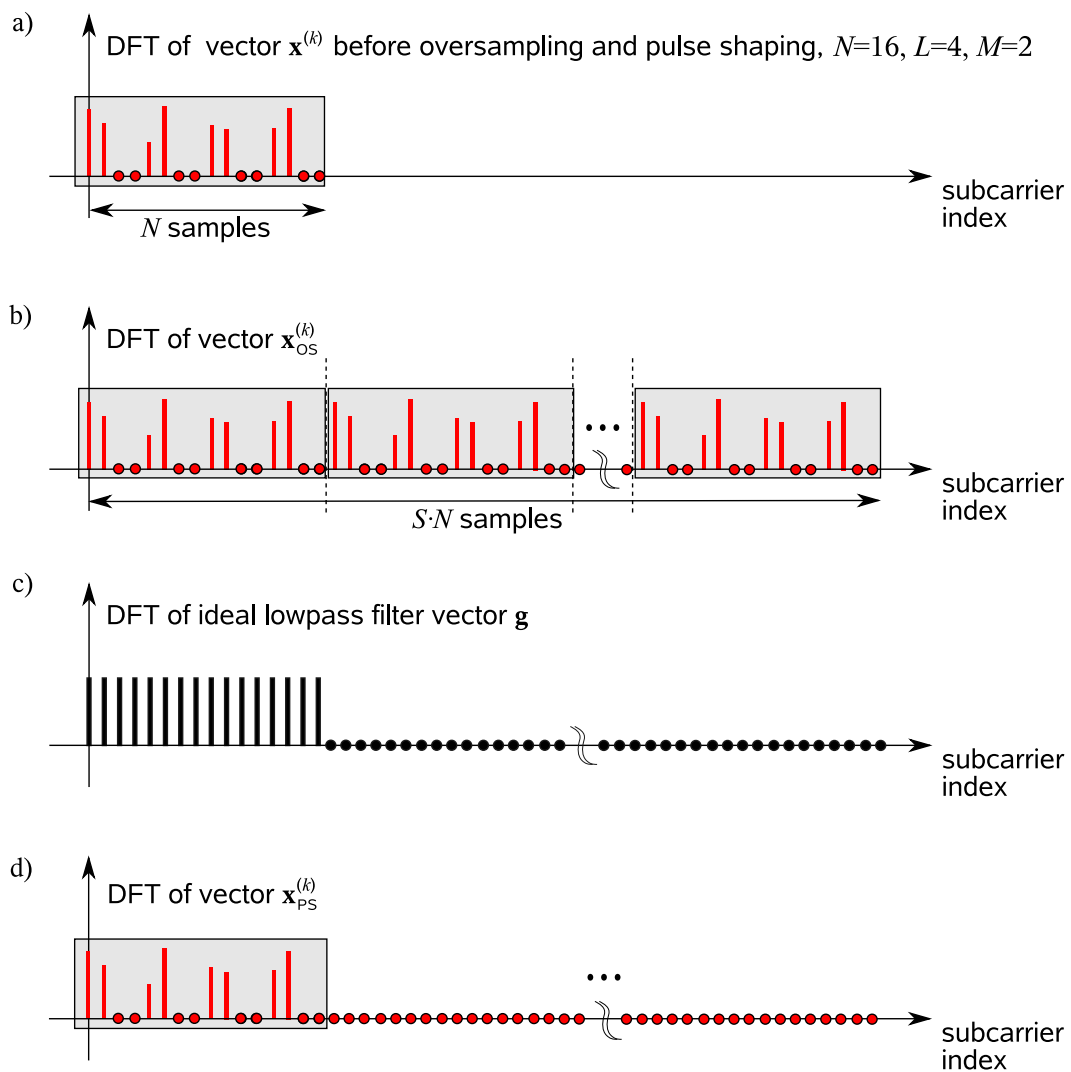
Figure 4.25: Illustration of the oversampling and pulse shaping that is used throughout this Section, cf. [vNP00], for $N = 16$, $L = 4$ and $M = 2$.

is given by

$$\mathbf{x}_{\mathrm{w}}^{(k)} = \mathbf{W} \cdot \mathbf{x}_{\mathrm{CP}}^{(k)}, \tag{4.44}$$

where $\mathbf{W}$ denotes an $S \cdot (N + N_{\mathrm{CP}}) \times S \cdot (N + N_{\mathrm{CP}})$ diagonal matrix carrying the elements w_s of vector $\mathbf{w}$ on its main diagonal given by

$$\mathbf{W} = \mathrm{diag}(\mathbf{w}). \tag{4.45}$$

4.4.3.3   Metrics for the Evaluation of the Signal Envelope

In this section, a selection of appropriate metrics for the evaluation of the signal envelope is recalled. A widely used metric is the Peak-to-Average Power Ratio (PAPR) per modulated data vector [vNP00] defined as

$$PAPR^{(k)} = \max_s \left\{ \frac{|x_{\mathrm{w},s}^{(k)}|^2}{E\{|x_{\mathrm{w},s}^{(k)}|^2\}} \right\}, \quad s = 0, \ldots, S \cdot (N_{\mathrm{CP}} + N) - 1, \tag{4.46}$$

where $E\{|x_{\mathrm{w},s}^{(k)}|^2\}$ denotes the expectation of the random process $|x_{\mathrm{w},s}^{(k)}|^2$ for a given user k. Defined according to (4.46), the PAPR gives the ratio of the peak power and the average power within a modulated data vector. However, dependent on the data symbols, the PAPR varies from modulated data vector to modulated data vector. Thus, in order to obtain meaningful results, not only the maximum PAPR but also the probability distribution of the PAPR over many consecutive modulated data vectors has to be regarded.

Recently, a new metric denoted as Cubic Metric (CM) [SSJ06] has been receiving wide interest in 3GPP LTE. The CM is based on the fact that the primary cause of distortions due to envelope fluctuations of the transmit signal is the third order non-linearity of the amplifier gain characteristic [SSJ06]. A metric of the intensity of the third order non-linearity is given by normalizing the absolute values of the elements $x_{\mathrm{w},s}^{(k)}$ of the transmit signal vector $\mathbf{x}_{\mathrm{w}}^{(k)}$ to a root mean square (RMS) value equal to one and then calculating the RMS of the cubed normalized signal according to

$$RCM^{(k)} = 20\log_{10}\left(\mathrm{RMS}\left(\left(\frac{|x_{\mathrm{w},s}^{(k)}|}{\mathrm{RMS}\left(x_{\mathrm{w},s}^{(k)} \right)} \right)^3 \right) \right), \tag{4.47}$$

where

$$\mathrm{RMS}\left(x_{\mathrm{w},s}^{(k)} \right) = \sqrt{ \frac{1}{S \cdot (N_{\mathrm{CP}} + N)} \sum_{s=0}^{S \cdot (S \cdot + N) - 1} |x_{\mathrm{w},s}^{(k)}|^2 } \tag{4.48}$$

denotes the RMS of the elements $x_{\mathrm{w},s}^{(k)}$ of vector $\mathbf{x}_{\mathrm{w}}^{(k)}$. The metric $RCM^{(k)}$ is known as Raw Cubic Metric (RCM) and is often used in comparison to a reference signal with the RCM CM_{ref} of a Wideband Code Division Multiple Access (W-CDMA) signal that is equal to $CM_{\mathrm{ref}} = 1.52$ [3GP04].

Together with a non-linear amplifier, a fluctuating signal envelope results in undesired out-of-band radiation [FDLLS07]. In order to meet a certain spectral mask of the signal, which is usually predefined by regulatory authorities, a certain power back-off is required for the amplifier. The higher the required power back-off, the lower the power efficiency of the amplifier [FDLLS07]. Thus, a further metric for evaluation of the envelope fluctuations of a signal is the required amplifier power back-off in order to meet a given spectral mask for a given amplifier model. In the following, the Rapp model [vNP00] is used in order to model the non-linear power amplifier. The output of the amplifier according to the Rapp model is given by

$$y_{\mathrm{w},s}^{(k)} = \frac{x_{\mathrm{w},s}^{(k)}}{\left(1 + \left(\frac{x_{\mathrm{w},s}^{(k)}}{x_{\mathrm{sat}}}\right)^{2p}\right)^{\frac{1}{2p}}}, \qquad (4.49)$$

where p denotes the Rapp-Parameter and x_{sat} denotes the saturation level of the amplifier. Large values of p, e.g., $p = 10$, model a highly linear amplifier whereas with decreasing values of p the non-linearity of the amplifier increases. The relation between the saturation level x_{sat}, the power P_{in} of the input signal $x_{\mathrm{w},s}^{(k)}$ and the input power back-off IBO is given by

$$IBO = 10\log_{10}\left(\frac{|x_{\mathrm{sat}}|^2}{P_{\mathrm{in}}}\right). \qquad (4.50)$$

Another important effect of transmitting a signal with fluctuating envelope over a non-linear amplifier is that due to the non-linear distortions the orthogonality of the subcarriers is destroyed. Thus, the performance of the received signal degrades with a decreasing power back-off of the amplifier. Consequently, the performance degradation, e.g., in terms of BERs is a further metric in order to evaluate the effect of envelope fluctuations in presence of non-linear amplifiers. In the following, the BER degradation for transmission over an AWGN channel is regarded. The reason to use an AWGN channel for transmission is that the different regarded subcarrier allocations provide different amounts of frequency diversity when transmitted over a frequency selective channel. Performance degradations due to non-orthogonal subcarriers and performance gains due to frequency diversity should, however, be well separated in this analysis.

4.4.3.4   Analysis of the Signal Envelope

In this section, the envelope of the B-IFDMA transmit signal is analyzed. For that purpose, a B-IFDMA signal according to the extended signal model from Section 4.4.3.2 is regarded and the metrics presented in Section 4.4.3.3 are used. In particular, the following results are presented:

At first, results for the impact of the

- oversampling, pulse shaping and windowing,

- bit mapping scheme,

- DFT pre-coding, and

- allocation of the subcarrier blocks

on the signal envelope based on the PAPR distribution are presented, with the number M of subcarriers per block as a parameter.

Subsequently, the required power back-off in order to meet a given spectral mask is investigated and results for the required power back-off in order to provide a low BER degradation are presented and discussed.

Finally, results for the envelope fluctuations of B-IFDMA and OFDMA transmit signals are presented in terms of

- the raw cubic metric,

- the mean PAPR, and

- the required power back-off of the power amplifier,

with the number M of subcarriers per block as a parameter.

In the following, results for the analysis of the impact of oversampling, pulse shaping and windowing on the envelope of the B-IFDMA transmit signal are presented. For that purpose, the cumulative probability density function (CDF) of the PAPR of a B-IFDMA signal without oversampling, i.e., $S = 1$, is analyzed and compared to the CDF of the PAPR of a B-IFDMA signal with oversampling, pulse shaping and windowing.

Figures 4.26 and 4.27 depict the CDF of the PAPR of a B-IFDMA signal with $S = 1$ using QPSK and 64QAM, respectively, with the number M of subcarriers per block as a parameter. The number N of subcarriers in the system is $N = 1024$. $Q = 64$ subcarriers are assigned to a user.

For QPSK with $M = 1$, a PAPR of 0 dB is provided. The reason is that for $M = 1$, B-IFDMA signal generation reduces to a simple compression and repetition of the data symbol vector $\mathbf{d}^{(k)}$ and a subsequent user specific phase rotation [SDBS98]. Hence, using PSK in general and QPSK in particular, a constant envelope of the signal is provided. The PAPR increases for an increasing number M of subcarriers per block. The reason is that B-IFDMA can be regarded as a superposition of M single carrier signals, cf. Section 3.2.3.1. The steps in the graph in Figure 4.26 for low values of M can be explained as follows: In (3.13), for low values of M, there is only a low number of different summands for a given sample $x_n^{(k)}$ with index n of the B-IFDMA signal. Thus, the number of different possible peak amplitudes obtained by summing up different QPSK symbols that are weighted by different weighting factors $\Theta_n^{(\mu,k)}$ is low, too. This results in a low number of different possible peak powers within a modulated data vector. At the same time, the average power of a modulated data block is almost constant. Thus, there is only a low number of different possible PAPR values. For large values of M, the number of summands in (3.13) increases and, thus, for the calculation of each sample $x_n^{(k)}$ of the B-IFDMA signal, much more different combinations of weighted data symbols are possible compared to low values of M. Consequently, also the number of different possible peak amplitudes is much higher compared to the case with low values of M. Thus, large values of M result in a high number of different possible PAPR values and the CDF of the PAPR of a B-IFDMA signal becomes smooth for large values of M. In Figure 4.26, it can be seen that a smooth CDF is provided for $M \geq 8$.

For 64QAM, the PAPR is larger than the PAPR for QPSK and the constant signal envelope for $M = 1$ is lost. The reason is that for 64QAM, the data symbols $d_q^{(k)}$ have different amplitudes. Also for 64QAM, the PAPR increases with an increasing number M of subcarriers per block for the same reasons as for QPSK. The relative increase of the PAPR for 64QAM compared to QPSK is the higher the lower the number M of subcarriers per block. Note that for 64QAM the steps in the graph do not occur, cf. Figure 4.27, because there is already a large number of different possible amplitudes of the 64QAM symbols and, thus, the number of different possible peak amplitudes of the B-IFDMA signal is high even for low values of M due to the use of 64QAM bit mapping.

Figures 4.28 and 4.29 depict the CDF of the PAPR of a B-IFDMA signal with an

Figure 4.26: CDF of the PAPR for the B-IFDMA transmit signal with $N = 1024$ subcarriers in the system and $Q = 64$ subcarriers per user without oversampling using QPSK.
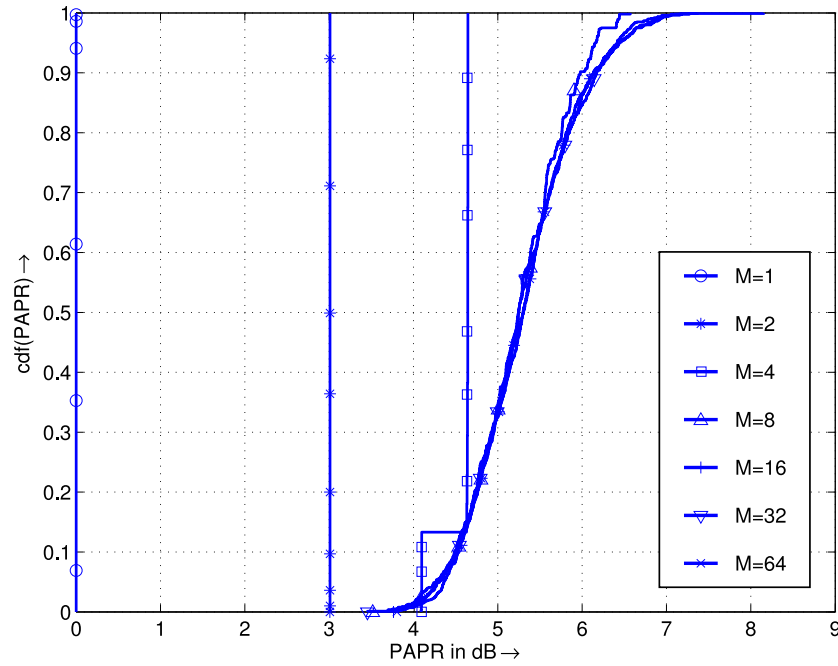

Figure 4.27: CDF of the PAPR for the B-IFDMA transmit signal with $N = 1024$ subcarriers in the system and $Q = 64$ subcarriers per user without oversampling using 64QAM.

oversampling factor $S = 8$ for QPSK and 64QAM, respectively. As a pulse shaping filter, an ideal lowpass filter in the DFT domain is considered, which is common for an oversampled OFDM transmit signal, cf. [vNP00]. Note that, as described in Section 4.4.3.2, in this case, the oversampling and pulse shaping is equivalent to a zero-padding in the DFT domain.

After oversampling and pulse shaping, the CP is inserted and a windowing according to (4.43) is applied. For the results presented throughout this section, the window $\mathbf{w}$ is chosen as a Raised Cosine window. The raising and the trailing edge of the window have a duration of altogether 5% of the duration of the modulated data vector with guard interval. Compared to the results for the PAPR without oversampling in Figures 4.26 and 4.27, the results with oversampling are different: Even for QPSK, due to the impact of the pulse shaping filter, B-IFDMA with $M = 1$ provides no constant envelope. Also for $M > 1$, the PAPR is increased compared to the PAPR of the B-IFDMA signal without oversampling for the same reason. In contrast to the PAPR of the B-IFDMA signal without oversampling, for small numbers M, the PAPR increases with increasing M, reaches a maximum and, for values of M greater than L, the PAPR decreases with increasing M. The PAPRs for $M = 1$ and $M = 64$ are similar as also the PAPRs for $M = 2$ and $M = 32 = Q/2$, and the PAPRs for $M = 4$ and $M = 16 = Q/4$. This effect can be explained as follows. The B-IFDMA signal with $M = 1$ is equivalent to an IFDMA signal. The respective time domain signal is, thus, given by the data symbol vector $\mathbf{d}^{(k)}$ that is compressed, repeated and phase rotated cf. [SDBS98], and, subsequently, oversampled by oversampling factor S and passed through an ideal lowpass filter in the DFT domain. Finally, the windowing is applied. Since a compression and repetition in time and a phase rotation does not change the envelope characteristics of the transmit signal, the PAPR of this signal is equivalent to the PAPR of the data symbol vector $\mathbf{d}^{(k)}$, where oversampling, pulse shaping and windowing is applied. Thus, the PAPR of B-IFDMA with $M = 1$ is equivalent to the PAPR of a single carrier signal with according pulse shaping filter. Note that, as the the raising and the trailing edge of the window are short, the impact of windowing is negligible. For the sake of illustration, the DFT of a B-IFDMA signal with $M = 1$ after oversampling and pulse shaping is depicted in Figure 4.30 a).

The B-IFDMA time domain signal with $M = Q$ can be explained as follows. Similar as for $M = 1$, the B-IFDMA signal is oversampled and a pulse shaping filter given by an ideal lowpass filter in frequency domain and windowing is applied. Note that the pass band of the ideal lowpass contains N samples. The DFT of a B-IFDMA signal with $M = Q$ after oversampling and pulse shaping is depicted in Figure 4.30 b). However, the signal from Figure 4.30 b) is equivalent to a signal that is obtained by oversampling of the data symbol vector $\mathbf{d}^{(k)}$ with oversampling factor $S \cdot N/Q$ and the application of
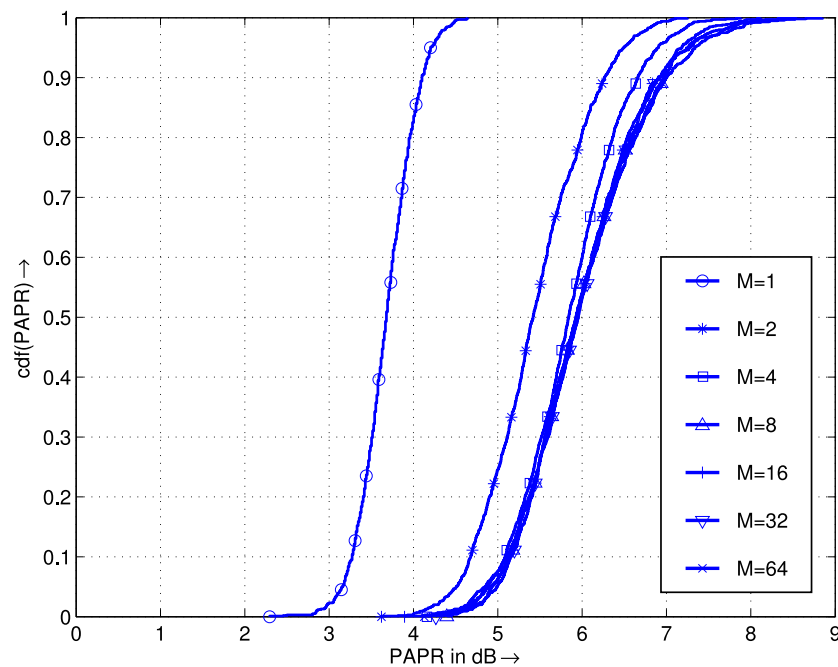
Figure 4.28: CDF of the PAPR for the B-IFDMA transmit signal with $N = 1024$ subcarriers in the system and $Q = 64$ subcarriers per user with oversampling factor $S = 8$, an ideal lowpass in DFT domain as pulse shaping filter and QPSK.
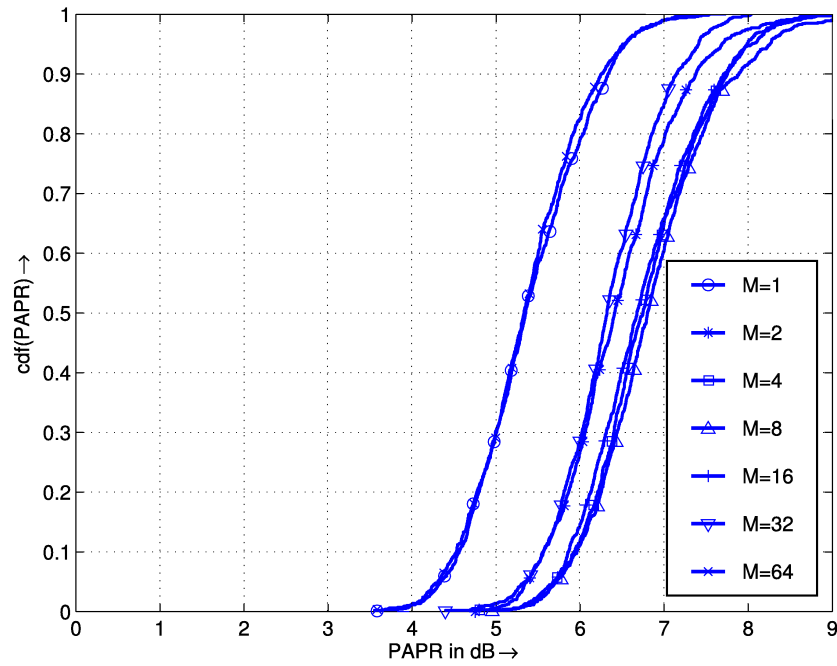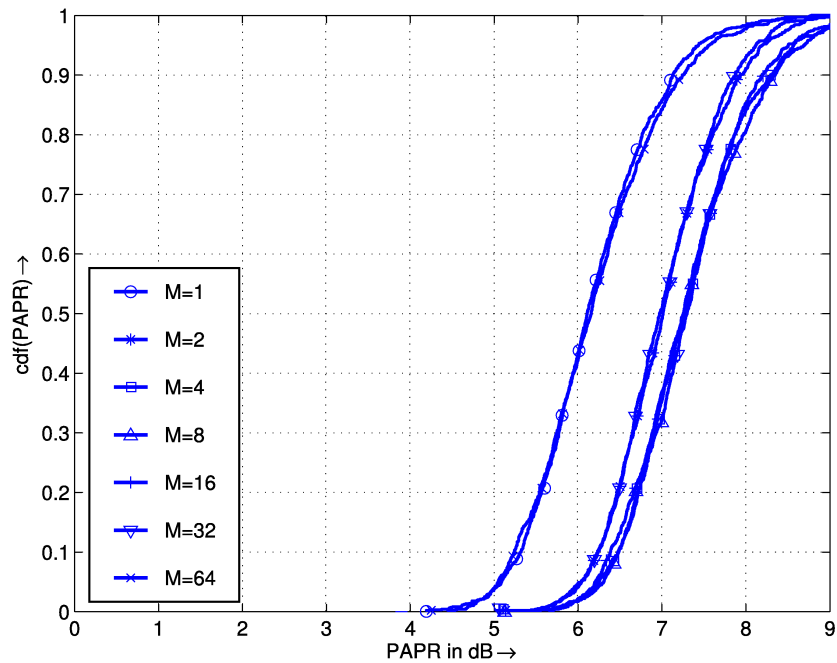

Figure 4.29: CDF of the PAPR for the B-IFDMA transmit signal with $N = 1024$ subcarriers in the system and $Q = 64$ subcarriers per user with oversampling factor $S = 8$, an ideal lowpass in DFT domain as pulse shaping filter and 64QAM.
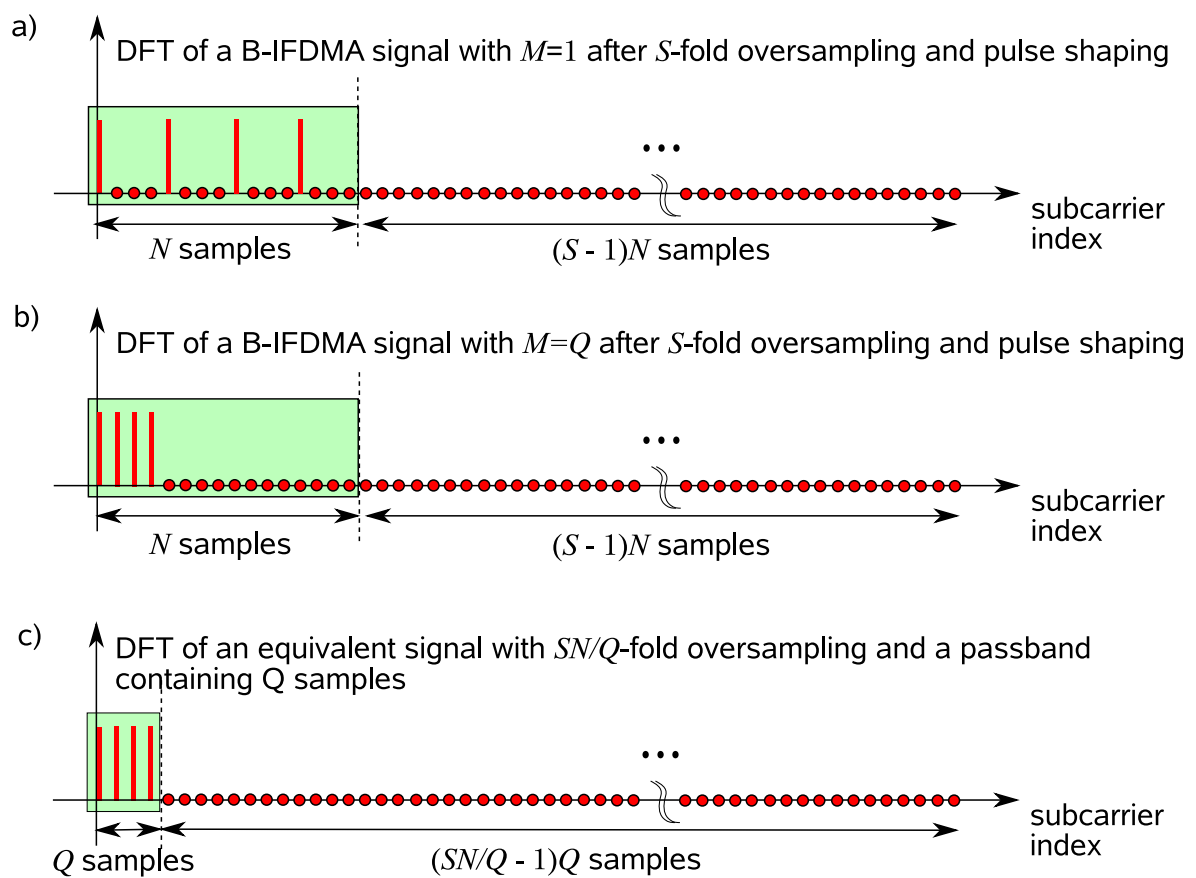
Figure 4.30: Illustration of the oversampling and pulse shaping for B-IFDMA with $M = 1$ and $M = Q$.

an ideal lowpass filter whose pass band contains Q samples, cf. Figure 4.30 c). Thus, also for this signal the PAPR is equivalent to the PAPR of the data symbol vector $\mathbf{d}^{(k)}$, where oversampling pulse shaping and windowing is applied. For large values S, the effect of both ideal lowpass filters for $M = 1$ and for $M = Q$ becomes similar and, thus, also the PAPRs of the B-IFDMA signal are similar for $M = 1$ and $M = Q$.

The similarity of the PAPRs of the B-IFDMA signals for $M = 2$ and $M = 32 = Q/2$ and for $M = 4$ and $M = 16 = Q/4$ can be explained as follows. In section 3.2.3.1, it has been shown that a B-IFDMA signal with $M > 1$ can be regarded as a superposition of M single carrier signals with different frequency shifts. Also the B-IFDMA signal with L subcarrier blocks can be regarded as a superposition of $L = Q/M$ single carrier signals with different frequency shifts. The generation of a B-IFDMA signal from a superposition of single carrier signals is illustrated in Figure 4.31 for $L = 2$. In Figure 4.31 it can be seen that, for that purpose, at first the elements $d_q^{(k)}$ of data symbol vector $\mathbf{d}^{(k)}$ have to be oversampled and low pass filtered. Subsequently, the oversampled and filtered data symbols are shifted in the DFT domain and added up. Note that the two signals that are added up are different but correlated. As both, the B-IFDMA signal with M subcarriers per block and the B-IFDMA signal with $L = Q/M$ subcarrier blocks can be regarded as a superposition of M and Q/M single carrier signals, respectively, both signals provide a similar PAPR.

The effect that the PAPR decreases for $M > L$ is not visible regarding the PAPR without oversampling because without oversampling the impact of the pulse shaping filter is not considered correctly. The reason why for an investigation without oversampling the PAPR of a B-IFDMA signal with a large number M of subcarriers per block is significantly higher than for an investigation with oversampling can be illustratively explained by the following example. A B-IFDMA signal with, e.g., $L = 2$ can be regarded as a superposition of $L = 2$ single carrier signals that are mutually shifted by $N/2$ samples in the DFT domain, cf. Figure 4.31. Without oversampling, this shift is obtained by multiplication with a phase rotation factor $e^{j\frac{2\pi}{N} \cdot N/2 \cdot n} = e^{j \cdot n \cdot \pi} = (-1)^n$ with $n = 0, \ldots, N - 1$ in time domain. Thus, the samples of both signals in time domain are added up with alternating sign and, consequently, the PAPR is significantly increased. Considering a B-IFDMA signal with oversampling and pulse shaping as generally illustrated in Figure 4.25, in case of $L = 2$, the mutual shift of the both signals is still $N/2$ samples in DFT domain. However, the time domain phase rotation factor is now given by $e^{j\frac{2\pi}{SN} \cdot N/2 \cdot s} = e^{j\frac{s \cdot \pi}{S}}$ with $s = 0, \ldots, SN - 1$. Thus, for a large oversampling factor S, the samples of both single carrier signals are added up almost in phase and, thus, the increase of the PAPR is much lower compared to the case without oversampling.

Data symbols and their DFT:

Oversampling and filtering:
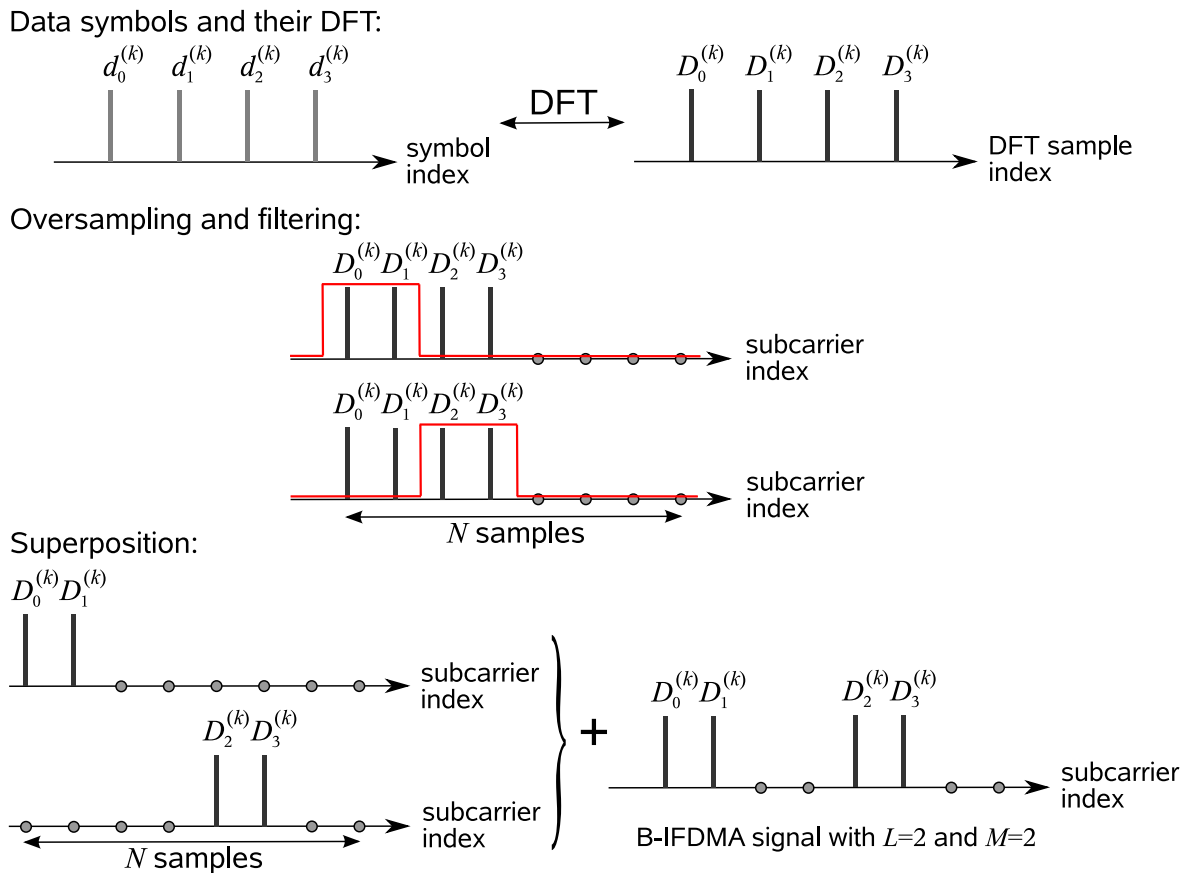
Superposition:

Figure 4.31: B-IFDMA signal with $L = 2$ and $M = 2$ as a superposition of $L = 2$ single carrier signals.

From the results in Figures 4.26 - 4.29 it can be concluded that, for the investigation of the envelope fluctuations of a B-IFDMA signal, the analysis of the transmit signal with $S = 1$ is misleading. Thus, in the sequel, the oversampled transmit signal is considered.

In the following, results for the analysis of the impact of the DFT pre-coding on the PAPR are presented. For that purpose, the CDF of the PAPR of a B-IFDMA signal is compared to the CDF of the PAPR of an OFDMA signal with the same subcarrier allocation. The same parameters as for the results in Figures 4.26 - 4.29 are assumed. A transmission using QPSK is considered.

In Figure 4.32, the CDFs of the PAPR of B-IFDMA signals with different values of M and the CDFs of the PAPR of OFDMA signals with corresponding subcarrier allocations are depicted. The results for B-IFDMA are the same as shown in Figure 4.28. For OFDMA, the CDF of the PAPR provides similar characteristics as for B-IFDMA. For low numbers M, the PAPR increases whereas for $M > L$ the PAPR decreases with increasing M. This can be understood noting that OFDMA with block interleaved
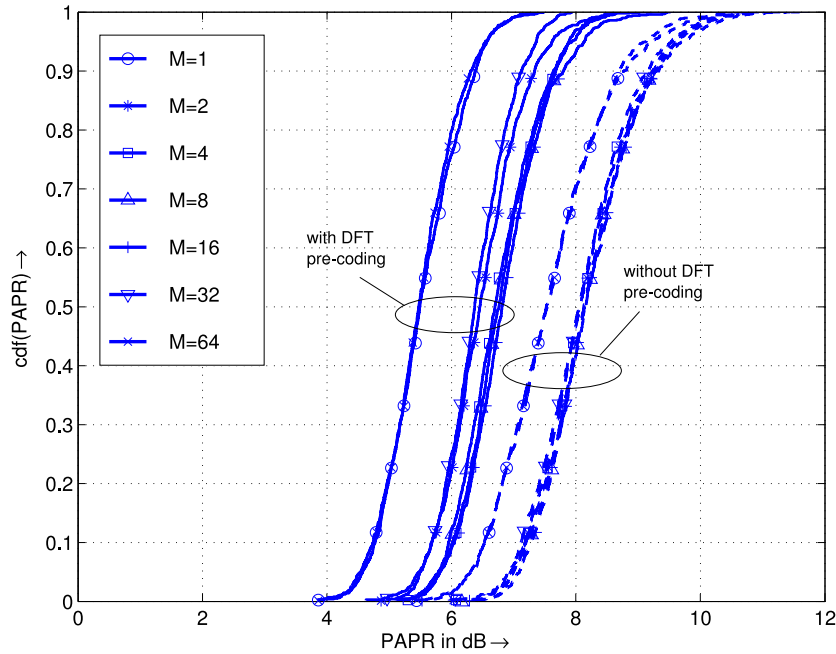
Figure 4.32: CDF of the PAPR for B-IFDMA (with pre-coding) and block-interleaved OFDMA (without DFT pre-coding) transmit signals with $N = 1024$ subcarriers in the system and $Q = 64$ subcarriers per user with oversampling factor $S = 8$ using QPSK.

subcarrier allocation can be regarded as B-IFDMA replacing the data symbols by their IDFT. However, it can be seen that for B-IFDMA, the PAPR is considerably lower than the PAPR for OFDMA for all numbers M of subcarriers per block. The difference of the PAPR of DFT pre-coded OFDMA compared to OFDMA without DFT pre-coding has been generally described in [XZG03]. From a B-IFDMA perspective, this effect can be understood as follows: As already discussed above, the reason for the low PAPR of B-IFDMA is that it can be regarded as a superposition of single carrier signals. Each of these single carrier signals benefits from its low PAPR due to the low PAPR of the data symbols. Thus, also the B-IFDMA signal provides a low PAPR. As OFDMA with block interleaved subcarrier allocation is obtained by replacing the data symbols by their IDFT, this advantage is lost, because the IDFT of the data symbol vector already provides a high PAPR. Thus, even for $M = 1$ or $L = 1$, the signal suffers from a high PAPR. Another explanation is that an OFDMA signal is the superposition of a number of mutually uncorrelated subcarriers because they carry the mutually independent data symbols, whereas in case of B-IFDMA the subcarriers are correlated because each subcarrier carries an element of the DFT of the data symbols.

In the following, the results of the analysis of the impact of the subcarrier allocation on the PAPR are presented. For that purpose, in Figure 4.33, the CDF of the PAPR of B-IFDMA signals with different numbers M and of DFT pre-coded OFDMA signals

with blocks of subcarriers of the same size as for B-IFDMA but with random allocation instead of a regular allocation of the blocks are depicted. The same parameters as for the results in Figure 4.32 are assumed. Again, the results for B-IFDMA are the same as shown in Figure 4.28.

In Figure 4.33 it can be seen that, for random subcarrier allocation, the PAPR increases with decreasing number M of subcarriers per block. Further on, the envelope fluctuations are significantly increased compared to B-IFDMA. A comparison to the results depicted in Figure 4.32 shows that, for the signal with DFT pre-coding and random allocation of the subcarrier blocks, the envelope fluctuations are even larger than for the signal without DFT pre-coding but with regular subcarrier allocation. For $M = Q$ and $M = Q/2$, the CDFs of the PAPR of B-IFDMA signals and of signals with random allocation of the subcarrier blocks are similar. The reason is that for $M = Q$, i.e., for $L = 1$ subcarrier block, B-IFDMA and DFT pre-coded OFDMA with random allocation of the subcarrier blocks are equivalent. Further on, for $M = Q/2$, i.e., $L = 2$, B-IFDMA and DFT pre-coded OFDMA with random allocation of the subcarrier blocks can be both regarded as superpositions of $L = 2$ single carrier signals. The only difference is that for DFT pre-coded OFDMA with random allocation of the subcarrier blocks the subcarrier blocks have a random distance in DFT domain, whereas for B-IFDMA the distance is fixed, cf. Figure 4.31. For $L > M$ the PAPR of B-IFDMA decreases with increasing L or decreasing M, respectively, whereas, for DFT pre-coded OFDMA scheme with random allocation, the PAPR increases. The reason is that, for the latter, due to the lack of a regular subcarrier allocation the signal cannot be interpreted as a sum of M single carrier signals as described in Section 3.2.3.1. Thus, the PAPR increases with increasing L, regardless of M.

Summarizing the results from Figures 4.32 and 4.33, it can be concluded that, especially for $L > M$, the low envelope fluctuations of B-IFDMA can be provided only due to the combination of both, DFT pre-coding and regular block-interleaved subcarrier allocation.

In the following, the impact of different bit mapping schemes such as 16QAM and 64QAM is analyzed. For that purpose, in Figures 4.34 and 4.35 the CDF of the PAPR is depicted for B-IFDMA signals with different numbers M and compared to the CDF of the PAPR of OFDMA signals with corresponding subcarrier allocation using 16QAM and 64QAM, respectively. The same parameters as for the results in Figure 4.33 are assumed. Figures 4.34 and 4.35 show that, for higher order bit mapping schemes such as 16QAM and 64QAM, the PAPR of B-IFDMA is increased compared to QPSK, whereas for OFDMA with corresponding subcarrier allocation the PAPR is almost independent of the bit mapping schemes that is used. However, from the results
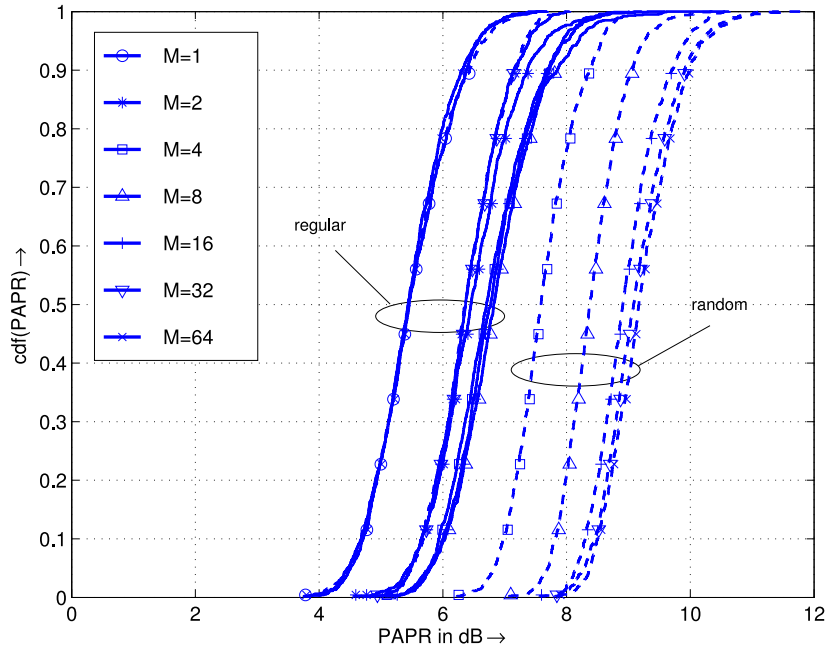
Figure 4.33: CDF of the PAPR for B-IFDMA transmit signals and DFT pre-coded OFDMA transmit signals with random allocation of the subcarrier blocks with $N = 1024$ subcarriers in the system and $Q = 64$ subcarriers per user with oversampling factor $S = 8$ using QPSK.

in Figures 4.34 and 4.35 it can be concluded that even for higher order bit mapping schemes like 64 QAM, B-IFDMA provides significantly lower envelope fluctuations of the transmit signal compared to OFDMA with corresponding subcarrier allocation.

In the following, the envelope of the B-IFDMA transmit signal is analyzed by applying the different metrics presented in Section 4.4.3.3. At first, in addition to the PAPR, the required power back-off for the amplifier is regarded.

For the determination of the required power back-off, a power amplifier model as described in Section 4.4.3.3 with Rapp factor $p = 2$ is assumed. The power spectral density of the signal at the output of the amplifier model is compared to a spectral mask according to [WIN06]. The power back-off has to be chosen such that the spectrum always lies below the spectral mask. In Figure 4.36, it is shown by an example that the effect of the non-linear amplifier is different for a B-IFDMA signal compared to an OFDMA signal with the same subcarrier allocation. The power spectral density for a B-IFDMA signal with $N = 1024$, $Q = 64$ and $M = 1$ and an OFDMA signal with corresponding parameters are depicted. For both schemes, QPSK is assumed as bit mapping scheme. For the OFDMA signal, a power back-off of 8.7 dB is used. It can be seen that using this power back-off of 8.7 dB, the power spectral density of the
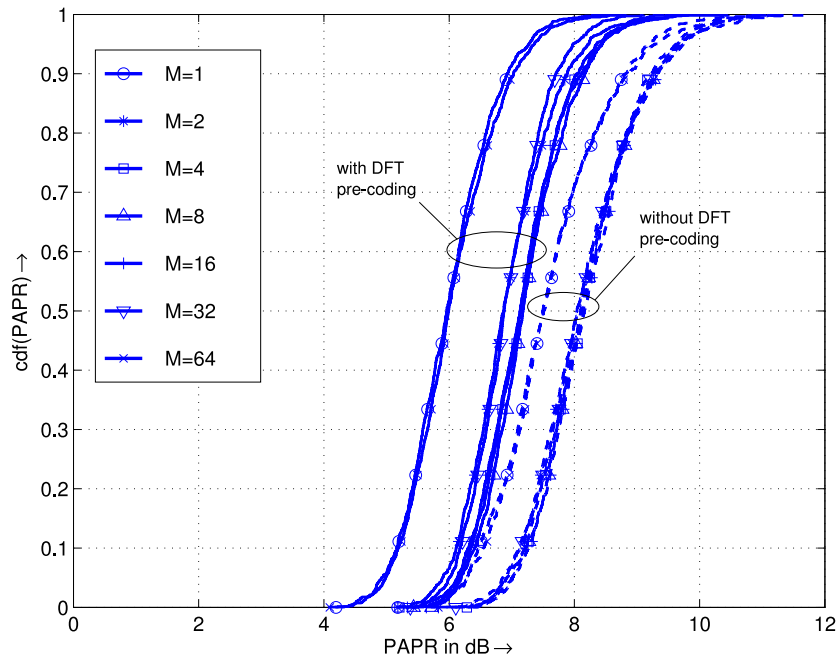
Figure 4.34: CDF of the PAPR for B-IFDMA and OFDMA transmit signals with $N = 1024$ subcarriers in the system and $Q = 64$ subcarriers per user with oversampling factor $S = 8$ using 16QAM.
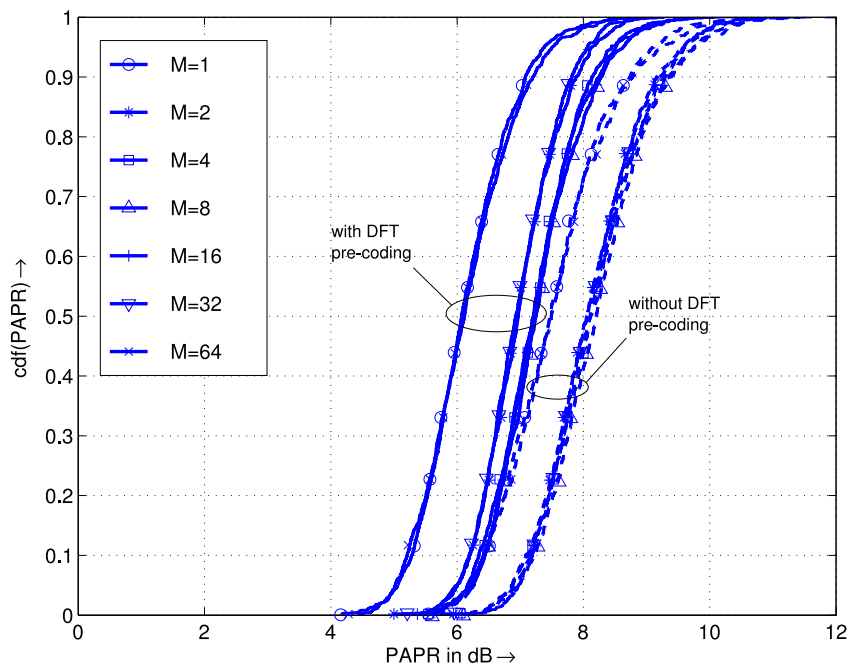
Figure 4.35: CDF of the PAPR for B-IFDMA and OFDMA transmit signals with $N = 1024$ subcarriers in the system and $Q = 64$ subcarriers per user with oversampling factor $S = 8$ using 64QAM.
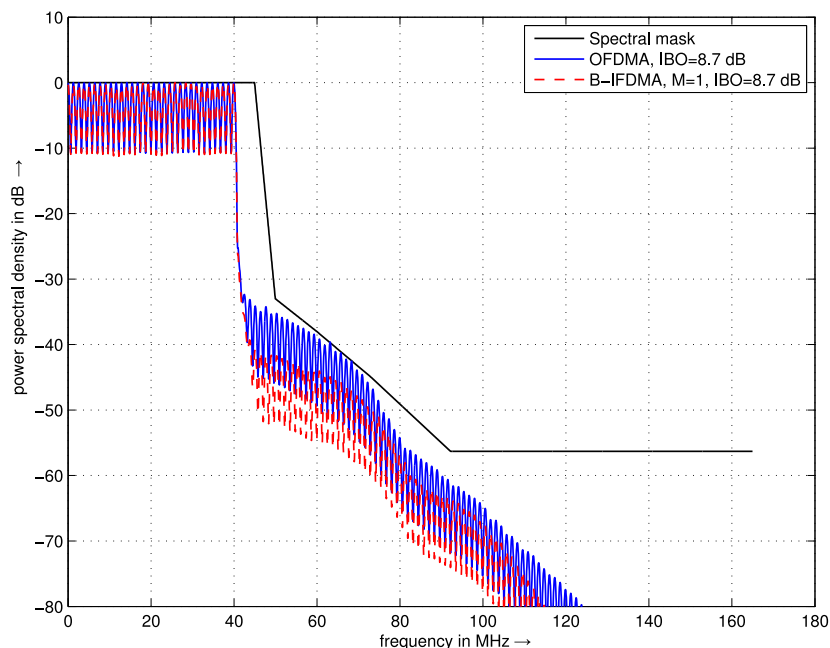
Figure 4.36: Power spectral density of a B-IFDMA signal with $N = 1024$, $Q = 64$ and $M = 1$ and OFDMA signal with corresponding parameters at the output of the amplifier model with a power back-off of 8.7 dB.

OFDMA signal meets the spectral mask. Further on, for the same power back-off of 8.7 dB, the out of band radiation for the B-IFDMA is significantly lower. Thus, for B-IFDMA, a lower power back-off could be chosen. A further analysis of the B-IFDMA signal with the given parameters has shown that the minimum possible power back-off that is required to meet the spectral mask is 6.9 dB.

In Figure 4.37, the uncoded BER performance at different power back-offs is depicted for the transmission of the signals analyzed in Figure 4.36 over an AWGN channel. In Figure 4.37, it can be seen that in case of OFDMA, for a power back-off of 8 dB, the performance degradation compared to the BER performance with a power back-off of 10 dB is negligible. For B-IFDMA, for a power back-off of 6 dB, the performance degradation compared to the BER performance with a power back-off of 10 dB is negligible. From Figure 4.37 it can be concluded that, assuming a power back-off such that the power spectral density of the signal meets the spectral mask, the BER degradation due to non-linear distortions of the amplifier is almost negligible. Thus, in general, the spectral mask can be considered as a stricter condition for the required power back-off. For that reason, in the following, the analysis of the BER degradation is omitted.

In the following, results for the mean PAPR, the RCM and the required power back-off
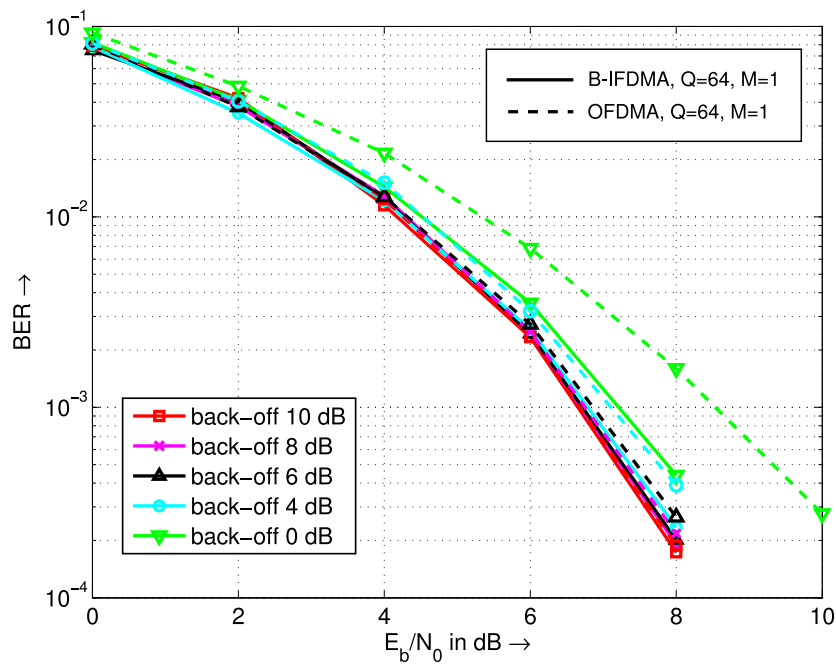
Figure 4.37: Bit error rate for B-IFDMA signal with $N = 1024$, $Q = 64$ and $M = 1$ and OFDMA signal with corresponding parameters for transmission over an AWGN channel for different power back-offs.

in order to meet the spectral mask from Figure 4.36 are presented and discussed.

Figures 4.38 - 4.40 depict the mean PAPR, the RCM and the required power back-off for a B-IFDMA signal and an OFDMA signal with corresponding parameters dependent on the number M of subcarriers per block for different bit mapping schemes.

In Figures 4.38 - 4.40 it can be seen that for B-IFDMA, the characteristic of the RCM as a function of the number M of subcarriers per block is similar to the characteristic of the mean PAPR dependent on M. For both metrics, for M close to $M = 1$, the RCM and the mean PAPR values are similar to the respective values for M close to $M = Q$. However, for OFDMA, this effect is much less pronounced. Especially the RCM results for OFDMA are almost independent of M.

In contrast to the RCM and the mean PAPR, for B-IFDMA as well as for OFDMA with corresponding subcarrier allocation, with increasing number M of subcarriers, the required power back-off in order to meet the spectral mask increases, even for values where the RCM and the mean PAPR decrease. This effect can be explained as follows. The broadening of the spectrum in the regarded out of band region is caused by the intermodulation products of the transmit signal. Thus, for a signal with a large number L of subcarrier blocks, the spectrum in the out of band region shows many peaks at
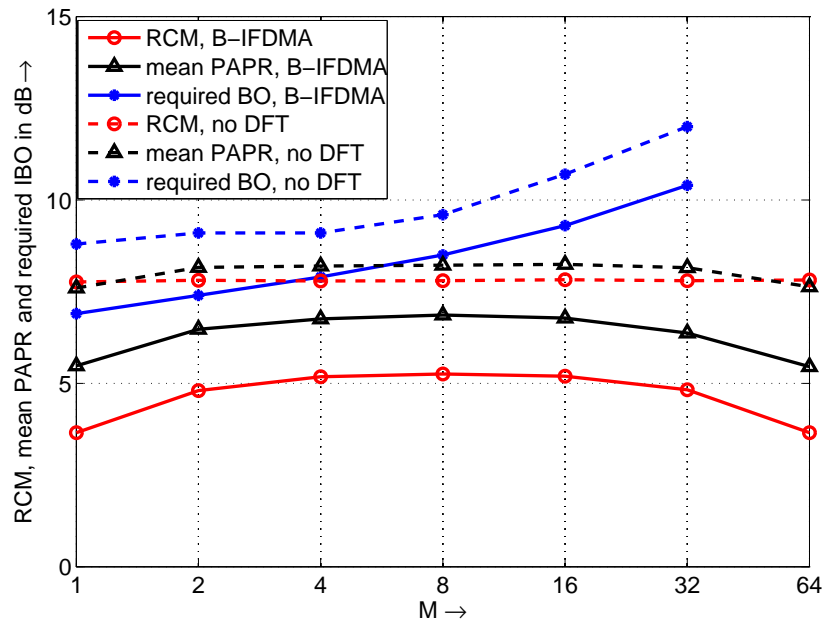
Figure 4.38: Different metrics for the envelope fluctuations of a B-IFDMA signal and an OFDMA signal with corresponding parameters dependent on M for $Q = 64$ using QPSK.
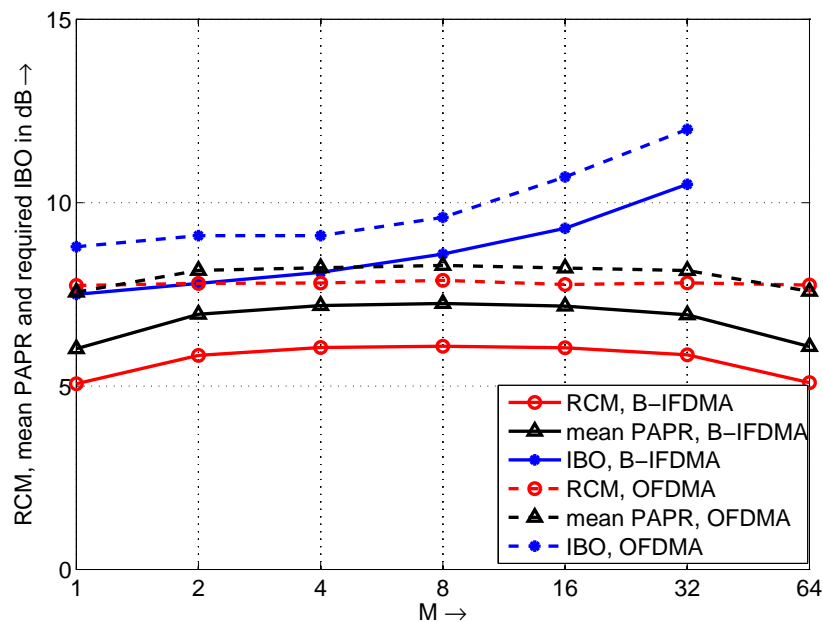
Figure 4.39: Different metrics for the envelope fluctuations of a B-IFDMA signal and an OFDMA signal with corresponding parameters dependent on M for $Q = 64$ using 16QAM.
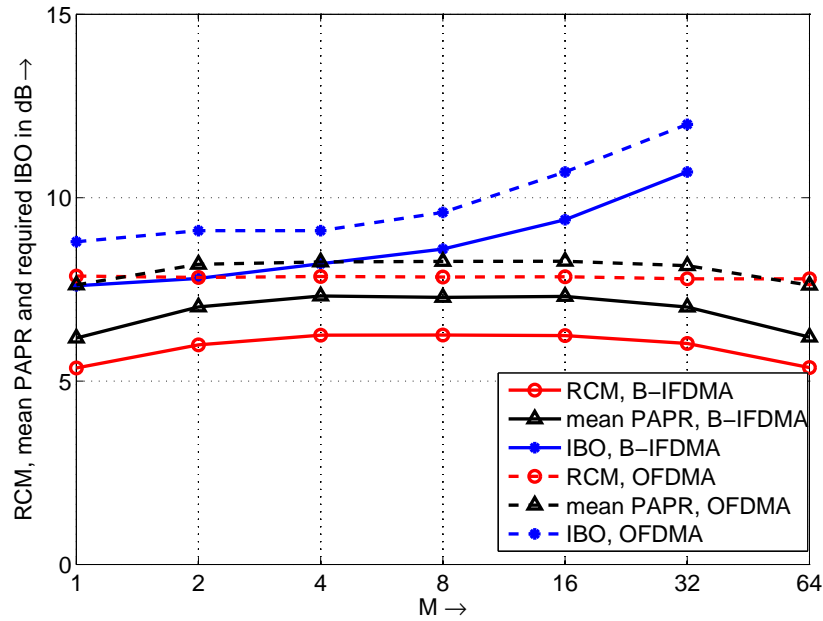
Figure 4.40: Different metrics for the envelope fluctuations of a B-IFDMA signal and an OFDMA signal with corresponding parameters dependent on M for $Q = 64$ using 64QAM.

positions that depend on the positions of the L subcarrier blocks in the pass band. For a low number L, the spectrum in the out of band region changes its shape. Due to the low number L of subcarrier blocks, the number of peaks in the out of band region is also low and the peak values are considerably increased compared to those of a signal with large values of L. For that reason, a much higher power back-off is required in order to guarantee that even these exposed peak values are below the spectral mask. Thus, it can be concluded that the required power back-off is not only dependent on the fluctuations of the signal envelope but, for low numbers L of subcarrier blocks, is dominated by the shape of the power spectral density in the out of band region of the signal.

In this context, the case $M = Q$, i.e. $L = 1$, can be considered as a special case. For $M = Q$, the whole spectrum in the pass band is concentrated in a small portion of the bandwidth of the pass band, whereas in case of $M < Q$, the signal is spread over the total bandwidth of the pass band. Thus, for a signal with $M = Q$, there are no peaks resulting from intermodulation products falling into the out of band spectrum between 45 MHz and 85 MHz where the regarded spectral mask is critical for $M < Q$. Consequently, the required power back-off to meet the spectral mask given in Figure 4.36 is extremely low. For that reason, in this special case $M = Q$,

the spectral mask given in Figure 4.36 has to be considered as not appropriate for the determination of the power back-off that will be used in practise. One reason is that in this special case the assumption that, if the spectral mask is met, the BER degradation is negligible, which has been introduced above, is not justified. Another reason is that, due to intermodulation, other requirements for the spectrum concerning the out of band radiations at integer multiples of the carrier frequencies might be missed. As, thus, for this special case, the back-off required to meet the spectral mask from Figure 4.36 is not expected to provide meaningful results, in Figures 4.38 - 4.40 the back-off for $M = Q$ is omitted. Note that, for practical applications, the case of low numbers L of subcarriers per block can be considered as not important for the application of B-IFDMA, because in this case only low frequency diversity is provided, cf. Section 4.2.2.

From Figures 4.38 - 4.40 it can be concluded that the presented results underline important properties of B-IFDMA that have been found regarding the CDF of the PAPR: Regardless of the metric,

- for B-IFDMA, the envelope fluctuations increase with increasing order of the bit mapping scheme and are the lowest for PSK, and

- for all considered bit mapping schemes, B-IFDMA provides significantly lower envelope fluctuations compared to OFDMA.

Further on, for low numbers M of subcarriers per block, which has been identified as important for B-IFDMA because in this case high frequency diversity is provided, cf. Section 4.2.2, it can be concluded that

- the envelope fluctuations of B-IFDMA decrease with decreasing number M and are the lowest for $M = 1$, i.e., for IFDMA.

Respective results for different numbers Q of subcarriers assigned to a user are given in Appendix C.1. The results show that the envelope properties of the B-IFDMA transmit signal are only weakly dependent on the number Q of subcarriers per user and, thus, on the instantaneous data rate.

Considering that the power efficiency of the power amplifier decreases with increasing envelope fluctuations as shown e.g. in [RAC$^+$02], the various results presented in this section show that B-IFDMA provides a significantly higher power efficiency than OFDMA, even for higher order bit mapping schemes such as 64QAM.

4.4.3.5 Power Efficiency Dependent on the Average Power within a Modulated Data Vector

In this section, the impact of the average power of the transmit signal within a modulated data vector on the power efficiency and its dependency on the B-IFDMA signal parameters are discussed. It is well known that the power efficiency of a power amplifier is the higher the closer the instantaneous output power to the maximum possible output power of the amplifier [RAC$^+$03]. Respective measurements for the power efficiency can be found, e.g., in [Cey05]. In the following, the average power efficiency for one modulated data vector is considered. It is the higher the closer the average power of a modulated data vector compared to the maximum power of the amplifier. Given that the power spectral density of the transmit signal is restricted by the spectral mask from Figure 4.36, it is reasonable to assume that the maximum possible average powers of all subcarriers of a B-IFDMA signal are identical. Thus, the maximum possible average power of a modulated data vector is proportional to the number Q of subcarriers assigned to a user and independent from the values of M and L.

As mentioned in Section 1.1, in future mobile radio applications, a wide range of different data rates has to be supported. As the number Q of subcarriers reflects the number of data symbols that is transmitted in a modulated data vector, together with information about the supported modulation schemes and code rates, the maximum data rate that shall be supported defines the maximum supported symbol rate that is required and, thus, the maximum supported number Q_{max} of subcarriers per user. Taking into account that, due to the envelope fluctuations of the signal discussed in Section 4.4.3.4, a certain power back-off is required, from Q_{max} the maximum power can be calculated the amplifier has to be designed for.

From the discussion above follows that, in order to provide a good average power efficiency for a modulated data vector, the average power of a modulated data vector should be as close to that maximum power as possible. Thus, the number Q of subcarriers should be as large as possible with $Q \leq Q_{max}$. This can be obtained as follows. Assuming that within a time frame of a certain length a number of $Q \cdot N_t$ data symbols shall be transmitted with N_t denoting the number of consecutive modulated data vectors assigned to a user. Note that assuming a certain length of a time frame and a certain modulation scheme and code rate this assumption is equivalent to the assumption of a certain average symbol rate. In order to provide a good power efficiency for the N_t consecutive modulated data vectors assigned to the user, large values of Q and low values of N_t should be used, i.e., the data transmission should be organized in a short burst within each frame with high instantaneous symbol rate. In this case,

the average power within the N_t modulated data vectors is large and, thus, the power amplifier is used in an efficient way.

4.4.3.6   Power Efficiency Improvements by Application of Sleep Modes

In this section, the impact of sleep modes on the power efficiency and its dependency on the B-IFDMA signal parameters is discussed. As discussed in Section 4.4.3.5, a good average power efficiency for the N_t modulated data vectors carrying the data symbols of a certain user can be obtained by organizing the transmission in short bursts with high instantaneous symbol rate. However, the overall power efficiency of the power amplifier is also dependent on the power consumption of the power amplifier in the time in-between successive bursts of N_t modulated data vectors, where no data is transmitted. Unfortunately, in general, power amplifiers that are switched on consume a considerable amount of power even if no input signal is present [FN01]. However, it has been shown in [FN01] that it is possible to switch off and to switch on again power amplifiers and other power consuming components of the mobile terminal within a few μs, which is well-known as joining a sleep mode [FN01]. Note that throughout this thesis the time required for transmission of a modulated data vector with CP is assumed to be 28.8 μs. Thus, the power consumption of the power amplifier in particular and of the mobile terminal in general can be improved by switching off the hardware components within a time frame when they that are not used. The power savings due to joining a sleep mode are the larger the longer the time interval within a given time frame where no data transmission is performed.

It can be concluded that, in order to efficiently apply sleep modes to B-IFDMA, similar as shown in Section 4.4.3.5, it is beneficial to organize the transmission of $Q \cdot N_t$ data symbols within a given time frame in short bursts, i.e., with a low number N_t of consecutive modulated data vectors assigned to a user with high instantaneous symbol rate, i.e., a high number Q of subcarriers assigned to a user. For the remaining time within the time frame the hardware components that are not required should be switched off.

4.5   Summary and Discussion

In this section, the results of the analysis presented in this chapter are summarized and discussed. The properties of B-IFDMA are compared to the properties of IFDMA and localized SC-FDMA with FH, that are considered as multiple access solutions in

3GPP LTE, and to the properties of OFDMA that is considered as multiple access solution in IEEE 802.16 WiMAX, cf. Section 1.1.3. Further on, based on the analysis presented in this chapter, generic trade-offs for the parameter design of B-IFDMA are identified and an exemplary parametrization of B-IFDMA for the non-adaptive uplink in a future mobile radio system is discussed.

The properties of B-IFDMA can be summarized as follows:

- B-IFDMA enables a good exploitation of frequency diversity by the choice of a large number L of subcarrier blocks. The amount of frequency diversity that is exploited increases with increasing number L and saturates for $L > B/B_c$, cf. Section 4.2.

- For B-IFDMA, time diversity can be exploited by application of channel coding and bit interleaving of the coded bits over several consecutive modulated data vectors. However, in Section 4.2.3 it is shown that, in order to provide low delays, in a typical future mobile radio system using packet switched data transmission, only a low number N_t of consecutive modulated data symbols should be assigned to a user. Further on, it has been shown that, for the assignment of low values of N_t, almost no performance improvement due to an exploitation of time diversity can be obtained. Thus, the exploitation of time diversity can be regarded as not appropriate in order to improve the performance in future mobile radio scenarios.

- B-IFDMA is well suited for the combination with multiple antenna schemes that exploit spatial diversity. Besides the advantages that have been shown in Section 3.3, Section 4.2.4 shows that the combination of B-IFDMA with STBCs and MRC provides a good performance due to a good exploitation of spatial diversity. However, even in presence of spatial diversity, the frequency diversity gains of B-IFDMA can be considered as important.

- B-IFDMA is well suited for non-adaptive transmission. In Section 4.2.5 it has been shown that adaptive transmission targeting at an exploitation of multi-user diversity is very demanding with respect to low delays between channel estimation, feedback of the CSI to the mobile terminal and start of the data transmission from the mobile terminal adapted to the channel conditions. The tough demands can be met only for scenarios with low user mobility. It has been shown that, if the these demands are not met, adaptive transmission exploiting multi-user diversity is outperformed by non-adaptive transmission using B-IFDMA exploiting frequency diversity by the assignment of a large number L of subcarrier blocks.

- B-IFDMA enables a reduction of the pilot symbol overhead for channel estimation with increasing number M of subcarriers per block and increasing number N_{t} of consecutive modulated data vectors assigned to a user, cf. Section 4.2.6. The pilot symbol overhead converges to a minimum for $M > B_{\mathrm{c}}/(F \cdot \Delta f)$ and $N_{\mathrm{t}} > T_{\mathrm{c}}/(F \cdot (T + T_{\mathrm{CP}}))$ where $F \approx 5$ is an appropriate choice for the oversampling factor, cf. Section 4.2.6.

- B-IFDMA provides a low computational complexity at the transmitter as well as at the receiver side for frequency domain implementation, cf. Section 4.3. For $M \leq 4$, the computational complexity of the transmitter can be further reduced by the application of the time domain implementation presented in Section 3.2.

- B-IFDMA provides a robustness to carrier frequency offsets that increases with increasing number M of subcarriers per block. Already for small values of M, a considerable robustness improvement is obtained compared to B-IFDMA with $M = 1$, cf. Section 4.4.2.

- B-IFDMA transmit signals provide low envelope fluctuations due to the combination of DFT pre-coding and a symmetric subcarrier allocation, even for higher order modulation such as 64QAM. This effect is shown for all metrics from Section 4.4.3.3. Thus, B-IFDMA enables a power efficient use of the power amplifier. Regarding the RCM and the mean PAPR, it can be concluded that the envelope fluctuations for $M = 1$ and $M = Q/1$, for $M = 2$ and $M = Q/2$, for $M = 4$ and $M = Q/4$ and so forth are similar. They are the lowest for $M = 1$ and $M = Q/1$, respectively and increase with increasing M for $M < L$ and increase with decreasing M for $M > L$. The maximum is obtained for $M = L$, cf. Section 4.4.3.4.

- B-IFDMA enables a further improved power efficiency by assigning small numbers N_{t} of consecutive modulated data vectors to a user due to two effects, cf. Sections 4.4.3.5 and 4.4.3.6: At first, for a given number $Q \cdot N_{\mathrm{t}}$ of data symbols to be transmitted within a given time frame, a small number N_{t} enables an efficient use of the amplifier because the average power of the N_{t} consecutive modulated data vectors assigned to a user is as close as possible to the maximum power of the amplifier. Secondly, within a given time frame, a low number N_{t} leads to a significant amount of time within a time frame where no data transmission is performed and, thus, hardware components could join a sleep mode in order to save power.

In the following, the properties of B-IFDMA are compared to the properties of IFDMA, localized SC-FDMA with FH and OFDMA. Note that IFDMA is equivalent to the

special case of B-IFDMA with $M = 1$. Thus, a comparison of B-IFDMA and IFDMA means a comparison of B-IFDMA with $M \neq 1$ to its special case with $M = 1$.

- From Section 4.2.2 follows that IFDMA provides a good performance because a large amount of frequency diversity is exploited. However, as long as $L > B/B_c$, the performance of B-IFDMA is similar to the performance of IFDMA. This is true also for the application of spatial diversity, cf. Section 4.2.5.

- From Section 4.2.6 it can be concluded that for IFDMA, the pilot symbol overhead required for channel estimation is large because an interpolation between different subcarriers is not possible. Especially for low values of N_t, the pilot symbol overhead for IFDMA leads to severe performance degradations. For a given instantaneous data rate, B-IFDMA offers the possibility to effectively reduce the pilot symbol overhead compared to IFDMA by increasing the number M of subcarriers per block. Since, as mentioned above, at the same time for B-IFDMA, the performance saturates for $L > B/B_c$, increasing the number M of subcarriers per block does not affect the performance as long as $L \geq B/B_c$. Thus, B-IFDMA enables a transmission with high frequency diversity and with a much lower channel estimation overhead compared to IFDMA at low numbers N_t of consecutive modulated data vectors.

- Using the efficient implementation presented in Section 3.2.3, the computational complexity of the IFDMA transmitter is lower than for B-IFDMA with $M > 1$, cf. Section 4.3.

- From the results presented in Section 4.4.2 it follows that, for B-IFDMA, increasing the number M of subcarriers per block results in an increased robustness to carrier frequency offsets compared to IFDMA. Already for small values of M, considerable improvements of the robustness of B-IFDMA are provided compared to IFDMA. Thus, B-IFDMA enables the combination of an increased robustness to carrier frequency offsets compared to IFDMA with a similar performance compared to IFDMA due to the good exploitation of frequency diversity.

- The envelope fluctuations of an IFDMA transmit signal are slightly higher than those of a B-IFDMA transmit signal with $1 < M < Q$ and similar to the envelope fluctuations of a B-IFDMA signal with $M = Q$, cf. Section 4.4.3.4.

- The possibility of a transmission with good performance and low channel estimation overhead using low values of N_t increases the power efficiency compared to IFDMA due to an efficient use of the power amplifier and due to the feasibility of micro-sleep periods, cf. Sections 4.4.3.5 and 4.4.3.6.

In the following, the properties of B-IFDMA are compared to the properties of localized SC-FDMA with FH. Note that localized SC-FDMA is equivalent to the special case of B-IFDMA with $M = Q$. Thus, a comparison of B-IFDMA and localized SC-FDMA with FH means a comparison of B-IFDMA in general to B-IFDMA with $M = Q$ combined with FH.

- B-IFDMA with $L > B/B_c$ provides a good performance even for low numbers N_t of consecutive modulated data vectors assigned to a user. For localized SC-FDMA combined with FH, considerably larger values of N_t are required in order to provide a comparable performance. Thus, B-IFDMA with large values of L provides a similar performance at considerably lower delays, cf. Section 4.2.2.

- The channel estimation overhead for B-IFDMA is significantly lower than for localized SC-FDMA with FH, because in contrast to localized SC-FDMA combined with FH, for B-IFDMA, an interpolation in time direction is possible, cf. Section 4.2.6.

- For localized SC-FDMA combined with FH and B-IFDMA, the computational complexity is similar. For B-IFDMA with low values of M, the computational complexity is slightly lower compared to SC-FDMA combined with FH, because the efficient implementation in time domain can be applied, cf. Section 4.3.

- With a parametrization aiming at a good exploitation of frequency diversity, i.e., large values of L, the robustness of B-IFDMA to carrier frequency offsets is lower compared to localized SC-FDMA, cf. Section 4.4.2.

- The envelope fluctuations of localized SC-FDMA signals combined with FH are similar to the envelope fluctuations of B-IFDMA with $M = Q$ and $M = 1$ and slightly lower than for B-IFDMA with $1 < M < Q$, cf. Section 4.4.3.4.

- Due to the lower numbers N_t of consecutive modulated data vectors that is possible for B-IFDMA compared to localized SC-FDMA with FH, the power efficiency of B-IFDMA is expected to be higher than for localized SC-FDMA with FH, cf. Sections 4.4.3.5 and 4.4.3.6.

In the following, the properties of B-IFDMA are compared to the properties of OFDMA. In order to provide a fair comparison, a similar subcarrier allocation is assumed for OFDMA and B-IFDMA.

- Compared to OFDMA, for coded transmission, B-IFDMA provides a performance that is similar to that of OFDMA with corresponding subcarrier allocation. Note that for B-IFDMA the frequency diversity gains are even provided without channel coding, whereas this is not the case for OFDMA, cf. Section 4.2.2.

- The channel estimation overhead for B-IFDMA and OFDMA is similar.

- At the mobile terminal, for implementation in frequency domain, the computational complexity of B-IFDMA is slightly higher than the computational complexity of OFDMA due to the additional DFT required for pre-coding. For the implementation in time domain, the computational complexity of B-IFDMA is slightly lower than the computational complexity of OFDMA due to the additional IDFT that is required for OFDMA, cf. Section 4.3.1. At the base station, for implementation in frequency domain and for implementation in time domain, the computational complexity of B-IFDMA is slightly higher than the computational complexity of OFDMA due to the additional DFT required for compensation of the pre-coding, cf. Section 4.3.2. However, especially at the transmitter side, the differences are marginal.

- For all regarded metrics, the envelope fluctuations of the B-IFDMA transmit signal are lower than the envelope fluctuations of the OFDMA transmit signal, even for high order bit mapping schemes such as 64QAM. Thus, B-IFDMA provides a higher power efficiency of the amplifier due to a lower required power back-off compared to OFDMA.

- As both, B-IFDMA and OFDMA, can be used applying low numbers N_t of consecutive modulated data vectors assigned to a user, the power efficiency that is obtained by a high average power within a modulated data vector and due to application of micro sleep modes are similar for B-IFDMA and OFDMA.

Analyzing the results in this chapter, for the parametrization of B-IFDMA, the following generic trade-offs can be identified:

For a given number Q of subcarriers assigned to a user, either the number M of subcarriers per block or the number L of subcarrier blocks can be chosen. On the one hand, increasing the number M of subcarriers per block results in a reduced pilot symbol overhead and in an increased robustness to carrier frequency offsets. On the other hand, due to $Q = L \cdot M$, increasing the values of M causes decreased values of L that, for $L \leq B/B_c$, result in a decreased performance. Moreover, for $M < L$, increasing the values of M increases the signal envelope. Thus, there is a generic trade-off between the provision of a low pilot symbol overhead and an increased robustness

to carrier frequency offsets on the one hand and a good performance due to a good exploitation of frequency diversity and a low signal envelope on the other hand. Note that a limitation of M to $M \leq 4$ could be an interesting option in order to provide low cost terminals with a signal generation using the efficient implementation in time domain introduced in Section 3.2.3.1. In this case, it has to be also considered that the computational complexity increases with increasing values of M.

For a given number of $Q \cdot N_t$ to be transmitted within a certain time frame, either Q or N_t can be chosen. Reducing N_t, on the one hand, increases the power efficiency of the mobile terminal, reduces the delays, and increases the instantaneous symbol rate within a modulated data vector and, thus, the performance through the provision of a higher frequency diversity. On the other hand, increasing the values of N_t causes a reduced pilot symbol overhead because the interpolation in time direction is limited. Thus, there is a generic trade-off between a good power efficiency of the mobile terminal, low delays and a good performance through the provision of a higher frequency diversity on the one hand, and a low pilot symbol overhead on the other hand.

In order to find an optimum parametrization for B-IFDMA, the above mentioned trade-offs have to be balanced in a reasonable way. In general, an optimization of the parameters for B-IFDMA requires a detailed knowledge of the scenario, the hardware platform and the application B-IFDMA shall be optimized for and, thus, cannot be presented throughout this work. However, in the following, a simple and exemplary parametrization for the application of B-IFDMA to the non-adaptive uplink of future mobile radio systems is presented that is aiming at a balancing of the aforementioned advantages and disadvantages based on the results presented in the previous sections.

Assuming a system with parameters chosen according to Table 4.2, in general, the reduction of the pilot symbol overhead in frequency direction is rather low for $M > B_c/(F \cdot \Delta f)$. With $F = 5$, which is a reasonable assumption, cf. Section 4.2.6, $B_c/(F \cdot \Delta f) \approx 3$. Since, according to Section 3.5, the values of Q, L and M are preferably chosen as powers of 2, a reasonable choice for M is, thus, $M = 4$. Assuming an instantaneous data rate of 1.11 Mbps, i.e., $Q = 32$ subcarriers per user within a modulated data vector, and $M = 4$, the number L of subcarrier blocks results in $L = 8$. From the results in Section 4.2 it can be seen that for $L = 8$ still a good performance is provided. Note that for higher instantaneous data rates, assuming $M = 4$, larger values of L are obtained and, thus, the performance is even better. Lower instantaneous data rates result in a performance that is worse and, thus, should be avoided. In presence of spatial diversity, for $L = 8$, the performance degradation compared to $L = Q$ is small, cf. Section 4.2.4. Moreover, the results from Section 4.4.2 show that for $M = 4$, the robustness to carrier frequency offsets is already considerably improved compared

to $M = 1$. Further on, at $M = 4$, B-IFDMA still provides a low signal envelope and a low computational complexity that, however, is not optimum. Thus, $M = 4$ represents a good compromise between good performance, low overhead, acceptable envelope fluctuations and increased robustness.

For $M = 4$ and $N_\mathrm{t} = 1$, which would be the preferred choice aiming at maximum power efficiency, minimum delays and maximum frequency diversity due to a high instantaneous data rate, the pilot symbol overhead is very large, cf. Section 4.2.6. In order to reduce the pilot symbol overhead, the value of N_t has to be increased. Taking into account that the exploitation of spatial diversity using STBCs according to Section 3.3 requires a value of N_t that is an integer multiple of the number of transmit antennas, assuming $n_\mathrm{T} = 2$, $N_\mathrm{t} = 4$ is a reasonable choice, because for $N_\mathrm{t} = 4$ the overhead is significantly reduced. Note that for a frame structure as proposed in WINNER, cf. [WIN05], a frame consists of 24 modulated data vectors. Thus, the assignment of $N_\mathrm{t} = 4$ modulated data vectors with $Q = 32$ to a user within each frame results in an average data rate of 1.11 Mbps/6 = 183 kbps. As the frames are short, even lower average data rates can be obtained if $N_\mathrm{t} = 4$ modulated data vectors are assigned to a certain user less than once per frame.

The exemplary parametrization shows that, for a given scenario, the properties of B-IFDMA can be flexibly designed by the choice of its signal parameters. Thus, B-IFDMA enables to adapt the properties of the scheme in a flexible way to the requirements in a given scenario.

Chapter 5

Conclusions

This thesis has dealt with the new multiple access scheme B-IFDMA and its application in the non-adaptive uplink of future mobile radio systems.

In Chapter 1, an overview of current activities targeting at an evolution of today's mobile radio systems has been presented. Further on, the requirements of a future mobile radio system as formulated by the ITU have been summarized and several multiple access solutions that are considered as promising candidates for a future mobile radio system have been identified. Finally, open problems and the contribution of this thesis have been formulated.

In Chapter 2, a new general system model has been formulated that enables a joint description of B-IFDMA and other important multiple access schemes that are based on block transmission with CP. From the general system model, a system model for B-IFDMA has been derived. Based on a new metric, B-IFDMA has been shown not to suffer from MAI even for transmission over a time dispersive channel. Thus, B-IFDMA provides a receiver structure with low computational complexity that is based on user separation and channel equalization in frequency domain. Further on, B-IFDMA has been shown to be a generalization of SC-FDMA including localized SC-FDMA and distributed SC-FDMA, that is also known as IFDMA, as special cases. Moreover, the relation of B-IFDMA to other important multiple access schemes based on block transmission with CP has been systematically described.

In Chapter 3, several algorithms have been introduced for B-IFDMA that are required for the application of the scheme in a future mobile radio system. In particular, a new low complexity implementation in time domain has been presented, a new method for an appropriate application of STBCs to B-IFDMA and a corresponding low complexity implementation has been introduced, the application of SDMA to B-IFDMA has been described and a new method for the reduction of the computational complexity of B-IFDMA with SDMA has been proposed. Finally, a new approach for an efficient accommodation of different data rates within one cell has been introduced for B-IFDMA. Chapter 3 shows that B-IFDMA can be implemented efficiently, is well suited for the combination with STBCs and SDMA and, further on, enables an efficient accommodation of different data rates within one cell providing low signalling effort.

In Chapter 4, an extensive analysis of the properties of B-IFDMA has been presented dependent on the B-IFDMA signal parameters. B-IFDMA has been shown to provide a good performance due to the provision of high frequency diversity even if no reliable CSI is available at the transmitter. Moreover, the new approach for application of STBCs has been shown to further improve the performance of B-IFDMA due to the exploitation of frequency diversity. Even in presence of spatial diversity, the good exploitation of frequency diversity can be regarded as an important advantage of B-IFDMA. Moreover, B-IFDMA has been shown to provide low overhead for pilot symbols for channel estimation. B-IFDMA is, further on, shown to provide low complexity, good robustness to carrier frequency offsets and high power efficiency. The properties of B-IFDMA have been compared to the properties of other well known multiple access schemes. It has been shown that B-IFDMA provides similar performance, but higher power efficiency, lower pilot symbol overhead and higher robustness to carrier frequency offsets as IFDMA, similar performance and slightly lower robustness to carrier frequency offsets but lower delays, lower pilot symbol overhead for channel estimation and higher power efficiency as localized SC-FDMA with frequency hopping, and significantly lower envelope fluctuations compared to OFDMA. Finally, the design of the B-IFDMA signal parameters has been discussed and an exemplary parametrization has been proposed.

In summary, the results presented throughout this thesis show that B-IFDMA combines many advantages of well-known multiple access schemes. Further on, B-IFDMA can be flexibly adapted to the demands in different scenarios. The scheme meets the requirements for the radio interface as formulated in the IMT-Advanced concept and provides several advantages compared to other well-known multiple access solutions. Thus, B-IFDMA can be regarded as a promising candidate multiple access scheme for the non-adaptive uplink of future mobile radio systems.

Appendix A

A.1 Overview of Different Block-Transmission-Based Multiple Access Schemes

A.1.1 Introduction

Many well-known multiple access schemes are based on block transmission with CP. Defining the matrices in (2.11), transmitter models for different multiple access schemes are obtained. In the following, the matrices for

- Multi Carrier Time Division Multiple Access (MC-TDMA),

- Block Transmission Code Division Multiple Access (BT-CDMA),

- Multi Carrier Code Division Multiple Access (MC-CDMA),

- Code Division Multiple Access with Frequency Domain Orthogonal Signature Sequences (FDOSS-CDMA),

- Spread Spectrum Multi Carrier Multiple Access (SS-MC-MA), and

- Variable Spreading and Chip Repetition Factor Code Division Multiple Access (VSCRF-CDMA)

are presented.

A.1.2 Multi Carrier Time Division Multiple Access

MC-TDMA is a multi-user variant of OFDM that is also known as OFDM-TDMA, where the K_t different users with index k, $k = 0, \ldots, K_\mathrm{t} - 1$, are separated by TDMA [FK03, IEE99, IEE00]. For MC-TDMA, $K_\mathrm{f} = K_\mathrm{c} = 1$ and $Q = N$, cf. Section 2.3.3. In order to describe MC-TDMA,

$$\mathbf{S}^{(k_\mathrm{c})} = \mathbf{I}_\mathrm{N}, \tag{A.1}$$

i.e., no CDMA is used,

$$\mathbf{P} = \mathbf{I}_\mathrm{N}, \tag{A.2}$$

i.e., no pre-coding is used, and

$$\mathbf{M}^{(k_\mathrm{f})} = \mathbf{I}_\mathrm{N}, \tag{A.3}$$

i.e., no FDMA is used.

With (2.4) and (2.11), the modulated data vector is given by

$$\mathbf{x}^{(k)}_\mathrm{MC-TDMA} = \mathbf{F}^\mathrm{H}_\mathrm{N} \cdot \mathbf{d}^{(k)}. \tag{A.4}$$

For MC-TDMA, the insertion of the matrices from (A.1), (A.2) and (A.3) in (2.20) leads to

$$\left(\mathbf{g}^{(k)}_p\right)^\mathrm{H} \cdot \mathbf{g}^{(\kappa)}_q = 0 \ \ \forall \ \ p,q = 0,\dots,Q-1; \ \ k,\kappa = 0,\dots,K-1; \ \ k \neq \kappa, \tag{A.5}$$

i.e., the received signal is MAI-free. Moreover,

$$\left(\mathbf{g}^{(k)}_p\right)^\mathrm{H} \cdot \mathbf{g}^{(k)}_q = 0 \ \ \forall \ \ p,q = 0,\dots,Q-1; \ \ p \neq q; \ \ k = 0,\dots,K-1, \tag{A.6}$$

i.e., the received signal is also ISI-free.

A.1.3   Block Transmission Code Division Multiple Access

BT-CDMA is a single carrier scheme that performs user separation by CDMA within a block structure with CP [Mar04]. For BT-CDMA, $K_\mathrm{f} = 1$ and, thus, $K = K_\mathrm{c}$ and $k = k_\mathrm{c}$, cf. Section 2.3.3. Further on, $Q = N/K$. Let $\mathbf{s}^{(k)} = \left[s^{(k)}_0, \dots, s^{(k)}_{K-1}\right]^\mathrm{T}$ denote a CDMA spreading sequence of length K for user k. In order to describe BT-CDMA,

$$\mathbf{S}^{(k_\mathrm{c})} = \mathbf{S}^{(k)}_\mathrm{C} = \begin{bmatrix} \mathbf{s}^{(k)} & \mathbf{0}_\mathrm{Q} & \cdots & \mathbf{0}_\mathrm{Q} \\ \mathbf{0}_\mathrm{Q} & \mathbf{s}^{(k)} & \cdots & \mathbf{0}_\mathrm{Q} \\ \vdots & \vdots & \ddots & \vdots \\ \mathbf{0}_\mathrm{Q} & \mathbf{0}_\mathrm{Q} & \cdots & \mathbf{s}^{(k)}_\mathrm{Q} \end{bmatrix}, \tag{A.7}$$

where $\mathbf{S}^{(k)}_\mathrm{C}$ is an $N \times Q$ matrix and $\mathbf{0}_\mathrm{Q}$ is a column vector of Q elements equal to zero. Moreover,

$$\mathbf{P} = \mathbf{F}_\mathrm{N}, \tag{A.8}$$

i.e., a DFT pre-coding is used, and

$$\mathbf{M}^{(k_\mathrm{f})} = \mathbf{I}_\mathrm{N}, \tag{A.9}$$

i.e., no FDMA is used.

With (2.4) and (2.11), the modulated data vector is given by

$$\mathbf{x}_{\text{BT}-\text{CDMA}}^{(k)} = \mathbf{S}_{\text{C}}^{(k)} \cdot \mathbf{d}^{(k)}. \tag{A.10}$$

For BT-CDMA, inserting the matrices from (A.7), (A.8) and (A.9) in (2.20), the condition

$$\left(\mathbf{g}_p^{(k)}\right)^{\text{H}} \cdot \mathbf{g}_q^{(\kappa)} = 0 \ \ \forall \ \ p, q = 0, \dots, Q-1; \ \ k, \kappa = 0, \dots, K-1; \ \ k \neq \kappa \tag{A.11}$$

is violated i.e., the received signal contains MAI. Moreover, the condition

$$\left(\mathbf{g}_p^{(k)}\right)^{\text{H}} \cdot \mathbf{g}_q^{(k)} = 0 \ \ \forall \ \ p, q = 0, \dots, Q-1; \ \ p \neq q; \ \ k = 0, \dots, K-1 \tag{A.12}$$

is violated, i.e., the received signal contains ISI.

A.1.4 Multi Carrier Code Division Multiple Access

MC-CDMA is a multi carrier scheme that performs user separation by CDMA and transmits the elements of the spread signal on mutually orthogonal subcarriers [FK03]. For MC-CDMA, $K_{\text{f}} = 1$ and, thus, $K = K_{\text{c}}$ and $k = k_{\text{c}}$, cf. Section 2.3.3. Further on, $Q = N/K$. In order to describe MC-CDMA,

$$\mathbf{S}^{(k_{\text{c}})} = \mathbf{S}_{\text{C}}^{(k)}, \tag{A.13}$$

i.e., CDMA is used,

$$\mathbf{P} = \mathbf{I}_{\text{N}}, \tag{A.14}$$

i.e., no pre-coding is used, and

$$\mathbf{M}^{(k_{\text{f}})} = \mathbf{I}_{\text{N}}, \tag{A.15}$$

i.e., no FDMA is used.

With (2.4) and (2.11), the modulated data vector is given by

$$\mathbf{x}_{\text{MC}-\text{CDMA}}^{(k)} = \mathbf{F}_{\text{N}}^{\text{H}} \cdot \mathbf{S}_{\text{C}}^{(k)} \cdot \mathbf{d}^{(k)}. \tag{A.16}$$

For MC-CDMA, inserting the matrices from (A.13), (A.14) and (A.15) in (2.20), the condition

$$\left(\mathbf{g}_p^{(k)}\right)^{\text{H}} \cdot \mathbf{g}_q^{(\kappa)} = 0 \ \ \forall \ \ p, q = 0, \dots, Q-1; \ \ k, \kappa = 0, \dots, K-1; \ \ k \neq \kappa \tag{A.17}$$

is violated i.e., the received signal contains MAI. Moreover,

$$\left(\mathbf{g}_p^{(k)}\right)^{\text{H}} \cdot \mathbf{g}_q^{(k)} = 0 \ \ \forall \ \ p, q = 0, \dots, Q-1; \ \ p \neq q; \ \ k = 0, \dots, K-1, \tag{A.18}$$

i.e., the received signal is ISI-free.

A.1.5   Code Division Multiple Access with Frequency Domain Orthogonal Signature Sequences

FDOSS-CDMA is a single carrier scheme that uses a specific type of CDMA spreading sequences with elements that represent complex exponentials for user separation [CC00]. For FDOSS, $K_\mathrm{f} = 1$ and, thus, $K = K_\mathrm{c}$ and $k = k_\mathrm{c}$, cf. Section 2.3.3. Further on, $Q = N/K$. Let $\mathbf{f}^{(k)} = \left[f_0^{(k)}, \ldots, f_{K-1}^{(k)} \right]^\mathrm{T}$ denote a signature sequence of length K for user k out of a set of K frequency domain orthogonal signature sequences with elements

$$f_\kappa^{(k)} = e^{j\frac{2\pi}{N} k\kappa}, \quad k, \kappa = 1, \ldots, K - 1. \tag{A.19}$$

Thus, in order to describe FDOSS-CDMA,

$$\mathbf{S}^{(k_\mathrm{c})} = \mathbf{S}_\mathrm{F}^{(k)} = \begin{bmatrix} \mathbf{I}_\mathrm{Q} \cdot f_0^{(k)} \\ \mathbf{I}_\mathrm{Q} \cdot f_1^{(k)} \\ \vdots \\ \mathbf{I}_\mathrm{Q} \cdot f_{K-1}^{(k)} \end{bmatrix}. \tag{A.20}$$

Moreover,

$$\mathbf{P} = \mathbf{F}_\mathrm{N} \tag{A.21}$$

i.e., a DFT pre- coding is used, and

$$\mathbf{M}^{(k_\mathrm{f})} = \mathbf{I}_\mathrm{N}, \tag{A.22}$$

i.e., no FDMA is used.

With (2.4) and (2.11), the modulated data vector is given by

$$\mathbf{x}_\mathrm{FDOSS}^{(k)} = \mathbf{S}_\mathrm{F}^{(k)} \cdot \mathbf{d}^{(k)}. \tag{A.23}$$

For FDOSS-CDMA, the insertion of the matrices from (A.20), (A.21) and (A.22) in (2.20) leads to

$$\left(\mathbf{g}_p^{(k)} \right)^\mathrm{H} \cdot \mathbf{g}_q^{(\kappa)} = 0 \ \ \forall \ \ p, q = 0, \ldots, Q - 1; \ \ k, \kappa = 0, \ldots, K - 1; \ \ k \neq \kappa, \tag{A.24}$$

i.e., the received signal is MAI-free. Moreover, the condition

$$\left(\mathbf{g}_p^{(k)} \right)^\mathrm{H} \cdot \mathbf{g}_q^{(k)} = 0 \ \ \forall \ \ p, q = 0, \ldots, Q - 1; \ \ p \neq q; \ \ k = 0, \ldots, K - 1 \tag{A.25}$$

is violated, i.e., the received signal contains ISI.

A.1.6 Spread Spectrum Multi Carrier Multiple Access

SS-MC-MA is an OFDMA scheme with Walsh Hadamard pre-coding [KF97]. For SS-MC-MA, $K_c = 1$ and, thus, $K = K_f$ and $k = k_f$, cf. Section 2.3.3. Further on, $Q = N/K$. In order to describe SS-MC-MA,

$$\mathbf{S}^{(k_c)} = \mathbf{I}_Q, \tag{A.26}$$

i.e., no CDMA is used, and

$$\mathbf{P} = \mathbf{W}_Q, \tag{A.27}$$

where $\mathbf{W}_Q$ denotes a $Q \times Q$ Walsh Hadamard matrix for pre-coding. Moreover,

$$\mathbf{M}^{(k_f)} = \mathbf{M}_{\mathrm{BI}}^{(k)} \tag{A.28}$$

with $M = 1$ and $\mathbf{M}_{\mathrm{BI}}^{(k)}$ of (2.38), i.e., an interleaved FDMA scheme is used.

With (2.4) and (2.11), the modulated data vector is given by

$$\mathbf{x}_{\mathrm{SS-MC-MA}}^{(k)} = \mathbf{F}_N^{\mathrm{H}} \cdot \mathbf{M}_{\mathrm{int}}^{(k)} \cdot \mathbf{W}_Q \cdot \mathbf{d}^{(k)}. \tag{A.29}$$

For SS-MC-MA, the insertion of the matrices from (A.26), (A.27) and (A.28) in (2.20) leads to

$$\left(\mathbf{g}_p^{(k)} \right)^{\mathrm{H}} \cdot \mathbf{g}_q^{(\kappa)} = 0 \ \ \forall \ \ p, q = 0, \ldots, Q-1; \ \ k, \kappa = 0, \ldots, K-1; \ \ k \neq \kappa, \tag{A.30}$$

i.e., the received signal is MAI-free. Moreover, the condition

$$\left(\mathbf{g}_p^{(k)} \right)^{\mathrm{H}} \cdot \mathbf{g}_q^{(k)} = 0 \ \ \forall \ \ p, q = 0, \ldots, Q-1; \ \ p \neq q; \ \ k = 0, \ldots, K-1 \tag{A.31}$$

is violated, i.e., the received signal contains ISI.

A.1.7 Variable Spreading and Chip Repetition Factor Code Division Multiple Access

VSCRF-CDMA is a hybrid Code Division and Frequency Division Multiple Access scheme combining IFDMA and CDMA [GKAS03]. For VSCRF-CDMA, $K = K_f \cdot K_c$ and $k = k_f + k_c \cdot K_f$, cf. Section 2.3.3. Let $\mathbf{u}^{(k_c)} = \left[u_0^{(k_c)}, \ldots, u_{K_c-1}^{(k_c)} \right]^{\mathrm{T}}$ denote a CDMA spreading sequence of length K_c. In order to describe VSCRF-CDMA,

$$\mathbf{S}^{(k_c)} = \bar{\mathbf{S}}_{\mathrm{C}}^{(k_c)} = \begin{bmatrix} \mathbf{u}^{(k_c)} & \mathbf{0}_{\mathrm{R}} & \cdots & \mathbf{0}_{\mathrm{R}} \\ \mathbf{0}_{\mathrm{R}} & \mathbf{u}^{(k_c)} & \cdots & \mathbf{0}_{\mathrm{R}} \\ \vdots & \vdots & \ddots & \vdots \\ \mathbf{0}_{\mathrm{R}} & \mathbf{0}_{\mathrm{R}} & \cdots & \mathbf{u}_{\mathrm{R}}^{(k_c)} \end{bmatrix}, \tag{A.32}$$

where $\mathbf{0}_\mathrm{R}$ is a column vector of $R = N/(K_\mathrm{f} \cdot K_\mathrm{c})$ elements equal to zero, i.e., the users are separated by CDMA. Moreover,

$$\mathbf{P} = \mathbf{F}_{N/K_\mathrm{f}}, \tag{A.33}$$

where $\mathbf{F}_{N/K_\mathrm{f}}$ denotes an $N/K_\mathrm{f} \times N/K_\mathrm{f}$ Discrete Fourier Transform matrix, i.e, a DFT pre-coding is used. Finally,

$$\mathbf{M}^{(k)} = \bar{\mathbf{M}}_\mathrm{int}^{(k)} \tag{A.34}$$

with elements

$$\left[\bar{\mathbf{M}}_\mathrm{int}^{(k)}\right]_{n,q} = \begin{cases} 1 & n = q \cdot K_\mathrm{f} + k, \quad q = 0, \ldots, N/K_\mathrm{f} - 1 \quad n = 0, \ldots, N - 1 \\ 0 & \text{else,} \end{cases} \tag{A.35}$$

i.e., the users are separated by an interleaved FDMA scheme.

With (2.4) and (2.11), the modulated data vector is given by

$$\mathbf{x}_\mathrm{VSCRF}^{(k)} = \mathbf{F}_N^\mathrm{H} \cdot \bar{\mathbf{M}}_\mathrm{int}^{(k)} \cdot \mathbf{F}_{N/K_\mathrm{f}} \cdot \bar{\mathbf{S}}_\mathrm{C}^{(k_\mathrm{c})} \cdot \mathbf{d}^{(k)}. \tag{A.36}$$

For VSCRF-CDMA, inserting the matrices from (A.32), (A.33) and (A.34) in (2.20), the condition

$$\left(\mathbf{g}_p^{(k)}\right)^\mathrm{H} \cdot \mathbf{g}_q^{(\kappa)} = 0 \;\; \forall \;\; p,q = 0, \ldots, Q-1; \;\; k, \kappa = 0, \ldots, K-1; \;\; k \neq \kappa \tag{A.37}$$

is violated, i.e., the received signal contains MAI. Moreover, the condition

$$\left(\mathbf{g}_p^{(k)}\right)^\mathrm{H} \cdot \mathbf{g}_q^{(k)} = 0 \;\; \forall \;\; p,q = 0, \ldots, Q-1; \;\; p \neq q; \;\; k = 0, \ldots, K-1 \tag{A.38}$$

is violated, i.e., the received signal contains ISI.

Appendix B

B.1 Comparison of the PAPR for STBCs and STFCs

B.1.1 Introduction

In the following, the envelope fluctuations of a B-IFDMA signal with STBCs as proposed in Section 3.3 are compared to the envelope fluctuations of a B-IFDMA signal with SFBC as described, e.g., in [BP00]. For the investigation, as an approximation of the continuous time transmit signal at a certain transmit antenna, the respective oversampled transmit signal including pulse shaping and windowing is analyzed. A detailed description of the transmit signal considering pulse shaping and windowing is given in Section 4.4.3.2. As metrics for the envelope fluctuations the mean PAPR and the raw cubic metric (RCM) are used. A definition of both metrics can be found in Section 4.4.3.3. The considered code is the well known Alamouti code, cf. [Ala98], that, for STBC, is applied to consecutive modulated data vectors and, for SFBC, to pairs of adjacent subcarriers within a block. The considered B-IFDMA signal provides $Q = 32$ subcarriers per user at $N = 1024$ subcarriers in the system and is investigated for different numbers M of subcarriers per block. The modulation scheme that is used is QPSK.

B.1.2 Results

In Figure B.1, the results for the envelope fluctuations of B-IFDMA with STBC and SFBC, respectively, are depicted. Note that for $M = 1$, i.e., for IFDMA, SFBC cannot be applied cf. Section 3.3.2.

From the results in Figure B.1 it can be seen that for $M = 2$ the envelope fluctuations are similar for STBC and SFBC. For an increasing number $M > 2$ of subcarriers per block, the difference between the envelope fluctuations for STBC and SFBC increases. The reason for the different envelope fluctuations of STBC and SFBC is that, on the one hand, the approach described in Section 3.3 for application of STBC to B-IFDMA leaves the envelope of the B-IFDMA unchanged compared to the single antenna transmission. On the other hand, in general, for SFBC, the elements of the DFT of the
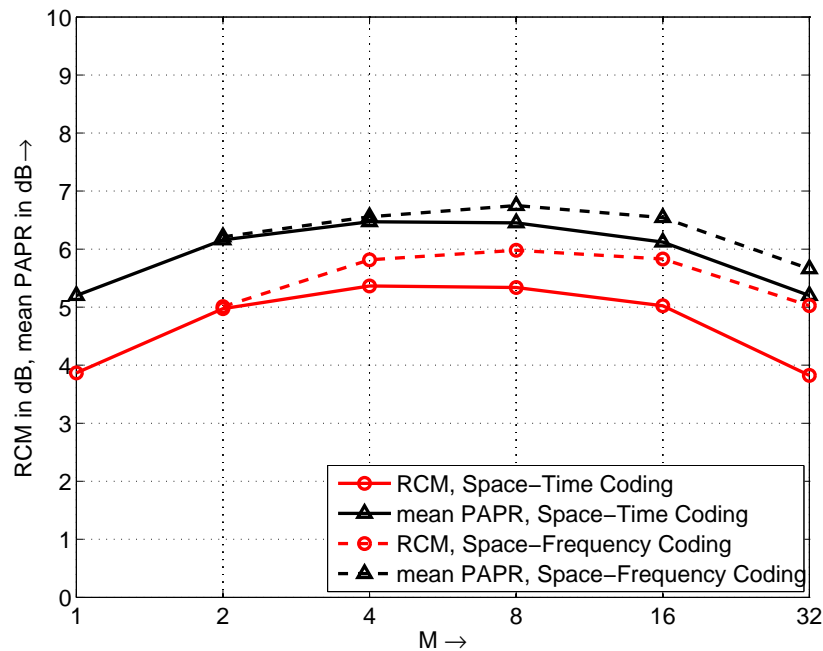
Figure B.1: Different metrics for the envelope fluctuations of a B-IFDMA signal for STBC and SFBC dependent on M for $Q = 32$ using QPSK.

data symbols are manipulated. In particular, for the Alamouti code the elements of the DFT are complex conjugated and pairwise interchanged. Due to the manipulation of the elements of the DFT the resulting signal is no longer an authentic DFT pre-coded OFDMA signal and, thus, the envelope fluctuations are increased compared to those of B-IFDMA.

The results that are shown in in Figure B.1 can be regarded as a motivation for the approach for the application of STBC to B-IFDMA presented in Section 3.3, because this approach combines the exploitation of spatial diversity due to the application of multiple transmit antennas with a better power efficiency due to lower envelope fluctuations of the transmit signal compared to B-IFDMA with SFBC.

B.2 Examples of Code Matrices for Different STBCs

B.2.1 Introduction

In the following, based on the generalized approach for the application of STBCs to B-IFDMA introduced in Section 3.3, examples of code matrices are given for different well known STBCs. For mobile terminals such as laptops or handheld computers not only 2 but also 3 or 4 transmit antennas may be feasible. Thus, in the following, in addition to the example of a STBC for 2 antennas in Section 3.3.3.2, examples for STBCs for 3 and 4 antennas are presented. The examples are obtained by applying a certain well known STBC from the literature to the elements of the DFT of the data vector as described in Section 3.3.3.1. The examples include orthogonal STBCs with different code rates as well as an example for a non-orthogonal STBC.

B.2.2 Orthogonal STBC for 3 Tx Antennas, Rate 1/2

In the following, an orthogonal STBC for $n_{\mathrm{T}} = 3$ transmit antennas that is described, e.g., in [PNG03] is considered. It is assumed that the channel does not change for the duration of the transmission of $N_{\mathrm{t}} = 8$ consecutive modulated data vectors. The number A of encoded data vectors $\mathbf{d}_a^{(k)}$ is given by $A = 4$ and $a = 0, \ldots, 3$. The code rate results in

$$R = \frac{A}{N_{\mathrm{t}}} = \frac{1}{2}. \tag{B.39}$$

For this code,

$$
\begin{aligned}
\mathcal{V}_1 \;=\; & \{(0,0), (0,1), (0,2), (0,3), \\
& (1,0), (1,1), (1,2), (1,3), \\
& (2,0), (2,1), (2,2), (2,3)\}
\end{aligned} \tag{B.40}
$$

and

$$
\begin{aligned}
\mathcal{V}_2 \;=\; & \{(0,4), (0,5), (0,6), (0,7), \\
& (1,4), (1,5), (1,6), (1,7), \\
& (2,4), (2,5), (2,6), (2,7)\} \,.
\end{aligned} \tag{B.41}
$$

Further on,

$$
\begin{aligned}
f_{0,0} \;=\; & f_{0,4} = f_{1,0} = f_{1,0} = f_{1,1} = f_{1,2} = f_{1,4} = f_{1,5} = f_{1,6} = f_{2,0} \\
\;=\; & f_{2,2} = f_{2,3} = f_{2,4} = f_{2,6} = f_{2,7} = 1
\end{aligned} \tag{B.42}
$$

and

$$f_{0,1} = f_{0,2} = f_{0,3} = f_{0,5} = f_{0,6} = f_{0,7} = f_{1,4} = f_{1,7} = f_{2,1} = f_{2,5} = -1. \qquad \text{(B.43)}$$

Since $f_{m,n} \in \{-1; +1\}$, the application of the STBC from (B.45) does not change the envelope characteristics of the B-IFDMA transmit signal per transmit antenna compared to single antenna transmission.

With (3.37), for this code, matrix $\mathbf{C}^{(k)}$ of (3.32) is given by

$$\mathbf{C}^{(k)} = \begin{bmatrix} \mathbf{u}_0^{(k)} & -\mathbf{u}_1^{(k)} & -\mathbf{u}_2^{(k)} & -\mathbf{u}_3^{(k)} & \left(\mathbf{u}_0^{(k)}\right)^* & -\left(\mathbf{u}_1^{(k)}\right)^* & -\left(\mathbf{u}_2^{(k)}\right)^* & -\left(\mathbf{u}_3^{(k)}\right)^* \\ \mathbf{u}_1^{(k)} & \mathbf{u}_0^{(k)} & \mathbf{u}_3^{(k)} & -\mathbf{u}_2^{(k)} & \left(\mathbf{u}_1^{(k)}\right)^* & \left(\mathbf{u}_0^{(k)}\right)^* & \left(\mathbf{u}_3^{(k)}\right)^* & -\left(\mathbf{u}_2^{(k)}\right)^* \\ \mathbf{u}_2^{(k)} & -\mathbf{u}_3^{(k)} & \mathbf{u}_0^{(k)} & \mathbf{u}_1^{(k)} & \left(\mathbf{u}_2^{(k)}\right)^* & -\left(\mathbf{u}_3^{(k)}\right)^* & \left(\mathbf{u}_0^{(k)}\right)^* & \left(\mathbf{u}_1^{(k)}\right)^* \end{bmatrix}$$

(B.44)

with $\mathbf{u}_a^{(k)}$ of (3.30). Consequently, with (3.38) to (3.41), matrix $\mathbf{\Xi}^{(k)}$ of (3.42) is given by

$$\mathbf{\Xi}^{(k)} = \begin{bmatrix} \mathbf{d}_0^{(k)} & -\mathbf{d}_1^{(k)} & -\mathbf{d}_2^{(k)} & -\mathbf{d}_3^{(k)} & \left(\bar{\mathbf{d}}_0^{(k)}\right)^* & -\left(\bar{\mathbf{d}}_1^{(k)}\right)^* & -\left(\bar{\mathbf{d}}_2^{(k)}\right)^* & -\left(\bar{\mathbf{d}}_3^{(k)}\right)^* \\ \mathbf{d}_1^{(k)} & \mathbf{d}_0^{(k)} & \mathbf{d}_3^{(k)} & -\mathbf{d}_2^{(k)} & \left(\bar{\mathbf{d}}_1^{(k)}\right)^* & \left(\bar{\mathbf{d}}_0^{(k)}\right)^* & \left(\bar{\mathbf{d}}_3^{(k)}\right)^* & -\left(\bar{\mathbf{d}}_2^{(k)}\right)^* \\ \mathbf{d}_2^{(k)} & -\mathbf{d}_3^{(k)} & \mathbf{d}_0^{(k)} & \mathbf{d}_1^{(k)} & \left(\bar{\mathbf{d}}_2^{(k)}\right)^* & -\left(\bar{\mathbf{d}}_3^{(k)}\right)^* & \left(\bar{\mathbf{d}}_0^{(k)}\right)^* & \left(\bar{\mathbf{d}}_1^{(k)}\right)^* \end{bmatrix}.$$

(B.45)

B.2.3   Orthogonal STBC for 3 Tx Antennas, Rate 3/4

In the following, an orthogonal STBC for $n_\mathrm{T} = 3$ transmit antennas that is described, e.g., in [LS03] is considered. It is assumed that the channel does not change for the duration of the transmission of $N_\mathrm{t} = 4$ consecutive modulated data vectors. The number A of encoded data vectors $\mathbf{d}_a^{(k)}$ is given by $A = 3$ and $a = 0, \ldots, 2$. The code rate results in

$$R = \frac{A}{N_\mathrm{t}} = \frac{3}{4}. \qquad \text{(B.46)}$$

For this code,

$$\mathcal{V}_1 = \{(0,0), (0,1), (0,2), (0,3), (1,0), (1,1), (2,1), (2,3)\} \qquad \text{(B.47)}$$

and

$$\mathcal{V}_2 = \{(1,2), (1,3), (2,0), (2,2)\}. \qquad \text{(B.48)}$$

Further on,

$$f_{0,0} = f_{0,2} = f_{1,1} = f_{1,2} = f_{1,3} = f_{2,2} = 1, \qquad \text{(B.49)}$$

$$f_{0,1} = f_{1,0} = f_{2,3} = 0 \tag{B.50}$$

and

$$f_{0,3} = f_{2,0} = f_{2,1} = -1. \tag{B.51}$$

Some factors $f_{m,n}$ are equal to zero. That means that for the duration of the respective m-th modulated data vector the transmission at antenna n is switched off. For the other modulated data vectors, the application of the STBC according to (B.53) does not change the envelope characteristics of the B-IFDMA transmit signal per transmit antenna compared to single antenna transmission, because the respective factors $f_{m,n}$ are either 1 or -1.

With (3.37), for this code, matrix $\mathbf{C}^{(k)}$ of (3.32) is given by

$$\mathbf{C}^{(k)} = \begin{bmatrix} \mathbf{u}_0^{(k)} & 0 & \mathbf{u}_1^{(k)} & -\mathbf{u}_2^{(k)} \\ 0 & \mathbf{u}_0^{(k)} & \left(\mathbf{u}_2^{(k)}\right)^* & \left(\mathbf{u}_1^{(k)}\right)^* \\ -\left(\mathbf{u}_1^{(k)}\right)^* & -\mathbf{u}_2^{(k)} & \left(\mathbf{u}_0^{(k)}\right)^* & 0 \end{bmatrix} \tag{B.52}$$

with $\mathbf{u}_a^{(k)}$ of (3.30). Consequently, with (3.38) to (3.41), matrix $\mathbf{\Xi}^{(k)}$ of (3.42) is given by

$$\mathbf{\Xi}^{(k)} = \begin{bmatrix} \mathbf{d}_0^{(k)} & 0 & \mathbf{d}_1^{(k)} & -\mathbf{d}_2^{(k)} \\ 0 & \mathbf{d}_0^{(k)} & \left(\bar{\mathbf{d}}_2^{(k)}\right)^* & \left(\bar{\mathbf{d}}_1^{(k)}\right)^* \\ -\left(\bar{\mathbf{d}}_1^{(k)}\right)^* & -\mathbf{d}_2^{(k)} & \left(\bar{\mathbf{d}}_0^{(k)}\right)^* & 0 \end{bmatrix}. \tag{B.53}$$

B.2.4   Orthogonal STBC for 4 Tx Antennas, Rate 3/4

In the following, an orthogonal STBC for $n_{\mathrm{T}} = 4$ transmit antennas that is described, e.g., in [LS03] is considered. It is assumed that the channel does not change for the duration of the transmission of $N_{\mathrm{t}} = 4$ consecutive modulated data vectors. The number A of encoded data vectors $\mathbf{d}_a^{(k)}$ is given by $A = 3$ and $a = 0, \dots, 2$. The code rate results in

$$R = \frac{A}{N_{\mathrm{t}}} = \frac{3}{4}. \tag{B.54}$$

For this code,

$$\mathcal{V}_1 = \{(0,0), (0,1), (0,2), (0,3), (1,0), (1,1), (2,1), (2,3), (3,1), (3,2)\} \tag{B.55}$$

and

$$\mathcal{V}_2 = \{(1,2), (1,3), (2,0), (2,2), (3,0), (3,3)\}. \tag{B.56}$$

Further on,

$$f_{0,0} = f_{0,2} = f_{1,1} = f_{1,2} = f_{1,3} = f_{2,2} = f_{3,0} = f_{3,3} = 1, \tag{B.57}$$

$$f_{0,1} = f_{1,0} = f_{2,3} = f_{3,2} = 0 \tag{B.58}$$

and

$$f_{0,3} = f_{2,0} = f_{2,1} = f_{3,1} = -1. \tag{B.59}$$

Again, some factors $f_{m,n}$ are equal to zero. That means that for the duration of the respective m-th modulated data vector the transmission at antenna n is switched off. For the other modulated data vectors, the application of the STBC according to (B.53) does not change the envelope characteristics of the B-IFDMA transmit signal per transmit antenna compared to single antenna transmission, because the respective factors $f_{m,n}$ are either 1 or -1.

With (3.37), for this code, matrix $\mathbf{C}^{(k)}$ of (3.32) is given by

$$\mathbf{C}^{(k)} = \begin{bmatrix} \mathbf{u}_0^{(k)} & 0 & \mathbf{u}_1^{(k)} & -\mathbf{u}_2^{(k)} \\ 0 & \mathbf{u}_0^{(k)} & \left(\mathbf{u}_2^{(k)}\right)^* & \left(\mathbf{u}_1^{(k)}\right)^* \\ -\left(\mathbf{u}_1^{(k)}\right)^* & -\mathbf{u}_2^{(k)} & \left(\mathbf{u}_0^{(k)}\right)^* & 0 \\ \left(\mathbf{u}_2^{(k)}\right)^* & -\mathbf{u}_1^{(k)} & 0 & \left(\mathbf{u}_0^{(k)}\right)^* \end{bmatrix} \tag{B.60}$$

with $\mathbf{u}_a^{(k)}$ of (3.30). Consequently, with (3.38) to (3.41), matrix $\mathbf{\Xi}^{(k)}$ of (3.42) is given by

$$\mathbf{\Xi}^{(k)} = \begin{bmatrix} \mathbf{d}_0^{(k)} & 0 & \mathbf{d}_1^{(k)} & -\mathbf{d}_2^{(k)} \\ 0 & \mathbf{d}_0^{(k)} & \left(\bar{\mathbf{d}}_2^{(k)}\right)^* & \left(\bar{\mathbf{d}}_1^{(k)}\right)^* \\ -\left(\bar{\mathbf{d}}_1^{(k)}\right)^* & -\mathbf{d}_2^{(k)} & \left(\bar{\mathbf{d}}_0^{(k)}\right)^* & 0 \\ \left(\bar{\mathbf{d}}_2^{(k)}\right)^* & -\mathbf{d}_1^{(k)} & 0 & \left(\bar{\mathbf{d}}_0^{(k)}\right)^* \end{bmatrix}. \tag{B.61}$$

B.2.5 Non-orthogonal STBC for 4 Tx Antennas, Rate 1

In the following, a non-orthogonal STBC for $n_\mathrm{T} = 4$ transmit antennas that is described, e.g., in [SgXM04] is considered. It is assumed that the channel does not change for the duration of the transmission of $N_\mathrm{t} = 4$ consecutive modulated data vectors. The number A of encoded data vectors $\mathbf{d}_a^{(k)}$ is given by $A = 4$ and $a = 0, \dots, 3$. The code rate results in

$$R = \frac{A}{N_\mathrm{t}} = 1. \tag{B.62}$$

For this code,

$$\mathcal{V}_1 = \{(0,0), (0,1), (0,2), (0,3), (2,0), (2,1), (2,2), (2,3)\} \tag{B.63}$$

and

$$\mathcal{V}_2 = \{(1,0),(1,1),(1,2),(1,3),(3,0),(3,1),(3,2),(3,3)\}. \tag{B.64}$$

Further on,

$$f_{0,0} = f_{0,1} = f_{0,2} = f_{0,3} = f_{1,1} = f_{1,3} = f_{2,0} = f_{2,1} = f_{2,2} = f_{2,3} = f_{3,1} = f_{3,3} = 1 \tag{B.65}$$

and

$$f_{1,0} = f_{1,2} = f_{3,0} = f_{3,2} = -1. \tag{B.66}$$

Since $f_{m,n} \in \{-1;+1\}$, the application of the STBC from (B.45) does not change the envelope characteristics of the B-IFDMA transmit signal per transmit antenna compared to single antenna transmission.

With (3.37), for this code, matrix $\mathbf{C}^{(k)}$ of (3.32) is given by

$$\mathbf{C}^{(k)} = \begin{bmatrix} \mathbf{u}_0^{(k)} & \mathbf{u}_1^{(k)} & \mathbf{u}_2^{(k)} & \mathbf{u}_4^{(k)} \\ -\left(\mathbf{u}_1^{(k)}\right)^* & \left(\mathbf{u}_0^{(k)}\right)^* & -\left(\mathbf{u}_3^{(k)}\right)^* & \left(\mathbf{u}_2^{(k)}\right)^* \\ \mathbf{u}_2^{(k)} & \mathbf{u}_3^{(k)} & \mathbf{u}_0^{(k)} & \mathbf{u}_1^{(k)} \\ -\left(\mathbf{u}_3^{(k)}\right)^* & \left(\mathbf{u}_2^{(k)}\right)^* & -\left(\mathbf{u}_1^{(k)}\right)^* & \left(\mathbf{u}_0^{(k)}\right)^* \end{bmatrix} \tag{B.67}$$

with $\mathbf{u}_a^{(k)}$ of (3.30). Consequently, with (3.38) to (3.41), matrix $\mathbf{\Xi}^{(k)}$ of (3.42) is given by

$$\mathbf{\Xi}^{(k)} = \begin{bmatrix} \mathbf{d}_0^{(k)} & \mathbf{d}_1^{(k)} & \mathbf{d}_2^{(k)} & \mathbf{d}_4^{(k)} \\ -\left(\bar{\mathbf{d}}_1^{(k)}\right)^* & \left(\bar{\mathbf{d}}_0^{(k)}\right)^* & -\left(\bar{\mathbf{d}}_3^{(k)}\right)^* & \left(\bar{\mathbf{d}}_2^{(k)}\right)^* \\ \mathbf{d}_2^{(k)} & \mathbf{d}_3^{(k)} & \mathbf{d}_0^{(k)} & \mathbf{d}_1^{(k)} \\ -\left(\bar{\mathbf{d}}_3^{(k)}\right)^* & \left(\bar{\mathbf{d}}_2^{(k)}\right)^* & -\left(\bar{\mathbf{d}}_1^{(k)}\right)^* & \left(\bar{\mathbf{d}}_0^{(k)}\right)^* \end{bmatrix} \tag{B.68}$$

B.3 Derivation of the Equalizer for Colored Noise

In the following, the matrix representation of the FDE based on the MMSE criterion that is used in Section 3.3.5.1 is derived. Let $\boldsymbol{\mathcal{E}}_{\mathrm{MMSE}}^{(k)}$ denote the $2AQ \times 2AQ$ matrix representation of the FDE. The FDE is based on the minimization of the expected squared error $\mathbf{e}^{(k)}$ between $\boldsymbol{\mathcal{E}}_{\mathrm{MMSE}}^{(k)} \cdot \mathrm{Re}\left\{\left(\mathbf{B}^{(k)}\right)^{\mathrm{H}} \cdot \bar{\boldsymbol{\nu}}^{(k)}\right\}$ and $\check{\mathbf{u}}^{(k)}$, cf. (3.82). Thus, the minimization problem can be formulated as

$$\underset{\boldsymbol{\mathcal{E}}_{\mathrm{MMSE}}^{(k)}}{\arg \min} \left\{ E\left\{ \left\| \boldsymbol{\mathcal{E}}_{\mathrm{MMSE}}^{(k)} \cdot \mathrm{Re}\left\{\left(\mathbf{B}^{(k)}\right)^{\mathrm{H}} \cdot \bar{\boldsymbol{\nu}}^{(k)}\right\} - \check{\mathbf{u}}^{(k)} \right\|^2 \right\} \right\}, \tag{B.69}$$

where $\|\cdot\|^2$ denotes the Euclidean norm of a vector and where $\underset{\mathbf{A}}{\arg \min}\{\cdot\}$ gives the matrix $\mathbf{A}$ that minimizes the expression in the curly brackets. With (3.82), the expected error $\mathbf{e}^{(k)}$ can be expressed as follows:

$$\begin{aligned} \mathbf{e}^{(k)} &= E\left\{ \left\| \boldsymbol{\mathcal{E}}_{\mathrm{MMSE}}^{(k)} \cdot \mathrm{Re}\left\{\left(\mathbf{B}^{(k)}\right)^{\mathrm{H}} \cdot \bar{\boldsymbol{\nu}}^{(k)}\right\} - \check{\mathbf{u}}^{(k)} \right\|^2 \right\} \\ &= E\left\{ \left\| \boldsymbol{\mathcal{E}}_{\mathrm{MMSE}}^{(k)} \cdot \left(\boldsymbol{\Delta}^{(k)} \cdot \check{\mathbf{u}}^{(k)} + \bar{\mathbf{w}}^{(k)}\right) - \check{\mathbf{u}}^{(k)} \right\|^2 \right\} \\ &= E\left\{ \left\| \boldsymbol{\mathcal{E}}_{\mathrm{MMSE}}^{(k)} \cdot \boldsymbol{\Delta}^{(k)} \cdot \check{\mathbf{u}}^{(k)} + \boldsymbol{\mathcal{E}}_{\mathrm{MMSE}}^{(k)} \cdot \bar{\mathbf{w}}^{(k)} - \check{\mathbf{u}}^{(k)} \right\|^2 \right\}. \end{aligned} \tag{B.70}$$

Since $\boldsymbol{\Delta}^{(k)}$ is a diagonal matrix, $\boldsymbol{\mathcal{E}}_{\mathrm{MMSE}}^{(k)}$ is a diagonal matrix, too. Let $\mathcal{E}_{\mathrm{MMSE},r,r}^{(k)}$ and $\Delta_{r,r}^{(k)}$ with $r = 0, \ldots, 2AQ - 1$ denote the diagonal element in the r-th row and column of $\boldsymbol{\mathcal{E}}_{\mathrm{MMSE}}^{(k)}$ and $\boldsymbol{\Delta}^{(k)}$, respectively. Let, further on, $\check{u}_r^{(k)}$ and $\bar{w}_r^{(k)}$ denote the r-th element of $\check{\mathbf{u}}^{(k)}$ and $\bar{\mathbf{w}}^{(k)}$, respectively. Thus, $\mathbf{e}^{(k)}$ can be written as

$$\begin{aligned} \mathbf{e}^{(k)} &= E\left\{ \sum_{r=0}^{2AQ-1} \left| \mathcal{E}_{\mathrm{MMSE},r,r}^{(k)} \cdot \Delta_{r,r}^{(k)} \cdot \check{u}_r^{(k)} + \mathcal{E}_{\mathrm{MMSE},r,r}^{(k)} \cdot \bar{w}_r^{(k)} - \check{u}_r^{(k)} \right|^2 \right\} \\ &= \sum_{r=0}^{2AQ-1} E\left\{ \left| \left(\mathcal{E}_{\mathrm{MMSE},r,r}^{(k)} \cdot \Delta_{r,r}^{(k)} - 1 \right) \cdot \check{u}_r^{(k)} + \mathcal{E}_{\mathrm{MMSE},r,r}^{(k)} \cdot \bar{w}_r^{(k)} \right|^2 \right\} \\ &= \sum_{r=0}^{2AQ-1} E\left\{ \left| \mathcal{E}_{\mathrm{MMSE},r,r}^{(k)} \cdot \Delta_{r,r}^{(k)} - 1 \right|^2 \cdot \left| \check{u}_r^{(k)} \right|^2 + \right. \\ &\qquad\qquad \left(\mathcal{E}_{\mathrm{MMSE},r,r}^{(k)} \cdot \Delta_{r,r}^{(k)} - 1 \right)^* \cdot \left(\check{u}_r^{(k)} \right)^* \cdot \mathcal{E}_{\mathrm{MMSE},r,r}^{(k)} \cdot \bar{w}_r^{(k)} + \\ &\qquad\qquad \left(\mathcal{E}_{\mathrm{MMSE},r,r}^{(k)} \cdot \Delta_{r,r}^{(k)} - 1 \right) \cdot \check{u}_r^{(k)} \cdot \left(\mathcal{E}_{\mathrm{MMSE},r,r}^{(k)} \right)^* \cdot \left(\bar{w}_r^{(k)} \right)^* + \\ &\qquad\qquad \left. \left| \mathcal{E}_{\mathrm{MMSE},r,r}^{(k)} \right|^2 \cdot \left| \bar{w}_r^{(k)} \right|^2 \right\} \end{aligned} \tag{B.71}$$

$$= \sum_{r=0}^{2AQ-1} \left|\mathcal{E}_{\text{MMSE},r,r}^{(k)} \cdot \Delta_{r,r}^{(k)} - 1\right|^2 \cdot E\left\{\left|\check{u}_r^{(k)}\right|^2\right\} +$$

$$\left(\mathcal{E}_{\text{MMSE},r,r}^{(k)} \cdot \Delta_{r,r}^{(k)} - 1\right)^* \cdot \mathcal{E}_{\text{MMSE},r,r}^{(k)} \cdot E\left\{\left(\check{u}_r^{(k)}\right)^* \cdot \bar{w}_r^{(k)}\right\} + \qquad \text{(B.72)}$$

$$\left(\mathcal{E}_{\text{MMSE},r,r}^{(k)} \cdot \Delta_{r,r}^{(k)} - 1\right) \cdot \left(\mathcal{E}_{\text{MMSE},r,r}^{(k)}\right)^* \cdot E\left\{\check{u}_r^{(k)} \cdot \left(\bar{w}_r^{(k)}\right)^*\right\} +$$

$$\left|\mathcal{E}_{\text{MMSE},r,r}^{(k)}\right|^2 \cdot E\left\{\left|\bar{w}_r^{(k)}\right|^2\right\}$$

As $\check{u}_r^{(k)}$ and $\bar{w}_r^{(k)}$ are statistically independent with mean value 0, the second and the third summand in (B.72) are equal to zero and, thus,

$$\mathbf{e}^{(k)} = \sum_{r=0}^{2AQ-1} \left|\mathcal{E}_{\text{MMSE},r,r}^{(k)} \cdot \Delta_{r,r}^{(k)} - 1\right|^2 \cdot E\left\{\left|\check{u}_r^{(k)}\right|^2\right\} + \left|\mathcal{E}_{\text{MMSE},r,r}^{(k)}\right|^2 \cdot E\left\{\left|\bar{w}_r^{(k)}\right|^2\right\}. \quad \text{(B.73)}$$

As all terms in the sum are real-valued and non-negative, the minimization of the sum is obtained by the minimization of the summands:

$$e_r^{(k)} = \left|\mathcal{E}_{\text{MMSE},r,r}^{(k)} \cdot \Delta_{r,r}^{(k)} - 1\right|^2 \cdot E\left\{\left|\check{u}_r^{(k)}\right|^2\right\} + \left|\mathcal{E}_{\text{MMSE},r,r}^{(k)}\right|^2 \cdot E\left\{\left|\bar{w}_r^{(k)}\right|^2\right\} \overset{!}{=} \min. \quad \text{(B.74)}$$

The partial derivative of (B.74) with respect to $\mathcal{E}_{\text{MMSE},r,r}^{(k)}$ and $\left(\mathcal{E}_{\text{MMSE},r,r}^{(k)}\right)^*$, respectively, is given by

$$\frac{\partial e_r^{(k)}}{\partial \mathcal{E}_{\text{MMSE},r,r}^{(k)}} = \left(\left(\mathcal{E}_{\text{MMSE},r,r}^{(k)}\right)^* \cdot \left(\Delta_{r,r}^{(k)}\right)^* - 1\right) \cdot \Delta_{r,r}^{(k)} \cdot E\left\{\left|\check{u}_r^{(k)}\right|^2\right\} + \left(\mathcal{E}_{\text{MMSE},r,r}^{(k)}\right)^* \cdot E\left\{\left|\bar{w}_r^{(k)}\right|^2\right\}$$

$$\text{(B.75)}$$

and

$$\frac{\partial e_r^{(k)}}{\partial \left(\mathcal{E}_{\text{MMSE},r,r}^{(k)}\right)^*} = \left(\mathcal{E}_{\text{MMSE},r,r}^{(k)} \cdot \Delta_{r,r}^{(k)} - 1\right) \cdot \left(\Delta_{r,r}^{(k)}\right)^* \cdot E\left\{\left|\check{u}_r^{(k)}\right|^2\right\} + \mathcal{E}_{\text{MMSE},r,r}^{(k)} \cdot E\left\{\left|\bar{w}_r^{(k)}\right|^2\right\}.$$

$$\text{(B.76)}$$

As $\Delta_{r,r}^{(k)}$ is real-valued, cf. (3.94), also $\mathcal{E}_{\text{MMSE},r,r}^{(k)}$ is real valued. The value for $\mathcal{E}_{\text{MMSE},r,r}^{(k)}$ that minimizes (B.74) is, thus, given by

$$\left(\mathcal{E}_{\text{MMSE},r,r}^{(k)} \cdot \Delta_{r,r}^{(k)} - 1\right) \cdot \Delta_{r,r}^{(k)} \cdot E\left\{\left|\check{u}_r^{(k)}\right|^2\right\} + \mathcal{E}_{\text{MMSE},r,r}^{(k)} \cdot E\left\{\left|\bar{w}_r^{(k)}\right|^2\right\} \overset{!}{=} 0$$

$$\mathcal{E}_{\text{MMSE},r,r}^{(k)} \cdot \left(\Delta_{r,r}^{(k)}\right)^2 \cdot E\left\{\left|\check{u}_r^{(k)}\right|^2\right\} + \mathcal{E}_{\text{MMSE},r,r}^{(k)} \cdot E\left\{\left|\bar{w}_r^{(k)}\right|^2\right\} = \Delta_{r,r}^{(k)} \cdot E\left\{\left|\check{u}_r^{(k)}\right|^2\right\}$$

$$\mathcal{E}_{\text{MMSE},r,r}^{(k)} \cdot \left(\left(\Delta_{r,r}^{(k)}\right)^2 \cdot E\left\{\left|\check{u}_r^{(k)}\right|^2\right\} + E\left\{\left|\bar{w}_r^{(k)}\right|^2\right\}\right) = \Delta_{r,r}^{(k)} \cdot E\left\{\left|\check{u}_r^{(k)}\right|^2\right\},$$

$$\text{(B.77)}$$

resulting in

$$\mathcal{E}_{\text{MMSE},r,r}^{(k)} = \frac{\Delta_{r,r}^{(k)}}{\left(\Delta_{r,r}^{(k)}\right)^2 + \frac{E\left\{\left|\bar{w}_r^{(k)}\right|^2\right\}}{E\left\{\left|\check{u}_r^{(k)}\right|^2\right\}}}. \qquad \text{(B.78)}$$

According to (3.72), (3.62) and (3.63), $\check{u}_r^{(k)}$ is given by the real part $\check{u}_{a,q}^{(k)}$ or the imaginary part $\tilde{u}_{a,q}^{(k)}$ of the elements $u_{a,q}^{(k)}$ of the DFT of the data symbol vector $\mathbf{d}_a^{(k)}$, respectively, with $a = 0, \ldots, A - 1$. Thus, $E\{|\check{u}_r^{(k)}|^2\} = 1/2 \cdot E\{|u_{a,q}^{(k)}|^2\}$. For the determination of $E\{|\bar{w}_r^{(k)}|^2\}$, let

$$\mathbf{w}_q^{(k)} = \left[w_0^{(k)}, \ldots, w_{2A-1}^{(k)} \right]^{\mathrm{T}} \tag{B.79}$$

with

$$\mathbf{w}_q^{(k)} = \left(\mathbf{B}_q^{(k)} \right)^{\mathrm{H}} \bar{\mathbf{n}}_q^{(k)}. \tag{B.80}$$

As the elements $\bar{n}_{n,q}^{(k)}$, $n = 0, \ldots, N_{\mathrm{t}} - 1$, $q = 0, \ldots, Q - 1$, of the noise vector $\bar{\mathbf{n}}_q^{(k)}$ are statistically independent,

$$E\{|w_r^{(k)}|^2\} = \mathrm{tr}\left\{ \mathbf{B}_q^{(k)} \cdot \left(\mathbf{B}_q^{(k)} \right)^{\mathrm{H}} \right\} \cdot E\{|\bar{n}_{n,q}^{(k)}|^2\}, \tag{B.81}$$

where $\mathrm{tr}\{\cdot\}$ denotes the trace of a matrix. As the real and the imaginary part of the complex white Gaussian noise vector $\bar{\mathbf{n}}_q^{(k)}$ have the same power, also the real and the imaginary part of $\mathbf{w}_q^{(k)}$ have the same power. Thus, with (B.81), the expectation of the elements $\bar{w}_r^{(k)}$ of vector $\bar{\mathbf{w}}^{(k)}$ that is equal to the expectation of the elements $\bar{w}_{n,q}^{(k)}$ of vector $\bar{\mathbf{w}}_q^{(k)} = \mathrm{Re}\left\{ \mathbf{w}_q^{(k)} \right\}$, cf. (3.76), is given by

$$E\{|\bar{w}_r^{(k)}|^2\} = \frac{1}{2}\mathrm{tr}\left\{ \mathbf{B}_q^{(k)} \cdot \left(\mathbf{B}_q^{(k)} \right)^{\mathrm{H}} \right\} \cdot E\{|\bar{n}_{n,q}^{(k)}|^2\}. \tag{B.82}$$

As $\mathbf{u}_a^{(k)}$ is the DFT of $\mathbf{d}_a^{(k)}$, cf. (3.30), and as $\bar{\mathbf{n}}_n^{(k)}$ is the representation of the noise $\mathbf{n}$ in the DFT domain, cf. (3.55), and assuming $|f_{m,n}| = 1$, with the above presented expressions for $E\{|\check{u}_r^{(k)}|^2\}$ and $E\{|\bar{w}_r^{(k)}|^2\}$,

$$\frac{E\{|\bar{w}_r^{(k)}|^2\}}{E\{|\check{u}_r^{(k)}|^2\}} = \mathrm{tr}\left\{ \mathbf{B}_q^{(k)} \cdot \left(\mathbf{B}_q^{(k)} \right)^{\mathrm{H}} \right\} \cdot \frac{\sigma_{\mathrm{d}}^2}{\sigma_{\mathrm{n}}^2}, \tag{B.83}$$

where σ_{d}^2 denotes the power of the data symbols and σ_{n}^2 denotes the power of the noise, cf. (2.32).

Thus, (B.78) can be rewritten as

$$\mathcal{E}_{\mathrm{MMSE},r,r}^{(k)} = \frac{\Delta_{r,r}^{(k)}}{\left(\Delta_{r,r}^{(k)} \right)^2 + \mathrm{tr}\left\{ \mathbf{B}_q^{(k)} \cdot \left(\mathbf{B}_q^{(k)} \right)^{\mathrm{H}} \right\} \cdot \frac{\sigma_{\mathrm{n}}^2}{\sigma_{\mathrm{d}}^2}}. \tag{B.84}$$

Collecting the elements of $\mathcal{E}_{\mathrm{MMSE},r,r}^{(k)}$ that belong to subcarrier q in one diagonal matrix $\boldsymbol{\mathcal{E}}_{\mathrm{MMSE},q}^{(k)}$ results in

$$\boldsymbol{\mathcal{E}}_{\mathrm{MMSE},q}^{(k)} = \left(\left(\boldsymbol{\Delta}_q^{(k)} \right)^{\mathrm{T}} \cdot \boldsymbol{\Delta}_q^{(k)} + \mathrm{tr}\left\{ \mathbf{B}_q^{(k)} \cdot \left(\mathbf{B}_q^{(k)} \right)^{\mathrm{H}} \right\} \cdot \frac{\sigma_{\mathrm{n}}^2}{\sigma_{\mathrm{d}}^2} \cdot \mathbf{I}_{2A} \right)^{-1} \cdot \left(\boldsymbol{\Delta}_q^{(k)} \right)^{\mathrm{T}}. \tag{B.85}$$

Appendix C

C.1 Analysis of the B-IFDMA Signal Envelope for Different Values of Q

In the following, results for the envelope fluctuations are presented in terms of the mean PAPR, the RCM and the required power back-off for a B-IFDMA signal and an OFDMA signal with corresponding parameters dependent on the number M of subcarriers per block for different bit mapping schemes and different numbers Q of subcarriers per user. The parameters and assumptions are the same as for the results in 4.38 - 4.40.

Figures C.1, C.2 and C.3 show results for the different metrics from Section 4.4.3.3 describing the envelope fluctuations of B-IFDMA and OFDMA signals with $Q = 32$ subcarriers per user using QPSK, 16QAM and 64QAM as bit mapping schemes, respectively. Figures C.4, C.5 and C.6 show respective results for B-IFDMA and OFDMA signals with $Q = 128$ subcarriers per user using QPSK, 16QAM and 64QAM as bit mapping schemes, respectively.

A comparison of the results from Figures C.1 - C.6 to the results from Figures 4.38 - 4.40 shows that the results are almost independent from the number Q of subcarriers assigned to a certain user, i.e., from the instantaneous data rate.

Figure C.1: Different metrics for the envelope fluctuations of a B-IFDMA signal and an OFDMA signal with corresponding parameters dependent on M for $Q = 32$ using QPSK.

Figure C.2: Different metrics for the envelope fluctuations of a B-IFDMA signal and an OFDMA signal with corresponding parameters dependent on M for $Q = 32$ using 16QAM.

Figure C.3: Different metrics for the envelope fluctuations of a B-IFDMA signal and an OFDMA signal with corresponding parameters dependent on M for $Q = 32$ using 64QAM.
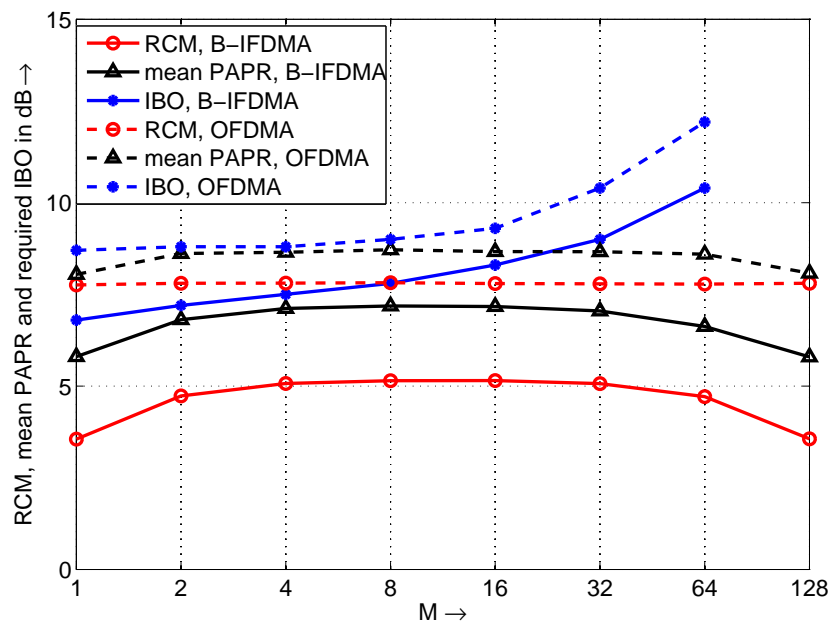
Figure C.4: Different metrics for the envelope fluctuations of a B-IFDMA signal and an OFDMA signal with corresponding parameters dependent on M for $Q = 128$ using QPSK.
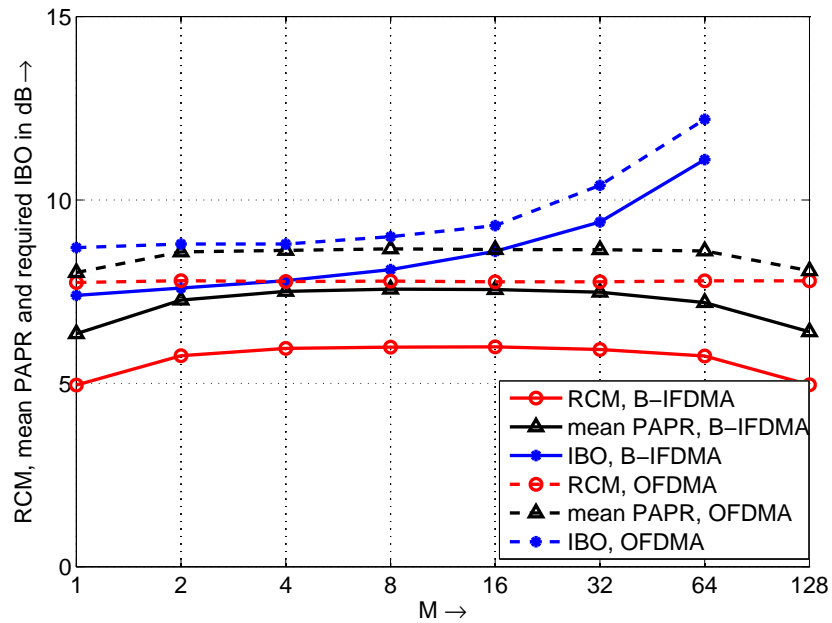
Figure C.5: Different metrics for the envelope fluctuations of a B-IFDMA signal and an OFDMA signal with corresponding parameters dependent on M for $Q = 128$ using 16QAM.
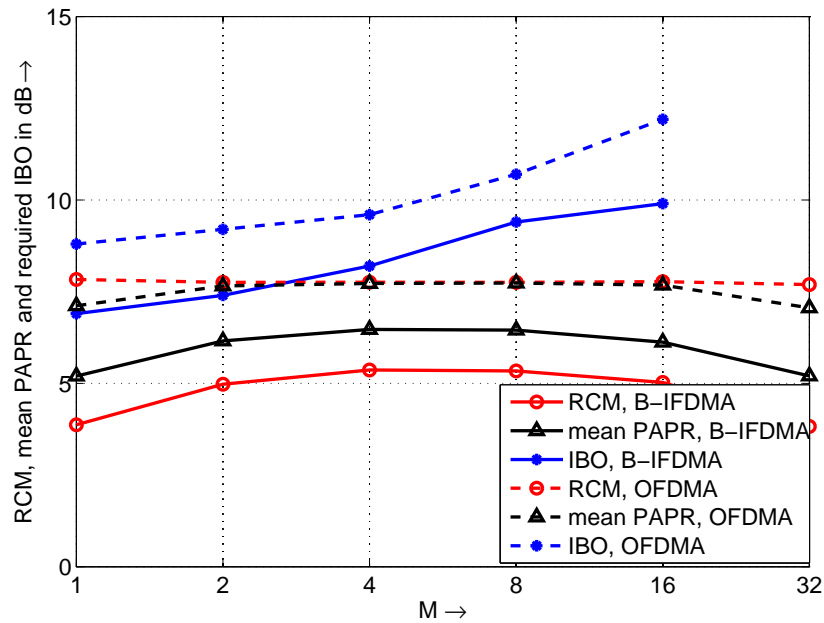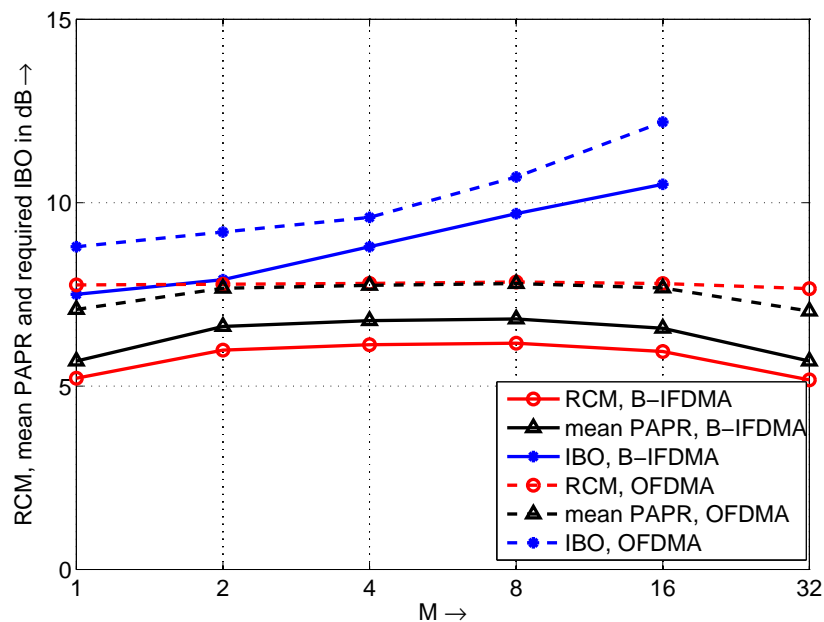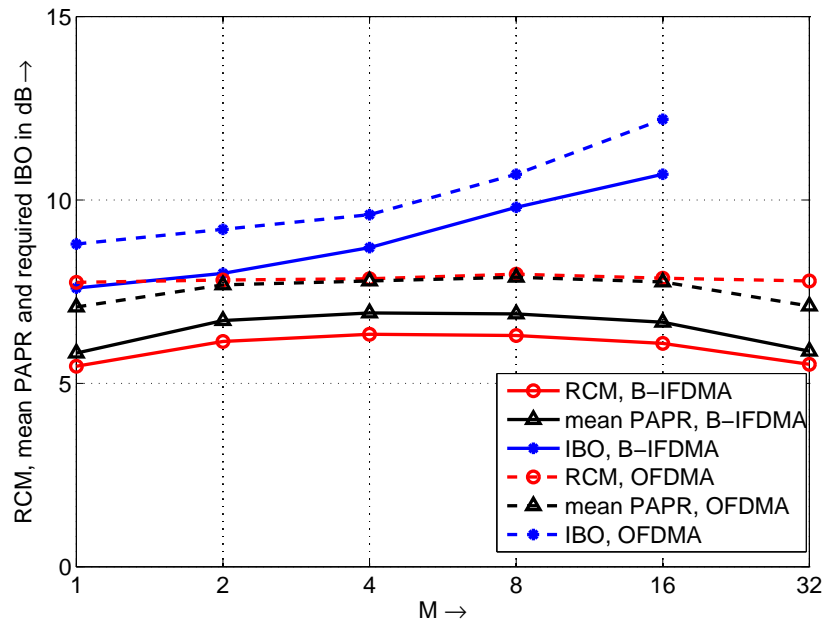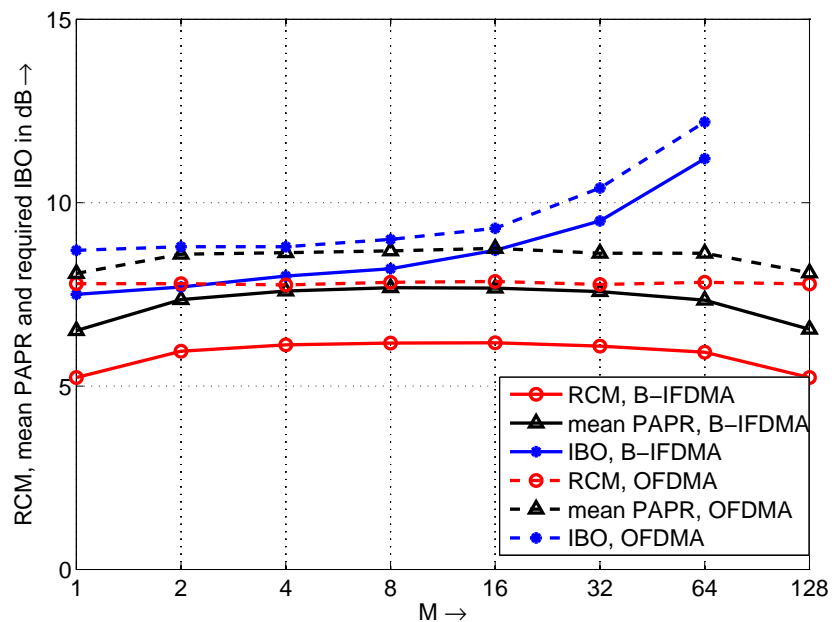

Figure C.6: Different metrics for the envelope fluctuations of a B-IFDMA signal and an OFDMA signal with corresponding parameters dependent on M for $Q = 128$ using 64QAM.

List of Acronyms

1G	First Generation
2G	Second Generation
3G	Third Generation
3GPP	Third Generation Partnership Project
4G	Fourth Generation
A/D	Analog to Digital
AWGN	Additive White Gaussian Noise
B-EFDMA	Block Equidistant Frequency Division Multiple Access
B-IFDMA	Block Interleaved Frequency Division Multiple Access
BER	Bit Error Rate
BO	Back-off
BT-CDMA	Block Transmission Code Division Multiple Access
CDF	Cumulative Probability Density Function
CDMA	Code Division Multiple Access
CM	Cubic Metric
CP	Cyclic Prefix
CSI	Channel State Information
D/A	Digital to Analog
DCA	Dynamic Code Assignment
DECT	Digital Enhanced Cordless Telecommunications
DFT	Discrete Fourier Transform
DSP	Digital Signal Processor
EDGE	Enhanced Data Rates for GSM Evolution
EU	European Union

FDD	Frequency Division Duplex
FDMA	Frequency Division Multiple Access
FDE	Frequency Domain Equalizer
FDOSS	Frequency Domain Orthogonal Signature Sequences
FFT	Fast Fourier Transform
FH	Frequency Hopping
FIR	Finite Impulse Response
GSM	Global Systems for Mobile Communications
HIPERLAN	High Performance Local Area Network
I-OFDMA	Interleaved Orthogonal Frequency Division Multiple Access
ICI	Inter Carrier Interference
IDFT	Inverse Discrete Fourier Transform
IEEE	Institute of Electrical and Electronics Engineers
IFDMA	Interleaved Frequency Division Multiple Access
IMT	International Mobile Telecommunications
IP-OFDMA	Internet Protocol - Orthogonal Frequency Division Multiple Access
ISI	Inter Symbol Interference
ITU	International Telecommunication Union
LFDMA	Localized Frequency Division Multiple Access
LTE	Long Time Evolution
MAI	Multiple Access Interference
MBMS	Multimedia Broadcast Multicast Service
MC-CDMA	Multi Carrier Code Division Multiple Access
MC-TDMA	Multi Carrier - Time Division Multiple Access
MCS	Modulation and Coding Scheme

ML	Maximum Likelihood
MLSE	Maximum Likelihood Sequence Estimation
MMAC	Multimedia Mobile Project Access Communications Systems
MMSE	Minimum Mean Square Error
MRC	Maximum Ratio Combining
MUD	Multiuser Detection
OFDM	Orthogonal Frequency Division Multiplex
OFDMA	Orthogonal Frequency Division Multiple Access
OVSF	Orthogonal Variable Spreading Factor
P/S	Parallel to Serial
PAPR	Peak to Average Power Ratio
PDA	Personal Digital Assistant
PSK	Phase Shift Keying
QAM	Quadrature Amplitude Modulation
QPSK	Quaternatary Phase Shift Keying
RCM	Raw Cubic Metric
RMS	Root Mean Square
S/P	Serial to Parallel
SC-FDE	Single Carrier - Frequency Domain Equalizer
SC-FDMA	Single Carrier - Frequency Division Multiple Access
SC-FDMA	Single Carrier - Frequency Division Multiple Access
SC-TDMA	Single Carrier - Time Division Multiple Access
SDMA	Space Division Multiple Access
SFBC	Space Frequency Block Coding
SI	Self Interference

SNR	Signal to Noise Ratio
SS-MC-MA	Spread Spectrum Multi Carrier Multiple Access
STBC	Space Time Block Coding
STC	Space Time Block Code
TD-CDMA	Time Division - Code Division Multiple Access
TDMA	Time Division Multiple Access
TD-SCDMA	Time Division - Synchronous Code Division Multiple Access
TDD	Time Division Duplex
UMTS	Universal Mobile Telecommunications Systems
UTRA	Universal Terrestrial Radio Access
VoIP	Voice over Internet Protocol
VSCRF	Variable Spreading and Chip Repetition Factor
W-CDMA	Wideband Code Division Multiple Access
WiMAX	Worldwide Interoperability for Microwave Access
WINNER	Wireless World Initiative New Radio
WLAN	Wireless Local Area Network
ZF	Zero Forcing

List of Symbols

$(\cdot)^\dagger$	pseudo inverse of a vector or a matrix, respectively
$(\cdot)^{-1}$	inverse of a vector or a matrix, respectively
$(\cdot)^H$	hermitian of a vector or a matrix, respectively
$(\cdot)^T$	transpose of a vector or a matrix, respectively
$[\cdot]_{m,n}$	element of a matrix in the m-th row and the n-th column
$\lfloor\cdot\rfloor$	returns the closest integer $\leq$ the argument
$\lceil\cdot\rceil$	returns the closest integer $\geq$ the argument
$\mathrm{tr}\{\cdot\}$	trace of a matrix
$\mathrm{diag}\{\cdot\}$	returns a diagonal matrix when the argument is a vector, or returns a vector containing the elements of the main diagonal when the argument is a matrix
$\otimes$	Kroenecker product
$\circledast$	circular convolution
$E\{\cdot\}$	expectation
$\mathbf{\Gamma}^{(k)}$	overall channel matrix
$\mathbf{\Gamma}^{(k,\kappa)}$	overall channel of user k assuming $\mathbf{M}^{(\kappa)}$
$\hat{\mathbf{\Gamma}}^{(k,\kappa)}$	estimate of overall channel of user k assuming $\mathbf{M}^{(\kappa)}$
$\Gamma_{m,q}^{(k)}$	diagonal elements of the overall channel matrix for the m-th transmit antenna
$\mathbf{\Gamma}_q^{(k)}$	vector of all $\Gamma_{m,q}^{(k)}$ belonging to the same subcarrier q
$\Gamma_q^{(k)}$	diagonal elements of the overall channel matrix
$\mathbf{\Delta}^{(k)}$	matrix describing encoding of $u_{a,q}^{(k)}$, overall channel and decoding jointly for all subcarriers
Δf	subcarrier bandwidth
$\Delta f_{\mathrm{CFO}}^{(k)}$	frequency offset for user k
$\Delta \bar{f}_{\mathrm{CFO}}^{(k)}$	frequency offset for user k normalized to the subcarrier bandwidth Δf
$\Delta \bar{f}_{\mathrm{CFO,max}}^{(k)}$	maximum normalized frequency offset for user k
$\mathbf{\Delta}_q^{(k)}$	matrix describing encoding of $u_{a,q}^{(k)}$, overall channel and decoding jointly for subcarrier q
$\Delta\tau$	channel delay spread
ΔT	duration of the transmission of N_t consecutive modulated data vectors with CP
ΔT_f	time interval between reception of pilot symbols and adapted transmission

$\Theta_n^{(\mu,k)}$	complex weighting factors for efficient implementation of B-IFDMA modulation
λ	wave length
$\bar{\boldsymbol{\nu}}^{(k)}$	vector stacking all $\bar{\mathbf{v}}_q^{(k)}$
$\boldsymbol{\xi}_{m,n}^{(k)}$	time domain equivalent of $\mathbf{c}_{m,n}^{(k)}$
$\boldsymbol{\Xi}^{(k)}$	time domain equivalent of STBC encoding matrix
ρ	correlation between $\mathbf{t}_{\mathrm{OD}}^{(k,\kappa)}$ and $\mathbf{t}^{(k,\kappa)}$
$\boldsymbol{\rho}^{(k)}$	demodulated signal vector
$\rho_q^{(k)}$	elements of the demodulated signal vector
σ_{d}^2	variance of $d_q^{(k)}$
σ_{n}^2	variance of n_n
$\sigma_{\underline{\mathrm{n}}}^2$	variance of $n_{\eta,q}$
$\sigma_{\underline{\mathrm{u}}}^2$	variance of $u_q^{(\kappa)}$
Υ	SNR degradation due to pilot symbol overhead in dB for B-IFDMA
$\bar{\Upsilon}$	SNR degradation due to pilot symbol overhead in dB for LFDMA with FH
$\Psi_n^{(\nu,k)}$	complex weighting factors for efficient implementation of B-IFDMA demodulation
$\mathbf{0}_{X \times Y}$	$X \times Y$ matrix with all elements equal to zero
A	number of consecutive data symbol vectors that are jointly encoded by a STBC
$\mathbf{A}$	system matrix
$\breve{\mathbf{A}}$	block-diagonal matrix with the matrices $\underline{\mathbf{A}}_q$ on its main diagonal
$\bar{\mathbf{A}}^{(\eta,\kappa)}$	submatrix of $\mathbf{A}$ describing the overall channel between the transmit terminal of user κ and the η-th receive antenna
$\bar{A}_{q,q}^{(\eta,\kappa)}$	diagonal element of $\bar{\mathbf{A}}^{(\eta,\kappa)}$ in q-th row and q-th column
$\underline{\mathbf{A}}_q$	$n_{\mathrm{R}} \times N_{\mathrm{s}}$ matrix with all elements $\bar{A}_{q,q}^{(\eta,\kappa)}$ belonging to the same subcarrier q
B	bandwidth
B_{c}	coherence bandwidth
B_{D}	Doppler bandwidth
$\mathbf{B}_q^{(k)}$	matrix describing encoding of $u_{a,q}$ and overall channel jointly for subcarrier q
$\mathbf{B}_{\mathrm{Re},q}^{(k)}$	matrix describing encoding of $\breve{u}_{a,q}^{(k)}$ and overall channel jointly for subcarrier q
$\mathbf{B}_{\mathrm{Im},q}^{(k)}$	matrix describing encoding of $\tilde{u}_{a,q}^{(k)}$ and overall channel jointly for subcarrier q

$\mathbf{C}^{(k)}$	STBC encoding matrix
c_0	speed of light
$\mathbf{c}_{m,n}^{(k)}$	vector of encoded elements of the DFT of the data symbol vector
$c_{m,n,q}^{(k)}$	encoded elements of the DFT of the data symbol vector
$\mathbf{C}_q^{(k)}$	$n_\mathrm{T} \times N_\mathrm{t}$ matrix with all $c_{m,n,q}^{(k)}$ belonging to the same subcarrier q
$D^{(k)}$	distance between subcarrier blocks of user k
$\mathbf{d}$	vector stacking all vectors $\mathbf{d}^{(\kappa)}$
$\mathbf{d}^{(k)}$	data symbol vector
$\mathbf{d}^{(\kappa)}$	data symbol vector of users separated by SDMA
$\hat{\mathbf{d}}^{(k)}$	estimate of the data symbol vector
$\hat{\mathbf{d}}^{(\kappa)}$	estimate of data symbol vector of users separated by SDMA
$\mathbf{d}_a^{(k)}$	a-th data symbol vector
$\bar{\mathbf{d}}_a^{(k)}$	permuted version of a-th data symbol vector
$\hat{\mathbf{d}}_a^{(k)}$	estimate of the a-th data symbol vector
$d_{a,q}^{(k)}$	data symbols contained in vector $\mathbf{d}_a^{(k)}$
$\hat{d}_{a,q}^{(k)}$	estimate of data symbol $d_{a,q}^{(k)}$ contained in vector $\mathbf{d}_a^{(k)}$
$DIV_{\mathrm{B-EFDMA,Rx}}^{(t)}$	number of complex divisions required for the B-EFDMA base station receiver with demodulation in time domain
$DIV_{\mathrm{B-IFDMA,Rx}}^{(f)}$	number of complex division required for the B-IFDMA base station receiver with demodulation in frequency domain
$DIV_{\mathrm{B-IFDMA,Rx}}^{(f)}$	number of complex divisions required for the B-IFDMA base station receiver with demodulation in time domain
$DIV_{\mathrm{OFDMA,Rx}}^{(f)}$	number of complex divisions required for the OFDMA base station receiver with demodulation in frequency domain
$d_q^{(k)}$	data symbol
E_b	energy per bit
$\mathbf{E}_{\mathrm{MMSE}}^{(k)}$	MMSE equalizer matrix
$\boldsymbol{\mathcal{E}}_{\mathrm{MMSE}}^{(k)}$	STBC MMSE frequency domain equalizer matrix
$\mathbf{E}_{\mathrm{ZF}}^{(k)}$	zero-forcing equalizer matrix
F	oversampling factor for channel estimation
f_0	carrier frequency
$f_{\mathrm{D,max}}$	maximum Doppler frequency
$f_{m,n}$	real-valued weighting factor
$\mathbf{F}_\mathrm{N}$	N-point FFT matrix
$\mathbf{F}_\mathrm{N}^\mathrm{H}$	N-point IFFT matrix

$\mathbf{g}$	vector representation of the pulse shaping filter
$\mathbf{G}^{(k)}$	combined modulation and channel matrix
$g_n^{(k)}$	elements of vector $\mathbf{g}_q^{(k)}$
$\mathbf{g}_q^{(k)}$	column vectors of the combined modulation and channel matrix
g_r	elements of vector $\mathbf{g}$
$\mathbf{H}$	$n_\mathrm{R} \times K_\mathrm{s}$ channel matrix for all users separated by SDMA and for all receive antennas
$\mathbf{H}^{(k)}$	circulant channel matrix
$\mathbf{h}^{(k)}$	channel vector
$\bar{\mathbf{h}}^{(k)}$	channel vector complemented with zeros
$\mathbf{H}_m^{(k)}$	circulant channel matrix for m-th transmit antenna
$\bar{\mathbf{h}}_m^{(k)}$	channel vector complemented with zeros for the m-th transmit antenna
$h_n^{(k)}$	elements of the channel vector
$\bar{h}_n^{(k)}$	elements of the channel vector that is complemented with zeros
$\mathbf{H}^{(\eta,\kappa)}$	channel for the m-th receive antenna
IBO	input back-off
$I^{(k)}$	index of subcarrier with the lowest frequency assigned to user k
$I_{l,m}$	possible values of $I^{(k)}$
$\mathbf{I}_N$	N-point identity matrix
$J_0(\cdot)$	zero-order Bessel function
K	number of users
$\mathbf{K}_a$	a-th matrix describing STBC encoding of $\breve{u}_{a,q}^{(k)}$
K_c	number of orthogonal codes
K_f	number of orthogonal frequency resources
K_s	number of users separated by SDMA
L	number of subcarrier blocks
L_0	minimum number of subcarrier blocks
$\mathbf{L}_a$	a-th matrix describing STBC encoding of $\tilde{u}_{a,q}^{(k)}$
L_c	number of samples of the channel vector
$L^{(k)}$	number of subcarrier blocks assigned to user k
L_l	possible values of $L^{(k)}$, levels of the tree for $L^{(k)}$
M	number of subcarriers per block
M_0	minimum number of subcarriers per block
$\mathbf{M}_\mathrm{BI}$	block-interleaved subcarrier allocation matrix of users separated by SDMA

$M^{(k)}$	number of subcarriers per block assigned to user k
$\mathbf{M}^{(\kappa)}$	κ-th subcarrier set that can be assigned to user k
$\mathbf{M}^{(k_\mathrm{f})}$	subcarrier allocation matrix
$\mathbf{M}_\mathrm{BI}^{(k)}$	block-interleaved subcarrier allocation matrix
M_m	possible values of $M^{(k)}$, levels of the tree for $M^{(k)}$
$MUL_\mathrm{B-IFDMA,Tx}^{(f)}$	number of complex multiplications required for B-IFDMA signal generation in frequency domain
$MUL_\mathrm{B-IFDMA,Rx}^{(f)}$	number of complex multiplications required for the B-IFDMA base station receiver with demodulation in frequency domain
$MUL_\mathrm{OFDMA,Tx}^{(f)}$	number of complex multiplications required for OFDMA signal generation in frequency domain
$MUL_\mathrm{OFDMA,Rx}^{(f)}$	number of complex multiplications required for the OFDMA base station receiver with demodulation in frequency domain
$MUL_\mathrm{B-IFDMA,Tx}^{(t)}$	number of complex multiplications required for B-IFDMA signal generation in time domain
$MUL_\mathrm{B-IFDMA,Rx}^{(t)}$	number of complex multiplications required for the B-IFDMA base station receiver with demodulation in time domain
$MUL_\mathrm{B-EFDMA,Tx}^{(t)}$	number of complex multiplications required for B-EFDMA signal generation in time domain
$MUL_\mathrm{B-EFDMA,Rx}^{(t)}$	number of complex multiplications required for the B-EFDMA base station receiver with demodulation in time domain
N	number of subcarriers in a system
$\mathbf{n}$	AWGN vector
$\bar{\mathbf{n}}$	vector stacking all vectors $\mathbf{n}_\eta$
$\bar{\mathbf{n}}^{(k)}$	noise part of DFT of the n-th received signal vector after subcarrier demapping
$\mathbf{n}_\eta$	AWGN vector at η-th receive antenna
$n_{\eta,q}$	elements of vector $\mathbf{n}_\eta$
N_CP	number of samples at sample rate K/T_s of the CP
$\mathbf{n}_\mathrm{e}$	normalized Gaussian noise vector
$n_{\mathrm{e},q}$	elements of the normalized Gaussian noise vector
n_n	elements of the AWGN vector $\mathbf{n}$
$\mathbf{n}_n$	n-th AWGN vector
$\bar{\mathbf{n}}_q^{(k)}$	vector of all $\bar{n}_{n,q}^{(k)}$ belonging to the same subcarrier q
$\bar{n}_{n,q}^{(k)}$	elements of n-th AWGN vector
$\underline{n}_q$	vector of all $n_{\eta,q}$ belonging to the same subcarrier q
N_f	number of adjacent subcarriers with identical channel coefficients

n_{R}	number of receive antennas
n_{T}	number of transmit antennas
N_{t}	number of consecutive modulated data vectors
P	total number of pilot symbols
p	Rapp factor
$\mathbf{P}$	pre-coding matrix
P_{f}	number of pilot symbols in frequency direction
P_{in}	input power of the amplifier
P_{pilot}	pilot symbol power
p_r	factors of N
P_{t}	number of pilot symbols in time direction for B-IFDMA
$\bar{P}_{\mathrm{t}}$	number of pilot symbols in time direction for LFDMA with FH
Q	number of data symbols per user
$Q^{(k)}$	number of subcarriers assigned to user k
$Q^{(k,\kappa)}$	channel quality metric for the overall channel of user k
Q_{max}	maximum number of supported subcarriers assigned to a user
R	number of factors of N
$\mathbf{r}$	received signal vector
$\bar{\mathbf{r}}$	vector stacking all vectors $\mathbf{r}_\eta$
$\mathbf{r}_\eta$	received signal vector at η-th receive antenna
R_{f}	number of samples of the pulse shaping filter at sample rate $S \cdot K/T_{\mathrm{s}}$
$\mathbf{r}_n$	n-th received signal vector
r_n	elements of the received signal vector $\mathbf{r}$
S	oversampling factor
$\mathbf{S}^{(k_{\mathrm{c}})}$	spreading matrix
$\mathbf{s}$	vector stacking all vectors $\mathbf{s}_\eta$
$\mathbf{s}_\eta$	received signal vector at η-th receive antenna after IDFT and subcarrier demapping
S_l	number of nodes at level L_l in the tree for $L^{(k)}$
s_l	index of the nodes at level L_l in the tree for $L^{(k)}$
S_m	number of nodes at level M_m in the tree for $M^{(k)}$
s_m	index of the nodes at level M_m in the tree for $M^{(k)}$
$S_{NN}(f)$	two-sided power spectral density of the noise
T	length of a modulated data vector
T_{c}	coherence time

T_{CP}	length of the cyclic prefix
$\mathbf{T}^{(k)}$	modulation matrix
$\breve{\mathbf{t}}^{(k,\kappa)}$	vector of diagonal elements of $\hat{\boldsymbol{\Gamma}}^{(k,\kappa)}$
$\mathbf{t}^{(k,\kappa)}$	normalized version of vector $\breve{\mathbf{t}}^{(k,\kappa)}$
$\mathbf{t}_{\mathrm{OD}}^{(k,\kappa)}$	vector of outdated channel coefficients
$1/T_{\mathrm{s}}$	symbol rate
$\mathbf{u}$	vector stacking all vectors $\mathbf{u}^{(\kappa)}$
$\mathbf{u}^{(\kappa)}$	DFT of data symbol vector of users separated by SDMA
$\hat{\mathbf{u}}^{(\kappa)}$	estimate of data symbol vector after DFT pre-coding of users separated by SDMA
$\mathbf{u}^{(k)}$	DFT pre-coded data symbol vector
$\bar{\mathbf{u}}^{(k)}$	DFT pre-coded data symbol vector after subcarrier mapping
$\breve{\mathbf{u}}^{(k)}$	vector stacking all $\breve{\mathbf{u}}_q^{(k)}$
$\left(\breve{\mathbf{u}}^{(k)}\right)'$	estimate of vector $\breve{\mathbf{u}}^{(k)}$
$\mathbf{u}_a^{(k)}$	a-th DFT pre-coded data symbol vector
$\left(\breve{\mathbf{u}}_a^{(k)}\right)'$	vector with all elements of vectors $\left(\breve{\mathbf{u}}_q^{(k)}\right)'$ belonging to the a-th data symbol vector
$\left(\tilde{\mathbf{u}}_a^{(k)}\right)'$	vector with all elements of vectors $\left(\tilde{\mathbf{u}}_q^{(k)}\right)'$ belonging to the a-th data symbol vector
$u_{a,q}^{(k)}$	elements of a-th DFT pre-coded data symbol vector
$\breve{u}_{a,q}^{(k)}$	real part of $u_{a,q}^{(k)}$
$\tilde{u}_{a,q}^{(k)}$	imaginary part of $u_{a,q}^{(k)}$
$u_q^{(\kappa)}$	elements of vector $\mathbf{u}^{(\kappa)}$
$u_q^{(k)}$	elements of the DFT pre-coded data symbol vector
$\breve{\mathbf{u}}_q^{(k)}$	vector of all $\breve{u}_{a,q}^{(k)}$ belonging to the same subcarrier q
$\tilde{\mathbf{u}}_q^{(k)}$	vector of all $\tilde{u}_{a,q}^{(k)}$ belonging to the same subcarrier q
$\breve{\mathbf{u}}_q^{(k)}$	vector stacking $\breve{\mathbf{u}}_q^{(k)}$ and $\tilde{\mathbf{u}}_q^{(k)}$
$\left(\breve{\mathbf{u}}_q^{(k)}\right)'$	estimate of vector $\breve{\mathbf{u}}_q^{(k)}$
$\bar{u}_r^{(k)}$	elements of the DFT pre-coded data symbol vector after subcarrier mapping
$\left(\breve{\mathbf{u}}_q^{(k)}\right)'$	estimate of $\breve{\mathbf{u}}_q^{(k)}$
$\left(\tilde{\mathbf{u}}_q^{(k)}\right)'$	estimate of $\tilde{\mathbf{u}}_q^{(k)}$
$\underline{\mathbf{u}}_q$	vector of all $u_q^{(\kappa)}$ belonging to the same subcarrier q
$\hat{\underline{\mathbf{u}}}_q$	estmate of $\underline{\mathbf{u}}_q$
$\mathcal{V}$	set of possible index couples (m, n)

v	velocity of the user terminal
$\mathcal{V}_1$	subset of $\mathcal{V}$
$\mathcal{V}_2$	relative complement of $\mathcal{V}_1$ in $\mathcal{V}$
$v_{\eta,q}$	elements of vector $\mathbf{s}_\eta$
$\bar{\mathbf{v}}$	DFT of the received signal vector
$\bar{\mathbf{v}}^{(k)}$	DFT of the received signal vector after subcarrier demapping
$\bar{v}_n$	elements of the DFT of the received signal vector
$\bar{\mathbf{v}}_n^{(k)}$	DFT of the n-th received signal vector after subcarrier demapping
$\bar{v}_{n,q}^{(k)}$	elements of the DFT of the n-th received signal vector after subcarrier demapping
$\bar{v}_q^{(k)}$	elements of vector $\bar{\mathbf{v}}^{(k)}$
$\bar{\mathbf{v}}_q^{(k)}$	vector of all $\bar{v}_{n,q}^{(k)}$ belonging to the same subcarrier q
$\underline{\mathbf{v}}_q$	vector of all $v_{\eta,q}$ belonging to the same subcarrier q
$\mathbf{W}$	diagonal matrix with the elements w_s on its main diagonal
$\mathbf{w}$	vector representation of the window
$\bar{\mathbf{w}}^{(k)}$	vector stacking all $\bar{\mathbf{w}}_q^{(k)}$
$\bar{\mathbf{w}}_q^{(k)}$	noise vector after decoding
$\underline{\mathbf{W}}_q$	receive filter for subcarrier q
w_s	elements of $\mathbf{w}$
$\mathbf{x}$	vector stacking all vectors $\mathbf{x}^{(\kappa)}$
$\mathbf{x}^{(\kappa)}$	modulated data vector of users separated by SDMA
$\mathbf{x}^{(k)}$	modulated data vector
$\mathbf{x}_{\mathrm{BI}}^{(k)}$	modulated data vector for B-IFDMA
$\mathbf{x}_{\mathrm{BT-CDMA}}^{(k)}$	modulated data vector for BT-CDMA
$\mathbf{x}_{\mathrm{FDOSS}}^{(k)}$	modulated data vector for FDOSS-CDMA
$x_m^{(k)}$	elements of the modulated data vector $\mathbf{x}^{(k)}$
$\mathbf{x}_{\mathrm{MC-CDMA}}^{(k)}$	modulated data vector for MC-CDMA
$\mathbf{x}_{\mathrm{MC-TDMA}}^{(k)}$	modulated data vector for MC-TDMA
$\mathbf{x}_{m,n}^{(k)}$	n-th modulated data vector transmitted from m-th transmit antenna
$x_n^{(k)}$	elements of the modulated data vector
$\mathbf{x}_{\mathrm{OFDMA}}^{(k)}$	modulated data vector for OFDMA
$\mathbf{x}_{\mathrm{OS}}^{(k)}$	oversampled modulated data vector
$x_{\mathrm{OS},n}^{(k)}$	elements of the oversampled modulated data vector
$\mathbf{x}_{\mathrm{PS}}^{(k)}$	modulated data vector after pulse shaping

x_{sat}	saturation value of the amplifier
$\mathbf{x}_{\mathrm{SS-MC-MA}}^{(k)}$	modulated data vector for SS-MC-MA
$\mathbf{x}_{\mathrm{VSCRF}}^{(k)}$	modulated data vector for VSCRF-CDMA
$\mathbf{x}_{\mathrm{w}}^{(k)}$	modulated data vector after windowing
$x_{\mathrm{w},s}^{(k)}$	elements of $\mathbf{x}_{\mathrm{w}}^{(k)}$
z	arbitrary prime number

Bibliography

[3GP04]   3GPP, "Comparison of PAR and Cubic Metric for Power-Derating," TSG RAN WG4 31, Technical Document TDoc R4-040367, May 2004.

[3GP06]   ——, "Physical layer aspects for evolved Universal Terrestrial Radio Access (UTRA)," TSG RAN, Technical Report TR 25.814 v7.1.0, Oct. 2006.

[3GP08a]   ——, "Evolved Universal Terrestrial Radio Access (E-UTRA) and Evolved Universal Terrestrial Radio Access Network (E-UTRAN); Overall description; Stage 2 (Release 8)," TSG RAN, Technical Report TR 36.300 v8.7.0, Dec. 2008.

[3GP08b]   ——, "Evolved Universal Terrestrial Radio Access (E-UTRA); Long Term Evolution (LTE) Physical Layer; General Description," TSG RAN, Technical Specification TS 36.201 v8.2.0, Dec. 2008.

[3GP08c]   ——, "Evolved Universal Terrestrial Radio Access (E-UTRA); User Equipment (UE) Radio Transmission and Reception," TSG RAN, Technical Specification TS 36.101 v8.4.0, Dec. 2008.

[3GP08d]   ——, "Physical Layer on the Radio Path; General Description," TSG GSM/EDGE, Technical Specification TS 45.001 v8.0.0, Dec. 2008.

[3GP08e]   ——, "Radio Access Network; Radio Transmission and Reception," TSG GSM/EDGE, Technical Specification TS 45.005 v8.3.0, Nov. 2008.

[3GP08f]   ——, "Requirements for Further Advancements for E-UTRA (LTE-Advanced)," TSG RAN, Technical Report TR 36.913 v8.0.0, Jun. 2008.

[3GP08g]   ——, "User Equipment (UE) Radio Transmission and Reception (TDD)," TSG RAN, Technical Specification TS 25.102 v8.2.0, Dec. 2008.

[3GP09]   ——, "User Equipment (UE) Radio Transmission and Reception (FDD)," TSG RAN, Technical Specification TS 25.101 v8.5.1, Jan. 2009.

[Ach78]   D. Achilles, *Die Fourier Transformation in der Signalverarbeitung*, 1st ed. Berlin, Heidelberg, New York: Springer Verlag, 1978.

[AD01]   N. Al-Dhahir, "Single-Carrier Frequency-Domain Equalization for Space-Time Block-Coded Transmission Over Frequency-Selective Channels," *IEEE Communication Letters*, vol. 5, no. 7, pp. 304–306, Jul. 2001.

[AFK10]   A. U. T. Amah, T. Frank, and A. Klein, "On Combining SDMA and B-IFDMA: Multi-User Detection and Channel Estimation," in *Proc. of International ITG Workshop on Smart Antennas (WSA) 2010*, Bremen, Germany, Feb. 2010, pp. 434–441.

[Ala98]   S. M. Alamouti, "A Simple Transmit Diversity Technique for Wireless Communications," *IEEE Journal on Selected Areas in Communications*, vol. 16, no. 8, pp. 1451–1458, Oct. 1998.

[BP00] H. Bölcskei and A. Paulraj, "Space-frequency coded broadband OFDM systems," in *Proc. WCNC 2000*, Chicago, Illinois, USA, Sep. 2000, pp. 1–6.

[BR98] K. Brüninghaus and H. Rohling, "Multi-Carrier Spread Spectrum and its relation to Single-Carrier Transmission," in *Proc. IEEE Vehicular Technology Conference*, Ottawa, Ontario, Canada, May 1998, pp. 2329–2332.

[CC00] C.-M. Chang and K.-C. Chen, "Frequency-Domain Approach to Multiuser Detection in DS-CDMA," *IEEE Communication Letters*, vol. 4, pp. 331–333, Nov. 2000.

[Cey05] N. Ceylan, "Linearization of power amplifiers by means of digital predistortion," Ph.D. dissertation, Erlangen, Germany, 2005, Universität Erlangen-Nürnberg.

[CVY05] Z. Chen, B. Vucetic, and J. Yuan, "Asymptotic Performance of Space-time Block Codes with Imperfect Transmit Antenna Selection," *Electronics Letters*, pp. 538–540, Apr. 2005.

[DEC97] DECT Forum, "The DECT Standard Explained," www.dect.org, Standard, Feb. 1997.

[Deg05] C. Degen, "Frequency-Domain Signal Processing for Space-Division Multiple Access with Consideration of Front-End Imperfections," Ph.D. dissertation, Aachen, Germany, 2005, RWTH Aachen.

[DLF04] R. Dinis, C. T. Lam, and D. Falconer, "Carrier Synchronization Requirements for CDMA Systems with Frequency-Domain Orthogonal Signature Sequences," in *Proc. of ISSSTA2004*, Sydney, Australia, Aug./Sep. 2004, pp. 821–825.

[DMO09] M. Döttling, W. Mohr, and A. Osseiran, *Radio Technologies and Concepts for IMT-Advanced*, 1st ed. John Wiley & Sons, 2009.

[Ea06] H. Ekström and al., "Technical Solutions for the 3G Long-Term Evolution," *IEEE Communications Magazine*, pp. 38–45, Mar. 2006.

[ECV03] M. Ergen, S. Coleri, and P. Varaiya, "QoS Aware Adaptive Resource Allocation Techniques for Fair Scheduling in OFDMA Based Broadband Wireless Access Systems," *IEEE Transactions on Broadcasting*, vol. 49, no. 4, pp. 362–370, Dec. 2003.

[ETS99] ETSI, "Broadband radio access networks HIPERLAN Type 2 functional specification - Part I: Physical layer," ETSI HIPERLAN/2, Sophia-Antipolis, France, Technical Specification 101 475, Sep. 1999.

[FABSE02] D. Falconer, S. L. Ariyavisitakul, A. Benyamin-Seeyar, and B. Eidson, "Frequency domain equalization for single-carrier broadband wireless systems," *IEEE Communications Magazine*, vol. 40, pp. 58–66, Apr. 2002.

[FC07]   A. Filippi and E. Costa, "Low-Complexity Interleaved Subcarrier Allocation in Multicarrier Multiple-Access Systems," *IEEE Transactions on Communications*, vol. 55, pp. 35–39, Jan. 2007.

[FDLLS07] D. Falconer, F. Danilo-Lemaine, C.-T. Lam, and M. Sabbaghian, "Power Backoff Reduction for Generalized Multicarrier Waveforms," in *Proc. EU-SIPCO07*, Poznan, Poland, Sep. 2007, pp. 693–697.

[FG98]   G. J. Foschini and M. J. Gans, "On limits of wireless communications in a fading environment when using multiple antennas," *Wireless Personal Communications*, vol. 6, no. 5, pp. 311–335, Mar. 1998.

[FGH07]   M. Fuchs, G. D. Galdo, and M. Haardt, "Low-Complexity Space-Time-Frequency Scheduling for MIMO Systems With SDMA," *IEEE Transactions on Vehicular Technology*, vol. 56, pp. 2775–2784, Sep. 2007.

[FK03]   K. Fazel and S. Kaiser, *Multi-Carrier Spread Spectrum Systems*, 1st ed. John Wiley & Sons Ltd, 2003.

[FKC07a]   T. Frank, A. Klein, and E. Costa, "An Efficient Implementation for Block-IFDMA," in *Proc. PIMRC 2007*, Athens, Greece, Sept. 2007.

[FKC07b]   ——, "IFDMA: A Scheme Combining the Advantages of OFDMA and CDMA," *IEEE Wireless Communications Magazine*, vol. 14, no. 3, pp. 9–17, Jun. 2007.

[FKCK06]   T. Frank, A. Klein, E. Costa, and A. Kühne, "Low Complexity and Power Efficient Space-Time-Frequency Coding for OFDMA," in *Proc. of 15th Mobile & Wireless Communications Summit*, Mykonos, Greece, Jun. 2006.

[FKCS04]   T. Frank, A. Klein, E. Costa, and E. Schulz, "Robustness of IFDMA as Air Interface Candidate for Future High Rate Mobile Radio Systems," in *Advances in Radio Science*, Miltenberg, Germany, Oct. 2004.

[FKCS05a] ——, "IFDMA - A Promising Multiple Access Scheme for Future Mobile Radio Systems," in *Proc. PIMRC 2005*, Berlin, Germany, Sep. 2005.

[FKCS05b] ——, "Interleaved Orthogonal Frequency Division Multiple Access with Variable Data Rates," in *Proc. International OFDM Workshop 2005*, Hamburg, Germany, Aug./Sep. 2005, pp. 179–183.

[FKCS05c] ——, "Low Complexity Equalization with and without Decision Feedback and its Application to IFDMA," in *Proc. PIMRC 2005*, Berlin, Germany, Sep. 2005.

[FKH08]   T. Frank, A. Klein, and T. Haustein, "A survey on the envelope fluctuations of DFT precoded OFDMA," in *Proc. International International Conference on Communications*, Beijing, China, Mai 2008.

[FN01]   L. M. Feeney and M. Nilsson, "Investigating the Energy Consumption of a Wireless Network Interface in an Ad Hoc Networking Environment," in *Proc. of 20th Annual Joint Conference of the IEEE Computer and Communications Societies*, Anchorage, Alaska, Apr. 2001, pp. 1548–1575.

[GC98]   A. J. Goldsmith and S. Chua, "Adaptive coded modulation for fading chan-
            nels," *IEEE Trans. Commun.*, vol. 46, pp. 595–602, Mai 1998.

[GKAS03]   Y. Goto, T. Kawamura, H. Atarashi, and M. Sawahashi, "Variable Spread-
            ing and Chip Repetition Factors (VSCRF)-CDMA," in *Proc. of PIMRC 02*,
            Bejing, China, Sep. 2003, pp. 254–259.

[GRC$^+$02] D. Galda, H. Rohling, E. Costa, H. Haas, and E. Schulz, "A Low Com-
            plexity Transmitter Structure for OFDM-FDMA Uplink Systems," in *Proc.
            IEEE Vehicular Technology Conference*, Birmingham, United Kingdom,
            May 2002, pp. 1737–1741.

[GS01a]   G. Ganesan and P. Stoica, "Space Time Block Codes: A Maximum SNR
            Approach," *IEEE Transactions on Information Theory*, pp. 1650–1656, May
            2001.

[GS01b]   ——, "Space-time block codes: a maximum SNR approach," *IEEE Trans.
            Inf. Theory*, pp. 1650–1656, May 2001.

[HEK05]   J. Hartung, B. Elpelt, and K.-H. Klüsener, *Lehr- und Handbuch der ange-
            wandten Statistik*, 14th ed.   Muenchen, Wien: R. Oldenbourg, 2005.

[IEE99]   IEEE, "LAN/MAN specific requirements - Part 2: Wireless MAC and PHY
            specifications - high speed physical layer in the 5 GHz band," IEEE-802.11,
            Technical Specification P802.11aD6.0, May 1999.

[IEE00]   ——, "Air interface for fixed broadband wireless access systems - Part A:
            Systems between 2 and 11 GHz," IEEE-802.16, Technical Report P802.16ab-
            01/01, Jun. 2000.

[ITU01]   ITU, "Detailed specifications of the radio interfaces of International Mo-
            bile Telecommunications-2000 (IMT-2000)," International Telecommunica-
            tion Union (ITU), Radiocommunication Sector, Technical Report ITU-R
            M.1457-6, Jan. 2001.

[ITU08]   ——, "Requirements related to technical performance for IMT-Advanced
            radio interface(s)," International Telecommunication Union (ITU), Radio-
            communication Sector, Technical Report ITU-R M.2134, Dec. 2008.

[JB04]   E. Jorswieck and H. Boche, "Optimal transmission strategies and impact
            of correlation in multiantenna systems with different types of channel state
            information," *IEEE Transactions on Signal Processing*, vol. 52, pp. 3440–
            3453, Dec. 2004.

[JWY05]   A. Jamalipour, T. Wada, and T. Yamazato, "A Tutorial on Multiple Ac-
            cess Technologies for Beyond 3G Mobile Networks," *IEEE Communications
            Magazine*, vol. 43, pp. 110–117, Feb. 2005.

[Kam08]   K.-D. Kammeyer, *Nachrichtenübertragung*, 4th ed.   Stuttgart, Deutschland:
            B.G. Teubner, Reihe Informationstechnik, Mar 2008.

[Ker04]   K.-P. Kerbusk, "Autobahn ohne Aussicht," *DER SPIEGEL*, pp. 90–94, Jun. 2004.

[KF97]   S. Kaiser and K. Fazel, "A flexible spread-spectrum multi-carrier multiple-access system for multi-media applications," in *Proc. IEEE International Symposium on Personal Indoor and Mobile Communications (PIMRC'97)*, Helsinki, Finland, Sep. 1997, pp. 100–104.

[LFDLD06] C.-T. Lam, D. Falconer, F. Danilo-Lemoine, and R. Dinis, "Channel estimation for SC-FDE systems using frequency domain multiplexed pilots," in *Proceedings of the 64th IEEE Vehicular Technology Conference (VTC '06)*, Montreal, Canada, Sep. 2006, pp. 1438–1442.

[LS03]   E. G. Larsson and P. Stoica, *Space-time block coding for wireless communications*, 1st ed.   Cambridge University Press, 2003.

[Mac08]   T. Maciel, "Suboptimal Resource Allocation for Multi-User MIMO-OFDMA Systems," Ph.D. dissertation, Darmstadt, Germany, 2008, Technische Universität Darmstadt.

[Mar04]   I. Martoyo, "Frequency Domain Equalization in CDMA Detection," Ph.D. dissertation, Karlsruhe, Germany, 2004, Universität Karlsruhe (TH).

[MLG06]   H. G. Myung, J. Lim, and D. J. Goodman, "Peak-to-Average Power Ratio of Single Carrier FDMA Signals with Pulse Shaping," in *Proc. of PIMRC06*, Helsinki, Finland, Sep. 2006.

[Moh06]   W. Mohr, "The WINNER (Wireless World Initiative New Radio) Project - Development of a Radio Interface for Systems Beyond 3G," *International Journal of Wireless Information Networks*, vol. 14, no. 2, pp. 67–78, Dec. 2006.

[MP00]   S. Mudulodu and A. Paulraj, "A Transmit Diversity Scheme for Frequency Selective Fading Channels," in *Proc. GLOBECOM 2000*, Nov./Dec. 2000, pp. 1089–1093.

[MS00]   T. Minn and K. Siu, "Dynamic assignment of orthogonal variable-spreading-factor codes in W-CDMA," *IEEE Journal on Selected Areas in Communications*, vol. 18, no. 8, pp. 429–1440, 2000.

[Pae99]   M. Paetzold, *Mobilfunkkanäle*, 1st ed.   Vieweg, 1999.

[PF01]   C. B. Papadias and G. J. Foschini, "A space-time coding approach for systems employing four transmit antennas," in *IEEE International Conference on Acoustics, Speech, and Signal Processing*, May 2001.

[PL07]   Y. Pei and Y.-C. Liang, "Subcarrier-Based Block-Iterative GDFE (BI-GDFE) Receivers for MIMO Interleaved FDMA," in *VTC Spring*, Dubin, Ireland, 2007, pp. 2033–2037.

[PNG03]   A. Paulraj, R. Nabar, and D. Gore, *Introduction to space-time wireless communications*, 1st ed.   Cambridge University Press, 2003.

[Pro95]   J. G. Proakis, *Digital Communications*, 3rd ed., ser. Electrical Engineering Series.   McGraw-Hill, 1995.

[RAC+02] F. H. Raab, P. Asbeck, S. Cripps, P. B. Kennington, Z. B. Popovic, N. Pothecary, J. F. Sevic, and N. O. Sokal, "Power Amplifiers and Transmitters for RF and Microwave," *IEEE Trans. on Microwave Theory and Techniques*, vol. 50, no. 3, pp. 814–826, Mar. 2002.

[RAC+03] F. H. Raab, P. Asbeck, S. Cripps, P. B. Kenington, Z. B. Popovic, N. Pothecary, J. F. Sevic, and N. O. Sokal, "RF and microwave power amplïer and transmitter technologies - part 1," *High Frequency Electronics*, p. 22â36, May 2003.

[RHV97]   P. Robertson, P. Höher, and E. Villebrun, "Optimal and sub-optimal maximum a posteriori algorithms suitable for turbo decoding," *IEEE Trans. on Telecommunications*, vol. 8, pp. 119–125, Mar./Apr. 1997.

[RMBG99] H. Rohling, T. May, K. Brüninghaus, and R. Grünheid, "Broad-Band OFDM Radio Transmission for Multimedia Applications," *Proc. of the IEEE*, vol. 87, Oct. 1999.

[RP03]   L. M. R. Prasad, *WLANs and WPANs towards 4G wireless*, 1st ed.   Boston, London: Artech House, 2003.

[SDBS98]   U. Sorger, I. De Broeck, and M. Schnell, "IFDMA - A New Spread-Spectrum Multiple-Access Scheme," in *Proc. ICC'98*, Atlanta, Georgia, USA, Jun. 1998, pp. 1013–1017.

[SFE+09]   T. Svensson, T. Frank, T. Eriksson, D. Aronsson, M. Sternad, and A. Klein, "Block Interleaved Frequency Division Multiple Access for Power Efficiency, Robustness, Flexibility and Scalability," *EURASIP Journal on Wireless Communications and Networking*, Article ID 720973, 2009.

[SFF+07]   T. Svensson, T. Frank, D. Falconeer, M. Sternad, E. Costa, and A. Klein, "B-IFDMA - A Power Efficient Multiple Access Scheme for Non-frequency-adaptive Transmission," in *Proc. 16th Mobile & Wireless Communications Summit*, Budapest, Hungary, Jul. 2007.

[SFK06]   A. Sohl, T. Frank, and A. Klein, "Channel Estimation for DFT precoded OFDMA with blockwise and interleaved subcarrier allocation," in *Proc. International OFDM Workshop 2006*, Hamburg, Germany, Aug. 2006.

[SgXM04]   W. Su, X. gen Xia, and S. Member, "Signal constellations for quasi-orthogonal space-time block codes with full diversity," *IEEE Trans. Inform. Theory*, vol. 50, pp. 2331–2347, 2004.

[SH03]   R. P. S. Hara, *Multicarrier Techniques for 4G Mobile Communications*, 1st ed.   Boston, London: Artech House, 2003.

[SK07]   A. Sohl and A. Klein, "Comparison of localized, interleaved and block-interleaved FDMA in terms of pilot multiplexing and channel estimation," in *Proc. 15th European Signal Processing Conference*, Pozan, Poland, Sep. 2007.

[SK09]   ——, "Block-IFDMA – iterative channel estimation versus estimation with interpolation filters," in *Proc. International Multi-Carrier Systems & Solutions Workshop*, Herrsching, Germany, May 2009.

[SKJ94]   H. Sari, G. Karam, and I. Jeanclaude, "Frequency Domain Equalization of Mobile Radio Terrestrial Broadcast Channels," in *Proc. GLOBECOM*, San Francisco, USA, Nov./Dec. 1994, pp. 1–5.

[SSJ06]   A. Skrzypczak, P. Siohan, and J.-P. Javaudin, "Power Spectral Density and Cubic Metric for the OFDM/OQAM Modulation," in *Proc. of ISSPIT2006*, 2006, pp. 846–850.

[SW02]   A. Springer and R. Weigl, *UMTS The Physical Layer of the Universal Mobile Telecommunications System*.   Berlin, Germany: Springer, 2002.

[Sza05]   G. V. Szabo, "Optimization Problems in Mobile Communication," Ph.D. dissertation, Zürich, Switzerland, 2005, ETH Zürich.

[TIA99]   TIA/EIA/IS-cdma2000, "Physical layer standard for cdma2000 spread spectrum systems," Standard, Aug. 1999.

[TIA04]   K. Takeda, T. Itagaki, and F. Adachi, "Application of space-time transmit diversity to single-carrier transmission with frequency-domain equalisation and receive antenna diversity in a frequency-selective fading channel," *IEE IEE Proc.-Commun.*, vol. 151, no. 6, pp. 627–632, Dec. 2004.

[TJC99a]   V. Tarokh, H. Jafarkhani, and A. Calderbank, "Space-time block codes from orthogonal designs," *IEEE Transactions on Information Theory*, vol. 45, no. 5, pp. 1456–1467, Jul. 1999.

[TJC99b]   ——, "Space-time block coding for wireless communications: performance results," *IEEE Journal on Selected Areas in Communications*, vol. 17, no. 3, pp. 451–460, Mar. 1999.

[TV05]   D. Tse and P. Viswanath, *Fundamentals of Wireless Communication*.   UK: Cambridge University Press, 2005.

[VdPG+00]   P. Vandenameele, L. V. der Perre, B. Gyselinckx, M. Engels, M. Moonen, and H. D. Man, "A single-carrier frequency-domain SDMA basestation," in *ICASSP '00: Proceedings of the Acoustics, Speech, and Signal Processing, 2000. on IEEE International Conference*.   Washington, DC, USA: IEEE Computer Society, 2000, pp. 3714–3717.

[vNP00]   R. van Nee and R. Prasad, *OFDM for Wireless Multimedia Communications*, 1st ed.   Artech House, 2000.

[WG00]   Z. Wang and G. B. Giannakis, "Wireless Multicarrier Communications,"
          IEEE Signal Processing Magazine, pp. 29–48, May 2000.

[WIN05]   WINNER, "Final report on identified RI key technologies, system concept,
          and their assessment," WINNER-2003-507581, Deliverable D2.10 v. 1.0,
          Dec. 2005.

[WIN06]   WINNER II, "The WINNER II Air Interface: Refined Multiple Access
          Concepts," IST-4-027756 WINNER II, www.ist-winner.org/WINNER2-
          Deliverables/D4.6.1.pdf, Deliverable D4.6.1, v. 1.0, Nov. 2006.

[WIN07a] ——, "Final CG "local area" description for integration into overall System
          Concept and assessment of key technologies," IST-4-027756 WINNER II,
          www.ist-winner.org/WINNER2-Deliverables/D6.13.12v1.0.pdf, Deliverable
          D6.13.12 V1.0, Nov. 2007.

[WIN07b] ——, "Final CG "metropolitan area" description for integration into overall
          System Concept and assessment of key technologies," IST-4-027756 WIN-
          NER II, www.ist-winner.org/WINNER2-Deliverables/D6.13.11v1.0.pdf,
          Deliverable D6.13.11 V1.0, Nov. 2007.

[WIN07c] ——, "Final CG "wide area" description for integration into overall System
          Concept and assessment of key technologies," IST-4-027756 WINNER II,
          www.ist-winner.org/WINNER2-Deliverables/D6.13.10v1.0.pdf, Deliverable
          D6.13.10 V1.0, Nov. 2007.

[WIN07d] ——, "Final WINNER II System Requirements," IST-4-027756 WIN-
          NER II, www.ist-winner.org/WINNER2-Deliverables/D6.11.4.pdf, Deliver-
          able D6.11.4 V1.0, Jun. 2007.

[WIN07e] ——, "State-of-the-art evaluation (issue 2)," IST-4-027756 WINNER
          II, www.ist-winner.org/WINNER2-Deliverables/D6.13.9.pdf, Deliverable
          D6.13.9, v. 1.0, Jun. 2007.

[WIN07f] ——, "WINNER II Channel Models: Part I Channel Models," IST-4-027756
          WINNER II, www.ist-winner.org/WINNER2-Deliverables/D1.1.2.zip, De-
          liverable D1.1.2 v1.2, Sep. 2007.

[WJ94]   J. W.C. Jakes, *Mircowave Mobile Communications*. New York: IEEE Press,
          1994.

[XZG03]   P. Xia, S. Zhou, and G. B. Giannakis, "Bandwidth- and Power-Efficient
          Multicarrier Multiple Access," *IEEE Trans. on Communications*, vol. 51,
          pp. 1828–1837, Nov. 2003.

[ZG03]   S. Zhou and G. Giannakis, "Single-Carrier Space-Time Block-Coded Trans-
          missions Over Frequency Selective Fading Channels," *IEEE Transactions
          on Information Theory*, vol. 49, pp. 164–179, Jan. 2003.